

**Towards the
innate immunity phenotype
of newly emerging viruses**

INAUGURAL-DISSERTATION

zur Erlangung des akademischen Grades

`doctor rerum naturalium`

(Dr. rer. nat.)

des Fachbereichs 08 – Biologie und Chemie

der Justus-Liebig-Universität Gießen

vorgelegt von

Ulrike Elke Felgenhauer

Justus-Liebig-Universität Gießen

Gießen, Oktober 2021

Die vorliegende Arbeit wurde von Oktober 2017 bis Oktober 2021 in der Arbeitsgruppe von Prof. Dr. Friedemann Weber am Institut für Virologie des Fachbereichs Veterinärmedizin der Justus-Liebig-Universität Gießen angefertigt.

Erstgutachterin: Prof. Dr. Sandra Hake
Fachbereich Biologie und Chemie
Institut für Genetik
Justus-Liebig-Universität Gießen

Zweitgutachter: Prof. Dr. Friedemann Weber
Fachbereich Veterinärmedizin
Institut für Virologie
Justus-Liebig-Universität Gießen

Eidesstattliche Erklärung

Ich erkläre: Ich habe die vorgelegte Dissertation selbständig und ohne unerlaubte fremde Hilfe und nur mit den Hilfen angefertigt, die ich in der Dissertation angegeben habe. Alle Textstellen, die wörtlich oder sinngemäß aus veröffentlichten Schriften entnommen sind, und alle Angaben, die auf mündlichen Auskünften beruhen, sind als solche kenntlich gemacht. Ich stimme einer evtl. Überprüfung meiner Dissertation durch eine Antiplagiat-Software zu. Bei den von mir durchgeführten und in der Dissertation erwähnten Untersuchungen habe ich die Grundsätze guter wissenschaftlicher Praxis, wie sie in der „Satzung der Justus-Liebig-Universität Gießen zur Sicherung guter wissenschaftlicher Praxis“ niedergelegt sind, eingehalten.

Ulrike Felgenhauer

1 Contents

1	Contents.....	4
2	Abstract	8
3	Zusammenfassung	9
4	Introduction	10
4.1	The innate immune system	10
4.1.1	Interferons	10
4.1.2	Type I/III interferon induction.....	11
4.1.2.1	Toll-like receptor signalling	11
4.1.2.2	RIG-I-like receptor signalling	13
4.1.3	Interferon signalling	14
4.1.3.1	Type I interferon signalling	14
4.1.3.2	Type III interferon signalling	15
4.1.4	Interferon-stimulated genes	16
4.1.4.1	ISGs with direct antiviral activity.....	17
4.1.4.2	Other antiviral effectors.....	18
4.1.4.3	Regulators of interferon signalling.....	19
4.1.5	Pro-inflammatory cytokines and signalling.....	19
4.2	Phleboviruses.....	21
4.2.1	Overview and classification	21
4.2.2	Phlebovirus genome organisation and morphology	22
4.2.3	Phlebovirus replication cycle	22
4.2.4	Sandfly-borne phleboviruses	24
4.2.5	Antagonism of the innate immune response by phleboviruses	25
4.3	Coronaviruses.....	26
4.3.1	Overview and classification	26
4.3.2	Coronavirus genome organisation and morphology.....	27
4.3.3	Coronavirus replication cycle.....	28
4.3.4	Highly pathogenic human coronaviruses	30
4.3.4.1	Epidemiology	30
4.3.4.2	SARS coronaviruses and the innate immune response	31
4.4	Objective of this work	34
5	Materials.....	35
5.1	Viruses.....	35
5.2	Eukaryotic cells	35
5.3	Prokaryotic cells.....	36
5.4	Cell culture and transfection reagents	36

5.5	Buffers and solutions	37
5.6	PCR reagents	39
5.7	Antibodies and Fluorescence Dyes	39
5.8	Plasmids.....	40
5.9	Oligonucleotides.....	42
5.10	Commercial reagents	45
5.11	Kits	46
5.12	Consumables and other materials.....	47
5.13	Instruments and software.....	47
6	Methods	49
6.1	Eukaryotic cell culture.....	49
6.1.1	Maintenance and seeding of eukaryotic cells	49
6.1.2	Mycoplasma test.....	49
6.1.3	Transient transfection of eukaryotic cells.....	50
6.1.3.1	Transfection with plasmid DNA	50
6.1.3.2	Transfection with viral RNA	50
6.1.4	Cytokine and inhibitor assays.....	50
6.1.5	Generation of stable cell lines by lentiviral transduction	51
6.2	Virological methods	51
6.2.1	Virus infection of eukaryotic cells	51
6.2.2	Production of virus stocks	52
6.2.2.1	Phleboviruses.....	52
6.2.2.2	SARS coronaviruses.....	52
6.2.3	Virus titre determination by plaque assay	52
6.2.4	Virological work under BSL-3 conditions	53
6.3	Co-immunoprecipitation.....	53
6.4	Immunofluorescence analysis	54
6.5	Luciferase reporter assays	54
6.5.1	Dual luciferase reporter assay	54
6.5.2	Interferon bioassay	55
6.6	Molecular cloning and prokaryotic cell culture.....	55
6.6.1	Subcloning of genes of interest into desired vector backbone	55
6.6.1.1	Insert amplification.....	56
6.6.1.2	Restriction endonuclease digest and ligation.....	56
6.6.2	Transformation of bacteria	57
6.6.3	Insert verification.....	58
6.6.3.1	Colony PCR.....	58
6.6.3.2	Sanger sequencing.....	58

6.7	Molecular biological methods	59
6.7.1	Plasmid DNA isolation from bacteria	59
6.7.2	RNA isolation from eukaryotic cells	59
6.7.3	Quantitative real-time PCR	59
6.7.3.1	Two-step SYBR® green qRT-PCR.....	60
6.7.3.2	Two-step probe qRT-PCR.....	60
6.7.3.3	One-step probe qRT-PCR.....	61
6.8	Protein biochemical methods	61
6.8.1	SDS polyacrylamide gel electrophoresis.....	61
6.8.2	Semidry Western blotting.....	62
6.8.3	Antibody staining	62
6.9	“Omics” approaches.....	62
6.9.1	Proteomic analyses	62
6.9.2	Transcriptomic analyses	63
7	Results	65
7.1	Innate immunity characterization of novel phlebovirus Ntapes virus (NTPV).....	65
7.1.1	Human cell line susceptibility to NTPV and related phleboviruses	65
7.1.2	Differential regulation of innate immune genes upon phlebovirus infection	67
7.1.3	Sensitivity of NTPV and related phleboviruses to type I and type III IFN	68
7.1.4	Effect of the JAK/STAT inhibitor Ruxolitinib on NTPV replication	70
7.1.5	Characterization of virulence factor NSs of novel phleboviruses	71
7.1.5.1	Novel phlebovirus NSs proteins antagonize IFN-β activation	72
7.1.5.2	Novel phlebovirus NSs proteins antagonize IFN-β activation at different signalling steps	74
7.1.5.3	Novel phlebovirus NSs proteins weakly antagonize dsRNA induced ISG54 expression.....	75
7.1.5.4	Novel phlebovirus NSs proteins antagonize NF-κB-dependent gene induction	76
7.1.5.5	Novel phlebovirus NSs proteins antagonize IFN signalling	77
7.1.5.6	Evaluation of tagged phlebovirus NSs constructs	80
7.1.5.7	Subcellular location of phlebovirus NSs	84
7.1.5.8	Interactome analysis of novel phlebovirus NSs proteins with host factors	84
7.2	Innate immunity characterization of SARS coronavirus 2 (SARS-CoV-2).....	96
7.2.1	Sensitivity of SARS-CoV-2 to type I IFN.....	96
7.2.2	Sensitivity of SARS-CoV-2 to type III IFN.....	98
7.2.3	Effect of the JAK/STAT inhibitor Ruxolitinib on SARS-CoV-2 replication.....	99
7.2.4	Comparison of Calu-3 and Vero E6 cell lines	100
7.2.5	Differential regulation of innate immune genes upon SARS-CoV-2 infection in human lung cell lines.....	102

7.2.6	IFN and ISG expression upon SARS-CoV-2 infection in human lung cell lines.....	106
7.2.7	Transcriptomic analysis of SARS-CoV-infected human lung cell lines	108
8	Discussion	117
8.1	Newly discovered phleboviruses with potential implications for human health.....	117
8.1.1	Innate immunity characterization of novel phlebovirus Ntepes virus suggests low pathogenicity in humans.....	117
8.1.2	Non-structural proteins NSs of novel phleboviruses exhibit distinct anti-innate immunity characteristics.....	119
8.2	Pandemic coronavirus SARS-CoV-2	129
8.2.1	Inhibition of SARS-CoV-2 by type I and type III interferons.....	129
8.2.2	Imperfect inhibition of interferons, cytokines and antiviral gene activation by SARS-CoV-2	130
9	List of abbreviations.....	135
10	List of figures	137
11	List of tables	138
12	References	140
13	Addendum	172
13.1	Peer-reviewed publications	172
13.2	Conference presentations.....	172
14	Danksagung.....	173
15	Annex	175

2 Abstract

The innate immune system, orchestrated by interferons (IFNs), is the host's first line of defence against intruding viruses. Therefore, pathogenic viruses have evolved a wide variety of IFN-antagonistic strategies. The sensitivity of viruses to IFNs as well as the quality and strength of IFN evasion can be an important determinant of virulence. This work aims to characterize this so-called innate immunity phenotype of newly emerging viruses with zoonotic potential. For this, the novel phlebovirus Ntepes virus (NTPV) of unknown implications for human health was analyzed, as well as the causative agent of the current COVID-19 pandemic, severe acute respiratory syndrome coronavirus 2 (SARS-CoV-2).

NTPV is a novel phlebovirus of unknown pathogenicity that was recently found to infect humans. This work provides the first comprehensive characterization of its innate immunity profile in human cells, compared to the related Rift Valley fever virus (RVFV) and an attenuated RVFV (clone 13), which lacks a functional virulence factor NSs. Thereby, transcriptional IFN and IFN-stimulated gene (ISG) induction upon NTPV infection and its sensitivity to exogenously added type I and type III IFNs were comparable to responses to the avirulent clone 13. Nonetheless, NTPV encoded an NSs which counteracted the promoter transactivation of several innate immune genes, as did three out of four other novel phleboviruses. However, each of the tested NSs proteins exhibited a distinct antagonistic profile, suggesting virus-specific pathways of IFN antagonism. Further, mass spectrometry analyses identifying host cell interaction partners of NSs proteins revealed a considerable overlap of interactors between viruses. Still, distinct host binding partners were identified for each NSs, again implying different ways to manipulate the host cell environment. In summary, NTPV exhibited a lower capability for IFN evasion than the pathogenic RVFV. However, the general ability of NTPV NSs to counteract IFN induction and signalling and its ability to infect humans emphasize the zoonotic potential of NTPV.

The recently emerged SARS-CoV-2 is the causative agent of the devastating COVID-19 lung disease pandemic. Here, its innate immunity phenotype was evaluated in comparison to the 2003-emerged SARS-CoV-1. Thereby, SARS-CoV-2 was inhibited by both IFNs of type I and type III in a dose-dependent manner, and generally exhibited a greater IFN sensitivity than SARS-CoV-1. Moreover, SARS-CoV-2 replication was boosted by proposed drug candidate Ruxolitinib, an inhibitor of IFN signalling. Further, only SARS-CoV-2 robustly induced an early antiviral response characterized by the transcriptional upregulation of IFNs, cytokines, and ISGs, which also translates to the protein level. However, this potent antiviral response was limited to the human lung cell line Calu-3, as it was absent or severely diminished in human lung cell lines H1299 and A549-ACE2, respectively. Comparison of the transcriptomic profiles of the three cell lines suggests that Calu-3 cells exhibit a "pre-stimulated" state which could account for the observed imperfect inhibition of innate immune induction in these cells. To conclude, this work showed that SARS-CoV-2 is sensitive to type I and III IFNs and unable to counteract IFN induction in all settings, differentiating it from the highly pathogenic SARS-CoV-1.

3 Zusammenfassung

Das von Interferonen (IFNs) gesteuerte angeborene Immunsystem ist die erste Abwehrlinie des Wirts gegen eindringende Erreger, z.B. Viren. Pathogene Viren entwickelten daher eine große Bandbreite an Anti-IFN-Strategien. Die IFN-Sensitivität eines Virus sowie die Qualität und Stärke seiner IFN-Evasion stellen wichtige Virulenzkriterien dar. Das Ziel dieser Arbeit ist es, diesen sogenannten Phänotyp der angeborenen Immunität neu auftretender Viren mit zoonotischem Potential zu bestimmen. Es wurden das neu gefundene Phlebovirus Ntepes Virus (NTPV), dessen Implikationen für die menschliche Gesundheit unbekannt sind, sowie das pandemische Virus *Severe Acute Respiratory Syndrome Coronavirus 2* (SARS-CoV-2), welches die COVID-19-Pandemie verursacht, untersucht.

Von NTPV, einem neuen Phlebovirus unbekannter Pathogenität, wurde kürzlich nachgewiesen, dass es Menschen infizieren kann. Hier wird die erste Charakterisierung seines Phänotyps der angeborenen Immunität präsentiert, im Vergleich mit dem verwandten *Rift Valley* Fieber Virus (RVFV) und einem avirulenten RVFV (*Clone 13*), dem der Virulenzfaktor NSs fehlt. Die transkriptionelle Induktion von IFN und IFN-stimulierten Genen (ISGs) nach NTPV-Infektion, sowie dessen Sensitivität gegenüber Typ I und III IFN waren vergleichbar mit Reaktionen auf *Clone 13*-Infektion. Dennoch kodierte NTPV für ein NSs-Protein, das der Promotoraktivierung einiger antiviraler Gene entgegenwirkt. Gleichermaßen taten dies die NSs-Proteine von drei von vier weiteren neuen Phleboviren. Jedoch wies hierbei jedes der untersuchten NSs-Proteine ein eigenes Profil auf, was auf virusspezifische IFN-Antagonisierung hindeutet. Des Weiteren zeigten Massenspektrometrie-Analysen zur Bestimmung zellulärer NSs-Interaktionspartner eine ausgeprägte Überschneidung der NSs-Interaktoren. Nichtsdestotrotz wurden einzigartige Bindungspartner der einzelnen NSs-Proteine identifiziert, was abermals verschiedene Wege der Wirtszellmanipulation impliziert. Zusammenfassend zeigte NTPV ein geringeres IFN-Evasionspotenzial als das pathogene RVFV. Die IFN-antagonistische Fähigkeit des NTPV NSs und die Tatsache, dass NTPV Menschen infizieren kann, unterstreichen jedoch sein zoonotisches Potenzial.

Das kürzlich aufgetretene SARS-CoV-2 verursacht die verheerende COVID-19-Pandemie. Hier wird dessen Phänotyp der angeborenen Immunität bestimmt, im Vergleich mit SARS-CoV-1, das 2003 aufgetreten war. SARS-CoV-2 wurde sowohl von Typ I als auch von Typ III IFNs auf dosisabhängige Weise gehemmt. Generell wies SARS-CoV-2 eine höhere IFN-Sensitivität als SARS-CoV-1 auf. Weiterhin aktivierte nur SARS-CoV-2 die antivirale Antwort mit transkriptioneller Induktion von IFN und ISGs, was auch auf Protein-Ebene zu beobachten war. Allerdings beschränkte sich diese Immunantwort auf die humane Lungenzelllinie Calu-3 und war in anderen Zelllinien nicht nachzuweisen. Vergleichende Transkriptom-Analysen der untersuchten Zelllinien legen nahe, dass sich Calu-3-Zellen in einem „vorstimulierten“ Zustand befinden, was die beobachtete mangelhafte Hemmung der Immunaktivierung erklären könnte. Somit wurde gezeigt, dass das IFN-sensitive SARS-CoV-2 die IFN-Induktion nicht konsequent hemmen kann, was es von dem hochpathogenen SARS-CoV-1 unterscheidet.

4 Introduction

4.1 The innate immune system

The innate immune system is the host's first line of defence against intruding viruses. In contrast to the adaptive immune system, which is highly specific and therefore takes longer to spring into action, it is fast-acting through the recognition of conserved structural patterns shared by many viruses and other pathogens, the so-called pathogen-associated molecular patterns (PAMPs). The key players of the innate immune system in animals are interferons (IFNs), which govern the nature and extent of this first disease counteraction. They render the host cells in an alert, antimicrobial state by regulating the expression of a vast number of IFN-stimulated genes (ISGs) with a broad range of functions.

4.1.1 Interferons

IFNs are a diverse family of cytokines that are secreted upon the detection of viral infection. They are crucial for immunity by rendering infected as well as bystander cells in an antiviral state through ISG induction, fine-tuning and balancing innate immune responses, as well as impacting adaptive immune responses.

There are three classes of IFNs. Classical type I IFNs in humans comprise the well described IFN- α , of which there are 13 subtypes, and a single IFN- β , as well as the more distantly related IFN- ϵ , IFN- κ and IFN- ω (LaFleur *et al.* 2001; Pestka *et al.* 2004b; Fung *et al.* 2013; Negishi *et al.* 2018). While most cell types can produce IFN- β , IFN- α is secreted by haematopoietic cells, predominantly plasmacytoid dendritic cells (Ivashkiv and Donlin 2014). Type I IFNs signal through the heterodimeric IFN- α receptor (IFNAR), consisting of IFNAR1 and IFNAR2 chains, which is expressed on all nucleated cells.

Type II IFNs contain IFN- γ as a single member, which is secreted mainly by immune cells. It binds to the IFN- γ receptor (IFNGR), which consists of IFNGR1 and IFNGR2 subunits and is expressed on a broad tissue range. IFN- γ displays limited antiviral activity, instead its main function is the modulation of innate and adaptive immunity (Negishi *et al.* 2018).

The family of type III IFNs consists of the four members IFN- λ 1 (IL-29), IFN- λ 2 (IL-28A), IFN- λ 3 (IL-28B) and IFN- λ 4 (Kotenko *et al.* 2003; Sheppard *et al.* 2003; Prokunina-Olsson *et al.* 2013). The IFN- λ receptor (IFNLR), consisting of IFNLR1 (IL-28R α) and IL-10R2 (IL-10R β) chains, in contrast to the IFNAR, is not ubiquitously expressed but limited to mucosal epithelial surfaces and to a subset of immune cells (Stanifer *et al.* 2019; Odendall and Kagan 2015).

IFN gene expression involves different sequence-specific transcription factors which are activated through intricate signalling cascades (chapter 4.1.2). IFN- α gene expression mainly engages members of the IFN regulatory factor (IRF) transcription factor family, with IRF3 and IRF7 playing the most important roles. As distinct IRFs display varying promoter affinities, this might function as a regulatory

mechanism for the different members of the IFN- α family (Levy *et al.* 2011). IFN- β gene expression involves a more complex promoter structure, with four positive regulatory domains (PRDI-IV) serving as overlapping binding sites for IRF3 (PRDI), NF- κ B (nuclear factor kappa B; PRDII), IRF7 (PRDIII) and AP-1 (Activator protein 1; PRDIV) (Goodbourn 1990; Levy *et al.* 2011). Concerted action of all transcription factors, *i.e.* the engagement of the so-called enhanceosome, is needed for efficient IFN- β induction (Iversen and Paludan 2010). IFN- λ gene expression is mediated by IRF and NF- κ B promoter binding sites: IFN- λ 1 depends on IRF3 and NF- κ B, while IFN- λ 2/3 relies on IRF7 binding. Because IRFs and NF- κ B can act independently on the IFN- λ promoters, type III IFN induction is said to be more flexible than that of type I IFN (Iversen and Paludan 2010).

As IFNs are such potent modulators of cell physiology, their unchecked expression can lead to a variety of diseases including autoimmune disease. Thus, their expression is tightly regulated and fine-tuned by diverse feed-forward and feedback loops. In the absence of stimulus, IFN gene expression is kept at very low levels through the engagement of a repressive machinery.

4.1.2 Type I/III interferon induction

Type I and type III IFNs can be produced by almost all cell types upon viral infection. For this, virus infection must first be detected by the host. A diverse group of germline-encoded pattern recognition receptors (PRRs), located in various compartments of the cell, is activated by the recognition of conserved viral PAMPs and this activation induces IFNs through complex signalling cascades.

4.1.2.1 Toll-like receptor signalling

Toll-like receptors (TLRs), expressed in various immune cells, can sense extracellular viruses and virus-infected cells. TLRs involved in virus recognition include TLR3, TLR7, TLR8 and TLR9 which sense nucleic acids in the endosome, and TLR2, TLR4 and TLR6 which detect viral surface proteins in the extracellular space (reviewed in Carty *et al.* 2021; Hartmann 2017; Fitzgerald and Kagan 2020). Specifically, TLR3 detects double-stranded RNA (dsRNA), TLR7 and 8 bind viral single-stranded RNA (ssRNA) and TLR9 is responsible for the sensing of hypomethylated CpG DNA (Carty *et al.* 2021). Upon ligand binding, TLRs dimerize and signal through either the adapter protein MyD88 (myeloid differentiation primary response 88) or TRIF (TIR-domain containing adapter inducing IFN- β) (Fitzgerald and Kagan 2020). MyD88 recruits IRAK (interleukin-1 receptor-associated kinase) proteins which in turn are autophosphorylated to recruit the E3 ubiquitin ligase TRAF6 (TNF receptor-associated factor 6). Next, TRAF6 activates TAK1 (transforming growth factor beta-activated kinase 1) which leads to the stimulation of transcription factors NF- κ B and AP-1 through IKK (inhibitor of κ B kinases) and MAPK (mitogen-activated protein kinase) proteins, respectively. This pathway is employed by all TLRs except for TLR3 and TLR4. Those signal in a MyD88-independent manner by association with TRIF. This adapter recruits TRAF6 to induce NF- κ B signalling as described above, and TRAF3 to induce IRF3 and IRF7 signalling. For this, TRAF3 recruits TBK1 (TANK-binding kinase 1), IKK ϵ and

NEMO (NF- κ B essential modifier), which form the TANK (TRAF family member associated NF- κ B activator) complex. This leads to the activation of transcription factors IRF3 and IRF7 by phosphorylation. Activated transcription factors translocate to the nucleus and induce expression of their respective target genes (**Figure 1**; Fitzgerald and Kagan 2020; Carty *et al.* 2021).

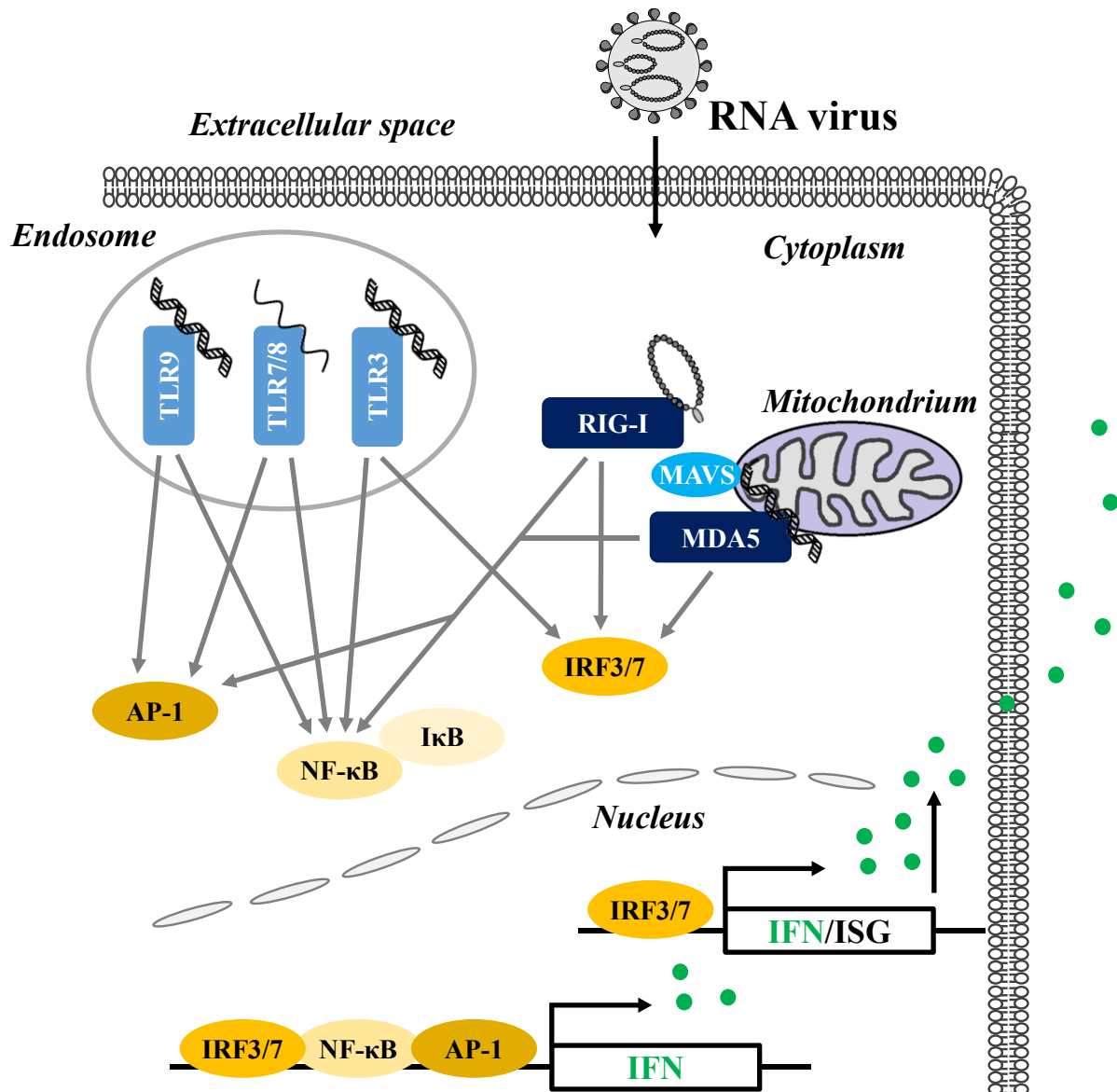


Figure 1: Interferon (IFN) induction through Toll-like receptor (TLR) and RIG-I-like receptor (RLR) signalling. Upon RNA virus infection, pattern recognition receptors (PRRs) located in the host cellular endosome and cytoplasm become activated by the sensing of viral genomes as pathogen-associated molecular patterns. PRR activation triggers signalling cascades culminating in transcription factor activation leading to IFN and IFN-stimulated gene induction. TLR, Toll-like receptor; RIG-I, Retinoic acid inducible gene I; MDA5, Melanoma differentiation-associated protein 5; MAVS, Mitochondrial antiviral signalling protein; IRF, IFN regulatory factor; NF- κ B, Nuclear factor kappa B; AP-1, Activator protein 1; IFN, Interferon; ISG, IFN-stimulated gene. Adapted from Levy *et al.* 2011 and Goubau *et al.* 2013.

4.1.2.2 RIG-I-like receptor signalling

Cytosolic sensing of RNA virus infection engages RIG-I-like receptors (RLRs). This family of DExD/H box-containing RNA helicases consists of structurally related sensors RIG-I (retinoic acid-inducible gene I), MDA5 (melanoma differentiation-associated protein 5) and LGP2 (laboratory of genetics and physiology 2). RIG-I is able to recognize as its main ligand uncapped, blunt-ended dsRNA containing a triphosphate (ppp) moiety at its 5' end, but is also activated by uncapped RNA with 5' diphosphate or a 5' nucleotide unmethylated at its 2'O position (Rehwinkel and Gack 2020; Hornung *et al.* 2006; Pichlmair *et al.* 2006; Schlee *et al.* 2009; Schmidt *et al.* 2009). MDA5 agonists are less well characterized but have been shown to include long dsRNAs of a higher order structure (Pichlmair *et al.* 2009; Rehwinkel and Gack 2020; Kato *et al.* 2008). RNA virus infection can be sensed by either RIG-I or MDA5, or by both PRRs, depending on the virus group (Goubau *et al.* 2013).

Both RIG-I and MDA5 are composed of N-terminal tandem caspase activation and recruitment domains (CARD), a helicase domain, and a C-terminal domain. In its inactive state, RIG-I is present in an auto-repressed conformation where the CARD domains are sterically unavailable for signalling. Upon ligand binding, RIG-I undergoes a conformational change from the resting state to an open conformation with exposed CARD domains (Kowalinski *et al.* 2011). The subsequent ubiquitination at CARD2 position K172 by E3 ligase TRIM25 (tripartite motif 25) serves as a prerequisite for RIG-I oligomerization (Gack *et al.* 2007; Jiang *et al.* 2012). This leads to the transport of RIG-I to the mitochondrial membrane with the help of the 14-3-3 ϵ protein. There, RIG-I associates with MAVS (mitochondrial antiviral signalling protein) via CARD-CARD interactions, which leads to large prion-like MAVS aggregates on the mitochondrial membrane to amplify antiviral signalling (Takeuchi and Akira 2010; Hou *et al.* 2011). RIG-I-MAVS interaction is the basis for the recruitment and activation of TBK1, MAP and IKK family kinases through ubiquitin ligases TRAF2, TRAF3 and TRAF6. TBK1 and IKK ϵ phosphorylate and thereby activate IRF3 and IRF7, while MAPKs cause the activation of AP-1, and IKK α and IKK β lead to phosphorylation and activation of NF- κ B inhibitor I κ B. This causes its dissociation from NF- κ B leaving NF- κ B unrestricted. In their activated state, the transcription factors translocate into the nucleus and cause the expression of their target genes. Amongst those are type I and type III interferons, pro-inflammatory cytokines and a subset of ISGs (**Figure 1**; reviewed in Goubau *et al.* 2013; Levy *et al.* 2011).

In contrast to RIG-I, MDA5 activation is less well described. It seems not to follow a strict conformational change upon activation, but rather flexibly exists in an equilibrium of open and closed conformations in the resting state. Ligand binding might favour the form which supports multimerization by causing filamentous aggregation of MDA5 along dsRNA (Berke and Modis 2012; Fan and Jin 2019; Brisse and Ly 2019). The involvement of K63-linked ubiquitination of MDA5 has long been controversial; however, the E3 ubiquitinase TRIM65 has recently been shown to interact with MDA5 to deliver K63-linked ubiquitination at K473, which catalyzes oligomerization (Lang *et al.* 2017). Like

RIG-I, MDA5 triggers IRF3/7 and NF- κ B induction via the CARD-CARD association with adapter molecule MAVS, as described above (**Figure 1**).

LGP2 differs from the structure of RIG-I and MDA5 in that it lacks the CARD domains. Consequently, it is unable to signal through MAVS. Different positive and negative regulatory roles for RIG-I and MDA5 have been described for LGP2, among those are the inhibition of RIG-I through prevention of binding to MAVS or ubiquitination by TRIM25 (Quicke *et al.* 2019; Rehwinkel and Gack 2020), and on the other hand support of MDA5-mediated antiviral responses (Bruns *et al.* 2014).

4.1.3 Interferon signalling

IFNs exert their manifold functions in an autocrine (on infected IFN-producing cells) as well as in a paracrine (on uninfected neighbouring cells) manner. IFN binding to their respective receptors (chapter 4.1.1) triggers a signalling cascade culminating in the induction of a large number of ISGs. Some ISGs have direct antiviral activity, while others are involved in, for example, host cell metabolism or regulation of IFN signalling.

4.1.3.1 Type I interferon signalling

Interferons of type I (IFN- α/β , chapter 4.1.1) are the ligands of the IFN- α receptor (IFNAR), a heterodimeric complex consisting of IFNAR1 and IFNAR2 chains which is present on all nucleated cells. Across type I IFNs, IFN- β displays the strongest receptor affinity (Mesev *et al.* 2019). Concerning IFNAR receptor subunits, IFNAR2 displays a high affinity for its ligands, whereas IFNAR1 shows lower affinity but rather is responsible for distinguishing different IFN subtypes (de Weerd *et al.* 2007; Jaks *et al.* 2007). The binding of type I IFN to IFNAR2 and the subsequent formation of a ternary receptor complex with IFNAR1 activates the JAK/STAT pathway (reviewed in Ivashkiv and Donlin 2014; Mesev *et al.* 2019; Stanifer *et al.* 2019). Thereby, first, protein tyrosine kinases located on the cytoplasmic tails of receptor subunits are activated by structural receptor rearrangements that render cytoplasmic receptor chains in close proximity: JAK1 (Janus kinase 1, associated with IFNAR2) and TYK2 (tyrosine kinase 2, associated with IFNAR1) cross-phosphorylate as well as phosphorylate receptor chains to create binding sites for STAT (signal transducer and activator of transcription) proteins. In a second step, recruited STATs are thus activated by phosphorylation. In humans, there are seven STAT proteins, namely STAT1, STAT2, STAT3, STAT4, STAT5A, STAT5B and STAT6. Upon phosphorylation, STAT proteins form various homo- and heterodimeric complexes (Levy and Darnell 2002). IFNAR signalling mainly induces STAT1:STAT2 heterodimers that associate with IRF9 to form the IFN-stimulated gene factor 3 (ISGF3) complex. ISGF3 acts as a transcription factor that binds so-called IFN-stimulated response elements (ISRE) upstream of ISG loci, thus inducing the transcription of ISGs (**Figure 2**). In some cases, STAT1 homodimers are formed, which act on gamma-activated sequences (GAS) of ISGs in the nucleus. Of note, ISGs promoter regions can contain an ISRE or GAS alone, or a combination of both. Importantly, STAT1 homodimers induced upon type I (and type II) IFN

signalling are responsible for IRF1 induction, which leads to a strong pro-inflammatory signature (**Figure 2**; Forero *et al.* 2019).

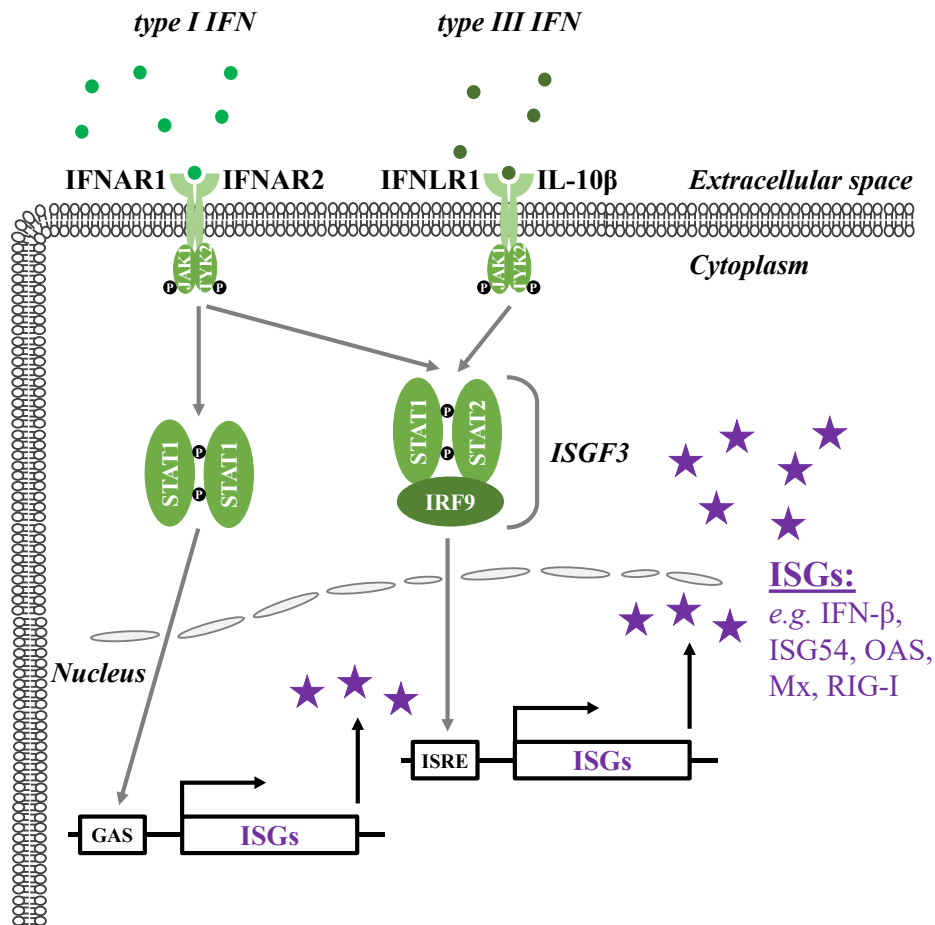


Figure 2: Type I and type III interferon signalling. Type I and type III interferon binding to their cognate receptors, consisting of IFNAR1/IFNAR2 or IFNLR1/IL-10 β chains, respectively, triggers a signalling cascade leading to the induction of transcription factor IFN-stimulated gene factor 3 (ISGF3, complex of STAT1:STAT2 heterodimer associated with IRF9) acting on IFN-stimulated response elements (ISRE) for IFN-stimulated gene (ISG) induction. Additionally, upon type I IFN signalling, STAT1 homodimers can be formed, which act on gamma-activated sequences (GAS) for ISG induction. IFN, Interferon; IFNAR, IFN alpha receptor; IFNLR, IFN lambda receptor; IL, Interleukin; IRF, IFN regulatory factor; JAK, Janus kinase; Mx, Myxovirus resistance protein; OAS, 2',5'-Oligoadenylate synthase; RIG-I, Retinoic acid-inducible gene I; STAT, Signalling transducer and activator of transcription; TYK, Tyrosine kinase. Adapted from Ivashkiv and Donlin 2014 and Schneider *et al.* 2014.

4.1.3.2 Type III interferon signalling

Type III IFNs (IFN- λ 1–4, chapter 4.1.1) bind to the IFN- λ receptor (IFNLR). Like IFNAR, this receptor is a heterodimeric complex formed by the IFNLR1 (IL-28R α) and the IL-10R2 (IL-10R β) chains, where receptor engagement also triggers a JAK/STAT signalling cascade (reviewed in Wack *et al.* 2015; Stanifer *et al.* 2019). Notably, the IL-10R2 chain is shared by members of the IL-10 family (Sheppard *et al.* 2003; Pestka *et al.* 2004a). Type III and type I IFN responses induce overlapping ISG signatures. While early work after the discovery of the type III IFN family primarily focused on its similarity with

the type I IFN response, recent work has elucidated several important differences between the two cytokine families.

The most fundamental disparity lies in the places of action: in contrast to ubiquitous IFNAR expression, IFNLR expression is limited through IFNLR1 subunit expression to epithelial cells including hepatocytes, and to specific immune cells (Sommereyns *et al.* 2008; Mordstein *et al.* 2010). Thus, type III IFNs confer protection at mucosal anatomic barriers. Further, type I and type III IFN signatures differ substantially with respect to their kinetics. While the transcriptional response upon type I IFN stimulation is quick, strong and transient, that of type III is delayed and weaker, but displays a much more prolonged activation (Pervolaraki *et al.* 2018). Lower levels of IFNLR cannot account for these profound kinetic differences between the two IFN classes; while IFNLR overexpression increased the magnitude of ISG expression, the delayed but sustained ISG induction is intrinsic to the signalling pathway and not associated with receptor abundance (Pervolaraki *et al.* 2018). However, these differences could in part be explained by the different induction kinetics of IFN signalling regulators. Suppressor of cytokine signalling 1 (SOCS1) leads to IFNAR1 downregulation through ubiquitination-induced TYK2 destabilization. It is itself an ISG but is induced much earlier following type I (Pestka *et al.* 2004b) than type III IFN stimulus (Pervolaraki *et al.* 2018; Stanifer *et al.* 2019). While SOCS1 acts on both type I and type III IFN signalling, ubiquitin-specific protease USP18 is a negative regulator of IFN- α signalling by inhibiting IFNAR2-JAK1 interaction that has no effect on type III IFN signalling (Blumer *et al.* 2017). Another key difference between type I and type III IFNs is the fact that in contrast to type I IFNs, IFN- λ signalling does not induce a pro-inflammatory response. This is due to the low IFNLR abundance which is insufficient to induce STAT1 homodimers that lead to IRF1 expression. In the absence of the IRF1-driven expression of pro-inflammatory cytokines, type III IFNs rather induce a transcriptional programme which is directed at tissue repair and maintenance of barrier integrity (Forero *et al.* 2019). Further, signalling pathways engaged upon type I or type III IFN stimulation can differ. For instance, the IFN- λ signalling pathway is still able to function in the absence of TYK2 (Fuchs *et al.* 2016).

Therefore, although type I and type III IFNs induce a similar ISG signature, their actions are not redundant. It is believed that type III IFNs act as a frontline defence against intruding viruses at mucosal surfaces by inducing a local antiviral state without causing profound inflammation. However, when barrier integrity is breached by intruding pathogens, a type I IFN response is mounted for systemic actions. Since this type I IFN response is accompanied by a strong pro-inflammatory response, its fast termination is crucial to prevent tissue damage. In contrast, type III IFN action is prolonged.

4.1.4 Interferon-stimulated genes

IFN-stimulated genes (ISGs) are transcripts whose expression is induced upon IFN signalling due to ISRE or GAS elements in their promoter or enhancer regions. The vast repertoire of ISGs comprises on

the one hand effectors with direct antiviral functions and sensors of viral infection, but on the other hand also cytokines, chemokines, and their receptors to mediate cell-cell communication, positive and negative regulators of IFN signalling, or proapoptotic proteins. “Classic ISGs” with profound antiviral functions have been known for a long time. However, the family of ISGs is an ever-growing class of proteins. Since the first large-scale ISG-screen describing novel antiviral factors was performed (Schoggins *et al.* 2011), identification of additional ISGs is constitutively reported. For example, a recent interferome study described a set of approx. 60 “core ISGs”, some of previously unknown association with IFN, which are shared between several vertebrate species (Shaw *et al.* 2017).

4.1.4.1 ISGs with direct antiviral activity

ISGs can directly combat virus infection by interfering with every step of the viral life cycle from virus entry, followed by translation and replication, to virus egress from the host cell.

Viral entry can be affected for example by IFITM and Mx proteins or CH25H. IFN-induced transmembrane (IFITM) proteins, located in endosomal and lysosomal cellular compartments, impede fusion of viral and endolysosomal membranes following virus endocytosis. IFITMs exert their antiviral functions for example on influenza viruses, members of the flavivirus family, Rift Valley fever virus (RVFV) or severe acute respiratory syndrome coronavirus 1 (SARS-CoV-1) (Perreira *et al.* 2013; Zhao *et al.* 2018) and SARS-CoV-2 (Zang *et al.* 2020). Human myxovirus resistance protein 1 (Mx1 or MxA), encoded by the *Mx1* gene, belongs to the family of dynamin-like GTPases. It is a cytosolic protein which traps viral nucleocapsids to prevent transcription. MxA expression strictly relies on IFN signalling and is not induced in direct response to virus infection (Haller and Kochs 2011). Viruses targeted by MxA include influenza virus (Matzinger *et al.* 2013) or RVFV and other phleboviruses (Frese *et al.* 1996; Habjan *et al.* 2009a), but not SARS-CoV-1 (Spiegel *et al.* 2004). However, single nucleotide polymorphisms in MxA promoter regions were demonstrated to alter susceptibility to SARS-CoV-1 (He *et al.* 2006; Ching *et al.* 2010). Cholesterol-25-hydroxylase (CH25H) depletes membrane cholesterol by converting it to 25-hydroxycholesterol (25HC), thereby inhibiting membrane fusion-mediated cell entry of enveloped viruses like vesicular stomatitis virus (VSV), RVFV (Liu *et al.* 2013) or SARS-CoV-2 (Wang *et al.* 2020d; Zang *et al.* 2020).

Viral translation and replication are complex processes antagonized by many different ISGs, either by targeting translation in general or by virus-specific effects. Members of the IFN-induced protein with tetratricopeptide repeats (IFIT) family are highly induced upon IFN stimulation but are also upregulated through IRF3 following virus infection (Fensterl and Sen 2011). They are able to inhibit host and viral gene translation via eukaryotic translation initiation factor 3 (eIF3) binding. It has also been shown that several IFIT proteins form a multimeric complex where IFIT1 sequesters viral 5'ppp RNAs (Pichlmair *et al.* 2011). Antiviral activity of IFIT proteins has been demonstrated for example against VSV and influenza viruses (Sadler and Williams 2008). Protein kinase R (PKR) is another ISG which interferes

with general translation. Before its upregulation following IFN stimulation, it is constitutively expressed at basal levels in an inactive form. Upon activation through recognition of dsRNA, it phosphorylates eukaryotic translation initiation factor 2 α (eIF2 α), thereby halting host and viral mRNA translation (Pindel and Sadler 2011). PKR displays profound activity against members of the phlebovirus family and is therefore targeted by viral evasion strategies (Kainulainen *et al.* 2016; Wuerth *et al.* 2020). Foreign RNAs are further sensed by 2',5'-oligoadenylate synthase (OAS) proteins to mediate the activation of ribonuclease L (RNaseL) which in turn degrades host and viral RNA, thereby interfering with viral replication while at the same time producing more PAMPs for IFN activation (Schneider *et al.* 2014). Since PKR and OAS are activated by similar ligands, viral inhibition or evasion of one pathway will likely also target the other. In addition to enzymatically active OAS1–3, humans also express an OAS-like (OASL) protein without catalytic function. Beside its regulatory role in the OAS-RNaseL pathway, OASL also possesses antiviral activity by augmenting RIG-I signalling (Drappier and Michiels 2015; Ibsen *et al.* 2015).

Viral egress is mainly opposed by viperin, encoded by the *Rsad2* gene, and tetherin, encoded by *BST2*. Viperin, which is also induced directly following virus infection, interferes with viral release from host cells by altering membrane structures through the disturbance of lipid rafts. This confers antiviral activity, among others, against influenza virus (Wang *et al.* 2007). Additionally, Viperin interferes with viral replication in tick-borne encephalitis virus (TBEV) infection (Upadhyay *et al.* 2014). Tetherin on the host membrane physically retains budding virions and thus prevents viral spread. Further, it is involved in NF- κ B induction and assumes various immunomodulatory roles (Tiwari *et al.* 2019).

4.1.4.2 Other antiviral effectors

ISGs are a heterologous group of effectors that antagonize viral infection through manifold functions that cannot always be stringently grouped. For example, IFN-stimulated gene 15 (ISG15) is a relatively small protein (~15 kDa) structurally related to ubiquitin. Like this relative, ISG15 can be covalently attached to proteins in a process called ISGylation. Unlike ubiquitination, however, that can target proteins for degradation, ISGylation rather acts in an activating manner, for example by stabilizing IRF3 (Shi *et al.* 2010). In addition, ISGylation of viral proteins can interfere with their respective functions (Dzimianski *et al.* 2019). The family of poly(ADP-ribose) polymerases (PARPs) has also gained attention as antiviral effectors. For example, PARP9 and PARP14 are involved in macrophage activation through opposing roles with PARP9 promoting pro-inflammatory genes and STAT1 phosphorylation (Iwata *et al.* 2016); further, PARP12 was identified as potent antagonist of Zika virus infection through ADP-ribosylation and subsequent degradation of viral proteins (Li *et al.* 2018).

4.1.4.3 Regulators of interferon signalling

Early in infection, multiple feed-forward mechanisms amplify pathogen sensing and signalling. However, just as crucial as the fast innate immune response is its timely termination to prevent harmful effects by an overshooting IFN response and to return to cellular homeostasis.

Zinc-finger antiviral protein (ZAP), encoded by the *ZC3HAV1* gene, has multiple splice variant isoforms with distinct antiviral functions (Li *et al.* 2019a). The best described isoforms are termed ZAPL, for long, and ZAPS, for short. In a directly antiviral mode of action, they bind to and cause the degradation of viral RNA (Schwerk *et al.* 2019). ZAPS, which is more potently induced upon IFN stimulation, further binds to RIG-I to enhance antiviral signalling (Hayakawa *et al.* 2011). It has recently been shown that both ZAPL and ZAPS restrict SARS-CoV-2 infection, in addition to its known inhibition of *e.g.* Alphaviruses or Filoviruses (Nchioua *et al.* 2020). DExD/H box helicase 60 (DDX60) belongs to the same family as PRRs RIG-I and MDA5, however is devoid of a CARD domain for signalling. Beside its ability to induce viral RNA degradation, it was shown to facilitate RIG-I activation by direct interaction (Miyashita *et al.* 2011; Oshiumi *et al.* 2015). However, another study was unable to reproduce RIG-I signalling potentiation upon DDX60 overexpression and also showed no effect on virus replication upon of DDX60 knockout in mice (Goubau *et al.* 2015). This might be attributed to a more complex manner of signalling mediation and/or species-specific differences.

Negative regulators of the IFN response are also upregulated with IFN signalling. Among those ISGs are for example the suppressor of cytokine signalling (SOCS) proteins or ubiquitin-specific peptidase 18 (USP18). SOCS proteins are induced early in the IFN response and mediate receptor degradation (Schneider *et al.* 2014). USP18 on the one hand binds to the IFNAR receptor to inhibit IFN- α but not IFN- β signalling, and on the other hand facilitates deISGylation. Notably, type III IFN signalling is insensitive to USP18 and SOCS3, but is negatively affected by SOCS1 (Blumer *et al.* 2017).

4.1.5 Pro-inflammatory cytokines and signalling

In addition to ISG induction, PRR and IFN signalling also leads to the secretion of cytokines, a group of small proteins that govern cell-cell communication, initiation of an adaptive immune response, and a pro-inflammatory reaction (Goubau *et al.* 2013). Consequently, cytokines are involved in the regulation of many biological and immune processes. According to structure and function, cytokines can be grouped into different classes, *e.g.* interleukins (IL), chemokines, growth factors, and IFNs themselves (Bixler and Goff 2015). The main source of cytokine secretion are immune cells such as monocytes, macrophages or dendritic cells, but other cell types like endothelial and epithelial cells or fibroblasts are involved in cytokine production as well (Betakova *et al.* 2017). Cytokines take on versatile functions and their dysregulation can result in the exacerbation of disease. In fact, an overshooting pro-inflammatory cytokine response (so-called “cytokine storm”) is involved in severe disease manifestation

caused by filo- and influenza viruses, as well as SARS-CoV-2 (Wack *et al.* 2011; Bixler and Goff 2015; Betakova *et al.* 2017; Fraser *et al.* 2020).

Chemokines exhibit chemotactic functions to attract various immune cells to the site of infection. Members of this sub-family include *e.g.* CCL5 (alternative name: RANTES), CCL4 (MIP-1 β), IL-8 (CXCL8) and CXCL10 (IP-10). CCL4 and CCL5 are upregulated following virus infection but not type I IFN stimulation (Hölzer *et al.* 2019), and both signal through the receptor CCR5 (Wack *et al.* 2011). CCL5 seems to play a dual role in virus infection: while mice deficient in CCR5 (with CCL5 as dominant ligand) are more susceptible to influenza virus infection, blocking of CCL5 during respiratory syncytial virus (RSV) infection reduces inflammation to alleviate infection (Wack *et al.* 2011). CXCL10, which facilitates chemotaxis of T cells, dendritic cells or macrophages, has been implicated in disease severity of SARS-CoV-2 (Yang *et al.* 2020a; Daamen *et al.* 2021).

The interleukin IL-6, produced primarily by macrophages, endothelial cells, and T or B cells, has been shown to be elevated in severe disease following SARS-CoV-2 (Han *et al.* 2020; Lagunas-Rangel and Chávez-Valencia 2020) and influenza virus infection (Betakova *et al.* 2017). In addition to its involvement in B and T effector cell regulation, IL-6 also aids in *STAT1* and *IRF9* gene expression (Betakova *et al.* 2017; Ivashkiv and Donlin 2014).

Other pro-inflammatory cytokines are members of the tumour necrosis factor (TNF) family, with TNF- α being the key player. Mainly produced by activated macrophages and other immune cells, it is involved in inflammatory processes such as fever development, immune cell attraction and regulation, coagulation, or apoptosis (Bixler and Goff 2015; Betakova *et al.* 2017). TNF- α signals through TNF-receptor (TNFR) 1 and 2, with the former being ubiquitously expressed while the latter is restricted to immune cells, neurons, and endothelial cells (Holbrook *et al.* 2019). TNF- α binding to TNFR1 causes a conformational change in the receptor-associated death domain, which leads to the recruitment of TRADD (TNFR1-associated death domain) and RIPK1 (receptor-interacting serine/threonine protein kinase 1). The ubiquitination status of RIPK1 determines further signalling towards cell survival or cell death. Cell survival is mediated by complex I formation consisting of TRADD, RIPK1, TRAF2/5, cIAP (cellular inhibitor of apoptosis protein) 1/2 and LUBAC (linear ubiquitin chain assembly complex). RIPK1 ubiquitination by the latter two leads to recruitment of TAB (TAK-binding protein) 2 and 3 and the IKK complex. Together these form the TAK1 complex which leads to the activation of transcription factors AP-1 and NF- κ B (see 4.1.2; Holbrook *et al.* 2019; Atretkhany *et al.* 2020). Signalling through TNFR2 promotes cell survival and AP-1/NF- κ B induction in a similar fashion. In contrast to TNFR1, however, TNFR2 does not possess a death domain and instead associates directly with TRAF1/2 for cIAP1/2 recruitment and complex I formation. Beside its strong pro-inflammatory capacities, TNF- α also influences the antiviral immune response through crosstalk with IFNs. A recent report demonstrated the synergistic effect of co-stimulation with IFN- β and TNF- α on a subset of genes including CXCL10, ISG20 and IRF1. Notably, this effect was independent of STAT1 in some genes, like CXCL10. Instead,

expression relies on STAT2 and IRF9 through the engagement of alternate ISRE promoter sites (Mariani *et al.* 2019). TNF- α is also known to induce low but sustained amounts of IFN- β through IRF1, which in an autocrine feed-forward loop leads to the late expression of ISGF3- and STAT1-dependent ISGs upon TNF- α signalling (Yarilina *et al.* 2008).

4.2 Phleboviruses

4.2.1 Overview and classification

Phleboviruses constitute one of 19 genera within the family *Phenuiviridae* of the order *Bunyavirales* (ICTV 2020; **Figure 3A**). Bunyaviruses are globally distributed and display a wide host range of vertebrates, invertebrates and plants (Léger and Lozach 2015). Most members of this order are arthropod-borne viruses (arboviruses), using blood-feeding mosquitoes, sandflies, ticks, and midges as vectors. The family *Hantaviridae* poses an exception, with transmission occurring through rodent reservoirs.

Of the 67 virus species annotated to the genus phlebovirus, many are able to infect humans (ICTV 2020; Elliott and Brennan 2014; Calisher and Calzolari 2021). Human pathogenic phleboviruses can cause a wide spectrum of illnesses, ranging from asymptomatic or mild disease to severe illness with potentially fatal outcomes (Léger and Lozach 2015). Phleboviruses of public health importance include, among others, Rift Valley fever virus (RVFV), Sandfly fever Sicilian virus (SFSV), Punta Toro virus (PTV) and Toscana virus (TOSV; Wuerth and Weber 2016; Wright *et al.* 2019).

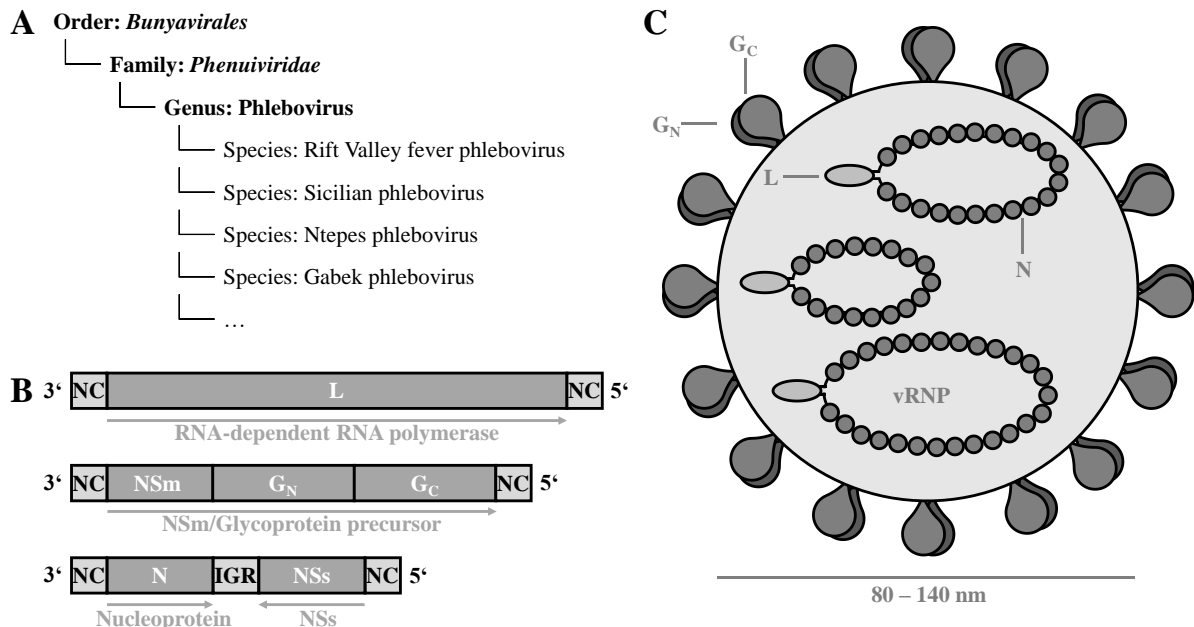


Figure 3: *Phlebovirus* taxonomy, genome organization, and virion. (A) Taxonomy of phleboviruses within the *Bunyavirales* order. (B) Phlebovirus genome organization. (C) Schematic representation of phlebovirus virion. G_C, glycoprotein G_C; G_N, glycoprotein G_N; IGR, intergenic region; L, RNA-dependent RNA polymerase; N, nucleoprotein; NC, non-coding region; NSm, medium non-structural protein; NSs, small non-structural protein; vRNP, viral ribonucleoprotein. Adapted from Wuerth and Weber 2016.

4.2.2 Phlebovirus genome organisation and morphology

Phleboviruses carry a tripartite, single-stranded RNA genome in negative orientation (**Figure 3B**; Elliott and Brennan 2014). The large genome segment (L segment) encodes the viral RNA-dependent RNA polymerase (RdRp), the medium segment (M segment) encodes the glycoproteins G_N and G_C , as well as the non-structural protein NSm in some species, like RVFV. The small genome segment (S segment) encodes the viral nucleoprotein N in negative sense orientation and, in ambisense orientation, the small non-structural protein NSs (Walter and Barr 2011).

Phleboviruses are enveloped, roughly spherical particles of 80 – 140 nm diameter (**Figure 3C**; Amroun *et al.* 2017). Inserted into their host-derived membrane they carry the two glycoproteins G_N and G_C which facilitate virus entry into the host cell and are the primary targets for neutralizing antibodies (Spiegel *et al.* 2016). Inside the virion lie the three genome segments, which are largely coated with the nucleoproteins N and associated with the polymerase L to form ribonucleoprotein (RNP) structures (Guu *et al.* 2012). These RNPs appear pseudo-circularized in electron microscopy studies (Amroun *et al.* 2017), a phenomenon that was long attributed to a so-called panhandle structure formation due to the strict complementarity of 5' and 3' non-coding regions of all segments (Amroun *et al.* 2017). However, this model has been revised as it was found that the polymerases of some Bunyaviruses bind the 5' and 3' genome ends in different binding sites (Amroun *et al.* 2017). Nonetheless, the near-circular form and the close association of the viral genome with N protect the RNPs from degradation.

4.2.3 Phlebovirus replication cycle

Before a virus can enter a host cell, it needs to attach to specific receptor molecules on the cellular surface (**Figure 4–1**). The receptors for phleboviruses are largely unidentified, although DC-SIGN (dendritic cell-specific intercellular adhesion molecule-3-grabbing non-integrin) was shown to be involved in RVFV, PTV and TOSV attachment, and heparan sulfate was shown to be required for RVFV entry (Spiegel *et al.* 2016). Since these surface molecules are not expressed on the whole target cell spectrum of phleboviruses, it is likely that additional receptors and attachment factors are involved.

The association of virus and receptor triggers internalization mechanisms via receptor-mediated endocytosis which vary for different phleboviruses (**Figure 4–2**; Spiegel *et al.* 2016; Amroun *et al.* 2017). In the endosome, receptor binding or low pH trigger a conformational change in the viral glycoprotein G_C . This leads to the fusion of viral and endosomal membranes and the subsequent release of the viral RNPs into the host cytoplasm (**Figure 4–3**; Spiegel *et al.* 2016).

Because the viral genomic RNA is orientated in negative sense, incoming virions need the RNP-associated polymerase L for primary mRNA transcription. Beside its function as RNA-dependent RNA polymerase, the viral L protein also displays exonuclease activity at its N-terminus, which is employed to acquire 5' cap structures from host mRNAs. In this process called “cap-snatching”, the polymerase cleaves host mRNA transcripts 10 – 20 nucleotides downstream of the cap with a strong sequence

preference (Ferron *et al.* 2017; Amroun *et al.* 2017). Subsequently, viral mRNAs are transcribed by the polymerase by elongating the acquired 5' caps, resulting in viral mRNA containing heterogeneous non-viral 5' sequences (Guu *et al.* 2012). Phleboviral mRNAs do not contain a 3' poly(A) tail, which during host cell translation binds the mRNA 3' end to the translation machinery to protect it from degradation. Instead, viral mRNA are described to form a 3' stem loop structure for exonuclease protection (Amroun *et al.* 2017).

Phlebovirus mRNA synthesis is strictly coupled to simultaneous protein translation (Barr 2007). For this, phleboviruses employ the host transcriptional machinery by using free ribosomes for N and L segment translation, and endoplasmic reticulum (ER)-associated ribosomes for M segment translation (**Figure 4–4**; Amroun *et al.* 2017). From the M segment mRNA, viral glycoproteins are synthesized as a precursor protein from a single open reading frame (ORF), and co-translationally processed into G_N and G_C by the host protease signal peptidase (Spiegel *et al.* 2016). A signal peptide within the G_N sequence leads to protein insertion into the ER membrane, where cleavage by the signal peptidase as well as glycosylation occurs (Spiegel *et al.* 2016). Thus resulting non-covalently associated G_N/G_C dimers subsequently migrate to the Golgi apparatus (Spiegel *et al.* 2016).

In addition to G_N and G_C, the M segment also contains the NSm protein ORF upstream of G_N. From this ORF, NSm-G_N (P78), NSm (P14) and NSm' (P13) can be produced (Spiegel *et al.* 2016). NSm is a virulence factor that is not required for viral replication in mammalian cells. However, the RVFV P78 protein is necessary for replication in the mosquito vector (Spiegel *et al.* 2016).

Replication of the phleboviral genome in the host cell occurs as a two-step process. First, a full-length intermediate RNA product in positive sense orientation (cRNA) is synthesized by the viral polymerase, which in turn serves as template for viral genomic RNA (vRNA) generation (Ferron *et al.* 2017). The fact that the polymerase is required to recognize the same sequences in these cRNA and vRNA transcripts explains the crucial complementarity of 5' and 3' non-coding regions (Ferron *et al.* 2017). Newly generated vRNA is immediately encompassed by viral nucleoproteins to form RNPs (**Figure 4–5**; Ferron *et al.* 2017). These RNPs associate with the viral glycoproteins at the Golgi apparatus, which leads to virus budding into the Golgi (**Figure 4–6**; Spiegel *et al.* 2016). This association between viral nucleo- and glycoproteins accounts for the missing matrix protein in phleboviruses in that it gives stability to the virions (Amroun *et al.* 2017). Newly formed virions subsequently exit the host cell through the exocytotic pathway (**Figure 4–7**; Spiegel *et al.* 2016).

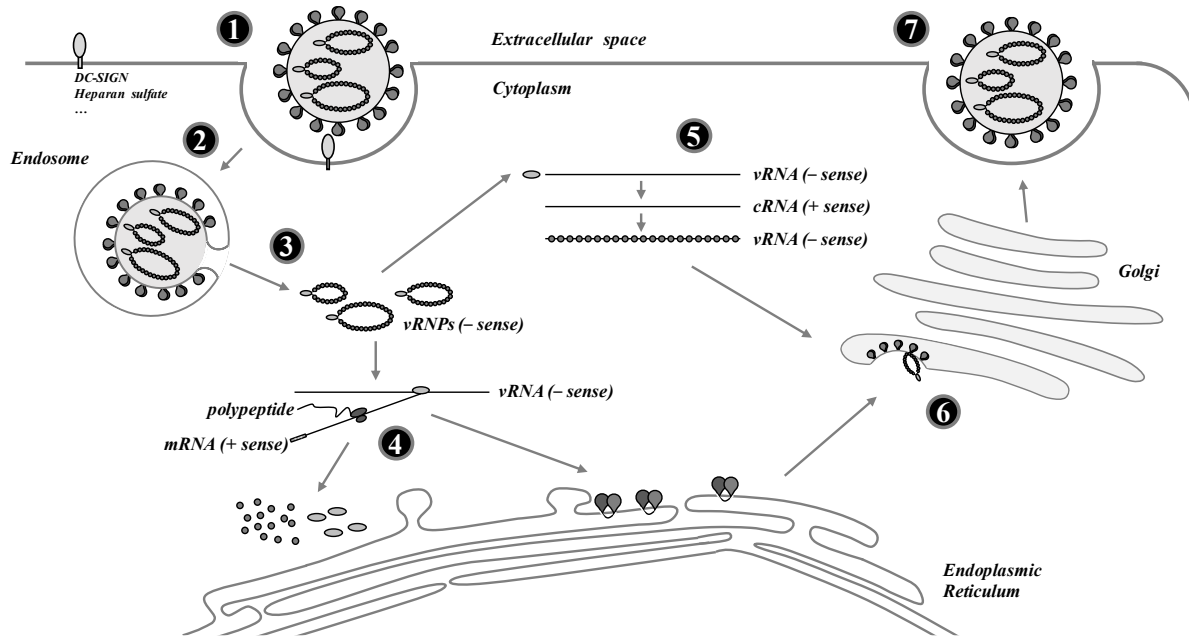


Figure 4: *Phlebovirus* replication cycle. Upon virus attachment to receptors on the cell surface (1), virions enter the cell via endocytosis (2). pH-dependent fusion of viral and endosomal membranes leads to vRNP release into the cytoplasm (3). Viral polymerase L transcribes negative-sense viral RNA into mRNA, which serves as template for protein synthesis at the host cellular ribosomal machinery (4). Replication of the viral genome involves the generation of positive-sense replication intermediates by the viral polymerase L, which serve as template for novel negative-sense vRNA genomes (5). Virion budding takes place into the Golgi apparatus (6) and newly formed virions are released through exocytosis (7). Adapted from Amroun *et al.* 2017 and Spiegel *et al.* 2016.

4.2.4 Sandfly-borne phleboviruses

Human actions and climate change result in an expanding vector territory, with an ever growing phlebovirus infection risk area (Esser *et al.* 2019; Ciota and Keyel 2019). Sandfly-borne phleboviruses are distributed on all continents and are divided into Old World and New World species. Virus transmission by different sandfly species dictates this strict discrimination (Alkan *et al.* 2017).

Old World sandfly-borne phleboviruses circulate in the Mediterranean, Africa, India, the Middle East, and Central Asia. Members of public health importance, which are endemic in the Mediterranean region, include for instance Sandfly fever Sicilian virus (SFSV), Sandfly fever Turkey virus (SFTV) and Toscana virus (TOSV) (Papa *et al.* 2011). The first two are associated with self-limiting febrile illness, while the latter exhibits a strong neurotropism which can manifest as meningitis and meningoencephalitis (Christova *et al.* 2020). Sandfly-transmitted phleboviruses in the New World include Punta Toro virus (PTV) as common cause of febrile illness in Panama (Palacios *et al.* 2015), as well as Candiru, Chilibre, and Frijoles viruses (Marklewitz *et al.* 2019).

Detection and isolation of novel phleboviruses occurs frequently but although in some cases seroprevalence studies confirm human infection, implications for human disease are mostly unknown. Over the past two decades, studies have persistently reported the identification, isolation, and human seropositivity of novel sandfly-borne phleboviruses in Portugal, Spain, France, Italy, Albania and Iran

(Charrel *et al.* 2009; Collao *et al.* 2010; Remoli *et al.* 2014; Amaro *et al.* 2015; Amaro *et al.* 2016; Alkan *et al.* 2017; Bino *et al.* 2019), Northern Africa (Zhioua *et al.* 2010; Bichaud *et al.* 2016), China (Wang *et al.* 2020a) and in Central and South America (Carvalho *et al.* 2018; Marklewitz *et al.* 2019). Less often can these novel viruses be associated with disease, owing to a short viremic period in phlebovirus infection, similar febrile symptoms and lacking molecular diagnostic methods (Anagnostou *et al.* 2011). Recently, a sandfly surveillance study conducted in Kenya in 2014 led to the detection and isolation of a previously unknown phlebovirus termed Ntepess virus (NTPV) (Tchouassi *et al.* 2019). Complete genome sequencing and phylogenetic analyses revealed NTPV as a member of the Karimabad species complex with its closest genetic relative being Gabek Forest virus (GFV). Seroprevalence studies determined 13.9% seropositivity of the Kenyan population at the site of sample collection as well as a remote site, thus confirming the potential of NTPV to infect humans (Tchouassi *et al.* 2019). However, no acute NTPV infection has been described to date and symptoms and disease spectrum caused by NTPV infections remain unknown.

A subsequent sandfly screening study conducted in the same area in Kenya in 2015/16 led to the discovery of four additional novel phleboviruses, termed Bogoria virus (BGRV), Embossos virus (EMBV), Perkerra virus (PERV) and Kiborgoch virus (KBGV) (Marklewitz *et al.* 2020). Complete genome sequencing and phylogenetic analyses showed the first three forming a monophyletic sister clade to the SFSV clade, whereas the latter was found to be related to TOSV (Marklewitz *et al.* 2020). Neither of these viruses could be successfully isolated. Notably, the re-discovery of NTPV in this follow-up study suggests a continuous circulation in Kenya (Marklewitz *et al.* 2020).

4.2.5 Antagonism of the innate immune response by phleboviruses

Pathogenic viruses can counteract the host innate immune system using manifold strategies to block IFN induction and signalling. In phleboviruses, the small non-structural protein termed NSs has been demonstrated for several species to exhibit anti-IFN characteristics and dictate pathogenicity (Eifan *et al.* 2013).

Highly pathogenic RVFV carries a multifunctional, early-acting NSs targeting several host pathways. It specifically blocks IFN- β gene transcription through stabilisation of a repressor complex on the IFN- β promoter, which inhibits histone acetyltransferase CBP recruitment, histone acetylation and therefore transcriptional activation (Le May *et al.* 2008). In addition, it later establishes a general block of host transcription, by sequestration of basal transcription factor TFIID subunit p44 and proteasomal degradation of TFIID subunit p62 (Le May *et al.* 2004; Kalveram *et al.* 2011; Kainulainen *et al.* 2014), and host translation, through an mRNA export block from the nucleus (Copeland *et al.* 2015). Furthermore, RVFV NSs mediates proteasomal degradation of antiviral PKR (Habjan *et al.* 2009b; Ikegami *et al.* 2009; Mudhasani *et al.* 2016). The natural RVFV variant clone 13 (C113) has a large in-frame deletion in its NSs gene and consequently expresses a truncated, non-functional NSs (Muller *et*

al. 1995). It is therefore profoundly attenuated and elicits an excellent type I IFN response in the host (Billecocq *et al.* 2004).

Intermediately virulent phleboviruses like SFSV, TOSV, or PTV express NSs proteins with certain anti-IFN characteristics, however unable to fully suppress the host innate immune response. SFSV NSs inhibits IFN- β gene transcription through obscuring the DNA-binding domain of IRF3 (Wuerth *et al.* 2018) and directly associates with translation initiation factor eIF2B to ensure ongoing viral protein synthesis in the presence of activated PKR (Wuerth *et al.* 2020). TOSV NSs was demonstrated to suppress IFN- β activation in overexpression experiments but not in an infection context (Gori Savellini *et al.* 2011; Brisbarre *et al.* 2013; Woelfl *et al.* 2020). Recently, however, it was demonstrated that TOSV NSs possesses E3 ubiquitin ligase activity and promotes the proteasomal degradation of RIG-I (Gori Savellini *et al.* 2019). The NSs of PTV Adames strain (PTV-A) inhibits IFN- β mRNA synthesis and was shown, like RVFV NSs, to induce a general host transcription block (Lihoradova *et al.* 2013; Wuerth *et al.* 2018). In contrast, the NSs protein of related PTV Balliet strain (PTV-B) has no effect on IFN- β activation (Perrone *et al.* 2007; Wuerth *et al.* 2018).

Strategies employed by NSs proteins of other phenuiviruses include, for instance, sequestration of key molecules for innate immune pathways to inclusion bodies by severe fever with thrombocytopenia syndrome virus (SFTSV), thereby inhibiting antiviral signalling (Wu *et al.* 2014; Ning *et al.* 2015; Hong *et al.* 2019; Min *et al.* 2020). The closely related Heartland virus employs a different strategy to block IFN induction, namely direct interaction with TBK1 to inhibit IRF3 activation (Ning *et al.* 2017).

Of note, not all NSs proteins function as potent IFN antagonists. For instance, non-pathogenic Uukuniemi virus (UUKV) expresses a functional NSs protein which acts as a considerably weak IFN antagonist, resulting in protective IFN upregulation upon UUKV infection (Rezelj *et al.* 2015; Rezelj *et al.* 2017). Thus, UUKV is unable to cause disease in humans.

4.3 Coronaviruses

4.3.1 Overview and classification

The *Coronaviridae* family lies within the order *Nidovirales*. It is further subcategorized into the subfamilies of *Letovirinae* and *Orthocoronavirinae*. The latter comprises the four genera alphacoronaviruses (alpha-CoVs), beta-CoVs, gamma-CoVs, and delta-CoVs (**Figure 5A**; Fung and Liu 2019; ICTV 2020). Alpha- and beta-CoVs solely infect mammals, while gamma- and delta-CoVs exhibit a broader host range. To date, seven human CoVs are known, causing respiratory and enteric diseases of varying severity. Human coronaviruses (HCoV) 229E, NL63 (alpha-CoVs), OC43, and HKU1 (beta-CoVs) are endemic in the human population and are associated with seasonal infections with “common cold” symptoms (Fehr and Perlman 2015; Fung and Liu 2019). In contrast, highly pathogenic severe acute respiratory syndrome CoV (SARS-CoV or SARS-CoV-1), Middle East respiratory syndrome CoV

(MERS-CoV) and the recently emerged SARS-CoV-2 can cause severe disease involving pneumonia and a variety of other symptoms that can be fatal (Fehr and Perlman 2015; V'kovski *et al.* 2021b, chapter 4.3.4).

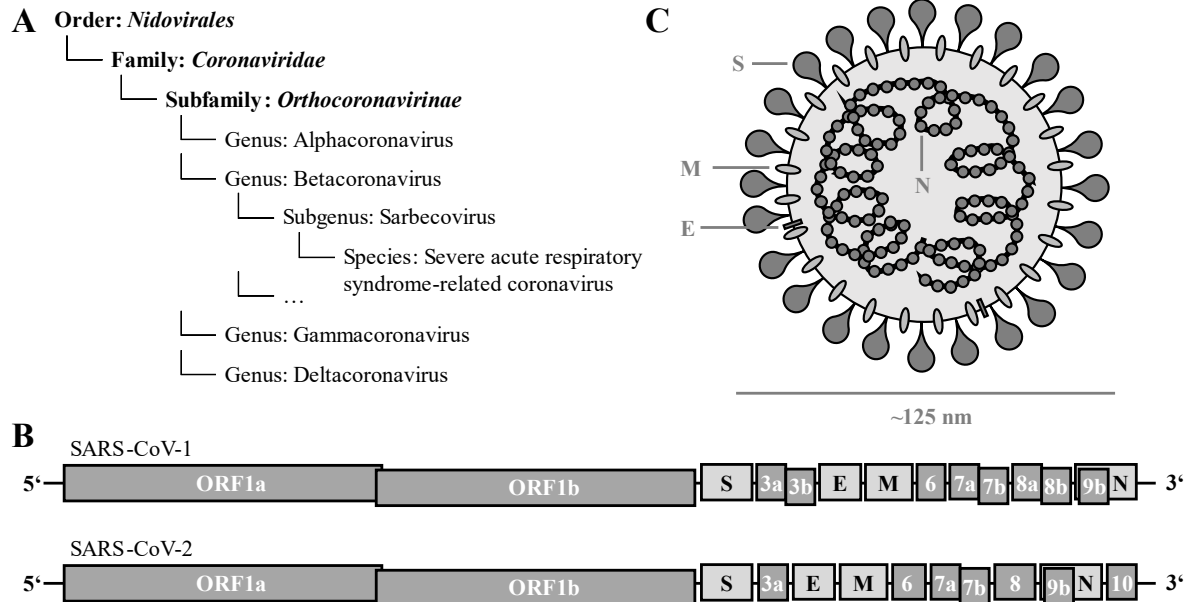


Figure 5: *Coronavirus taxonomy, genome organization, and virion.* (A) Taxonomy of coronaviruses within the *Nidovirales* order. (B) SARS-CoV-1 and SARS-CoV-2 genome organization. (C) Schematic representation of coronavirus virion. CoV, coronavirus; E, envelope protein; M, matrix protein; N, nucleoprotein; ORF, open reading frame; S, spike protein; SARS, severe acute respiratory syndrome. Adapted from V'kovski *et al.* 2021b.

4.3.2 Coronavirus genome organisation and morphology

CoVs carry a single-stranded RNA genome of positive polarity (ss(+)RNA). Spanning approx. 30 kb, it constitutes the largest known genome of all RNA viruses (**Figure 5B**). With a 5' cap structure and a 3' poly(A) tail, it resembles cellular messenger RNAs (mRNAs), allowing it to be directly translated by the host cell machinery. In addition, 5' and 3' untranslated regions confer important regulatory functions (Fehr and Perlman 2015). The 5' two thirds contain open reading frame (ORF) 1a and ORF1b, encoding for two polyproteins pp1a and pp1ab. These polyproteins are proteolytically cleaved by viral proteases PLpro and Mpro, resulting in the generation of 16 non-structural proteins with functions associated with viral replication. Further, on the 3' third of their genome, CoVs encode the four structural proteins S (spike protein), E (envelope protein), M (membrane protein), and N (nucleoprotein) as well as for a variable number of accessory proteins with various functions to combat the host immunity (chapter 4.3.4.2). The SARS-CoV-1 genome harbours eight ORFs coding for accessory proteins: 3a, 3b, 6, 7a, 7b, 8a, 8b and 9b (Fehr and Perlman 2015). The SARS-CoV-2 genome is still being investigated regarding protein-coding accessory ORFs. To date, five canonical ORFs, namely 3a, 6, 7a, 7b, and 8 are agreed upon. Downstream of the N gene there is an additional ORF named ORF10, however with questionable expression status (Finkel *et al.* 2021; Parker *et al.* 2021). Moreover, the SARS-CoV-2

genome possesses several non-canonical in-frame and out-of-frame ORFs, overlapping with canonical ORFs, with debatable expression profiles: an S gene-overlapping ORF2b, multiple ORF3a-overlapping ORFs termed 3c, 3d, 3d-2 and 3b, and two N gene-overlapping ORFs 9b and 9c (Jungreis *et al.* 2021; Finkel *et al.* 2021; Nelson *et al.* 2020). Ribosome profiling and subgenomic RNA sequencing studies postulate active translation of ORF3c, ORF3d, ORF3d-2, and ORF9b (Finkel *et al.* 2021; Nelson *et al.* 2020; Parker *et al.* 2021). CoV accessory genes often take up important functions in the natural host, but can be dispensable in laboratory cell culture (Forni *et al.* 2017).

CoV virions are spherical, enveloped particles of about 125 nm diameter (**Figure 5C**; Fehr and Perlman 2015). Inserted into the host-derived lipid bilayer membrane, they carry the S, E, and M proteins. The S protein is a heavily glycosylated homotrimeric class I fusion protein. Protruding from the virion body, it gives the CoV a crown-like appearance, hence the name coronavirus. The two S subunits mediate receptor-binding (S1) and membrane fusion (S2). The small M protein is the most abundant structural protein, giving the virus particle its shape. Lastly, the E protein is present in small amounts in the virus membrane and is involved in virion assembly and release (Fehr and Perlman 2015). Inside the virion lies the helically symmetrical nucleocapsid: the large ss(+)RNA genome coated by N proteins in a beads-on-a-string fashion (Fehr and Perlman 2015).

4.3.3 Coronavirus replication cycle

CoV attachment to the host cell is mediated by the receptor-binding domain (RBD) within the surface S protein (**Figure 6–1**). Different receptor usage has been reported for different CoVs, with angiotensin-converting enzyme 2 (ACE2) being employed by HCoV-NL63, SARS-CoV-1 and SARS-CoV-2, human aminopeptidase N (APN) by HCoV-229E, or dipeptidyl peptidase 4 (DPP4) by MERS-CoV (Perlman and Netland 2009; Hoffmann *et al.* 2020). Receptor tissue distribution and spike-receptor affinity thereby dictate coronavirus tropism. Prior to cell entry, acid-dependent proteolytic cleavage by host proteases like cell-surface serine protease Transmembrane protease serine 2 (TMPRSS2; SARS-CoV-1 and SARS-CoV-2) or endosomal cysteine proteases cathepsin B (CatB) or CatL (SARS-CoV-1) is needed to allow fusion of viral and cellular membranes. The first cleavage thereby separates the RBD from the fusion domain, the second exposes the fusion peptide within the fusion domain. Fusion can either take place directly with the cell membrane, or with endosomal membranes following receptor-mediated endocytosis (**Figure 6–2**; Fehr and Perlman 2015).

Since the genome structure of CoVs resembles that of cellular mRNA, after the release of the nucleocapsid into the cytoplasm (**Figure 6–3**) it can immediately be translated by the host machinery. First, the 5' ORFs 1a and 1b are translated into two polyproteins pp1a and pp1ab (**Figure 6–4**). Translation of the latter is the result of a programmed –1 ribosomal frameshift at the overlap of ORF1a and ORF1b (Perlman and Netland 2009). Viral proteases PLpro (papain-like protease, within nsp3) and Mpro (main protease, also referred to as 3C-like protease 3CLpro, within nsp5) co- and post-

translationally process pp1a and pp1ab polyproteins into 16 non-structural proteins (pp1a: nsp1 – 11, pp1ab: nsp1 – 10 and nsp12 – 16) (Fehr and Perlman 2015; V'kovski *et al.* 2021b). Fast proteolytic release of nsp1 and its host immune evasion capacities (chapter 4.3.4.2) facilitate viral translation. Nsp2 – 16 then assemble into the viral replicase-transcriptase complex (RTC; **Figure 6–5**), consisting of endoplasmic reticulum (ER)-derived double-membrane vesicles (DMVs), convoluted membranes and small double-membrane spherules. In this protective microenvironment, structurally supported by nsp2 – 11, viral genomic RNA replication and subgenomic RNA (sgRNA) transcription are mediated by nsp12 – 16 (Fehr and Perlman 2015; V'kovski *et al.* 2021b). Thereby, the nsp12 RNA-dependent RNA polymerase (RdRp) performs RNA synthesis, together with cofactors nsp7 and nsp8, whereas nsp13 – 16 assume RNA-modifying functions (V'kovski *et al.* 2021b): nsp14 harbours a 3'-5' exonuclease activity necessary for proofreading, RNA capping is mediated by 5' triphosphatase function of nsp13, and N7-methyltransferase and 2'-O-methyltransferase activities are conferred by nsp14 and nsp16, respectively. Nsp15 encodes an endonuclease, a feature unique to *Nidovirales*. Initially synthesized full-length negative-sense RNAs serve as templates for the production of new genomic RNAs (Fehr and Perlman 2015; V'kovski *et al.* 2021b). Additionally, a nested set of sgRNAs for the translation of structural and accessory proteins is produced by discontinuous transcription from negative-sense intermediates (**Figure 6–6**; Sola *et al.* 2015).

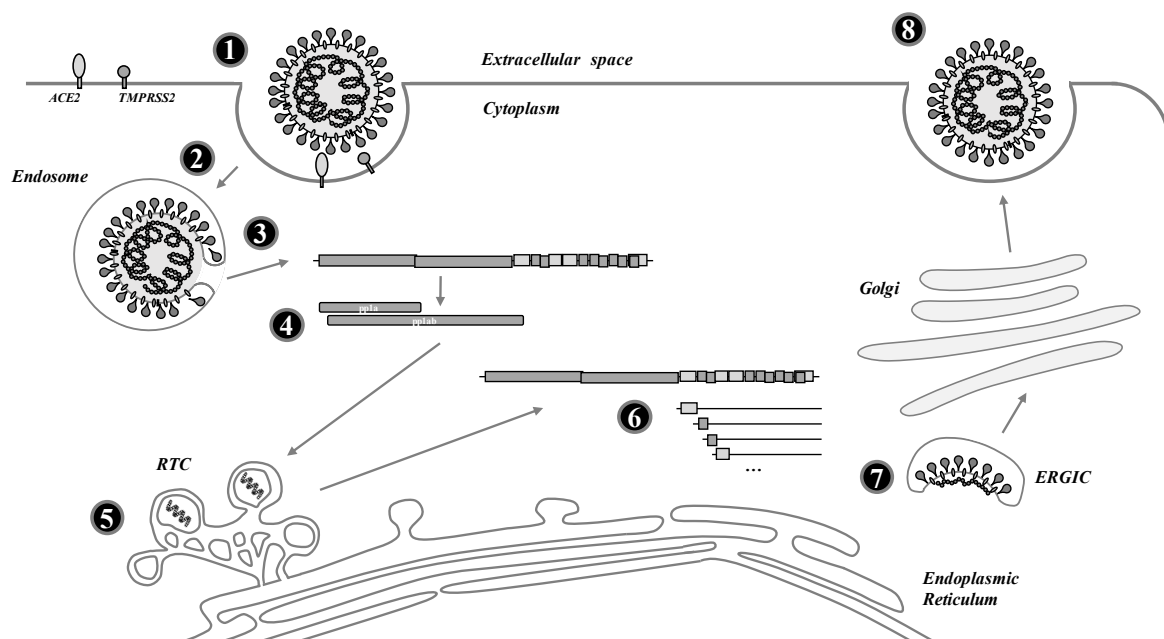


Figure 6: Coronavirus replication cycle. Upon virus attachment to cell surface receptors (1), virions enter the cell via endocytosis (2). pH-dependent fusion of viral and endosomal membranes leads to vRNP release into the cytoplasm (3). Viral pp1a and pp1ab ORFs are translated by the host cell machinery and processed by viral proteases into 16 nsps (4). Replication of the viral genome takes place in endoplasmic reticulum-associated RTCs (5). Translation of accessory proteins occurs through a nested set of subgenomic RNAs (6). Virion budding takes place into the ERGIC compartment (7) and newly formed virions are released through exocytosis (8). ACE2, angiotensin-converting enzyme 2; ERGIC, ER-Golgi intermediate compartment; nsp, non-structural protein; pp, polyprotein; RTC, replicase-transcriptase complex; TMPRSS2, Transmembrane protease serine 2. Adapted from V'kovski *et al.* 2021b.

Newly synthesised structural proteins are subsequently inserted into the ER. Budding of new virions takes place in the ER-Golgi intermediate compartment (ERGIC) by binding of N protein, which encompasses the newly synthesized genomic RNA, to the M protein (**Figure 6–7**). Mature virions transit through the exocytotic pathway until their release at the cell surface (**Figure 6–8**). Alternatively, it was recently postulated for mouse hepatitis virus (MHV) and SARS-CoV-2, as representatives of beta-CoVs, to exit the host cell via the lysosomal pathway (Ghosh *et al.* 2020). Of note, the CoV S protein can also migrate to the cell surface to mediate cell-cell fusion which allows for virus spread through syncytia formation (Fehr and Perlman 2015).

4.3.4 Highly pathogenic human coronaviruses

4.3.4.1 Epidemiology

SARS-CoV-1 emerged in 2002/2003 in Guangdong, China, and caused an outbreak with more than 8,000 infections and a fatality rate of approx. 10% (Zhong *et al.* 2003; Ksiazek *et al.* 2003; WHO 2003). Due to the virus mainly targeting the lower respiratory tract, resulting in a relatively poor human-to-human transmissibility, the SARS-CoV-1 outbreak was contained in 2003. SARS-CoV-1 likely originated from bats, where a large number of related viruses can be found, and was transferred to humans via civet cats (Corman *et al.* 2018). In 2012, another novel CoV, MERS-CoV, led to a series of severe respiratory infections in the Middle East. Since then, more than 2,500 human cases have been reported with a fatality rate of 36% (Zaki *et al.* 2012; V'kovski *et al.* 2021b). Like for SARS-CoV-1, a bat origin was found for MERS-CoV, and dromedary camels were identified as an intermediate host (Corman *et al.* 2018). The outbreak of SARS-CoV-2 in late 2019/early 2020 led to an ongoing, in modern times unprecedented, global pandemic (Zhu *et al.* 2020). SARS-CoV-2 infections can be asymptomatic or associated with mild disease; however, severe progression of the disease called COVID-19 (coronavirus disease 2019) with pronounced lung and other organ damage and potentially fatal immune activation also occurs (Harrison *et al.* 2020). At the time of writing, more than 222 million infections and approx. 4.5 million deaths have been reported (COVID-19 Dashboard, Johns Hopkins University, accessed on 08 September 2021).

Although SARS-CoV-2 and SARS-CoV-1 are closely related, their epidemiology and implications for global health are markedly different. While SARS-CoV-1 caused a relatively short epidemic with most patients experiencing severe symptoms with acute lung pathology, SARS-CoV-2 quickly spread to become a global pandemic that, at the time of writing, has been ongoing for 18 months and causes a wide symptomatic spectrum from asymptomatic to lethal (Huang *et al.* 2020). Both SARS coronaviruses use the same receptor and similar proteases for cell entry, however their receptor affinity and tissue infection ability differs (Chu *et al.* 2020; V'kovski *et al.* 2021b). This might explain the different tropism (upper respiratory tract for SARS-CoV-2 and lower respiratory tract for SARS-CoV-1) and the resulting different transmissibility. In addition, mutations in SARS coronavirus accessory proteins can account for the observed different pathogenicity (chapter 4.3.4.2).

4.3.4.2 SARS coronaviruses and the innate immune response

During the course of CoV infection, dsRNA replication intermediates are produced by the viral RdRp, that act as PAMPs for innate immune PRR sensors (Birra *et al.* 2020; see 4.1.2). Employment of particular sensors for these CoV dsRNA PAMPs has been shown to be cell-type dependent (Frieman *et al.* 2007a). Thereby, MDA5 acts as predominant RLR sensor for newly synthesized viral RNAs during CoV infection (Kasuga *et al.* 2021; Yin *et al.* 2021). In addition, RIG-I was recently reported to combat SARS-CoV-2 infection in an IFN signalling-independent manner, through binding to 3'UTRs of viral genomes and thereby inhibiting RdRp-dependent replication (Yamada *et al.* 2021). TLRs involved in SARS-CoV-1 sensing include TLR2, TLR3, TLR7 and TLR4, of which the first three have so far been shown to sense SARS-CoV-2 infection as well (Kasuga *et al.* 2021). Notably, aside from PRRs, CoV infection can also be sensed by other innate immune actors, like IFIT proteins (for SARS-CoV-1; Menachery *et al.* 2014) or PKR (for MERS-CoV; Rabouw *et al.* 2016). For SARS-CoV-2 infection, cell type-dependent activation of PKR and the OAS/RNaseL pathway has been reported (Li *et al.* 2021).

Although viral PAMPs are generated in the course of CoV infection, innate immune activation including type I and type III IFN production are often prevented or interrupted by viral evasion mechanisms directly targeting viral sensors or impeding downstream antiviral signalling (Kindler *et al.* 2016; Kasuga *et al.* 2021). SARS-CoV-1 induces little IFN in cell culture (Spiegel *et al.* 2005; Zielecki *et al.* 2013) and so far, SARS-CoV-2 IFN induction seems to be cell-type dependent (Wyler *et al.* 2021; Lowery *et al.* 2021). However, poor IFN induction has been observed in some COVID-19 patients (Cao *et al.* 2021).

Quickly after initial vRNA translation, nsp1 is proteolytically released from the pp1a/pp1ab polyproteins to fulfil several roles in the modulation of host cell pathways. It creates a favourable environment for virus replication through the inhibition of host cell protein synthesis by impeding mRNA nuclear export, inducing host mRNA degradation, and directly blocking host translation through binding to ribosomal subunits (Huang *et al.* 2011; Kindler *et al.* 2016; Thoms *et al.* 2020; Vazquez *et al.* 2021; Kasuga *et al.* 2021).

SARS coronaviruses further counteract the induction of IFN through a plethora of mechanisms. First, compartmentalisation of viral replication in DMVs and viral RNA association with the nucleoprotein N shield dsRNA PAMPs from exposure to host sensors (V'kovski *et al.* 2021b). Second, viral non-structural and accessory proteins directly inhibit innate immune signalling. For this, nsp3 can suppress IFN induction by binding the transcription factor IRF3 to prevent its phosphorylation, dimerization, and nuclear translocation (Devaraj *et al.* 2007). Further, nsp3 deubiquitination activity also impairs host IFN induction pathways. Interestingly, SARS-CoV-1 nsp3 mainly targets ubiquitin chains, while SARS-CoV-2 nsp3 processes ISGylated proteins (Klemm *et al.* 2020; Shin *et al.* 2020). PRR signalling is further hampered by SARS-CoV-2 nsp6 and nsp13 binding to TBK1 and proposed nsp8 binding to

the MDA5 CARD domains to impede its ubiquitination and subsequent signalling (Xia *et al.* 2020; Vazquez *et al.* 2021; Yang *et al.* 2020b). SARS-CoV-1 ORF3b is located at the outer mitochondrial membrane where it blocks the MAVS-mediated IFN induction pathways (Freundt *et al.* 2009). Importantly, SARS-CoV-2 expresses a considerably shorter 22 aa ORF3b protein and harbours three additional 3a-overlapping putative ORFs (ORF3c, ORF3d, ORF3d-2) within the ORF3a gene (Jungreis *et al.* 2021). Reports on SARS-CoV-2 ORF3b have been confounded by inconsistent terminology and interchangeable use of the name ORF3b for different transcripts. However, the truncated 22 aa protein has been shown to be a potent antagonist of type I IFN induction (Konno *et al.* 2020). SARS-CoV-1 ORF9b mediates the degradation of adapter molecules MAVS, TRAF3 and TRAF6 (Shi *et al.* 2014). A recent report attributes SARS-CoV-2 ORF9b with a different function, namely the binding to mitochondrial import receptor subunit TOM70, to block IFN induction (Jiang *et al.* 2020). For overexpressed SARS-CoV-2 ORF9c (former ORF14) an interaction with peroxisomal membrane protein PEX14 has been shown, potentially impacting matrix protein import and peroxisomal immune signalling (Knoblach *et al.* 2021) but the expression status of ORF9c during infection is still questionable (Nelson *et al.* 2020; Finkel *et al.* 2021). Finally, SARS coronavirus structural proteins N and M also possess anti-IFN induction capacities through interactions with various members of the PRR signalling cascades (Hu *et al.* 2017; Siu *et al.* 2014; Zheng *et al.* 2020b).

Moreover, SARS coronaviruses employ several vRNA modification strategies carried out by nsp13 – 16. For this, nsp13 mediates 5'ppp removal which could otherwise function as RIG-I ligand (Ivanov *et al.* 2004; Shu *et al.* 2020). Viral RNA capping, mediated by N7-methyltransferase activity of nsp14 and 2'O-methyltransferase activity of nsp16, is another mechanism by which CoVs prevent recognition (Chen *et al.* 2009; Chen *et al.* 2011; Krafcikova *et al.* 2020). In addition, the endonuclease activity of nsp15 suppresses dsRNA-activated early host responses by viral RNA 5'polyuridine cleavage (Kindler *et al.* 2017; Hackbart *et al.* 2020).

In addition to abrogating IFN induction, SARS coronaviruses also interfere with IFN signalling and ISG induction in multiple ways. For instance, the SARS-CoV-1 ORF3a protein mediates the degradation of the IFNAR1 IFN receptor chain (Minakshi *et al.* 2009). Further, although SARS-CoV-1 and SARS-CoV-2 ORF6 proteins show the highest amino acid sequence divergence (Lokugamage *et al.* 2020), both are potent IFN antagonists (Schroeder *et al.* 2021), thereby interfering with the host nuclear import and export machinery to block translocation of STAT proteins (Frieman *et al.* 2007b; Kopecky-Bromberg *et al.* 2007; Xia *et al.* 2020; Miorin *et al.* 2020). Phosphorylation and nuclear translocation of STAT1 and STAT2 has further been shown to be counteracted by the multifunctional nsp1, by nsp6 and by SARS-CoV-2 N protein (Wathelet *et al.* 2007; Mu *et al.* 2020; Xia *et al.* 2020). Nonetheless, despite these IFN antagonistic functions, both SARS-CoV-1 and SARS-CoV-2 are sensitive to exogenous IFN, with SARS-CoV-2 displaying a greater sensitivity (Zielecki *et al.* 2013; Felgenhauer *et al.* 2020).

Lastly, SARS coronaviruses are also known to directly antagonize host antiviral functions. For instance, ORF7a associates with Tetherin to block its activity (Taylor *et al.* 2015). Further, while SARS-CoV-1 infection leads to the activation of PKR, it is insensitive to its antiviral action (Krähling *et al.* 2009).

Overall, highly pathogenic SARS coronaviruses interfere with the host antiviral innate immune response in a multitude of ways, targeting almost all steps of IFN induction and signalling.

Nonetheless, dysregulated or overshooting immune responses also contribute to SARS coronavirus pathology. Thereby, immune responses mainly display an exuberant predominantly pro-inflammatory signature, termed hypercytokinemia or “cytokine storm” (Kasuga *et al.* 2021). In that, overexpression of pro-inflammatory cytokines and chemokines, such as TNF- α , IL-1, IL-6, IL-12, CXCL10 or also type I and type II IFNs, may lead to pathophysiological changes that can result in fatal multi-organ failure (Fajgenbaum and June 2020).

4.4 Objective of this work

The innate immune system acts as the host's first-line defence against intruding pathogens. It is governed by interferons (IFNs), of which mainly type I (IFN- α/β) and type III (IFN- λ) orchestrate the antiviral response. They are secreted upon the cellular recognition of pathogen-associated molecular patterns by pattern recognition receptors. IFNs induce an antiviral state in the host cells, combating infection and preventing its spread. Consequently, pathogenic viruses have evolved manifold strategies to counteract the innate immune response. The inhibition of IFN induction poses an efficient way to antagonize host cell responses, as this prevents both the establishment of an antiviral state in the surrounding cells and the attraction of immune cells. The interplay between the virus and the host cell's innate immune response, *i.e.* the quality and strength of IFN evasion, can be an important determinant of virulence. Therefore, the objective of this work was to describe this so-called innate immunity phenotype of newly emerging viruses with zoonotic potential.

Molecular characterizations of the viral innate immunity phenotype can provide insights into a virus' implications for human health, with more pathogenic viruses usually exhibiting more efficient and more variable ways to antagonize the IFN system. Therefore, two novel viruses were characterized to this regard in the course of this work. For this, on the one hand the recently isolated phlebovirus Ntepes virus (NTPV) was chosen. Although having been shown to be able to infect humans, NTPV's disease potential in humans is currently unknown. On the other hand, the novel coronavirus severe acute respiratory syndrome coronavirus 2 (SARS-CoV-2) was selected. Being the causative agent of the current devastating coronavirus disease 2019 (COVID-19) lung disease pandemic, SARS-CoV-2 is of nearly unprecedented interest concerning global human health. Gaining new insights into novel viruses' interactions with the innate immune system can help to better understand and with this combat human infection with these viruses.

5 Materials

5.1 Viruses

Table 1: Viruses used in this work

Abbreviation	Virus	Description, Origin	Reference
GFV	Gabek Forest virus	Gabek Forest virus strain Sud AN 754-61, from Sandra Junglen, Charité Berlin	Kemp <i>et al.</i> 1974
NTPV	Ntepes virus	Ntepes Virus strain MRG54-KE-2014, from Sandra Junglen, Charité Berlin	Tchouassi <i>et al.</i> 2019
RVFV clone 13	Rift Valley fever virus	Rift Valley Fever virus strain clone 13, NSs-deficient attenuated isolate	Muller <i>et al.</i> 1995
RVFV MP-12	Rift Valley fever virus	Rift Valley Fever virus strain MP-12, artificially attenuated vaccine strain	Caplen <i>et al.</i> 1985
RVFV-delNSs::Renilla	Rift Valley fever virus	recombinant Rift Valley Fever virus strain ZH548 with NSs gene replaced by <i>Renilla</i> luciferase ORF; from Matthias Habjan (formerly University of Freiburg)	Kuri <i>et al.</i> 2010
SARS-CoV-1	Severe acute respiratory syndrome coronavirus 1	SARS-CoV-1 patient isolate Frankfurt strain, from Christian Drosten, Charité Berlin	AY310120
SARS-CoV-2	Severe acute respiratory syndrome coronavirus 2	SARS-CoV-2 patient isolate 984, BetaCoV/Munich/BavPat1/2020, from Christian Drosten, Charité Berlin	EPI_ISL_406862

5.2 Eukaryotic cells

Table 2: Eukaryotic cell lines used in this work

Name	Organism	Type and origin	Reference
A549	<i>Homo sapiens</i> , human	lung, adenocarcinomic alveolar basal epithelial cell line	Wuerth <i>et al.</i> 2020
A549-ACE2	<i>Homo sapiens</i> , human	lung, <i>see above</i> ; transduced with lentivirus for stable expression of human angiotensin converting enzyme 2 (ACE2)	Chapter 6.1.5
BHK	<i>Mesocricetus auratus</i> , hamster	kidney, fibroblast cell line	Habjan <i>et al.</i> 2008b
Caco-2	<i>Homo sapiens</i> , human	colon, colorectal adenocarcinomic epithelial cell line	Eric Miska, The Gurdon Institute, University of Cambridge
Calu-3	<i>Homo sapiens</i> , human	lung, adenocarcinomic epithelial cell line derived from pleural effusion	Felgenhauer <i>et al.</i> 2020
H1299	<i>Homo sapiens</i> , human	lung, non-small cell lung carcinoma epithelial cell line derived from lymph node	Wyler <i>et al.</i> 2021
HEK293	<i>Homo sapiens</i> , human	kidney, embryonic cell line	Wuerth <i>et al.</i> 2020
HeLa	<i>Homo sapiens</i> , human	cervix, cervical cancer epithelial cell line	Lau and Weber 2020
Huh7	<i>Homo sapiens</i> , human	liver, hepatocyte-derived carcinoma cell line	Schoen <i>et al.</i> 2020
Vero E6	<i>Cercopithecus aethiops</i> , African green monkey	kidney, epithelial cell line	Felgenhauer <i>et al.</i> 2020
Vero 76	<i>Cercopithecus aethiops</i> , African green monkey	kidney, epithelial cell line	Stephan Becker, Institute of Virology, Philipps University of Marburg

5.3 Prokaryotic cells

Table 3: Prokaryotic cells used in this work

Name	Organism	Genotype	Origin
DH10B	<i>Escherichia coli</i> , bacterium	F- mcrA Δ (mrr-hsdRMS-mcrBC) ϕ 80lacZ Δ M15 Δ lacX74 recA1 endA1 araD139 Δ (ara-leu)7697 galU galK λ - rpsL(StrR) nupG	Thermo Fisher Scientific, Schwerte
TOP10	<i>Escherichia coli</i> , bacterium	F- mcrA (mrr-hsdRMS-mcrBC) 80lacZM15 lacX74 recA1 ara139 (ara-leu)7697 galU galK rpsL (StrR) endA1 nupG>	Thermo Fisher Scientific, Schwerte
Stellar Competent Cells	<i>Escherichia coli</i> , bacterium	F-, endA1, supE44, thi-1, recA1, relA1, gyrA96, phoA, Φ 80d lacZ Δ M15, Δ (lacZYA-argF) U169, Δ (mrr-hsdRMS-mcrBC), Δ mcrA, λ -	Takara, Saint-Germain-en-Laye, France

5.4 Cell culture and transfection reagents

Table 4: Cell culture reagents for eukaryotic cells

Name	Supplier
CCM34	Viro Vet Diagnostik GmbH, Giessen Dulbecco's modified Eagle's medium (DMEM) + 17.8 mg/l L-alanine + 0.7 g/l glycine + 75 mg/l L-glutamic acid +25 mg/l L-proline + 0.1 mg/l biotin + 25 mg/l hypoxanthine + 3.7 g/l sodium bicarbonate
Cell culture medium (CCM34+10% FBS+1X P/S/Q)	CCM34 + 10% FBS + 1% penicillin-streptomycin (P/S) + 1% L-glutamine (Q)
DMEM (Dulbeccos's modified Eagle medium)	Gibco, Thermo Fisher Scientific, Schwerte
DMEM, low glucose, pyruvate	Gibco, Thermo Fisher Scientific, Schwerte
FBS (Fetal Bovine Serum)	BioChrom GmbH, Berlin
2X MEM (Temin's modification), no phenol red	Gibco, Thermo Fisher Scientific, Schwerte
OptiMEM	Gibco, Thermo Fisher Scientific, Schwerte
OptiPRO	Gibco, Thermo Fisher Scientific, Schwerte
Penicillin-Streptomycin-Glutamine (P/S/Q; 100X)	Gibco, Thermo Fisher Scientific, Schwerte
Puromycin	Sigma-Aldrich, Steinheim
2X Trypan blue (0.4% Trypan blue in H ₂ O, sterile filtered)	Merck, Darmstadt
0.05% Trypsin-EDTA (1X), phenol red	Gibco, Thermo Fisher Scientific, Schwerte
Trypsin-EDTA-Solution, pH 7.4	Viro Vet Diagnostik GmbH, Giessen

Table 5: Transfection reagents for eukaryotic cells

Name	Supplier
EndoFectin™ Max	Genecopoeia, Rockville, MD, U.S.A.
TransIT@-LT1	Mirus Bio LLC, Madison, WI, U.S.A.

Table 6: Cytokines and inhibitors

Name	Supplier/Reference
Recombinant pan-species IFN- α (B/D)	PBL Assay Science, Piscataway, NJ, U.S.A.
Recombinant human TNF- α protein (Active)	Abcam, Berlin
Recombinant IFN- λ 3	Provided by Rune Hartmann, Aarhus University, Denmark (Dellgren <i>et al.</i> 2009)
Ruxolitinib	Selleckchem, Munich

Table 7: Media and solutions for prokaryotic cells

Name	Composition	Supplier
LB agar	1.5% agar agar in LB medium	Roth, Karlsruhe
LB medium	10% tryptone/peptone 5% yeast extract 0.5% NaCl, pH 7.0 in ddH ₂ O	Roth, Karlsruhe Roth, Karlsruhe Sigma-Aldrich, Steinheim
SOC medium	0.5% yeast extract 2% tryptone/peptone 10 mM NaCl 2.5 mM KCl 10 mM MgCl ₂ 10 mM MgSO ₄ 20 mM glucose in ddH ₂ O	Roth, Karlsruhe Roth, Karlsruhe Sigma-Aldrich, Steinheim Roth, Karlsruhe Fluka, Seelze Fluka, Seelze Fluka, Seelze

5.5 Buffers and solutions

Table 8: Buffers and reagents for SDS PAGE

Name	Composition	Supplier
SDS running buffer	25 mM tris 192 mM glycine 0.1% SDS in ddH ₂ O	Roth, Karlsruhe Roth, Karlsruhe Roth, Karlsruhe
10% APS	10% APS in H ₂ O	Sigma-Aldrich, Steinheim
10% SDS	10% SDS in H ₂ O	Roth, Karlsruhe
4X SDS sample buffer	114 mM tris-HCl, pH 6.8 4.6% SDS 23% glycerol 20% β -mercaptoethanol 3.4 mM bromophenol blue in ddH ₂ O	Roth, Karlsruhe Roth, Karlsruhe Roth, Karlsruhe Sigma-Aldrich, Steinheim Sigma-Aldrich, Steinheim
Color Prestained Protein Standard, Broad Range (11–245 kDa)	<i>n.a.</i>	Cell Signaling Technology, Frankfurt a.M.
Rotiphorese® PAGE Matrixpuffer plus	<i>n.a.</i>	Roth, Karlsruhe

Table 9: Buffers for Western blot

Name	Composition	Supplier
10X Tris buffered saline (TBS)	200 mM tris, pH 7.6 1.37 M NaCl in ddH ₂ O	Roth, Karlsruhe Sigma-Aldrich, Steinheim
Blocking buffer (BSA)	5% bovine serum albumin (BSA) in 1X TBS-T	Sigma-Aldrich, Steinheim

Blocking buffer (milk)	10% milk powder in 1X TBS	dm Drogeriemarkt, Giessen
Harsh stripping buffer	62.5 mM tris-HCl, pH 6.7 2% SDS 100 mM β -mercaptoethanol in ddH ₂ O	Roth, Karlsruhe Roth, Karlsruhe Sigma-Aldrich, Steinheim
Mild stripping buffer	200 mM glycine 0.1% SDS 1% Tween20 in ddH ₂ O, pH 2.2	Roth, Karlsruhe Roth, Karlsruhe Serva Electrophoresis GmbH, Heidelberg
Transfer buffer (for semidry blotting)	48 mM tris 39 mM glycine 1.3 mM SDS 20% methanol in ddH ₂ O	Roth, Karlsruhe Roth, Karlsruhe Roth, Karlsruhe Roth, Karlsruhe
Wash buffer (TBS-T)	0.1% Tween20 in 1X TBS	Serva Electrophoresis GmbH, Heidelberg

Table 10: Lysis buffers

Name	Composition	Supplier
PXL lysis buffer	1% NP-40 (Igepal®) 0.5% DOC 0.1% SDS in 1X PBS _{def}	Sigma-Aldrich, Steinheim Fluka, Seelze Roth, Karlsruhe

Table 11: Buffers and solutions for immunofluorescence (IF)

Name	Composition	Supplier
IF blocking buffer	2% BSA 5% glycerol 0.2% Tween20 in 1X PBS _{def}	Sigma-Aldrich, Steinheim Roth, Karlsruhe Serva Electrophoresis GmbH, Heidelberg
IF fixation solution	4% PFA in 1X PBS _{def}	Roth, Karlsruhe
IF permeabilization buffer	0.5% Triton-X 100 in 1X PBS _{def}	Sigma-Aldrich, Steinheim

Table 12: Buffers and reagents for agarose gel electrophoresis

Name	Composition	Supplier
1X TAE buffer	40 mM tris 20 mM glacial acetic acid 1 mM EDTA in ddH ₂ O	Roth, Karlsruhe Roth, Karlsruhe Roth, Karlsruhe
Orange DNA Loading Dye (6X)	<i>n.a.</i>	Thermo Fisher Scientific, Schwerte
O'GeneRuler™ 1 kb Plus DNA Ladder, ready-to-use	<i>n.a.</i>	Thermo Fisher Scientific, Schwerte

Table 13: Additional buffers and solutions

Name	Composition	Supplier
Crystal violet staining solution	0.75% crystal violet 3.75% formaldehyde 20% ethanol, absolute 1% methanol in ddH ₂ O	Sigma-Aldrich, Steinheim Roth, Karlsruhe Roth, Karlsruhe Roth, Karlsruhe
1X Phosphate buffered saline (PBS _{def})	137 mM NaCl 2,7 mM KCl 10 mM NaHPO ₄ 1,76 mM KH ₂ PO ₄ in ddH ₂ O, pH 7.4	Sigma-Aldrich, Steinheim Roth, Karlsruhe Merck, Darmstadt Merck, Darmstadt

TE buffer	10 mM tris-HCl, pH 8.0 1 mM EDTA in ddH ₂ O	Roth, Karlsruhe Roth, Karlsruhe
-----------	--	------------------------------------

5.6 PCR reagents

Table 14: Polymerases

Product Name	Supplier
JumpStart™ Taq DNA Polymerase with MgCl ₂	Sigma-Aldrich, Steinheim
KOD Hot Start DNA Polymerase	Merck, Darmstadt
Phusion® High-Fidelity DNA Polymerase	New England Biolabs, Frankfurt a.M.

Table 15: Restriction Enzymes

Product Name	Supplier
BamHI-HF	New England Biolabs, Frankfurt a.M.
DpnI	New England Biolabs, Frankfurt a.M.
KpnI-HF	New England Biolabs, Frankfurt a.M.
XhoI	New England Biolabs, Frankfurt a.M.

Table 16: Other PCR reagents

Product Name	Supplier
Deoxynucleotide (dNTP) Solution Mix, 10mM each	New England Biolabs, Frankfurt a.M.
CutSmart Buffer	New England Biolabs, Frankfurt a.M.

5.7 Antibodies and Fluorescence Dyes

Table 17: Primary antibodies for Western blotting

#*	Target	Species	Specificity	Supplier	Dilution
38	FLAG™ tag	mouse	monoclonal	Sigma-Aldrich, Steinheim	1:1,000
99	IFIT1	rabbit	monoclonal	Georg Kochs, Institute of Virology, Freiburg	1:1,000
324	ISG15 (F-9)	mouse	monoclonal	Santa Cruz Biotechnology, Heidelberg	1:4,000
398	MxA	mouse	monoclonal	Sigma-Aldrich, Steinheim	1:1,000
394	phospho-STAT1	rabbit	monoclonal	Cell Signaling, Frankfurt a.M.	1:1,000
396	phospho-STAT2	rabbit	monoclonal	Cell Signaling, Frankfurt a.M.	1:1,000
315	RVFV-N	mouse	monoclonal	Alejandro Brun, Instituto Nacional de Investigación y Tecnología Agraria y Alimentaria, Madrid, Spain	1:1,000
427	SARS-CoV-N	rabbit	polyclonal	Biomol, Hamburg	1:2,000
395	STAT1	mouse	monoclonal	BD Biosciences, San Jose, CA, U.S.A.	1:1,000
397	STAT-2	mouse	monoclonal	BD Biosciences, San Jose, CA, U.S.A.	1:1,000
12	β-Tubulin	rabbit	polyclonal	Abcam, Berlin	1:1,000

Table 18: Secondary antibodies for Western blotting

#*	Name	Species	Specificity	Supplier	Dilution
3	Peroxidase-conjugated goat anti-mouse IgG	goat	polyclonal	Thermo Fisher Scientific, Schwerte	1:20,000
4	Peroxidase-conjugated goat anti-rabbit IgG	goat	polyclonal	Thermo Fisher Scientific, Schwerte	1:20,000

Table 19: Antibodies for immunofluorescence microscopy

#*	Target	Species	Specificity	Supplier	Dilution
7	Alexa Fluor 555 donkey anti-mouse IgG	donkey	polyclonal	Invitrogen, Thermo Fisher Scientific, Schwerte	1:200
38	FLAG TM tag	mouse	monoclonal	Sigma-Aldrich, Steinheim	1:500

*(Laboratory collection number)

5.8 Plasmids

Table 20: Expression plasmids for viral NSs proteins

#*	Name	Description	Accession No.	Source
1235	pI.18-NTPV_NSs	AmpR. Untagged Ntepes virus (NTPV) NSs (amplified with primers #1217 and #1219 from plasmid #1199) cloned into pI.18 backbone (#291) with <i>BamHI/XhoI</i>		this work
1199	pI.18-3×FLAG_NTPV_NSs	AmpR. Ntepes virus (NTPV) NSs with N-terminal 3×FLAG tag (amplified with primers #1218 and #1219 from NTPV cDNA) cloned into pI.18 backbone (#291) with <i>BamHI/XhoI</i>	MF695811.1 with ntT384C (silent)	created by Besim Berisha/Jennifer Wuerth
1290	pI.18_NTPV_NSs-3×FLAG	AmpR. Ntepes virus (NTPV) NSs with C-terminal 3×FLAG tag (amplified with primers #1217 and #1360 from plasmid #1199) cloned into pI.18 backbone (#291) with <i>BamHI/XhoI</i>		this work
1287	pI.18-GFV-NSs	AmpR. Untagged Gabek Forest virus (GFV) NSs (amplified with primers #1345 and #1347 from GFV cDNA) cloned into pI.18 backbone (#291) with <i>BamHI/XhoI</i>	KF297905.1	this work
1288	pI.18-3×FLAG-GFV-NSs	AmpR. Gabek Forest virus (GFV) NSs with N-terminal 3×FLAG tag (amplified with primers #1346 and #1347 from GFV cDNA) cloned into pI.18 backbone (#291) with <i>BamHI/XhoI</i>	KF297905.1 with ntA678G (silent)	this work
1289	pI.18-GFV-NSs-3×FLAG	AmpR. Gabek Forest virus (GFV) NSs with C-terminal 3×FLAG tag (amplified with primers #1345 and #1361 from GFV cDNA) cloned into pI.18 backbone (#291) with <i>BamHI/XhoI</i>	KF297905.1	this work
1263	pI.18-EMBV_NSs	AmpR. Untagged Embossos virus (EMBV) NSs (amplified with primers #1380 and #1364 from EMBV cDNA), cloned into pI.18 backbone (#291) with <i>KpnI/XhoI</i>		this work
1264	pI.18-3×FLAG_EMBV_NSs	AmpR. Embossos virus (EMBV) NSs with N-terminal 3×FLAG tag (amplified with primers #1381 and #1364 from EMBV cDNA) cloned into pI.18 backbone (#291) with <i>KpnI/XhoI</i>	MT270827.1	this work
1265	pI.18-EMBV_NSs-3×FLAG	AmpR. Embossos virus (EMBV) NSs with C-terminal 3×FLAG tag (amplified with primers #1380 and #1365 from EMBV cDNA) cloned into pI.18 backbone (#291) with <i>KpnI/XhoI</i>		this work
1266	pI.18-BGRV_NSs	AmpR. Untagged Bogoria virus (BGRV) NSs (amplified with primers #1366 and #1368 from BGRV cDNA), cloned into pI.18 backbone (#291) with <i>BamHI/XhoI</i>		this work
1267	pI.18-3×FLAG_BGRV_NSs	AmpR. Bogoria virus (BGRV) NSs with N-terminal 3×FLAG tag (amplified with primers #1367 and #1368 from BGRV cDNA), cloned into pI.18 backbone (#291) with <i>BamHI/XhoI</i>	MT270830.1	this work
1268	pI.18-BGRV_NSs-3×FLAG	AmpR. Bogoria virus (BGRV) NSs with C-terminal 3×FLAG tag (amplified with primers #1366 and #1369 from BGRV cDNA), cloned into pI.18 backbone (#291) with <i>BamHI/XhoI</i>		this work
1269	pI.18-KBGV_NSs	AmpR. Untagged Kiborgoch virus (KBGV) NSs (amplified with primers #1370 and #1372 from KBGV cDNA), cloned into pI.18 backbone (#291) with <i>BamHI/XhoI</i>	MT270833.1	this work

1270	pI.18-3×FLAG_KBGV_NSs	AmpR. Kiborgoch virus (KBGV) NSs with N-terminal 3×FLAG tag (amplified with primers #1371 and #1372 from KBGV cDNA), cloned into pI.18 backbone (#291) with <i>BamHI/XhoI</i>		this work
1271	pI.18-KBGV_NSs-3×FLAG	AmpR. Kiborgoch virus (KBGV) NSs with C-terminal 3×FLAG tag (amplified with primers #1370 and #1373 from KBGV cDNA), cloned into pI.18 backbone (#291) with <i>BamHI/XhoI</i>		this work
1272	pI.18-PERV.1_NSs	AmpR. Untagged Perkerra virus (PERV; ORF1 = longest ORF with CTG changed to ATG) NSs (amplified with primers #1374 and #1378 from PERV cDNA), cloned into pI.18 backbone (#291) with <i>BamHI/XhoI</i>		this work
1273	pI.18-3×FLAG_PERV.1_NSs	AmpR. Perkerra virus (PERV; ORF1 = longest ORF with CTG changed to ATG) NSs with N-terminal 3×FLAG tag (amplified with primers #1375 and #1378 from PERV cDNA), cloned into pI.18 backbone (#291) with <i>BamHI/XhoI</i>		this work
1274	pI.18-PERV.1_NSs-3×FLAG	AmpR. Perkerra virus (PERV; ORF1 = longest ORF with CTG changed to ATG) NSs with C-terminal 3×FLAG tag (amplified with primers #1374 and #1379 from PERV cDNA), cloned into pI.18 backbone (#291) with <i>BamHI/XhoI</i>	MT270836.1	this work
1275	pI.18-PERV.2_NSs	AmpR. Untagged Perkerra virus (PERV; ORF2 = starting from ATG at position 13) NSs (amplified with primers #1376 and #1378 from PERV cDNA), cloned into pI.18 backbone (#291) with <i>BamHI/XhoI</i>		this work
1276	pI.18-3×FLAG_PERV.2_NSs	AmpR. Perkerra virus (PERV; ORF2 = starting from ATG at position 13) NSs with N-terminal 3×FLAG tag (amplified with primers #1377 and #1378 from PERV cDNA), cloned into pI.18 backbone (#291) with <i>BamHI/XhoI</i>		this work
1277	pI.18-PERV.2_NSs-3×FLAG	AmpR. Perkerra virus (PERV; ORF2 = starting from ATG at position 13) NSs with C-terminal 3×FLAG tag (amplified with primers #1376 and #1379 from PERV cDNA), cloned into pI.18 backbone (#291) with <i>BamHI/XhoI</i>		this work
556	pI.18-RVSV_NSs-3×FLAG	AmpR. RVSV NSs (strain ZH-548) with C-terminal 3×FLAG tag (amplified with primers #166 [RVSV primer] and #166 [common primer] from plasmid #468), cloned into pI.18 backbone (#291) with <i>BamHI/XhoI</i>	DQ380151.1	created by Simone Lau
1137	pI.18-NSsSFSV-3×FLAG	AmpR, contains SFSV NSs with C-terminal 3×FLAG tag between <i>BamHI</i> and <i>XhoI</i> restriction sites; generated from plasmid #665 via excision of additional 3XFLAG via <i>PvuI</i> and <i>BamHI</i> followed by recircularization via rapid ligation kit	EF201822.1	created by Jennifer Wuerth
913	pI.18-3×FLAG-NSsPTV-A	AmpR, contains PTV-A NSs with N-terminal 3×FLAG tag between <i>BamHI</i> and <i>XhoI</i> restriction sites; insert excised from plasmid #244 via <i>BamHI</i> and <i>XhoI</i> and ligated pI.18 backbone (#291).	EF201835.1	created by Jennifer Wuerth
914	pI.18-3×FLAG-NSsPTV-B	AmpR, contains PTV-B NSs with N-terminal 3×FLAG tag between <i>BamHI</i> and <i>XhoI</i> restriction sites; insert excised from plasmid #245 via <i>BamHI</i> and <i>XhoI</i> and ligated into pI.18 backbone (#291)	KR912211.1	created by Jennifer Wuerth

Table 21: Expression plasmids for luciferase reporter assays

#*	Name	Description	Reference
43	p125-Luc	AmpR, firefly luciferase under control of the IFN- β promoter	Yoneyama <i>et al.</i> 1998
78	pGL3-MX1P	AmpR, firefly luciferase under control of the Mx1 promoter	Hug <i>et al.</i> 1988; Jorns <i>et al.</i> 2006
77	ISG54-Luc	AmpR, firefly luciferase under control of the ISG54 promoter. wt TATA box (TATATA)	Paulson <i>et al.</i> 2002

678	kB-Luc	AmpR, firefly luciferase under control of an NF- κ B-responsive promoter	Rodrigo <i>et al.</i> 2012
48	pRL-SV40	AmpR, constitutively expressing <i>Renilla</i> luciferase	commercial (Promega)
291	pI.18	AmpR, eukaryotic expression vector, contains CMV-promoter-intron A from CMV-MCS-pA	Verbruggen <i>et al.</i> 2011
664	pI.18-3 \times FLAG - Δ Mx	AmpR, codes for 3 \times FLAG -tagged Δ Mx ORF (5' <i>Bam</i> HI – 3 \times FLAG – Δ Mx ORF – 3' <i>Xho</i> I)	created by Jennifer Wuerth
219	pI.18 3 \times FLAG - Δ Mx	AmpR, codes for 3 \times FLAG -tagged Δ Mx ORF (3 \times FLAG – 5' <i>Bam</i> HI – Δ Mx ORF – 3' <i>Xho</i> I)	created by Andreas Schön
815	pCDNA3.1-TOPO-RIG-I CARD	AmpR, N terminus (aa 1 to 284 = CARD domain) of human RIG-I. Cloned by amplifying human cDNA with primers # 464 and #466	created by Valentina Wagner
936	pFLAG-CMV2-huIPS-1 FL	AmpR, contains the human MAVS full-length gene with an N-terminal 3 \times FLAG tag and CMV promoter control	Kawai <i>et al.</i> 2005
1082	pCDNA3.1(-) flag-tag TBK1	AmpR, expresses human TBK1 with an N-terminal 1 \times FLAG tag	Sharma <i>et al.</i> 2003
934	IRF3(5D-97A)-CMV	AmpR, subcloned from #844 (insert) and #866 (backbone) via <i>Eco</i> RV and <i>Not</i> I restriction sites; contains IRF3 phosphomimetic (5D) and phosphodeficient (97A) mutant, i.e. autophosphorylated IRF3 that translocates to the nucleus in a PTEN-independent manner	Lin <i>et al.</i> 1998

*(Laboratory collection number)

5.9 Oligonucleotides

Table 22: Primers for cloning NSs expression plasmids

#*	Name	nt	Description	Sequence (5' \rightarrow 3')
1217	NSsNTPV_fwd	38	forward primer for cloning untagged Ntepes virus (NTPV) NSs	TACCGAGCTCGGATCCATGACAACCA GATTCTGTACG
1218	3 \times FLAG-NSsNTPV_fwd	104	forward primer for cloning Ntepes virus (NTPV) NSs containing N-terminal 3 \times FLAG tag	TACCGAGCTCGGATCCATGGACTACA AAGACCATGACGGTGATTATAAAGAT CATGATATCGATTACAAGGATGACGA TGACAAGACAACCAGATTCTGTACG
1219	NSsNTPV_rev	40	reverse primer for cloning Ntepes virus (NTPV) NSs	TAGATGCATGCTCGAGCTACTCACTG TCTGAGCTGAAGTC
1360	3 \times FLAG-NSsNTPV_rev	106	reverse primer for cloning Ntepes virus (NTPV) NSs containing C-terminal 3 \times FLAG tag	TAGATGCATGCTCGAGCTACTTGCA TCGTCATCCTTGTAATCGATATCATGA TCTTTATAATCACCGTCATGGTCTTTG TAGTCCTCACTGTCTGAGCTGAAGTC
1345	NSsGFV_fwd	38	forward primer for cloning untagged Gabek Forest virus (GFV) NSs	TACCGAGCTCGGATCCATGACAACCA GATTCTGTATG
1346	3 \times FLAG-GFV_fwd	104	forward primer for cloning Gabek Forest virus (GFV) NSs containing N-terminal 3 \times FLAG tag	TACCGAGCTCGGATCCATGGACTACA AAGACCATGACGGTGATTATAAAGAT CATGATATCGATTACAAGGATGACGA TGACAAGACAACCAGATTCTGTATG
1347	NSsGFV_rev	40	reverse primer for cloning Gabek Forest virus (GFV) NSs	TAGATGCATGCTCGAGCTACTCACTG TCAGAGCTG
1361	3 \times FLAG-NSsGABV_rev	101	reverse primer for cloning Gabek Forest virus (GFV) NSs containing C-terminal 3 \times FLAG tag	TAGATGCATGCTCGAGCTACTTGCA TCGTCATCCTTGTAATCGATATCATGA TCTTTATAATCACCGTCATGGTCTTTG TAGTCCTCACTGTCTGAGCTG
1380	NSs_EMBV_fwd_KpnI	38	forward primer for cloning untagged Embossovirus (EMBV) NSs	TACCGAGCTCGGATCCATGCTAAAGT CAACTGAGAATT

1381	3×FLAG- NSs_EMBV_fwd _KpnI	104	forward primer for cloning Embossos virus (EMBV) NSs containing N-terminal 3×FLAG tag	TACCGAGCTCGGATCCATGGACTACA AAGACCATGACGGTGATTATAAAGAT CATGATATCGATTACAAGGATGACGA TGACAAGCTAAAGTCAACTGAGAATT
1364	NSs_EMBV_rev	34	reverse primer for cloning Embossos virus (EMBV) NSs	TAGATGCATGCTCGAGTCACATGTTT CTGAATAC
1365	3×FLAG- NSs_EMBV_rev	100	reverse primer for cloning Embossos virus (EMBV) NSs containing C-terminal 3×FLAG tag	TAGATGCATGCTCGAGTCACTTGTC TCGTCATCCTTGTAAATCGATATCATGA CTTTATAATCACCGTCATGGTCTTTG TAGTCCATGTTTCTGAATAC
1366	NSs_BGRV_fwd	38	forward primer for cloning untagged Bogoria virus (BGRV) NSs	TACCGAGCTCGGATCCATGTTGAAAG CAACCGAGAATT
1367	3×FLAG- NSs_BGRV_fwd	104	forward primer for cloning Bogoria virus (BGRV) NSs containing N-terminal 3×FLAG tag	TACCGAGCTCGGATCCATGGACTACA AAGACCATGACGGTGATTATAAAGAT CATGATATCGATTACAAGGATGACGA TGACAAGTTGAAAGCAACCGAGAATT
1368	NSs_BGRV_rev	37	reverse primer for cloning Bogoria virus (BGRV) NSs	TAGATGCATGCTCGAGTTATATGTTTC TGAACATCAC
1369	3×FLAG- NSs_BGRV_rev	103	reverse primer for cloning Bogoria virus (BGRV) NSs containing C-terminal 3×FLAG tag	TAGATGCATGCTCGAGTTACTTGTCAT CGTCATCCTTGTAAATCGATATCATGAT CTTTATAATCACCGTCATGGTCTTTGT AGTCTATGTTTCTGAACATCAC
1370	NSs_KBGV_fwd	35	forward primer for cloning untagged Kiborgoch virus (KBGV) NSs	TACCGAGCTCGGATCCATGTTGTCAA GGGCTGTGT
1371	3×FLAG- NSs_KBGV_fwd	101	forward primer for cloning Kiborgoch virus (KBGV) NSs containing N-terminal 3×FLAG tag	TACCGAGCTCGGATCCATGGACTACA AAGACCATGACGGTGATTATAAAGAT CATGATATCGATTACAAGGATGACGA TGACAAGTTGTCAAGGGCTGTGT
1372	NSs_KBGV_rev	35	reverse primer for cloning Kiborgoch virus (KBGV) NSs	TAGATGCATGCTCGAGTTATAGGGGT AAATCAAGG
1373	3×FLAG- NSs_KBGV_rev	101	reverse primer for cloning Kiborgoch virus (KBGV) NSs containing C-terminal 3×FLAG tag	TAGATGCATGCTCGAGTTACTTGTCAT CGTCATCCTTGTAAATCGATATCATGAT CTTTATAATCACCGTCATGGTCTTTGT AGTCTAGGGGTAATCAAGG
1374	NSs_PERV_ORF 1_fwd	38	forward primer for cloning untagged Perkerra virus (PERV; ORF1 = longest ORF with CTG changed to ATG) NSs	TACCGAGCTCGGATCCATGACTCTAG CCATGAGTTTTA
1375	3×FLAG- NSs_PERV_ORF 1_fwd	104	forward primer for cloning Perkerra virus (PERV; ORF1 = longest ORF with CTG changed to ATG) NSs containing N-terminal 3×FLAG tag	TACCGAGCTCGGATCCATGGACTACA AAGACCATGACGGTGATTATAAAGAT CATGATATCGATTACAAGGATGACGA TGACAAGACTCTAGCCATGAGTTTTA
1376	NSs_PERV_ORF 2_fwd	42	forward primer for cloning untagged Perkerra virus (PERV; ORF2 = starting from ATG at position 13) NSs	TACCGAGCTCGGATCCATGAGTTTTA TGTATGATCACCCAAA
1377	3×FLAG- NSs_PERV_ORF 2_fwd	108	forward primer for cloning Perkerra virus (PERV; ORF2 = starting from ATG at position 13) NSs containing N-terminal 3×FLAG tag	TACCGAGCTCGGATCCATGGACTACA AAGACCATGACGGTGATTATAAAGAT CATGATATCGATTACAAGGATGACGA TGACAAGAGTTTTATGTATGATCACC CAAA
1378	NSs_PERV_rev	35	reverse primer for cloning Perkerra virus (PERV) NSs	TAGATGCATGCTCGAGTTAGGCAGCT GACTTCTTT
1379	3×FLAG- NSs_PERV_rev	101	reverse primer for cloning Perkerra virus (PERV) NSs containing C-terminal 3×FLAG tag	TAGATGCATGCTCGAGTTACTTGTCAT CGTCATCCTTGTAAATCGATATCATGAT CTTTATAATCACCGTCATGGTCTTTGT AGTCGGCAGCTGACTTCTTT

Table 23: Sequencing primers

#*	Name	nt	Description	Sequence (5' → 3')
45	pI.18_for2	20	pI.18 sequencing primer forward	TCCATGGGTCTTTTCTGCAG
46	pI.18_rev2	21	pI.18 sequencing primer reverse	GTGACACGTTTATTGAGTAGG
698	pI.18 seq upstream	19	alternative pI.18 sequencing primer forward	GATGCAGGCAGCTGAGTTG

Table 24: Miscellaneous primers

#*	Name	nt	Description	Sequence (5' → 3')
437	GPO-3	24	forward primer for mycoplasma diagnosis-PCR	GGGAGCAAACACGATAGATACCCT
438	MGSO	27	reverse primer for mycoplasma diagnosis-PCR	TGCACCATCTGTCACTCTGTAAACCTC

Table 25: qRT-PCR primers and probes for viral gene targets

#*	Name	Reference	Description	Sequence (5' → 3')
168	RVFL-2912fwdGG		qRT-PCR primer RVFV forward, binding in L segment	TGAAAATTCCTGAGACACATGG
169	RVFL-2981revAC	Bird <i>et al.</i> 2007	qRT-PCR primer RVFV reverse, binding in L segment	ACTTCCTTGCATCATCTGATG
170	RVFL-probe-2950		qRT-PCR probe for RVFV, use with 168/169 primer pair	6FAM-CAATGTAAGGGGCTGTGTGGAC TTGTG-BHQ1
1242	NTPV fwd qRT-PCR		qRT-PCR primer NTPV forward, binding in L segment	GCAAGAAAGCACTGTGGTGG
1243	NTPV rev qRT-PCR	Tchouassi <i>et al.</i> 2019	qRT-PCR primer NTPV reverse, binding in L segment	CGTATGATGATCGGCCACCA
1244	NTPV qRT-PCR probe		qRT-PCR probe for NTPV, use with 1242/43 primer pair	6-FAM-ACAGCCACCTCTGATGATGC-BHQ1
1348	GFV fwd qRT-PCR	Designed to mimic NTPV qRT-PCR primers from Tchouassi <i>et al.</i> 2019	qRT-PCR primer GFV forward, binding in L segment	GCAAGAAAACACTGTGGTGG
1349	GFV rev qRT-PCR		qRT-PCR primer GFV reverse, binding in L segment	CGGATTATGATGGGCCACCA
1350	GFV qRT-PCR probe		qRT-PCR probe for GFV, use with 1348/49 primer pair	6-FAM-ACAGCCACCTCGGACGATGC-BHQ1
1357	E_Sarbeco_F		qRT-PCR SARS-CoV E gene forward primer	ACAGGTACGTTAATAGTTAATAG CGT
1358	E_Sarbeco_P1	Corman <i>et al.</i> 2020	qRT-PCR SARS-CoV E gene probe	FAM-ACACTAGCCATCCTTACTGCGCTT CG-BBQ
1359	E_Sarbeco_R		qRT-PCR SARS-CoV E gene reverse primer, use with 1357/1358 primer pair	ATATTGCAGCAGTACGCACACA

Table 26: *qRT-PCR primers for human gene targets*

#*	Target	Name	Product Number	Supplier
36	18S ribosomal RNA	Hs_RR18s	QT00199367	Qiagen, Hilden
85	CCL4	Hs_CCL4_1_SG	QT01008070	Qiagen, Hilden
24	CCL5	Hs_CCL5_1_SG	QT00090083	Qiagen, Hilden
86	CH25H	Hs_CH25H_1_SG	QT00202370	Qiagen, Hilden
23	CXCL10/IP-10	Hs_CXCL10_1_SG	QT01003065	Qiagen, Hilden
16	CXCL8/IL-8	Hs_CXCL8_1_SG	QT00000322	Qiagen, Hilden
19	IFIT1	Hs_IFIT1_1_SG	QT00201012	Qiagen, Hilden
18	IFN- β	Hs_IFNB1_1_SG	QT00203763	Qiagen, Hilden
73	IFN- λ 1	Hs_IFNL1_2_SG	QT01033564	Qiagen, Hilden
74	IFN- λ 2	Hs_IFNL2_1_SG	QT00222488	Qiagen, Hilden
17	IL-6	Hs_IL6_1_SG	QT00083720	Qiagen, Hilden
15	ISG15	Hs_ISG15_1_SG	QT00072814	Qiagen, Hilden
13	MX1	Hs_MX1_1_SG	QT00090895	Qiagen, Hilden
12	OAS1	Hs_OAS1_1_SG	QT00099134	Qiagen, Hilden
96	OAS2	Hs_OAS2_1_SG	QT01005256	Qiagen, Hilden
97	OAS3	Hs_OAS3_1_SG	QT01005277	Qiagen, Hilden
98	PARP14	Hs_PARP14_1_SG	QT00087444	Qiagen, Hilden
11	RSAD2/Viperin	Hs_RSAD2_1_SG	QT00005271	Qiagen, Hilden
94	TNFSF10/TRAIL	Hs_TNFSF10_1_SG	QT00079212	Qiagen, Hilden
9	TNF- α	Hs_TNF_3_SG	QT01079561	Qiagen, Hilden

*(Laboratory collection number)

5.10 Commercial reagents

Table 27: *Commercial reagents*

Name	Supplier
4',6-diamidino-2-phenylindole (DAPI)	Sigma-Aldrich, Steinheim
Acrylamid/Bis (Rotiphorese® Gel 30 (37.5:1))	Roth, Karlsruhe
Agar	Merck, Darmstadt
Agarose	SERVA, Heidelberg
Ammonium persulfate (APS)	Sigma-Aldrich, Steinheim
Ampicillin sodium salt (50 mg/ml)	Sigma-Aldrich, Steinheim
Avicel	FMC BioPolymer, Philadelphia, PA, U.S.A.
β -Mercaptoethanol	Sigma-Aldrich, Steinheim
β -Propiolactone	Acros Organics, Thermo Fisher Scientific, Schwerte
Complete Protease Inhibitor Cocktail Tablets	Roche/Merck, Darmstadt
Crystal violet	Sigma-Aldrich, Steinheim
Deoxycholate (DOC)	Fluka, Seelze
Dimethylsulfoxide (DMSO)	Sigma-Aldrich, Steinheim
Dynabeads® M-270 Epoxy beads	Thermo Fisher Scientific, Schwerte
Ethanol, absolute	Roth, Karlsruhe
Ethanol, denatured	Roth, Karlsruhe
Ethidium bromide	Promega, Walldorf
Ethylenediaminetetraacetic acid (EDTA)	Roth, Karlsruhe
FluorSave Reagent	Merck, Darmstadt
Formaldehyde (37%)	Roth, Karlsruhe
Glycerol	Roth, Karlsruhe
Glycine	Roth, Karlsruhe
Hydrochloric acid (HCl)	Roth, Karlsruhe
Immobilon® ECL Ultra Western HRP Substrate	Merck, Darmstadt
Isopropanol	Sigma-Aldrich, Steinheim
Methanol	Roth, Karlsruhe

Milk powder	dm Drogeriemarkt, Giessen
N,N,N',N'-tetramethylethylenediamine (TEMED)	Sigma-Aldrich, Steinheim
NaOH	Sigma-Aldrich, Steinheim
NP-40 (Igepal®)	Sigma-Aldrich, Steinheim
Paraformaldehyde	Roth, Karlsruhe
Sodium bicarbonate (7.5%)	Sigma-Aldrich, Steinheim
Sodium chloride (NaCl)	Sigma-Aldrich, Steinheim
Sodium dodecyl sulfate (SDS)	Merck, Darmstadt
SuperSignal™ West Femto Maximum Sensitivity Substrate	Thermo Fisher Scientific, Schwerte
Thiazolyl Blue Tetrazolium Bromide (MTT)	Merck, Darmstadt
Tris(hydroxymethyl)aminomethan	Acros Organics, Thermo Fisher Scientific, Schwerte
Triton X-100	Sigma-Aldrich, Steinheim
Tryptone/peptone	Merck, Darmstadt
Tween-20	Sigma-Aldrich, Steinheim
Yeast extract	Merck, Darmstadt

5.11 Kits

Table 28: Commercial kits for co-immunoprecipitation, DNA- and RNA-isolation

<i>Product Name</i>	<i>Supplier</i>
Dynabeads® Antibody Coupling Kit	Thermo Fisher Scientific, Schwerte
E.Z.N.A.® Plasmid DNA Mini Kit I, V-spin (capped)	Omega bio-tek, Norcross, GA, U.S.A.
E.Z.N.A.® Plasmid DNA Midi Kit	Omega bio-tek, Norcross, GA, U.S.A.
QIAamp® Viral RNA Mini Kit	Qiagen, Hilden
RNeasy® Mini Kit	Qiagen, Hilden
ZymoPure™ Plasmid Midiprep Kit	Zymo Research, Freiburg

Table 29: Commercial kits for cloning

<i>Product Name</i>	<i>Supplier</i>
E.Z.N.A.® Gel Extraction Kit	Omega bio-tek, Norcross, GA, U.S.A.
Rapid DNA Ligation Kit	Thermo Fisher Scientific, Schwerte

Table 30: Commercial kits for (q)RT-PCR

<i>Product Name</i>	<i>Supplier</i>
Premix <i>Ex Taq</i> ™ (probe qRT-PCR)	Takara, Saint-Germain-en-Laye, France
PrimeScript™ RT reagent Kit with gDNA Eraser	Takara, Saint-Germain-en-Laye, France
QuantiFast™ Probe PCR Kit	Qiagen, Hilden
TB Green™ Premix <i>Ex Taq</i> ™ II (Tli RNase H Plus)	Takara, Saint-Germain-en-Laye, France

Table 31: Commercial kits for luciferase assays

<i>Product Name</i>	<i>Supplier</i>
Dual Luciferase Reporter Assay system	Promega, Walldorf
<i>Renilla</i> Luciferase Assay System	Promega, Walldorf

5.12 Consumables and other materials

Table 32: Consumables and other materials

<i>Name</i>	<i>Supplier</i>
Biosafety container (Biotainer 1.8 l)	E3 Cortex, Mitry-Mory, France
Cell culture dishes, 6 cm/10 cm diameter	Sarstedt, Nuembrecht
Cell culture flasks, 25 – 175 cm ²	Greiner Bio-One, Frickenhausen
Cell culture plates, 6-, 12-, 24-, and 96-well	Greiner Bio-One, Frickenhausen
Coverslips, 12 mm diameter	R. Langenbrinck GmbH, Emmendingen
Cryotubes	Sarstedt, Nuembrecht
Dispensertips PD-Tips, BIO-CERT®	Brand, Wertheim Bestenheid
Disposable Pipetting Reservoirs, Polystyrene Reservoirs, 50 ml	VWR, Darmstadt
Graduated TipOne® Filter Tip (sterile), 0.1 – 1000 µl	Starlab, Hamburg
Malassez counting chamber	Ro Go, France
MicroAmp™ Optical Adhesive Film	Thermo Fisher Scientific, Schwerte
MicroAmp™ Fast Optical 96-Well Reaction Plate, 0.1 ml	Thermo Fisher Scientific, Schwerte
Microplate, PS, 96 well, F-bottom (chimney well), white, lumitrac	Greiner Bio-One, Frickenhausen
Microscope slide	Roth, Karlsruhe
Parafilm	Kobe, Marburg
PCR tubes, 0.2 ml	Biozym, Hessisch Oldendorf
Petri dishes	Sarstedt, Nuembrecht
Pipet tips, Tip-One, 0.1 – 1000 µl	Starlab, Hamburg
Polypropylen tubes (Falcon), 15 – 50 ml	Sarstedt, Nuembrecht
Protran Nitrocellulose Transfer Membrane	Whatman, Dassel
PVDF Membrane: Immobilon®-P Transfer Membrane	Millipore, Schwalbach
Reaction tubes, 1.5 ml	Sarstedt, Nuembrecht
Reaction tubes, 2 ml	Eppendorf, Wesseling-Berzdorf
Screw cap tubes, 1.5 ml	Sarstedt, Nuembrecht
Vivaspin® 20, 100 kDa MWCO Polyethersulfone	GE Healthcare/Merck, Darmstadt

5.13 Instruments and software

Table 33: Instruments

<i>Name</i>	<i>Supplier</i>
(Wide) Mini-Sub® Cell GT agarose gel chamber	Bio-Rad, Feldkirchen
2720 Thermal Cycler	Applied Biosystems, Thermo Fisher Scientific, Schwerte
Allegra® X-15R Centrifuge	Beckman Coulter, Krefeld
Allegra® X-30R Centrifuge	Beckman Coulter, Krefeld
ChemiDoc XRS+	Bio-Rad, Feldkirchen
Color Sprout Plus Mini Centrifuge	Biozym, Hessisch Oldendorf
DNA gel chamber	Bio-Rad, Feldkirchen
DS-11+ Spectrophotometer	DeNovix, Wilmington, DE, U.S.A.
EVOS® XL Core Imaging System	Thermo Fisher Scientific, Schwerte
Handy Step electronic	Brand, Wertheim Bestenheid
Heat block	Steute, Loehne
IKAMAG REO S6 Magnetic Stirrer	Ika, Staufen
INCU-Line bacterial incubator	VWR, Darmstadt,
Labotect Incubator C200	Labotect, Goettingen
Laser Scanning Inverted Confocal Microscope TCS SP5 II	Leica Microsystems, Wetzlar
Light microscope Telaval 31	Zeiss, Jena

Microfuge® 20R Centrifuge	Beckman Coulter, Krefeld
Mini-PROTEAN® Tetra System	Bio-Rad, Feldkirchen
Mini-Shaker	Adolf Kühner AG, Basel, Switzerland
MSC-Advantage biological safety cabinet	Thermo Fisher Scientific, Schwerte
NanoDrop Spektrophotometer ND-1000	PeqLab, VWR, Darmstadt
PowerPac™ basic	Bio-Rad, Feldkirchen
Precision scale	Sartorius, Goettingen
REAX top vortex mixer	Heidolph, Schwabach
Rotator SB2	Kobe, Marburg
Scale PB602	Mettler-Toledo, Giessen
Shaker	Infors AG, Bottmingen, Switzerland
SimpliAmp™ Thermal Cycler	Life Technologies, Thermo Fisher Scientific, Schwerte
StepOnePlus Real-Time PCR System	Applied Biosystems, Thermo Fisher Scientific, Schwerte
T100™ Thermal Cycler	Bio-Rad, Feldkirchen
ThermoMixer F1.5	Eppendorf, Wesseling-Berzdorf
Trans-Blot® Turbo Transfer System	Bio-Rad, Feldkirchen
TriStar ² Multimode Reader LB 942	Berthold, Bad Wildbad
Vacuum system Integra Vacusafe	Integra, Biebertal
Waterbath	Memmert, Schwabach

Table 34: Software

<i>Name</i>	<i>Supplier/Reference</i>
BioEdit Sequence Alignment Editor 7.0.5.3	Hall 1999
Citavi 6	Swiss Academic Software GmbH
Clustal X 2.1	Larkin <i>et al.</i> 2007
GraphPad PRISM 9.0.2	GraphPad Software, LLC
Instrument Control and Evaluation (ICE) software	Berthold
Image Lab 5.2.1	Bio-Rad
Leica LAS X	Leica Microsystems CMS GmbH
MaxQuant software version 1.6.17.0	Max Planck Institute of Biochemistry (Tyanova <i>et al.</i> 2016a)
MEGA X version 10.1.6	Kumar <i>et al.</i> 2018
Metascape (metascape.org)	Zhou <i>et al.</i> 2019
Microsoft Office Word, Excel, PowerPoint 2016	Microsoft
Perseus software version 1.6.14	Max Planck Institute of Biochemistry (Tyanova <i>et al.</i> 2016b)
StepOne software v2.3	Life Technologies Corporation

6 Methods

6.1 Eukaryotic cell culture

6.1.1 Maintenance and seeding of eukaryotic cells

All adherent eukaryotic cells were cultivated in sterile plastic flasks or dishes at 37°C in a 5% CO₂ atmosphere. A549, BHK, Calu-3, H1299, HEK293, HeLa, Huh7, Vero E6 and Vero 76 cells were maintained in cell culture medium (CCM34 with 10% fetal bovine serum (FBS) and 1X penicillin-streptomycin-glutamine [P/S/Q]), A549-ACE2 cells were maintained in cell culture medium with 0.5 µg/ml puromycin to ensure strong ACE2 expression, and Caco-2 cells were maintained in CCM34 with 15% FBS and 1X P/S/Q. At 80 – 100% confluency, cells were passaged for optimal growth. For this, cells were washed once with PBS_{def} to remove traces of FBS that would inhibit trypsin enzyme activity, and subsequently detached using a trypsin-EDTA solution. For passaging, once detached, cells were resuspended well in the respective cell culture medium, the desired fraction of resuspended cell solution was discarded, and remaining cells were topped up with fresh cell culture medium. For a 1:10 passage, cells were resuspended in 10 parts cell culture medium, 9 parts were discarded, and 1 part was kept in culture with fresh medium. For cell seeding, after trypsination, cells were resuspended in cell culture medium and pelleted by centrifugation at 800×g for 5 min. Supernatant was discarded, cells were resuspended in fresh cell culture medium, counted with a Malassez counting chamber and seeded into plates or dishes at the desired cell number.

6.1.2 Mycoplasma test

To ensure that cultured cells and virus stocks were free of mycoplasma contamination, a mycoplasma polymerase chain reaction (PCR) test was carried out approx. every one to two weeks. A sample of cell supernatant, preferably from cells whose last passage had been 3 – 4 days before, or an aliquot of virus stock (chapter 6.2.2) was used as input for nucleic acid isolation with the Qiagen “Viral RNA mini kit” according to the manufacturer’s instructions. Although specified for the isolation of RNA, this kit serves well for the extraction of mycoplasma DNA from cell supernatant. PCR was carried out as specified in **Table 35** in a T100™ or SimpliAmp™ Thermal Cycler.

Upon completion of the PCR, 5 µl PCR reaction were mixed with 1 µl 6X Orange DNA Loading Dye and separated electrophoretically on an agarose gel (2% in 1X TAE buffer). The DNA fragment amplified using the GPO-3/MGSO primer pair has a size of approx. 300 base pairs, which was verified using an O'GeneRuler™ 1 kb Plus DNA Ladder.

Table 35: PCR settings for mycoplasma PCR test

Reagent			Quantity for 1 reaction of 20 μ l [μ l]
ddH ₂ O			14.2
10X PCR buffer			2
dNTPs (2 mM)			2
Primer GPO-3 (100 μ M; van Kuppeveld <i>et al.</i> 1992, 1993)			0.2
Primer MGSO (100 μ M; van Kuppeveld <i>et al.</i> 1992, 1993)			0.2
JumpStart™ Taq DNA-Polymerase			0.4
Sample			1
Initial Denaturation	95°C	2 min	35 cycles
Denaturation	95°C	20 sec	
Annealing	55°C	10 sec	
Elongation	70°C	15 sec	
Final Elongation	70°C	10 min	
Hold	4°C	∞	

6.1.3 Transient transfection of eukaryotic cells

6.1.3.1 Transfection with plasmid DNA

To express proteins from plasmid DNA in eukaryotic cells, plasmid DNA is introduced into the cell by lipid-based transfection using TransIT®-LT1 reagent. For this, the desired plasmid amount was diluted in serum-free medium (OptiMEM or OptiPRO) and mixed with 3 μ l TransIT®-LT1 per 1 μ g DNA diluted in serum-free medium. After a 15 – 30 min incubation at RT, the transfection mix was added to the cells with gentle mixing. The cationic lipid-polymer mixture of the transfection reagent will encompass negatively charged DNA to allow for the uptake of DNA-lipopolyplexes into the cells.

6.1.3.2 Transfection with viral RNA

To induce activation of reporter plasmid gene expression (chapter 6.5.1), virus infection is mimicked by transfection of viral RNA. Here, RNA from Vesicular Stomatitis virus (VSV) was isolated by phenol-chloroform extraction from PEG8000-precipitated VSV particles (Habjan *et al.* 2008a). For cells in each well in a 96-well format, 50 ng VSV-RNA were diluted in 5 μ l serum-free medium and mixed with 0.5 μ l EndoFectin™ Max diluted in 5 μ l serum-free medium. After a 5 – 20 min incubation at RT, the transfection mix was added to the cells with gentle mixing. Like TransIT®-LT1 (chapter 6.1.3.1), EndoFectin™ Max also works via cationic lipid-mediated transfection. VSV-RNA used in this work was prepared by Andreas Schön (Institute for Virology, FB10, Justus Liebig University Giessen).

6.1.4 Cytokine and inhibitor assays

To assess the sensitivity of viruses to innate immune cytokines, as well as the competency of viruses to overcome the antiviral state induced by these cytokines, cells were pre-treated with type I (IFN- α) or type III (IFN- λ 3) interferon (IFN) or with the JAK/STAT inhibitor Ruxolitinib, which prohibits type I/III IFN signalling. For this, cells seeded into 24-well plates (5×10^4 per well) were treated for 16 h with 100, 500, or 1000 U/ml pan-species IFN- α (B/D) (Horisberger and Staritzky 1987), 10 or

100 ng/ml purified recombinant IFN- λ 3 (Dellgren *et al.* 2009), or with 1 μ M Ruxolitinib prior to infection (chapter 6.2.1).

To induce activation of reporter plasmid gene expression (chapter 6.5.1), cells in each well in a 96-well format were treated with 50 U/well pan-species IFN- α (B/D) (Horisberger and Staritzky 1987) or with 10 ng/ml recombinant human TNF- α for 18 h.

6.1.5 Generation of stable cell lines by lentiviral transduction

The human immortalized adenocarcinoma alveolar basal epithelial lung cell line A549 does not support infection with SARS-CoV-1 or SARS-CoV-2 due to low expression levels of the viral receptor angiotensin-converting enzyme 2 (ACE2; Harcourt *et al.* 2020; Hoffmann *et al.* 2020; Letko *et al.* 2020). To study this cell line in the context of SARS coronavirus infection, A549 cells were engineered to stably express ACE2 by employing the ViraPower™ Lentiviral Expression System by invitrogen as described elsewhere (Riedel *et al.* 2017; Konstantoulas and Indik 2014). Briefly, cells were seeded to approx. 30% confluency in a 6-well plate and infected with HIV VSV G-pseudoparticles carrying the coding region of the human ACE2 gene (accession number NM_001371415.1), which were generated in HEK293T cells. Selection for successful ACE2 gene integration took place by addition of 1 μ g/ml puromycin to the cell culture medium. ACE2 integration and expression were confirmed by Western blot analysis. A549-ACE2 cells used in this work were generated by Benjamin Lamp and Andreas Schön (Institute for Virology, FB10, Justus Liebig University Giessen).

6.2 Virological methods

6.2.1 Virus infection of eukaryotic cells

To perform virus infection of eukaryotic cells, cells were seeded at the desired cell number per well one day prior to infection. Cells were washed once with 1X PBS_{def} and subsequently infected by adding a virus suspension diluted in serum-free medium (OptiMEM or OptiPRO) containing the desired amount of virus for a specific multiplicity of infection (MOI). An MOI of 1 means 1 plaque forming unit (PFU; corresponds to 1 infectious virus particle) per cell. To calculate the volume of virus needed for a specific MOI, the following formula was applied:

$$\frac{\text{desired MOI} \times \text{cell number}}{\text{virus titre} \left[\frac{\text{PFU}}{\text{ml}} \right]} = \text{virus volume [ml]}$$

The virus dilution (inoculum) was added to the cells and cells were incubated for 1 h at 37°C in a 5% CO₂ atmosphere. To ensure that cells were evenly covered by the inoculum throughout the incubation time, cell culture plates or flasks were gently rocked every 15 min. After incubation, the inoculum was removed, and fresh cell culture medium was added to the cells.

6.2.2 Production of virus stocks

6.2.2.1 Phleboviruses

Rift Valley fever virus (RVFV) clone 13 (CI13) and Ntapes virus (NTPV) strain MRG54-KE-2014 (Tchouassi *et al.* 2019) were propagated on Vero E6 cells. RVFV strain MP-12 and RVFV-delNSs::Renilla were propagated on BHK cells. Gabek Forest virus (GFV) isolate Sud AN 754-61 was propagated on Vero 76 cells. Cells were seeded into T175 flasks and infected the following day with either 5×10^3 PFU/flask (RVF viruses) or 4×10^4 PFU/flask (NTPV and GFV). For all phlebovirus stocks, cell supernatant was collected 3 d post infection and centrifuged for 5 min at $800 \times g$ to remove cellular debris. All phlebovirus stocks were titrated by plaque assay on BHK cells (chapter 6.2.3). Virus stocks were confirmed to be mycoplasma-free by PCR (chapter 6.1.2).

6.2.2.2 SARS coronaviruses

SARS-CoV-2 (Patient isolate 985, BetaCoV/Munich/BavPat1/2020|EPI_ISL_406862) and SARS-CoV-1 (Frankfurt strain, NCBI accession number AY310120) were propagated on Vero E6 cells. Cells were seeded into T175 flasks and infected the following day with approx. 5×10^4 PFU/flask. After infection, DMEM containing 2% FBS was added. Cell supernatants were collected 3–4 d post infection, purified through Vivaspin columns according to manufacturer's instructions and resuspended in OptiPRO serum-free medium. All coronavirus stocks were titrated by plaque assay on Vero E6 cells (chapter 6.2.3). Cells used for virus stock production were confirmed to be mycoplasma-free by PCR (chapter 6.1.2).

6.2.3 Virus titre determination by plaque assay

To determine the virus titre, given in $\frac{PFU}{ml}$, of virus stocks or cell supernatant samples, titration by plaque assay was performed. For this, cells were seeded in 24-well plates to reach confluency at the time of infection. Virus-containing samples were serially diluted in serum-free medium in 10-fold steps and usually dilutions 10^{-3} to 10^{-8} were used to infect cells (chapter 6.2.1). After incubation, inoculum was removed and replaced by 500 μ l 1.5%-Avicel solution per well (1X MEM containing 1.5% Avicel, 5% FBS and 1X P/S/Q) to prevent the spread of newly produced virus particles across the cell monolayer. Instead, the Avicel overlay allows only for infection of neighbouring cells, leading to the formation of characteristic cell-free spots, the so-called plaques. Because the spread of viruses is prevented by Avicel, each plaque thus originates from one virus particle in a given sample. Cells were incubated for 3–4 d at $37^\circ C$ in a 5% CO_2 atmosphere and then stained. For this, cells were washed 1–2 times with PBS_{def} and then incubated for a minimum of 30 min in a biosafety container filled with 4% formaldehyde solution in PBS_{def} to inactivate virus. Formaldehyde solution was removed, and cells were stained with crystal violet solution (0.75% crystal violet, 3.75% formaldehyde, 20% ethanol, 1% methanol in ddH_2O) for approx. 15 min. Cell culture plates were washed twice in H_2O and dried completely before counting of plaques. Virus titre was determined as follows:

$$\frac{\text{plaque number}}{\text{dilution factor} \times \text{inoculum volume [ml]}} = \text{titre} \left[\frac{\text{PFU}}{\text{ml}} \right]$$

6.2.4 Virological work under BSL-3 conditions

Infection experiments with SARS coronaviruses were performed under biosafety level 3 (BSL-3) conditions with enhanced respiratory personal protection equipment.

To process samples from BSL-3 in a BSL-2 environment, infectious virus particles must be fully inactivated. For this, cells to be subjected to RNA isolation via the RNeasy® mini kit from Qiagen (chapter 6.7.2) were lysed in RLT buffer provided in the kit which contains guanidine-isothiocyanate for virus inactivation, supplemented with β -mercaptoethanol (1:100). Cell lysates were transferred to RNase-free 1.5 ml safe-lock tubes, heated for 10 min at 70°C while rocking at 400 rpm, and then exported. Cells to be subjected to SDS PAGE and Western blot analysis (chapter 6.8) were lysed in 1X sample buffer containing 1% SDS for virus inactivation. Cell lysates were transferred to 1.5 ml screw cap tubes, heated for 10 min at 100°C and then exported. Cell supernatants to be subjected to interferon bioassay (chapter 6.5.2) were mixed with 0.05% β -propiolactone for virus inactivation and 5% sodium bicarbonate for pH buffering, incubated for 72 h at 4°C and then exported. Cell culture plates for plaque assay staining (chapter 6.2.3) were exported in a biotainer, submerged in 4% formaldehyde-PBS_{def} solution, which was only opened after a minimum of 30 min incubation time.

6.3 Co-immunoprecipitation

To analyze the interaction of one protein with another, a co-immunoprecipitation assay is applied. Here, in a first step, antibody against the target protein is coupled to magnetic beads. Next, cell lysates are incubated with bead-coupled antibodies which will result in antibody-target protein binding. Stringent washing will subsequently remove all proteins not bound to the antibodies. All proteins now detectable by mass spectrometry (chapter 6.9.1) or SDS PAGE and Western blotting (chapter 6.8) are interactors of the target protein that was “pulled down” with co-immunoprecipitation.

For this, HEK293 cells seeded into 10 cm dishes (2×10^6 per dish) were transfected the following day with expression constructs for 3×FLAG-tagged NSs of NTPV, SFSV (C-terminal tag), GFV, EMBV, BGRV, KBGV, PERV (N-terminal tag) or with the control construct pI.18-3×FLAG- Δ Mx (15 μ g per dish) via the use of TransIT®-LT1 (chapter 6.1.3.1). 24 h post transfection, cells were lysed in 300 μ l PXL buffer (1% NP-40, 0.5% DOC, 0.1% SDS in 1X PBS_{def}) and frozen at -80°C. For co-immunoprecipitation, 2 mg M-270 Epoxy beads per sample were coupled with 15 μ g anti-Flag M2 monoclonal antibody for 2 days at 22°C with slow tilt rotation using the Dynabeads® Antibody Coupling Kit (Thermo Fisher Scientific) according to the manufacturer’s instructions. Co-immunoprecipitation was performed for 1 h at 4°C with slow tilt rotation. Beads with bound protein

complexes were washed 2 times with 1X PBS_{def} containing 0.01% Tween20 and once with 1X PBS_{def} and subjected to mass spectrometry analysis (chapter 6.9.1).

6.4 Immunofluorescence analysis

To visualize phlebovirus NSs proteins in the host cell, HeLa cells seeded onto glass coverslips in 6-well plates (3×10^5 per well) were reverse transfected with expression constructs for 3×FLAG-tagged NSs of NTPV (C-terminal tag), GFV, EMBV, BGRV, KBGV or PERV (N-terminal tag) (2.5 µg per well) via the use of TransIT®-LT1 (chapter 6.1.3.1). 24 h post transfection, cells were fixed for 30 min in 1X PBS_{def}-4% PFA at 4°C. The coverslips were then washed with PBS_{def}, and the cells were permeabilized with PBS_{def}-0.1% Triton X-100, washed again, and blocked in blocking buffer (2% BSA, 5% glycerol, 0.2% Tween20 in 1X PBS_{def}). Staining with primary antibodies diluted in blocking buffer (anti-Flag M2, 1:500) was performed overnight in a humid chamber. Afterward, the coverslips were washed with 1X PBS_{def} and incubated with secondary antibody (Alexa Fluor 555 donkey anti-mouse [A31570]; 1:200) and 4',6-diamidino-2-phenylindole (DAPI; 0.1 µg/ml) for 45 min in a humid chamber. Samples were washed again in PBS_{def}, rinsed in demineralized water, and mounted onto microscopic slides using FluorSave reagent. Confocal microscopy was performed using a Leica TCS SP5 confocal microscope and the accompanying software.

6.5 Luciferase reporter assays

Luciferase reporter assays are applied to measure the amount of luciferase expression that usually serves as a substitute readout for another gene product. Luciferases are oxidative enzymes which catalyze a reaction producing bioluminescent light as a by-product which is detected by a plate-based luminometer.

6.5.1 Dual luciferase reporter assay

To assess the anti-innate immune signalling capacities of phlebovirus NSs proteins, dual luciferase reporter assays were performed. To this end, cells were transfected with reporter plasmids containing the firefly luciferase gene under the control of the NF-κB-dependent, IFN-β-, Mx1- or ISG54-promoter, which allows for firefly (*Photinus pyralis*) luciferase readout as a measurement for promoter activation. Promoter activation upon transfection of empty vector and a plasmid expressing an unrelated control protein can be compared to promoter activation in the presence of the respective NSs proteins. Co-transfection of *Renilla* (*Renilla reniformis* or sea pansy) luciferase is used as transfection control, although not included in the final analysis because the well-described RVFV NSs inhibits *Renilla* luciferase expression due to a general transcription block.

For this assay, HEK293 cells seeded into 96-well plates (1.5×10^4 per well) were transfected the following day with firefly and *Renilla* luciferase reporter constructs (40 ng each), as well as expression constructs for NSs proteins or the control protein ΔMx (10 ng) via the use of TransIT®-LT1 (chapter 6.1.3.1). 24 h post transfection, cells were treated with 50 U/well IFN-α(B/D) (Horisberger and Staritzky

1987), 10 ng/ml TNF- α , or transfected with 50 ng/well viral RNA (isolated from Vesicular Stomatitis virus [VSV] by phenol-chloroform extraction from PEG8000-precipitated VSV particles [Habjan *et al.* 2008a]) via the use of EndoFectin™ Max for 18 h and then processed.

Alternatively, HEK293 cells seeded into 96-well plates (1.5×10^4 per well) were transfected the following day with firefly and *Renilla* luciferase reporter constructs (40 ng each), expression constructs for NSs proteins or the control protein Δ Mx (10 ng), as well as expression constructs for RIG-I CARD, MAVS, TBK1, or IRF3(5D-97A) (40 ng each) for stimulation of promoter activation. Cells were processed 24 h post transfection.

Luciferase activities were measured with a dual-luciferase reporter assay system (Promega) according to the manufacturer's recommendations on a TriStar² Luminometer. Background firefly luciferase values of unstimulated control samples (*e.g.* no IFN- α (B/D), no TNF- α , no VSV-RNA) were subtracted from values of stimulated samples, and the resulting values for the empty vector control were set to 100% within each biological replicate.

6.5.2 Interferon bioassay

An IFN bioassay to relatively quantify the amount of type I IFN in a given sample was conducted according to Kuri *et al.* (2010). This assay relies on the inhibition of an IFN-sensitive reporter virus in the presence of type I IFN. Here, a recombinant RVFV with its NSs protein replaced by the firefly luciferase gene (RVFV-delNSs::*Renilla*) was used. The deletion of NSs renders this virus highly sensitive to type I interferon, while the expression of *Renilla* luciferase allows for easy virus quantification.

For this assay, supernatants of Calu-3, H1299 and A549-ACE2 cells that were infected with SARS-CoV-2, SARS-CoV-1, or RVFV C113 at an MOI of 1 for 24 h (chapter 6.2.1) were treated with 0.05 % β -propiolactone and 5 % -sodium bicarbonate for 72 h at 4°C to inactivate virus particles while conserving type I IFN. A549 cells seeded in 96-well plates to 80 % confluency were incubated with 100 μ l cell supernatant for 7 h at 37°C, 5 % CO₂ before infection with the IFN-sensitive reporter virus RVFV-delNSs::*Renilla* at an MOI of 1 for 16 h at 37°C, 5 % CO₂. *Renilla* luciferase activity was measured with a *Renilla* luciferase reporter assay system (Promega) according to the manufacturer's recommendations on a TriStar² Luminometer.

6.6 Molecular cloning and prokaryotic cell culture

6.6.1 Subcloning of genes of interest into desired vector backbone

For overexpression experiments of proteins, genes of interest must be available in a certain vector backbone. Molecular cloning refers to the production of expression vector constructs by insert amplification and insertion into the desired vector background.

6.6.1.1 Insert amplification

In a first step, the insert, being the gene of interest (GOI), was amplified through polymerase chain reaction (PCR). Primers were designed to comprise an 18 – 20 base sequence complementary to the GOI sequence at the 3' end and the cutting target sequence for a certain restriction enzyme (which is not found within the GOI sequence) including a random base sequence of about 6 – 10 bases to facilitate restriction enzyme binding at the 5' end. For PCR, Phusion® or KOD polymerase systems were used.

Table 36: Phusion® polymerase protocol

Reagent	Quantity for 1 reaction of 20 µl [µl]		
ddH ₂ O	10.2		
5X Phusion® HF or GC buffer	4		
dNTPs (2 mM)	2		
Primer, forward (10 µM)	1		
Primer, reverse (10 µM)	1		
DMSO	0.6		
Phusion® DNA Polymerase (2 U/µl)	0.2		
Template DNA (10 ng/µl)	1		
Initial Denaturation	98°C	1 min	35 cycles
Denaturation	98°C	5 sec	
Annealing	<i>varies (see below)</i>	10 – 30 sec	
Elongation	72°C	15 – 30 sec per kb	
Final Elongation	72°C	15 min	
Hold	4°C	∞	

The annealing temperature (T_m) is dependent on the primer sequences and was calculated using the T_m calculator tool on the Thermo Fisher Scientific website.

Table 37: KOD polymerase protocol

Reagent	Quantity for 1 reaction of 25 µl [µl]		
ddH ₂ O	14.9		
10X Buffer for KOD Hot Start DNA Polymerase	2.5		
dNTPs (2 mM)	2.5		
Primer, forward (10 µM)	0.9		
Primer, reverse (10 µM)	0.9		
25 mM MgSO ₄	1.5		
KOD Hot Start DNA Polymerase (1 U/µl)	0.6		
Template DNA (10 ng/µl)	1.25		
Initial Denaturation	95°C	2 min	35 cycles
Denaturation	95°C	20 sec	
Annealing	<i>lowest primer T_m</i>	10 sec	
Elongation	70°C	10 – 25 sec per kb	
Final Elongation	70°C	10 min	
Hold	4°C	∞	

The T_m for each primer was calculated using the OligoCalc webtool (Kibbe 2007).

6.6.1.2 Restriction endonuclease digest and ligation

In a next step, the resulting PCR product was digested by restriction endonuclease enzymes. These enzymes, originating from bacteria and archaea, recognize and bind specific, often palindromic, base pair sequences of usually 4 – 8 nucleotides, and cleave the DNA within the target sequence producing

either blunt (no overhang) or “sticky” (5’ or 3’ overhang) ends. The vector backbone is digested in the same way, resulting in a linearized vector with identical restriction site ends.

The restriction reaction was prepared as follows and incubated at 37°C for approx. 18 h.

Table 38: Restriction endonuclease digest reaction

<i>Reagent</i>	<i>Quantity for 1 reaction of 50 µl [µl]</i>
Nuclease-free ddH ₂ O	To 50 µl
10X CutSmart buffer	5
Restriction enzyme 1	[10 units]
Restriction enzyme 2	[10 units]
DNA	1 µg

To verify the correct length of the digested insert and vector fragments, and to purify those fragments by removal of contaminating fragments, the whole of the restriction reaction was subsequently analyzed via agarose gel electrophoresis on a 1% agarose gel in 1X TAE buffer, run for approx. 45 min at 100 V. In a next step, the fragments of the correct size, verified using an O'GeneRuler™ 1 kb Plus DNA Ladder, were excised from the agarose gel with a scalpel, and DNA was extracted from the gel piece via the use of the E.Z.N.A.® Gel Extraction Kit according to manufacturer's recommendations.

To insert the GOI insert fragment into the vector backbone, insert and vector were ligated in a next step using the Rapid DNA Ligation Kit as follows and incubated for 30 min at 22°C.

Table 39: Ligation reaction

<i>Reagent</i>	<i>Quantity for 1 reaction of 20 µl [µl]</i>
Nuclease-free ddH ₂ O	To 20 µl
5X Rapid Ligation Buffer	4
Linearized vector	50 – 100 ng
Linear PCR product (insert)	1:3 molar ratio with vector
T4 DNA ligase (5 U/µl)	0.4

6.6.2 Transformation of bacteria

The resulting plasmids were next amplified and therefore transformed into bacteria. For this, *Escherichia coli* (*E. coli*) bacteria were carefully thawed on ice. Here, the strains DH10B, TOP10 or Stellar competent cells were used. 10 µl of the ligation reaction were added to 25 – 50 µl bacteria and incubated at 4°C for 30 min, followed by a heat shock at 42°C for 30 sec. After an additional incubation at 4°C for 2 min, 400 µl SOC growth medium were added to the reaction, which was then incubated at 37°C for 1 h while shaking at 400 rpm. 100 µl of this reaction were then plated on LB-agar plates containing 100 ng/ml ampicillin for the antibiotic selection of the correct plasmids. The bacteria plates were then incubated at 37°C overnight.

6.6.3 Insert verification

6.6.3.1 Colony PCR

To verify the insertion of the GOI into the vector backbone, first a colony PCR was performed. Here, the cloned construct is amplified either in full or in part with a primer pair of which either both primers bind in the vector backbone spanning the insert, or, for long inserts, one primer binds in the vector backbone and the other one in the insert. For this, a PCR reaction using JumpStart™ *Taq* DNA-Polymerase was prepared as follows:

Table 40: Colony PCR reaction

Reagent			Quantity for 1 reaction of 20 µl [µl]
ddH ₂ O			14
10X PCR buffer			2
dNTPs (2 mM)			2
Primer, forward (100 µM)			0.4
Primer, reverse (100 µM)			0.4
JumpStart™ <i>Taq</i> DNA-Polymerase			2.4
Initial Denaturation	94°C	1 min	35 cycles
Denaturation	94°C	30 sec	
Annealing	50°C	30 sec	
Elongation	72°C	1 min per kb	
Final Elongation	72°C	10 min	
Hold	4°C	∞	

Single colonies were picked with a 10 µl pipette tip from the bacteria plate and transferred to a new LB-agar plate containing 100 ng/ml ampicillin, which is also incubated at 37°C until visible growth of bacteria. The same tip was then used to inoculate the PCR reaction by dipping in the tip and swirling it for approx. 15 sec. Upon completion of the PCR programme, 5 µl of the PCR reaction were mixed with 1 µl 6X Orange DNA Loading Dye and separated electrophoretically on an agarose gel (1% in 1X TAE buffer). The correct size of the amplified insert fragment was verified using an O'GeneRuler™ 1 kb Plus DNA Ladder.

6.6.3.2 Sanger sequencing

Colonies exhibiting the correct PCR product size were further analyzed via Sanger sequencing. For this, the *E. coli* NightSeq® service by Microsynth Seqlab was employed. Bacteria were picked from the new LB-agar plate with a 10 µl pipette tip and used to inoculate the 1.5 ml buffer-containing tube provided by Microsynth Seqlab by dipping in the tip and swirling it for approx. 15 sec. Sequencing primers were prepared in a separate 1.5 ml screw cap tube and both vials were sent to Microsynth Seqlab for analysis. The obtained sequences were checked for the correct sequence using BioEdit software (Hall 1999).

6.7 Molecular biological methods

6.7.1 Plasmid DNA isolation from bacteria

To prepare a working stock of plasmid DNA for various experimental applications, bacteria were picked from the LB-agar plate described in chapter 6.6.3.1 with a 10 µl pipette tip and used to inoculate a 50 ml LB medium solution containing 100 ng/ml ampicillin. After incubation at 37°C for 16 h while rotating at approx. 120 rpm, the bacteria culture was transferred to a 50 ml falcon tube and pelleted for 30 min at 4,000×g at 4°C. Plasmid DNA isolation was carried out with the E.Z.N.A.® Plasmid DNA Midi Kit from Omega bio-tek according to manufacturer's instructions. Plasmid DNA concentration was measured with a DS-11+ Spectrophotometer.

6.7.2 RNA isolation from eukaryotic cells

To isolate RNA from eukaryotic cells, the RNeasy® mini kit from Qiagen was used according to the manufacturer's recommendations. This system employs purification of the RNA through a silica membrane in a column system. In a final step, the RNA was eluted in RNase-free water and the concentration was determined with a DS-11+ Spectrophotometer.

6.7.3 Quantitative real-time PCR

Quantitative real-time PCR (qRT-PCR) is a means to quantify nucleic acids while they are amplified (*i.e.* in real time). It relies on the measurement of fluorescence signals generated either upon the unspecific intercalation of fluorescence dyes (*e.g.* SYBR® green) into newly formed double-stranded DNA (dsDNA), or on the binding of oligonucleotide probes complementary to the amplified target sequence, that carry fluorescent reporters which allow detection only upon hybridization with the target. In case of unspecifically intercalating dyes, a melt curve protocol downstream of the PCR amplification protocol allows for verification of the specificity of primers, which means that only one product is amplified.

The so-called cycle threshold value (C_T) serves as a readout. It indicates the moment (cycle number) when the fluorescence signal reaches a certain threshold. To quantify nucleic acids in a relative manner, *i.e.* the amount found in different samples in relation to each other, the fold-change in nucleic acid amount between the query and a control sample is calculated using the $2^{-\Delta\Delta C_T}$ method according to Livak and Schmittgen (2001). First, a double difference value ($\Delta\Delta C_T$) between C_T s of query and control (CTRL) samples is calculated as follows, with the 18S ribosomal RNA as reference gene whose levels do not change upon (query) treatment:

$$\Delta\Delta C_T = [C_T(GOI_{query}) - C_T(reference_{query})] - [C_T(GOI_{CTRL}) - C_T(reference_{CTRL})]$$

Second, the fold change between query (virus-infected) and control (uninfected/mock) sample values is calculated as follows: $fold\ change = 2^{-\Delta\Delta C_T}$

6.7.3.1 Two-step SYBR® green qRT-PCR

This method was used to assess the differential regulation of cellular genes.

For two-step qRT-PCR, RNA isolated from cell lysates (chapter 6.7.2) is first transcribed into copy DNA (cDNA). For this, the PrimeScript™ RT reagent Kit with gDNA Eraser from Takara was employed according to manufacturer's instructions. With this kit, potentially contaminating genomic DNA is eliminated in a first step, followed by reverse transcription of the RNA into cDNA by a reverse transcriptase in a second step.

Differential regulation of cellular genes was analyzed using TB Green™ Premix *Ex Taq*™ II (Tli RNase H Plus; Takara) according to manufacturer's instructions with commercial, validated QuantiTect® primer assays (**Table 26** and **Table 41**).

Table 41: Two-step SYBR green qRT-PCR protocol

Initial Denaturation	95°C	30 sec	40 cycles
Denaturation	95°C	5 sec	
Annealing & Elongation	60°C	30 sec	
Melt curve stage	95°C	15 sec	
	60°C	1 min	
	[+ 0.3°C increase]		
	95°C	15 sec	

6.7.3.2 Two-step probe qRT-PCR

This method was used to quantify viral nucleic acids in a relative manner.

cDNA was created as described previously (chapter 6.7.3.1). Relative viral load was assessed using Premix *Ex Taq*™ (probe qRT-PCR; Takara) according to manufacturer's instructions with primers and probes listed in **Table 25** (**Table 42**).

Table 42: Two-step probe qRT-PCR protocol

Initial Denaturation	95°C	20 sec	40 cycles
Denaturation	95°C	1 sec	
Annealing & Elongation	60°C	20 sec	

Since per se no viral nucleic acids can be measured in the uninfected mock control sample, the $2^{-\Delta\Delta C_T}$ method is not applied here. Instead, relative viral load is indicated as the reciprocal value of $C_T(GOI_{query})/C_T(reference_{query})$. The reason for reciprocal values is that a lower C_T value is associated with a higher amount of nucleic acid, and a non-reciprocal representation would be counterintuitive.

6.7.3.3 One-step probe qRT-PCR

This method was used to quantify viral nucleic acids in an absolute manner.

Absolute viral load was assessed using the QuantiFast™ Probe PCR Kit from Qiagen according to manufacturer's instructions with primers and probes listed in **Table 25**. This kit involves a reverse transcriptase step before the qRT-PCR stage and thus RNA instead of cDNA is used as input (**Table 43**).

Table 43: One-step probe qRT-PCR protocol

Reverse Transcription	50°C	10 min	
Denaturation	95°C	5 min	
Denaturation	95°C	10 sec	40 cycles
Annealing & Elongation	60°C	30 sec	

Absolute quantification of viral RNA amount is achieved by including a standard curve with samples of known amounts of genome copies.

6.8 Protein biochemical methods

6.8.1 SDS polyacrylamide gel electrophoresis

Sodium dodecyl sulfate polyacrylamide gel electrophoresis (SDS PAGE) is applied to electrophoretically separate proteins by mass. Cells are lysed in SDS-containing sample buffer and subsequently boiled. This serves to denature proteins by breaking intra- and intermolecular bonds. Additionally, the SDS forms negatively charged complexes with the proteins, thereby concealing intrinsic protein charges while rendering proteins with similar mass-charge-ratio properties. In an electric field, these protein complexes are separated by mass which corresponds to their migration speed to the anode.

For this, cells were either directly lysed in 1X SDS sample buffer (**Table 8**), or lysed using an alternative lysis buffer (**Table 10**) which was ultimately supplemented with 4X SDS sample buffer to reach a concentration of 1X, and boiled for 5 – 10 min at 100°C. 10 µl of sample were then loaded onto an SDS gel consisting of a 4% stacking and a 12% separating gel according to **Table 44**.

Table 44: SDS gel composition

Component	4% stacking gel (for 12 gels)	12% separating gel (for 12 gels)
ddH ₂ O	21.6 ml	25.5 ml
Rotiphorese® Gel 30 (37.5:1)	4.7 ml	30 ml
Rotiphorese®-PAGE Matrix Buffer plus	8.75 ml	18.75 ml
10% APS solution	350 µl	750 µl
TEMED	35 µl	45 µl

Separation of proteins by mass occurred in an electric field of 100 V for approx. 45 min in a Mini-PROTEAN® Tetra System.

6.8.2 Semidry Western blotting

Proteins mass-separated by SDS PAGE were transferred to polyvinylidene fluoride (PVDF) membranes (Millipore) via semidry blotting in a Trans-Blot® Turbo Transfer System at 10 V for 1 h.

6.8.3 Antibody staining

To saturate unspecific binding sites, PVDF membranes were incubated for a minimum of 1 h with blocking buffer (either 10% milk powder in 1X TBS or 5% BSA in 1X TBS-T, see **Table 9**). Primary antibody staining was performed overnight at 4°C. After this, membranes were washed three times in TBS-T, stained with secondary antibodies for 45 min, and washed again three times in TBS-T and once in TBS. Finally, membranes were developed with a SuperSignal™ West Femto kit or with the Immobilon® ECL Ultra Western HRP Substrate and bands were visualized using a ChemiDoc imaging system. Antibodies for Western blotting are listed in **Table 17** and **Table 18**.

6.9 “Omics” approaches

6.9.1 Proteomic analyses

To elucidate binding partners of a query protein, proteomic analyses can be applied. For this, query proteins were subjected to co-immunoprecipitation as described in chapter 6.3. Subsequently, proteins bound to the query proteins were identified by liquid chromatography-tandem mass spectrometry (LC-MS/MS). For this, samples bound to magnetic beads were washed three times with 100 µL 0.1 M ammonium bicarbonate solution. Proteins were digested "on-bead" by the addition of 0.1 µg Sequencing Grade Modified Trypsin (Serva) in 80 µL ammonium bicarbonate buffer and incubated at 37°C for 45 min. Subsequently, the supernatant was transferred to fresh tubes and incubated at 37°C overnight.

DTT was added to a final concentration of 5 mM and after mixing, samples were incubated for 15 min at 95°C. Subsequently, iodoacetamide was added to a final concentration of 25 mM and after mixing, samples were incubated for 45 min at RT in the dark. Then, DTT was added to a final concentration of 50 mM and samples were incubated for 1 h at RT.

Peptides were desalted and concentrated using Chromabond C18WP spin columns (Macherey-Nagel, Part No. 730522). Finally, peptides were dissolved in 25 µL of water with 5% acetonitrile and 0.1% formic acid.

The mass spectrometric analysis of the samples was performed using a timsTOF Pro mass spectrometer (Bruker Daltonic). A nanoElute HPLC system (Bruker Daltonics), equipped with an Aurora column (25cm x 75µm) C18 RP column filled with 1.7 µm beads (IonOpticks) was connected online to the mass

spectrometer. A portion of approximately 200 ng of peptides corresponding to 2 μ L was injected directly on the separation column. Sample loading was performed at a constant pressure of 800 bar.

Separation of the tryptic peptides was achieved at 50°C column temperature with the following gradient of water/0.1% formic acid (solvent A) and acetonitrile/0.1% formic acid (solvent B) at a flow rate of 400 nL/min: Linear increase from 2% B to 17% B within 18 min, followed by a linear gradient to 25% B within 9 min and linear increase to 37% solvent B in additional 3 min. Finally, B was increased to 95% within 10 min and hold for additional 10 min. The built-in “DDA PASEF-standard_1.1sec_cycletime” method developed by Bruker Daltonics was used for mass spectrometric measurement.

The mass spectrometry data analysis was performed using MaxQuant (version 1.6.17.0, Tyanova *et al.* 2016a) with standard settings for timsTOF data and Andromeda search against UniProtKB/Swiss-Prot (Release 2019_06 of 03-Jul-2019) human protein sequence database. The option “match between runs” was not used.

The results were analysed using the software Perseus (version 1.6.14, Tyanova *et al.* 2016b). Specific interactors of query proteins in comparison to the Δ Mx control were determined by Student’s t test with correction for multiple testing by data permutation (250 times) with a cutoff of $p_{\text{corrected}} = q < 0.05$. Before applying the t test, missing values were replaced by zero values in order to include proteins enriched in specific samples but not present in Δ Mx control samples.

Mass spectrometry analyses were carried out by Uwe Linne and Tina Krieg (Department of Chemistry, Philipps University Marburg). Accompanying bioinformatic analyses were performed with the help of Axel Weber (Rudolf Buchheim Institute for Pharmacology, Justus Liebig University Giessen).

6.9.2 Transcriptomic analyses

To compare the transcriptomic profiles of different cell lines and conditions, the mRNA expression profile can be determined via RNA sequencing. For transcriptomic analyses of SARS-CoV-2- and SARS-CoV-1-infected human cell lines, total cellular RNA was extracted from Calu-3, H1299 and A549-ACE2 cells that had been infected with SARS-CoV-2 or SARS-CoV-1 at an MOI of 1 for 24 h using the RNeasy® mini kit as described in chapter 6.7.2. Total RNA quantity was determined using a DS-11+ Spectrophotometer. To assess the quality of total RNA, Bioanalyzer 2100 Total RNA nano chip (Agilent) and reagents were used. Total RNA was depleted using NEBNext® rRNA Depletion Kit v2 (Human/Mouse/Rat; New England Biolabs). NEBNext® Ultra™ II Directional RNA Library Prep Kit for Illumina® (New England Biolabs) was applied for library preparation according to the manufacturer’s instructions. During this process, NEBNext® Multiplex Oligos for Illumina® (96 Unique Dual Index Primer Pairs; New England Biolabs) were chosen to facilitate multiplex sequencing. Libraries were purified with Agencourt AMPure XP Reagent (Beckman Coulter). Quality and quantity of the amplified cDNA was assessed with DNA High Sensitivity Kit (Agilent). Libraries were pooled,

denatured, and then diluted to 1.8 mM. For next generation sequencing, NextSeq 500/550 High Output Kit v2.5 (75 cycles) reagents were used (Illumina) to generate single-end reads.

After image processing, base calling, and demultiplexing of sequenced reads, fastQ-files were obtained and mapped against *Homo sapiens* (NCBI GCA_000001405.28 GRCh38.p13). Reads were aligned using CLC Main Workbench (Qiagen) and then sorted by position with SAMtools (Li *et al.* 2009). Read counts per gene and library were calculated using the subread function featureCounts (Liao *et al.* 2013). Differential expression analyses were performed in R using the package DESeq2 (Love *et al.* 2014). For visualisation the R packages, pheatmap (<https://cran.r-project.org/web/packages/pheatmap/index.html>), ggplot2, reshape2 (Wickham 2016), ggrepel (Slowikowski *et al.* 2021), EnhancedVolcano (Blighe *et al.* 2019) and RColorBrewer (Neuwirth 2011) were used. Data was normalized per ‘regularized log’ transformation and shrunk using the adaptive shrinkage estimator from the ashR package (Stephens 2016). Genes were considered differentially expressed when adjusted p value was below or equal to 0.05 and absolute log₂FoldChange was above 2.

RNA sequencing, transcriptomic and bioinformatic analyses were performed by Torsten Hain and Benjamin Ott (Institute of Medical Microbiology, Justus Liebig University Giessen).

7 Results

7.1 Innate immunity characterization of novel phlebovirus Ntepes virus (NTPV)

The novel phlebovirus Ntepes virus (NTPV) was recently isolated from sandflies collected in Kenya (Tchouassi *et al.* 2019). Although it can infect humans, its pathogenicity and impact on human health are unknown. This work provides the first assessment of the interplay of NTPV with the human innate immune response. The present characterization of NTPV includes the comparison to related known phleboviruses. For this, the closest known genetic relative to NTPV, Gabek Forest virus (GFV), was chosen. GFV was first isolated from animal tissue pools in 1961 (Kemp *et al.* 1974; Palacios *et al.* 2014) and is known to infect sandflies, rodents, and humans (Kemp *et al.* 1974; Tesh *et al.* 1976; Traoré-Lamizana *et al.* 2001). GFV produces fulminating fatal illness in hamsters (Tesh and Duboise 1987; Fisher *et al.* 2003) but its disease spectrum in humans is unknown. NTPV and GFV were further compared to two strains of the well-characterized phlebovirus Rift Valley fever virus (RVFV). RVFV was first discovered in 1930 in Kenya, is transmitted by mosquitoes and is implicated in severe veterinary and human disease in Africa and the Middle East (Linthicum *et al.* 2016). Infection in ruminants leads to abortion storms and often death of the affected animal; in humans RVFV causes periodic epidemics characterized by febrile illness that can progress to fatal hemorrhagic fevers (Linthicum *et al.* 2016; Wright *et al.* 2019), leading to a 20% fatality rate in hospitalized RVFV patients (Bird *et al.* 2009). Wildtype strains of RVFV are known to efficiently counteract the induction and effects of interferons (IFNs) via their main virulence factor NSs (Eifan *et al.* 2013; Wuerth and Weber 2016). Here, the RVFV vaccine strain MP-12 (Caplen *et al.* 1985) and the avirulent isolate termed clone 13 (CI13) were used, which is naturally attenuated through a mutation that leads to the expression of a non-functional, truncated version of the NSs protein (Muller *et al.* 1995). CI13 strongly activates the innate immune system and is known to be highly IFN-sensitive (Bouloy *et al.* 2001; Billecocq *et al.* 2004).

The here presented innate immunity characterization of NTPV aimed to describe this novel phlebovirus in terms of its induction of host innate immune genes, its sensitivity to type I and type III IFNs, and the characteristics of its virulence factor NSs. With this, comparing NTPV to the described well-characterized related viruses, the potential of NTPV to cause human disease was to be derived.

7.1.1 Human cell line susceptibility to NTPV and related phleboviruses

An initial study by Tchouassi and colleagues demonstrated the susceptibility of cell lines derived from a broad range of species to NTPV, as shown by productive virus growth on rodent, bat, and livestock cell lines, and also HEK293T cells as representative human cell line (Tchouassi *et al.* 2019).

To expand on the knowledge on the infectability of human cell lines, first the susceptibility of different human cell lines to NTPV and related phleboviruses was investigated. To this end, *in vitro* growth experiments were performed in five cell lines of four human tissues: liver (Huh7), lung (A549 and H1299), intestine (Caco-2), and kidney (HEK293).

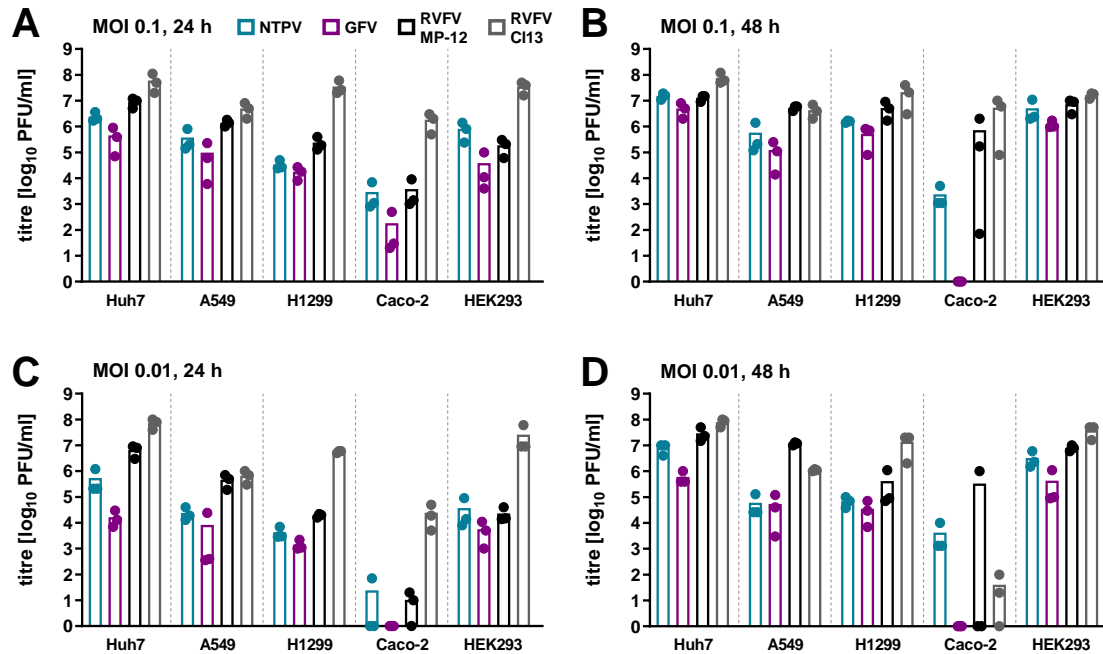


Figure 7: Human cell line susceptibility to NTPV and related phleboviruses. (A-D) Cells were infected with NTPV, GFV, RVPV MP-12 or RVPV C113 at an MOI of 0.1 or 0.01 and virus titres at 24 and 48 h post infection were assessed by plaque assay titration of supernatants. Individual titers (dots) and geometric mean values (bars) from three technical replicates are shown.

NTPV established productive infection in all tested cell lines at 24 and 48 h post infection, both at an intermediate (0.1) and low (0.01) multiplicity of infection (MOI) (Figure 7). Comparable virus titres, evaluated by plaque forming units (PFU) in the cell supernatant, were reached in Huh7, A549, H1299, and HEK293 cells, whereas titres in intestinal Caco-2 cells were consistently lower. GFV reached virus titres that were slightly lower but generally comparable to those of NTPV in all cell lines except for Caco-2 cells, where GFV was only detected at 24 h post infection at the intermediate MOI. RVPV viruses, as expected, productively infected Huh7, A549, H1299, and HEK293 cell lines, with RVPV C113 exhibiting an overall better growth than RVPV MP-12. In Caco-2 cells, both RVPV strains established reliable infection only at the intermediate MOI.

With this, a broad susceptibility of cell lines derived from different human tissues to NTPV and GFV was shown, comparable to RVPV.

7.1.2 Differential regulation of innate immune genes upon phlebovirus infection

Upon virus infection, cells rely on the rapid production of IFNs and other innate immune genes for efficient containment of early infection. To inhibit the spread of intruding viruses, IFNs and cytokines act on neighbouring cells to induce an antiviral state.

Therefore, the differential regulation of IFN and cytokine genes, as well as IFN-stimulated genes (ISGs) was examined upon infection with NTPV and related phleboviruses. For this, a set of host genes indicative of virus infection was compiled based on previous studies. This set of marker genes includes representative interferons IFN- β , IFN- λ 1 and IFN- λ 2 and cytokines CCL4, CCL5, CXCL10 (IP-10), IL-6, IL-8 (CXCL8), TNF- α and TNFSF10 (TRAIL) (Zhou *et al.* 2017; Sjaastad *et al.* 2018; Hölzer *et al.* 2019), as well as ISGs CH25H, IFIT1 (ISG56), ISG15, Mx1, OAS proteins, PARP14 and RSAD2 (Viperin) (Zhou *et al.* 2017; Shaw *et al.* 2017; Levitz *et al.* 2017; Sjaastad *et al.* 2018; Hölzer *et al.* 2019; Aso *et al.* 2019).

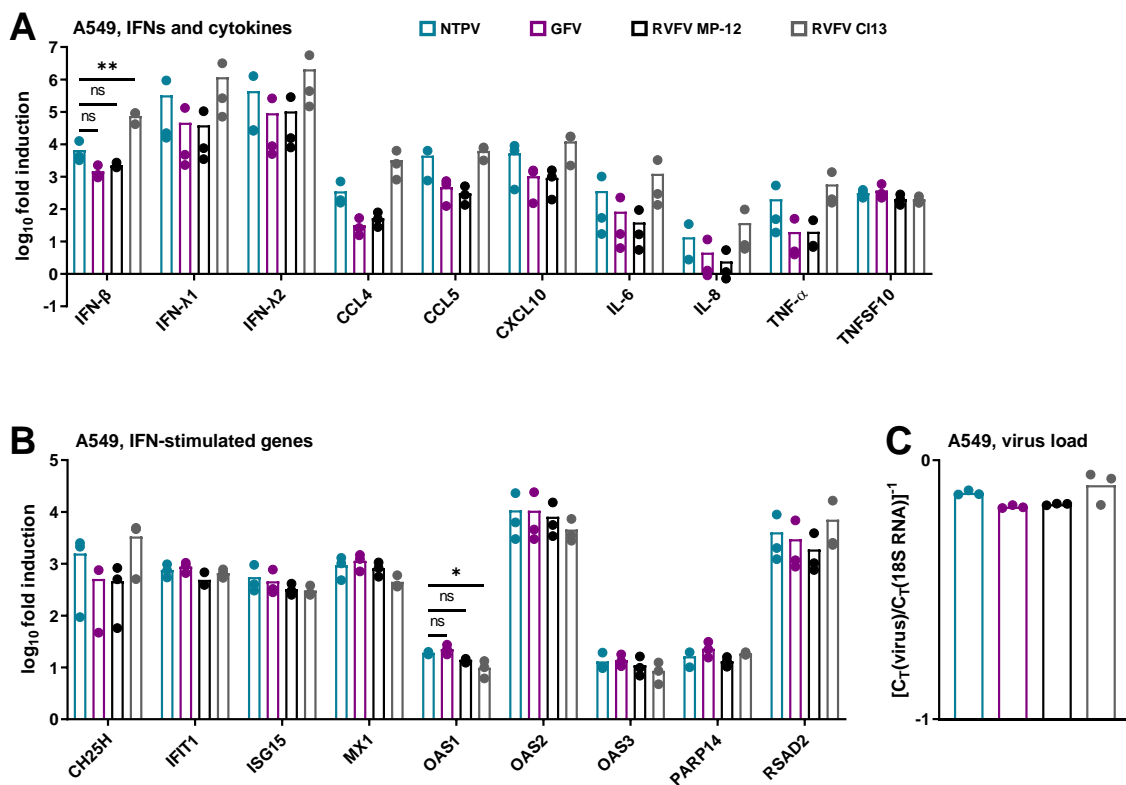


Figure 8: Differential regulation of innate immune genes upon phlebovirus infection. A549 cells were infected with NTPV, GFV, RVFV MP-12 or RVFV C113 at an MOI of 1 and harvested at 16 h post infection. Gene expression of select IFN and cytokine genes (A) and ISGs (B) was measured by quantitative real-time PCR analysis. Differential gene expression was calculated using the $\Delta\Delta C_T$ method and results are given as fold-induction over the uninfected mock control. 18S rRNA was used as a reference gene. Viral gene expression (C) is pictured as C_T value for viral L segment normalized to 18S rRNA control. Individual (dots) and geometric mean values (bars) from three biological replicates are shown. Values were analyzed by ordinary one-way ANOVA with Dunnett's post-test compared to NTPV. * $P < 0.0332$; ** $P < 0.0021$; ns, not significant (Graphpad Prism). No statistical information is given for genes where statistical significance compared to NTPV was not reached.

To evaluate the induction of innate immune genes upon phlebovirus infection, A549 cells were infected with a high MOI of 1 for 16 h and subsequently qRT-PCR was performed for the indicated genes. A549 cells were chosen for this assay because they have been shown to present a solid antiviral response upon infection (Sutejo *et al.* 2012). NTPV infection of A549 cells elicited an immune response lower than attenuated RVFV C113, which has previously been shown to be an excellent inducer of innate immune genes (Billecocq *et al.* 2004) but higher than GFV and RVFV MP-12: all tested IFN and cytokine genes were most strongly induced by RVFV C113 infection, followed by NTPV infection, except for TNFSF10 (TRAIL) which was induced to the same degree by all four phleboviruses (**Figure 8A**). IFN and cytokine gene induction by GFV was similar to that of RVFV MP-12 infection, and generally reduced by approximately one log compared to NTPV and RVFV C113 (**Figure 8A**). In contrast, ISGs were equally induced by all tested viruses with the exception of CH25H, where expression was again higher upon NTPV and RVFV C113 infection (**Figure 8B**). While gene induction upon NTPV infection did not reach statistical significance compared to GFV and RVFV MP-12, a trend points to higher IFN and cytokine gene induction in NTPV than in GFV and MP-12 infection. Notably, virus loads mimicked the gene induction pattern observed for IFNs and most cytokines (**Figure 8C**); however, since this induction pattern is not consistent (see TNFSF10, ISGs), the here presented data suggest that viral loads are not exclusively linked to the observed gene induction profiles.

7.1.3 Sensitivity of NTPV and related phleboviruses to type I and type III IFN

IFNs signal through their respective receptors to induce a vast number of ISGs. Pathogenic viruses are able to counteract IFN induction and signalling and thus circumvent the host immune system to gain a growth advantage.

Thus, in a next step, the sensitivity of NTPV and related phleboviruses to type I and type III interferons (IFNs) was investigated. For this, responses in the Huh7 hepatocyte-derived liver cell line and the A549 epithelial lung cell line were compared. Both cell lines express type I and III IFN receptors, and respond well to exogenously added type I and III IFNs (Bolen *et al.* 2014; Gerlach *et al.* 2017). Type I and type III IFNs induce a similar subset of genes but differ in their receptor distribution (chapters 4.1.1 and 4.1.3). While type I IFN (IFN- α/β) acts on the IFN- α receptor (IFNAR) that is ubiquitously present on most cell types, type III IFNs (IFN- $\lambda 1-4$) signal through the IFN- λ receptor (IFNLR) expressed almost exclusively on epithelial surfaces. Compared to type I IFN, type III IFN induces a weaker but longer-lasting immune response (Stanifer *et al.* 2019). Here cells were pre-treated for 16 h with IFN- α or IFN- λ and NTPV, GFV, and RVFV growth was evaluated after 24 and 48 h of infection.

Upon pre-treatment of Huh7 cells with IFN- α , 24 h post infection only RVFV strain MP-12 displayed a significant titre reduction (**Figure 9A**). However, this inhibition was fully compensated at 48 h post infection where comparable virus titres were reached in the presence and absence of IFN- α (**Figure 9B**).

In fact, only NTPV and GFV titres were significantly reduced by pre-treatment with IFN- α of Huh7 cells 48 h post infection (**Figure 9B**). By contrast, pre-treatment of A549 cells with IFN- α led to a strong titre reduction of all tested viruses at 24 h of infection, with NTPV being inhibited in a manner comparable to attenuated RVFV C113, and GFV and RVFV MP-12 to a lesser degree (**Figure 9C**). While this inhibition was partially compensated at 48 h post infection, titres of all tested viruses were still significantly reduced at this later timepoint (**Figure 9D**).

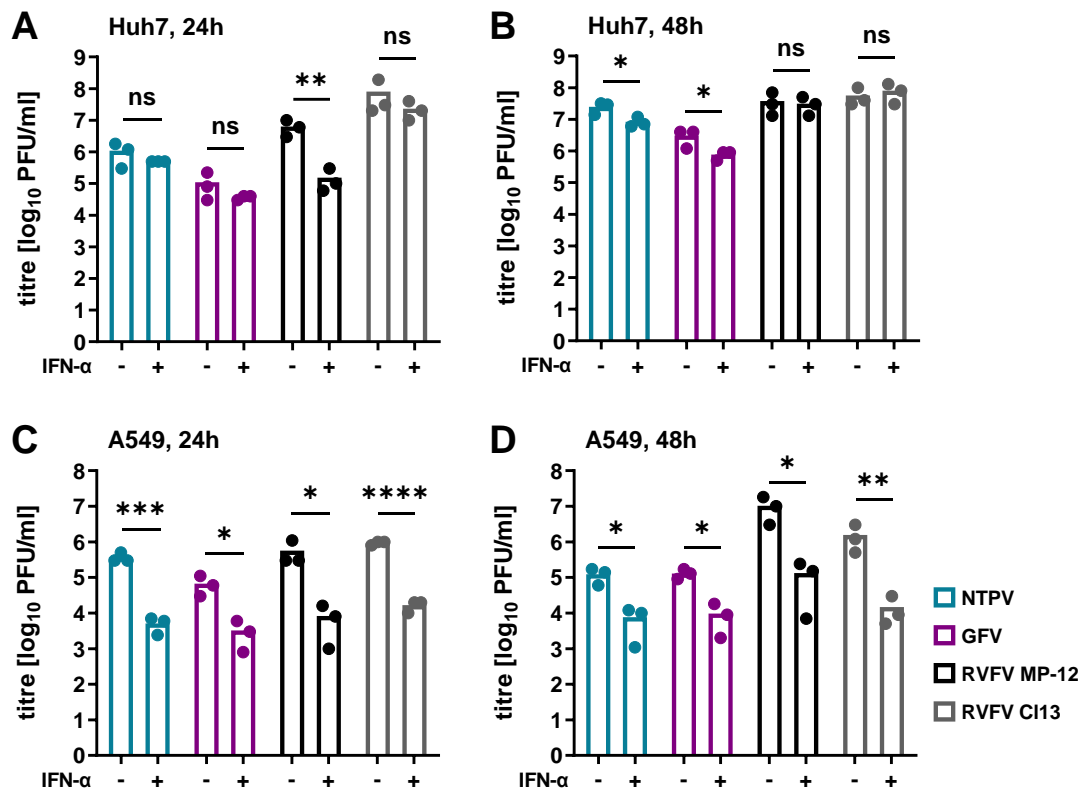


Figure 9: Sensitivity of phleboviruses to type I interferon. Huh7 (**A, B**) and A549 (**C, D**) cells were pre-treated with 1,000 U/ml recombinant IFN- α (**B, D**) for 16 h and infected with NTPV, GFV, RVFV MP-12 or RVFV C113 at an MOI of 0.01. Virus titres at 24 h (**A, C**) and 48 h (**B, D**) post infection were assessed by plaque assay titration of supernatants. Individual titers (dots) and geometric mean values (bars) from three biological replicates are shown. Log-transformed titres were analyzed by unpaired one-tailed Student's t test. * $P < 0.0332$; ** $P < 0.0021$; *** $P < 0.0002$; **** $P < 0.0001$; ns, not significant (Graphpad Prism).

Pre-treatment with IFN- λ had no effect on the replication of any tested phlebovirus in Huh7 cells at either timepoint (**Figure 10A, B**), although these cells are known to respond to type III IFN, albeit to a lesser degree than to type I IFN (Bolen *et al.* 2014). However, pre-treatment of A549 cells with IFN- λ caused a significant titre reduction at 24 h of all tested viruses with RVFV C113 growth being inhibited most consistently (**Figure 10C**). At 48 h post infection, only RVFV MP-12 was able to compensate type III IFN action as demonstrated by non-significant titre differences in the presence and absence of IFN- λ . NTPV, GFV, and RVFV C113 growth was still significantly inhibited at this timepoint (**Figure 10D**).

Consequently, NTPV replication is sensitive to exogenously added IFNs of type I and III, in a manner comparable to attenuated RVFV C113 strain, and this sensitivity, to some extent, is cell-line dependent.

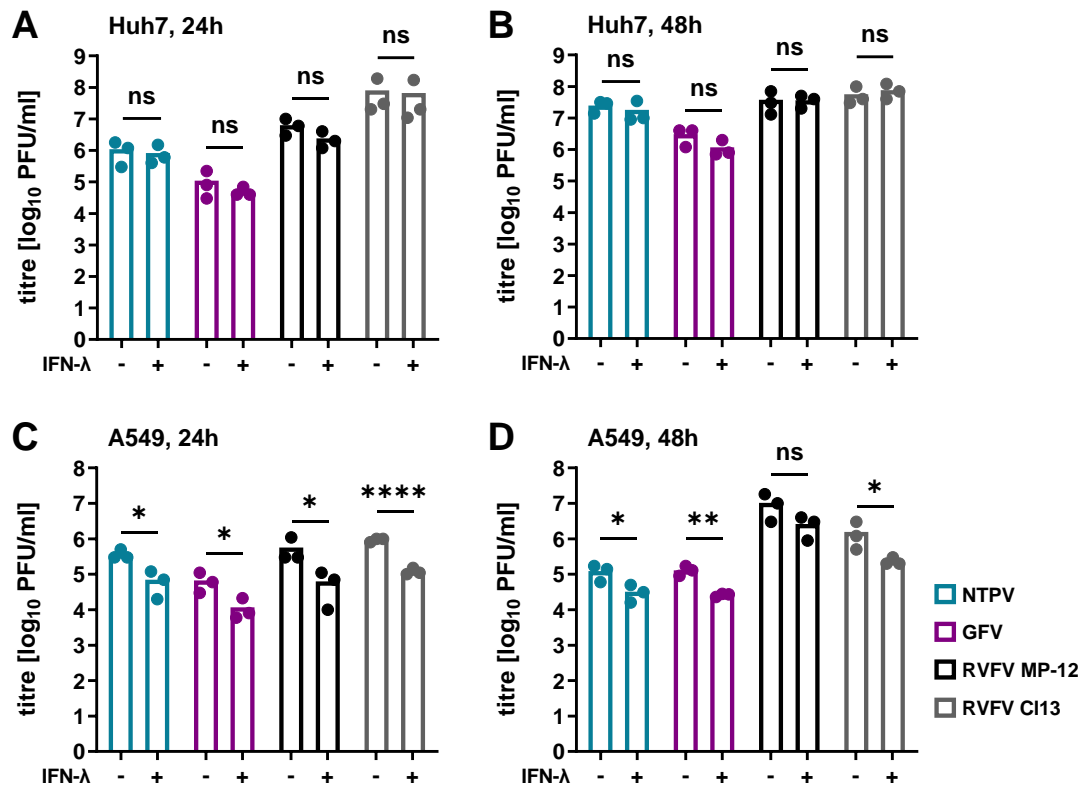


Figure 10: Sensitivity of phleboviruses to type III interferon. Huh7 (A, B) and A549 (C, D) cells were pre-treated with 100 ng/ml recombinant IFN-λ3 for 16 h and infected with NTPV, GFV, RVFV MP-12 or RVFV C113 at an MOI of 0.01. Virus titres at 24 h (A, C) and 48 h (B, D) post infection were assessed by plaque assay titration of supernatants. Individual titers (dots) and geometric mean values (bars) from three biological replicates are shown. Log-transformed titres were analyzed by unpaired one-tailed Student's t test. *P<0.0332; **P<0.0021; ****P<0.0001; ns, not significant (Graphpad Prism).

7.1.4 Effect of the JAK/STAT inhibitor Ruxolitinib on NTPV replication

Since IFN induction during NTPV infection and the sensitivity of NTPV to exogenously added IFN were demonstrated, it was hypothesized that blocking IFN signalling would augment virus replication.

To investigate this, inhibitor studies with the FDA (U.S. Food and Drug Administration)-approved drug Ruxolitinib were performed. This compound interferes with type I and III IFN signalling by targeting IFN-receptor associated Janus kinases (JAK)1/2 (Davis *et al.* 2011). Huh7 liver cells and A549 lung cells were pre-treated with Ruxolitinib for 16 h and virus titres were evaluated at 24 and 48 h post infection. In Huh7 cells, treatment with Ruxolitinib had no effect on the replication of either phlebovirus (Figure 11A – D). In contrast, in A549 cells, NTPV replication was significantly boosted upon Ruxolitinib treatment at 48 h post infection (Figure 11E), comparable to RVFV C113 (Figure 11H). On the other hand, neither GFV (Figure 11F) nor RVFV MP-12 titres (Figure 11G) were appreciably affected by Ruxolitinib treatment.

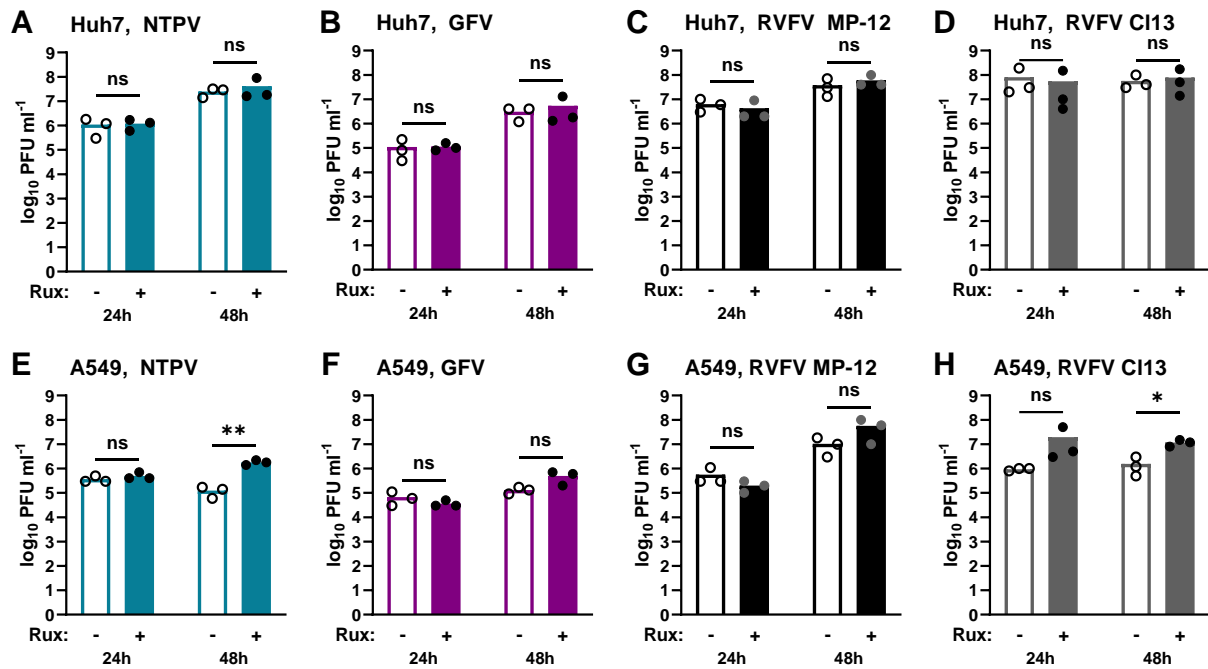
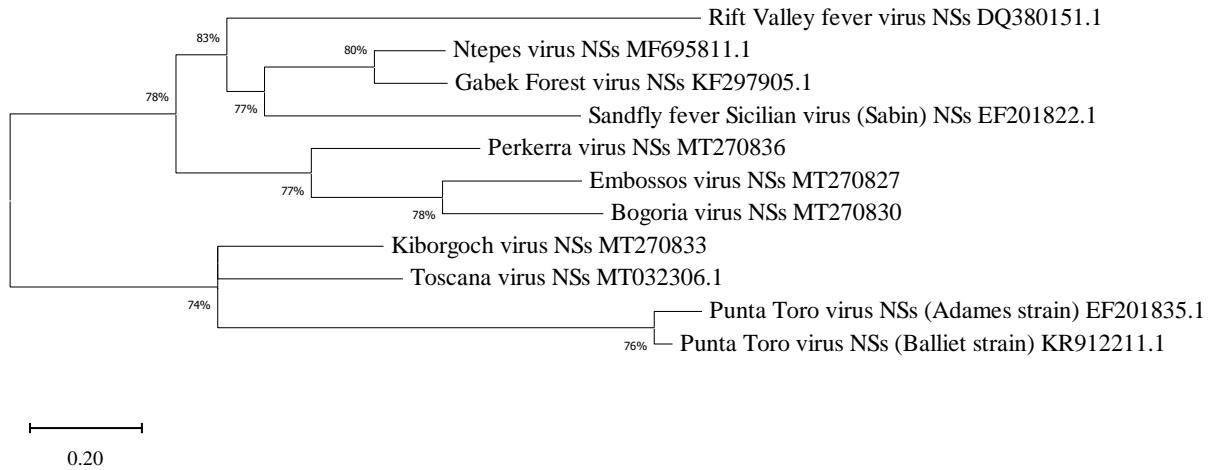


Figure 11: Effect of the JAK/STAT inhibitor Ruxolitinib on phlebovirus replication. Huh7 (A-D) and A549 (E-H) cells were pre-treated with 1 μ M Ruxolitinib (Rux) for 16 h, infected with NTPV, GFV, RVFV MP-12 or RVFV CI13 at an MOI of 0.01, and titers were determined at 24 and 48 h post infection by plaque assay titration of supernatants. Individual titers (dots) and geometric mean values (bars) from three biological replicates are shown. Log-transformed titres were analyzed by unpaired two-tailed Student's t test. * $P < 0.0332$; ** $P < 0.0021$; ns, not significant (Graphpad Prism).

These findings further support the evidence that NTPV is sensitive to type I and III IFNs, comparable to attenuated RVFV CI13, and that blocking of IFN signalling gives the virus a notable growth advantage.

7.1.5 Characterization of virulence factor NSs of novel phleboviruses

The next focus lay on the characterization of the virulence factor NSs of novel phleboviruses. For this, the NSs query spectrum was expanded by including NSs proteins of additional newly found phleboviruses, termed Embossos virus (EMBV), Bogoria virus (BGRV), Perkerra virus (PERV) and Kiborgoch virus (KBGV). Those viruses were discovered during another sandfly screening study conducted in Kenya in 2015/16 (Marklewitz *et al.* 2020 and chapter 4.2.4); however, to date none of those four additional viruses have been successfully isolated. Complete genome sequencing and phylogenetic analyses showed the first three forming a monophyletic sister clade to the Sandfly fever Sicilian virus (SFSV) clade, whereas the latter was found to be related to Toscana virus (TOSV) (Marklewitz *et al.* 2020 and **Figure 12**, top panel). NSs proteins are generally not well conserved on the amino acid level, as visualized by amino acid identity profiles in **Figure 12**, bottom panel. They serve heterogeneous functions, often involved in antagonism of the host innate immune response (chapter 4.2.5).



Amino acid identity (%)

NSs	NTPV	GFV	EMBV	BGRV	KBGV	PERV	SFSV	RVFV	PTV-A	PTV-B	TOSV
NTPV	100										
GFV	90	100									
EMBV	25	27	100								
BGRV	28	29	59	100							
KBGV	19	18	17	16	100						
PERV	30	31	39	41	18	100					
SFSV	31	29	26	23	17	26	100				
RVFV	27	27	21	23	17	24	25	100			
PTV-A	25	26	23	24	16	25	22	22	100		
PTV-B	25	25	25	25	15	26	22	21	96	100	
TOSV	15	15	17	15	50	15	14	14	13	13	100
	NTPV	GFV	EMBV	BGRV	KBGV	PERV	SFSV	RVFV	PTV-A	PTV-B	TOSV

Figure 12: Phylogenetic relationship and amino acid sequence identity of phlebovirus NSs proteins.
Top: The evolutionary history of select phlebovirus NSs proteins was inferred by using the Maximum Likelihood method and Tamura-Nei model (Tamura and Nei 1993). The tree with the highest log likelihood (-9830.13) is shown. The percentage of trees in which the associated taxa clustered together is shown next to the branches. Initial tree(s) for the heuristic search were obtained automatically by applying Neighbour-Join and BioNJ algorithms to a matrix of pairwise distances estimated using the Maximum Composite Likelihood (MCL) approach, and then selecting the topology with superior log likelihood value. The tree is drawn to scale, with branch lengths measured in the number of substitutions per site. The proportion of sites where at least 1 unambiguous base is present in at least 1 sequence for each descendent clade is shown next to each internal node in the tree. This analysis involved 11 nucleotide sequences. Codon positions included were 1st+2nd+3rd+Noncoding. There were a total of 995 positions in the final dataset. Evolutionary analyses were conducted in MEGA X (Kumar *et al.* 2018). Gen bank accession numbers are shown in addition to virus name. **Bottom:** Amino acid sequence identity of select phlebovirus NSs proteins was calculated as percent identity matrix by Clustal X 2.1 (Larkin *et al.* 2007). The sequences used were the same as in the top panel. Cell colour indicates the level of amino acid sequence identity; light grey, low; dark grey, high.

7.1.5.1 Novel phlebovirus NSs proteins antagonize IFN-β activation

Several phlebovirus NSs proteins are known to antagonize IFN-β promoter activation through distinct mechanisms. For instance, the potent RVFV NSs was shown to cause a general block of host transcription (Billecocq *et al.* 2004) while additionally inhibiting IFN activation by stabilizing a repressor complex on the IFN-β promoter (Le May *et al.* 2008). Additionally, SFSV NSs was

demonstrated to interfere with IFN- β promoter activation by obscuring the DNA-binding domain of transcription factor IRF3 (Wuerth *et al.* 2018).

To evaluate if NSs proteins of novel phleboviruses can also antagonize the transcriptional induction of IFN- β , a reporter system was employed which is based on luciferase expression under the control of the IFN- β promoter. For this, reporter constructs were co-transfected with expression constructs for native NSs proteins of NTPV, GFV, EMBV, BGRV, KBGV and PERV. As negative controls an empty vector plasmid as well as a plasmid coding for a C-terminally truncated, non-functional Mx1 protein, termed Δ Mx, were used. RVFV and SFSV NSs expression constructs were included as positive controls. Reporter gene expression was stimulated by mimicking virus infection through Vesicular stomatitis virus (VSV)-RNA transfection.

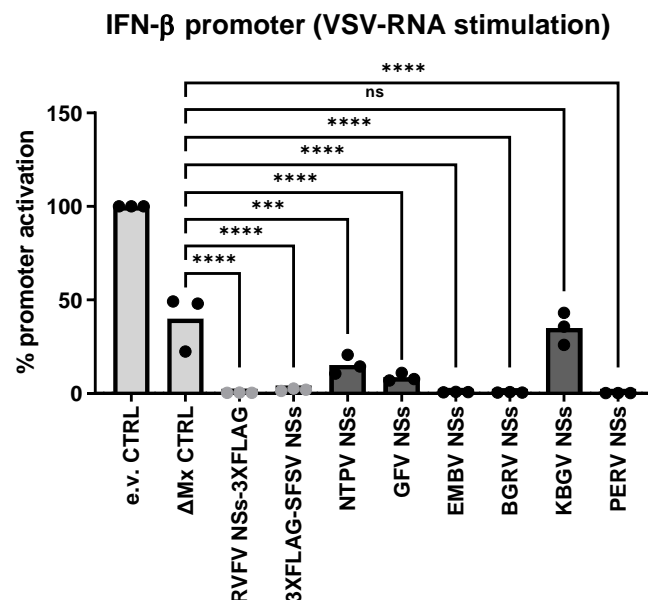


Figure 13: Antagonistic effect on IFN- β promoter induction of virulence factor NSs of novel phleboviruses. HEK293 cells were transfected with expression plasmids for untagged NSs of NTPV, GFV, EMBV, BGRV, KBGV, PERV, or 3 \times FLAG-tagged NSs of RVFV, SFSV or inactive control Δ Mx, or with empty pL18 vector (e.v.; 10 ng each), as well as stimulation-dependent firefly luciferase and constitutively active *Renilla* luciferase reporters. Firefly luciferase was under the control of the IFN- β promoter. 24 h post transfection, promoter activation was induced by VSV-RNA transfection (50 ng/well). Cell lysates were harvested 18 h after stimulation for dual-luciferase assays. Firefly luciferase values of unstimulated control samples were subtracted from values of stimulated samples, and the resulting values for the empty vector control were set to 100% within each biological replicate. Individual values (dots) and geometric mean values (bars) from three biological replicates are shown. Values were analyzed by ordinary one-way ANOVA with Dunnett's post-test compared to Δ Mx control. ***P<0.0002; ****P<0.0001; ns, not significant (Graphpad Prism).

Novel phlebovirus NSs proteins were able to counteract IFN- β promoter activation with the exception of KBGV NSs, which showed no effect (Figure 13). EMBV, BGRV and PERV NSs showed the greatest inhibitory effect, which was comparable to full inhibition by RVFV and SFSV NSs controls. NTPV and GFV NSs reduced IFN- β promoter activation, however to a lesser extent.

7.1.5.2 *Novel phlebovirus NSs proteins antagonize IFN- β activation at different signalling steps*

Mechanisms of IFN- β promoter inhibition by viral NSs proteins are manifold. Therefore, in a next step, the target of each NSs was to be pinpointed within the viral RNA-induced signalling cascade leading to IFN- β promoter induction. Viral RNA in the cytoplasm is detected by PRRs RIG-I or MDA5. Activation of these sensors promotes their CARD domain-mediated association with the adapter molecule MAVS, located on the outer mitochondrial membrane. This interaction triggers a signalling cascade involving TBK1, MAPK and IKK family kinases, which culminates in the activation of transcription factors IRF3 and IRF7, AP-1 and NF- κ B (Levy *et al.* 2011; Goubau *et al.* 2013 and chapter 4.1.2.2). Upon nuclear translocation, concerted action of these transcription factors induces IFN- β gene expression (Iversen and Paludan 2010). However, IRF3 alone can also induce IFN- β gene transcription (Jennings *et al.* 2005).

To address the question at which step the novel phlebovirus NSs proteins interfere with this signalling cascade, the same luciferase reporter system was employed as presented above. However, instead of using VSV-RNA, promoter induction was stimulated at consecutive steps of the RLR signalling pathway. This was achieved by co-transfection with either (i) a constitutively active truncated RIG-I consisting of the CARD domains, (ii) the adapter molecule MAVS, (iii) the kinase TBK1, or (iv) a constitutively active form of the transcription factor IRF3 [IRF3(5D)]. Of note, KBGV NSs was omitted for this essay because of its lack of effect in the previous experiment.

Stimulation of IFN- β promoter activation using overexpression of the RIG-I CARD domains (**Figure 14A**) was efficiently counteracted by NSs proteins of all tested phleboviruses. Stimulation of IFN- β promoter activation using overexpression of MAVS (**Figure 14B**) led to a reduction in NTPV and GFV NSs antagonistic effect; however, IFN- β promoter activation was still reduced compared to controls. EMBV, BGRV and PERV NSs still efficiently counteracted MAVS-induced IFN- β promoter activation. Stimulation of IFN- β promoter activation using overexpression of TBK1 (**Figure 14C**) completely abolished the ability to counteract promoter induction for NTPV and GFV NSs as well as for EMBV NSs. This suggests that these three NSs proteins target IFN- β induction upstream of TBK1 and probably downstream of MAVS. Stimulation of IFN- β promoter activation using overexpression of IRF3 (**Figure 14D**) could only be counteracted by RVFV and SFSV NSs, as expected, however none of the novel phlebovirus NSs showed any effect at this stage. Therefore, BGRV and PERV NSs proteins act upstream of IRF3 but downstream of TBK1.

Figure 14E schematically depicts the respective target steps of phlebovirus NSs proteins within the RIG-I signalling cascade to antagonize IFN- β promoter activation, as inferred from the described experiments. Question marks indicate that the exact step at which NTPV and GFV NSs proteins counteract IFN- β promoter activation could not be exclusively deduced from the presented experiments, as stimulation with MAVS lowered, but did not abrogate, IFN- β promoter inhibition.

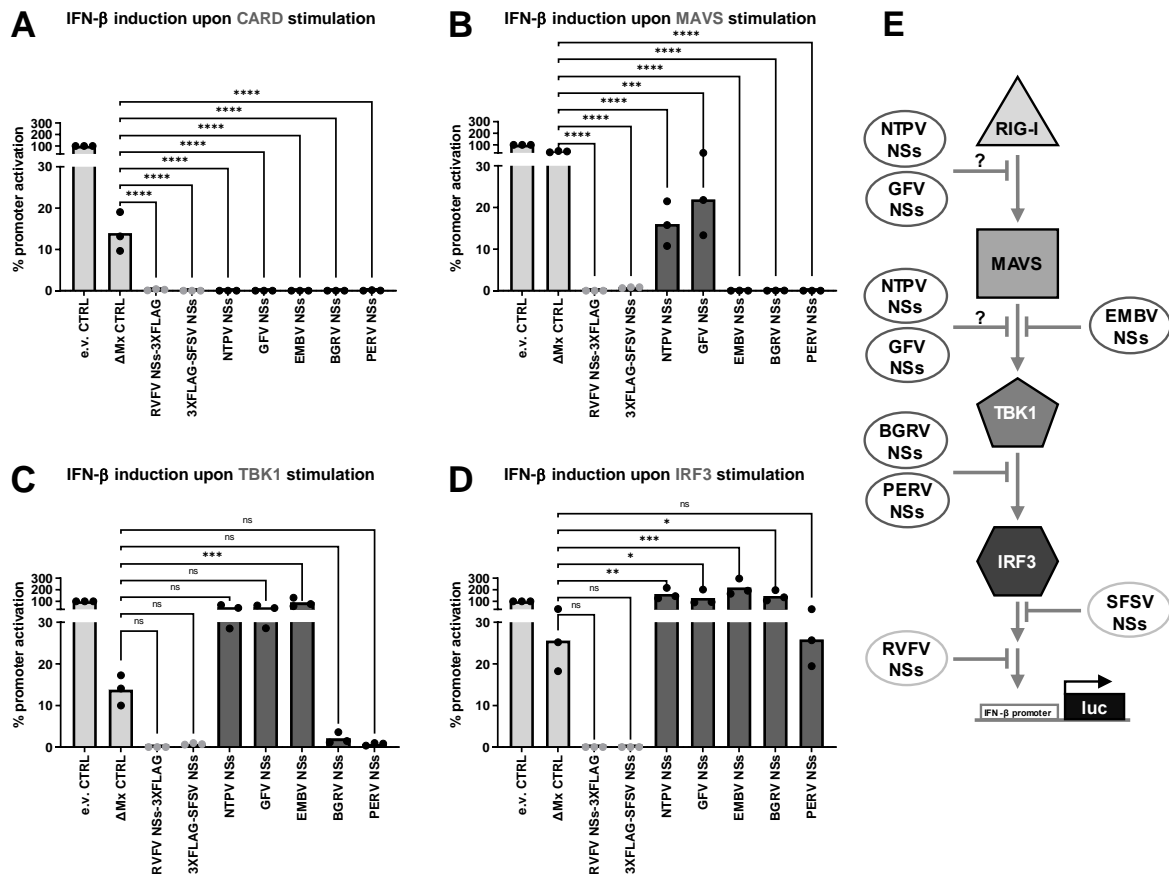


Figure 14: Antagonistic effect on pattern recognition receptor signalling cascade of virulence factor NSs of novel phleboviruses. HEK293 cells were transfected with expression plasmids for (A) RIG-I CARD, (B) MAVS, (C) TBK1 or (D) IRF3(5D-97A) (40 ng); untagged NSs of NTPV, GFV, EMBV, BGRV, PERV, or 3×FLAG-tagged NSs of RVFV, SFSV or inactive control Δ Mx, or with empty pI.18 vector (e.v.; 10 ng each), as well as stimulation-dependent firefly luciferase under the control of the IFN- β promoter, and constitutively active *Renilla* luciferase reporters. Cell lysates were harvested 24 h after transfection for dual-luciferase assays. Firefly luciferase values of unstimulated control samples were subtracted from values of stimulated samples, and the resulting values for the empty vector control were set to 100% within each biological replicate. Individual values (dots) and geometric mean values (bars) from three biological replicates are shown. Values were analyzed by ordinary one-way ANOVA with Dunnett's post-test compared to Δ Mx control. * $P < 0.0332$; ** $P < 0.0021$; *** $P < 0.0002$; **** $P < 0.0001$; ns, not significant (Graphpad Prism). (E) Schematic pattern recognition receptor signalling cascade with novel phlebovirus NSs targets as inferred from A–D. luc, luciferase.

7.1.5.3 Novel phlebovirus NSs proteins weakly antagonize dsRNA induced ISG54 expression

Innate immune gene promoters differ in their transcription factor binding sites. To expand on the IFN- β promoter activation data (chapters 7.1.5.1 and 7.1.5.2), the antagonism of another virus-induced innate immune gene, ISG54 (coding for IFIT2) by phlebovirus NSs proteins was evaluated. In contrast to the IFN- β promoter, the ISG54 promoter contains both an IRF3 binding site and an IFN-stimulated response element (ISRE; Daffis *et al.* 2007; Fensterl and Sen 2011), and is thus responsive to virus infection as well as to IFN stimulation.

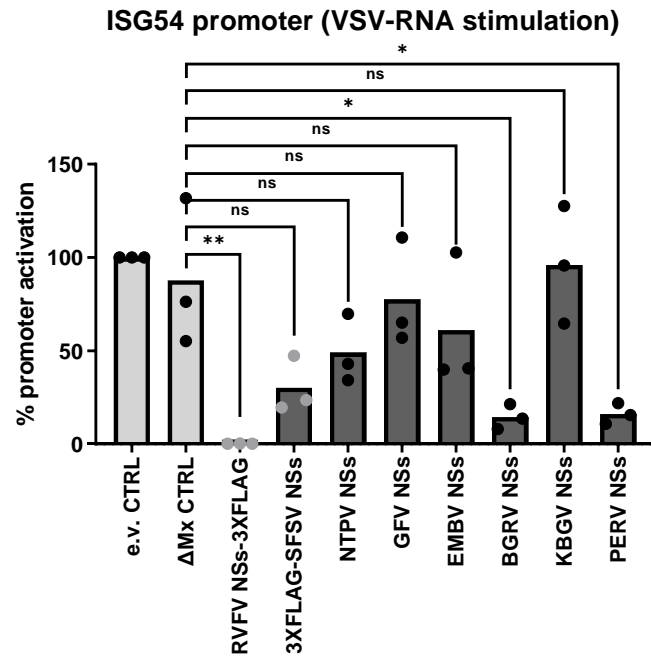


Figure 15: Antagonistic effect on ISG54 promoter induction of virulence factor NSs of novel phleboviruses. HEK293 cells were transfected with expression plasmids for untagged NSs of NTPV, GFV, EMBV, BGRV, KBGV, PERV, or 3×FLAG-tagged NSs of RVFV, SFSV or inactive control ΔMx, or with empty pL18 vector (e.v.; 10 ng each), as well as stimulation-dependent firefly luciferase and constitutively active *Renilla* luciferase reporters. Firefly luciferase was under the control of the ISG54 promoter. 24 h post transfection, promoter activation was induced by VSV-RNA transfection (50 ng/well). Cell lysates were harvested 18 h after stimulation for dual-luciferase assays. Firefly luciferase values of unstimulated control samples were subtracted from values of stimulated samples, and the resulting values for the empty vector control were set to 100% within each biological replicate. Individual values (dots) and geometric mean values (bars) from three biological replicates are shown. Values were analyzed by ordinary one-way ANOVA with Dunnett's post-test compared to ΔMx control. *P<0.0332; **P<0.0021; ns, not significant (Graphpad Prism).

In this scenario, RVFV NSs again fully inhibited ISG54 promoter induction upon VSV-RNA stimulation, while SFSV NSs showed a modest interference that was not statistically significant but repeatedly observed across replicate experiments (**Figure 15**). In fact, only BGRV and PERV NSs proteins could successfully counteract ISG54 promoter activation upon VSV-RNA stimulation. NTPV NSs showed a limited reduction of promoter activation, which, like in the case of SFSV NSs, was not statistically significant. GFV, EMBV and KBGV NSs had no effect on VSV-RNA induced ISG54 promoter activation. Hence, BGRV and PERV NSs proteins seem to act more broadly on innate immune promoters than the other tested novel NSs proteins.

7.1.5.4 Novel phlebovirus NSs proteins antagonize NF-κB-dependent gene induction

In addition to IRF3 activation, virus infection also leads to the induction of the transcription factor NF-κB (Goubau *et al.* 2013). In contrast to IRF-driven antiviral genes, NF-κB mainly induces genes that are involved in inflammation (Liu *et al.* 2017b). To determine if novel phlebovirus NSs proteins are also able to antagonize NF-κB-dependent promoter induction, luciferase reporter assays were repeated with

an NF- κ B-dependent promoter construct. Upon stimulation with VSV-RNA, NF- κ B-dependent promoter induction was efficiently abrogated in the presence of RVFV NSs, as expected (**Figure 16A**). SFSV NSs had no effect, confirming previous reports (Wuerth *et al.* 2018). Also, no impact was seen with NTPV and KBGV NSs proteins. In contrast, PERV NSs demonstrated complete antagonism of NF- κ B-driven genes upon viral RNA stimulation, while GFV, EMBV and BGRV NSs proteins exhibited a moderate counteraction.

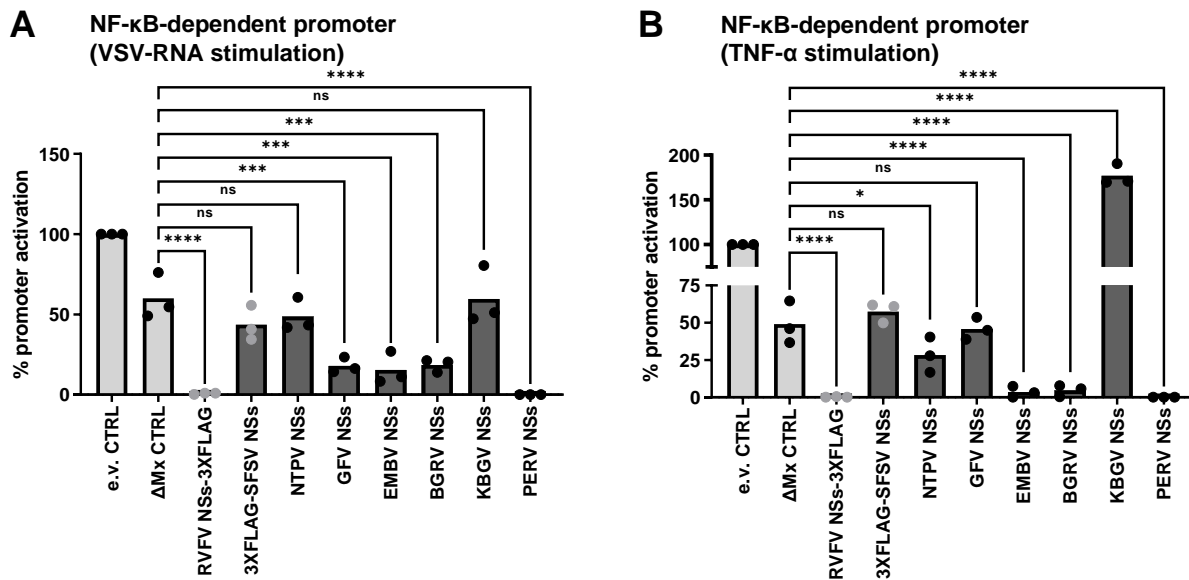


Figure 16: Antagonistic effect on NF- κ B-dependent promoter induction of virulence factor NSs of novel phleboviruses. HEK293 cells were transfected with expression plasmids for untagged NSs of NTPV, GFV, EMBV, BGRV, KBGV, PERV, or 3 \times FLAG-tagged NSs of RVFV, SFSV or inactive control Δ Mx, or with empty pI.18 vector (e.v.; 10 ng each), as well as stimulation-dependent firefly luciferase and constitutively active *Renilla* luciferase reporters. Firefly luciferase was under the control of an NF- κ B-dependent promoter. 24 h post transfection, promoter activation was induced by VSV-RNA transfection (**A**; 50 ng/well) or TNF- α (**B**; 10 ng/ml). Cell lysates were harvested 18 h after stimulation for dual-luciferase assays. Firefly luciferase values of unstimulated control samples were subtracted from values of stimulated samples, and the resulting values for the empty vector control were set to 100% within each biological replicate. Individual values (dots) and geometric mean values (bars) from three biological replicates are shown. Values were analyzed by ordinary one-way ANOVA with Dunnett's post-test compared to Δ Mx control. * $P < 0.0332$; *** $P < 0.0002$; **** $P < 0.0001$; ns, not significant (Graphpad Prism).

In addition to virus infection, NF- κ B-dependent transcripts are also induced upon signalling downstream of the inflammatory cytokine TNF- α . In this case, NF- κ B-dependent promoter activation upon TNF- α stimulation was fully antagonized by RVFV NSs, as well as by EMBV, BGRV and PERV NSs proteins (**Figure 16B**). NTPV NSs had a modest inhibitory effect, while SFSV, GFV and KBGV NSs showed no effect.

7.1.5.5 Novel phlebovirus NSs proteins antagonize IFN signalling

Type I IFN secreted upon virus infection acts on neighbouring cells to induce an antiviral state. IFN-binding to its cognate receptor triggers a JAK/STAT-mediated signalling cascade culminating in the

activation of the transcription factor ISGF3, consisting of STAT1, STAT2 and IRF9. ISGF3 binds to ISRE sites of promoter regions, thus upregulating a vast repertoire of antiviral and other ISGs (Ivashkiv and Donlin 2014 and chapter 4.1.3). To determine the influence of novel phlebovirus NSs proteins on IFN signalling, NSs influence on IFN- α -stimulated luciferase reporter constructs was evaluated: one under the control of the Mx1 promoter, which is purely IFN-driven, and another under the control of the ISG54-promoter, which is activated upon PRR- as well as IFN-signalling (see **Figure 15**).

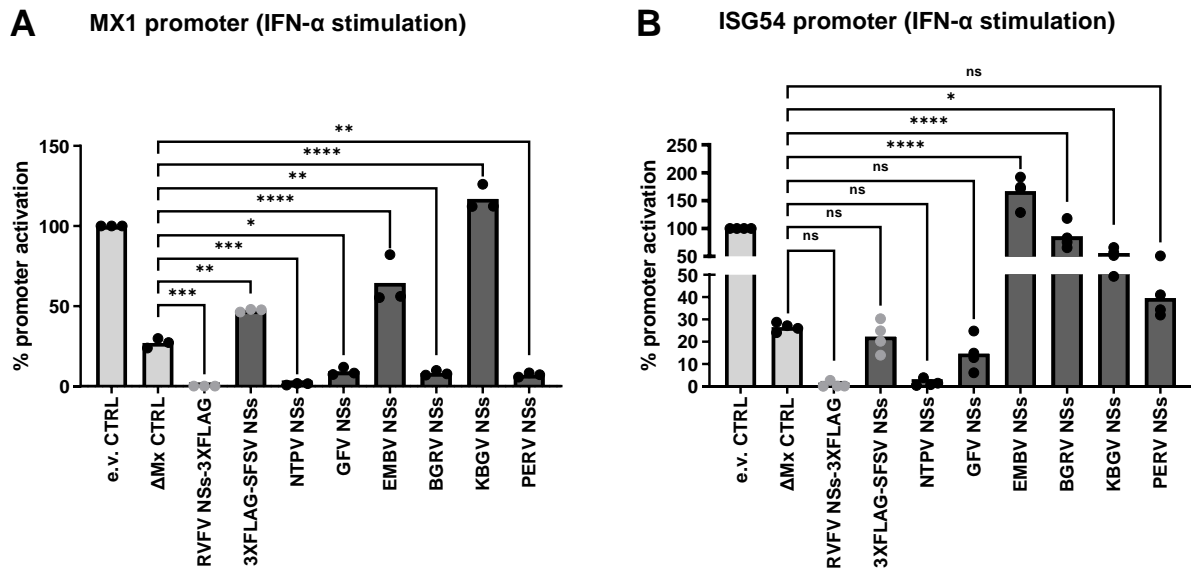


Figure 17: Antagonistic effect on type I IFN signalling of virulence factor NSs of novel phleboviruses. HEK293 cells were transfected with expression plasmids for untagged NSs of NTPV, GFV, EMBV, BGRV, KBGV, PERV, or 3 \times FLAG-tagged NSs of RVFV, SFSV or inactive control Δ Mx, or with empty pL18 vector (e.v.; 10 ng each), as well as stimulation-dependent firefly luciferase and constitutively active *Renilla* luciferase reporters. Firefly luciferase was under the control of (A) the Mx1 promoter or (B) the ISG54 promoter. 24 h post transfection, promoter activation was induced by IFN- α (B/D) (50 U/well). Cell lysates were harvested 18 h after stimulation for dual-luciferase assays. Firefly luciferase values of unstimulated control samples were subtracted from values of stimulated samples, and the resulting values for the empty vector control were set to 100% within each biological replicate. Individual values (dots) and geometric mean values (bars) from three or four biological replicates are shown. Values were analyzed by ordinary one-way ANOVA with Dunnett's post-test compared to Δ Mx control. * $P < 0.0332$; ** $P < 0.0021$; *** $P < 0.0002$; **** $P < 0.0001$; ns, not significant (Graphpad Prism).

NTPV NSs completely inhibited Mx1 promoter induction in a manner comparable to the RVFV NSs control (**Figure 17A**). GFV, BGRV and PERV NSs also exhibited a strong antagonism of Mx1 promoter induction; however, SFSV, EMBV and KBGV NSs showed no effect.

A different pattern was observed for IFN- α -stimulated ISG54 promoter induction (**Figure 17B**): Antagonism by NTPV and RVFV NSs was still strongest, but GFV NSs showed only a slight reduction at about 50% of control levels. However, in contrast to a suppression of Mx1 promoter induction, BGRV and PERV NSs showed no effect on ISG54 promoter induction, as did EMBV and SFSV NSs.

Figure 18 summarizes antagonistic effects displayed by the tested phlebovirus NSs proteins on different innate immunity promoters. As known, RVFV NSs potently suppressed gene induction under all conditions. In contrast, no antagonistic effect of KBGV was observed in any of the tested conditions. However, NSs proteins of other novel phleboviruses NTPV, EMBV, BGRV, PERV, as well as GFV NSs all exhibited distinct antagonistic profiles.

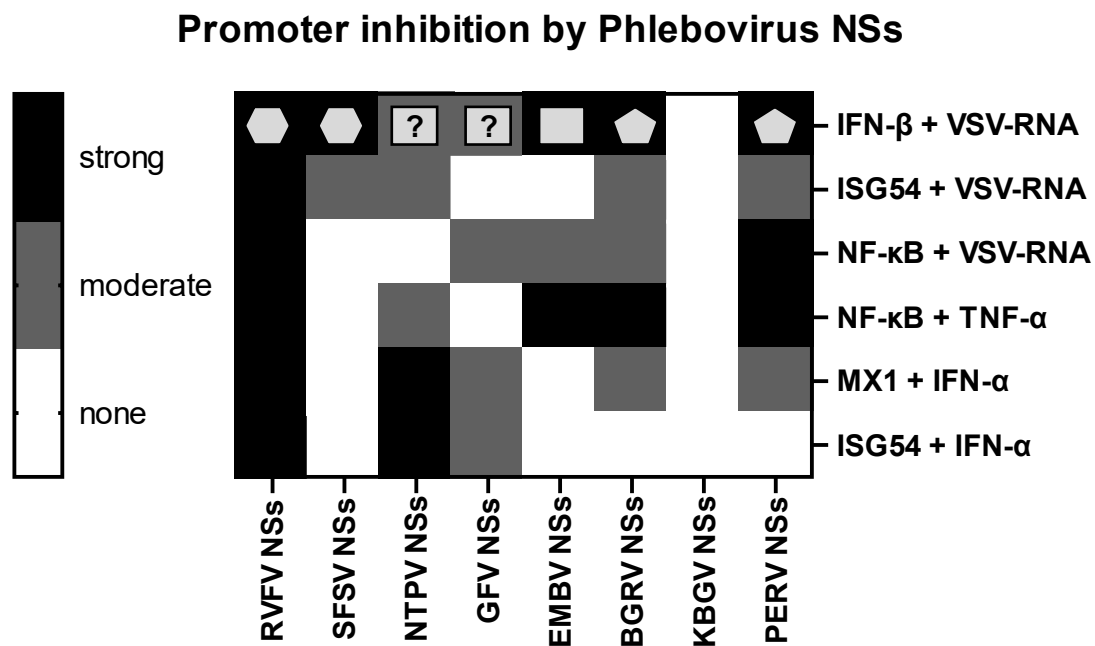


Figure 18: Heatmap summarizing the antagonistic effect of novel phlebovirus NSs proteins on innate immune gene induction. Antagonistic effect of phlebovirus NSs proteins obtained from reporter assay data (Figures 13 and 15–17) was grouped for no effect (white), moderate effect (grey) or strong effect (black). Symbols visualize the target PRR-signalling cascade step for IFN-β promoter antagonism according to Figure 14E: inhibition downstream of MAVS, rectangle; ...TBK1, pentagon; ...IRF3, hexagon.

Of note, the evaluation of the reporter assay data was focused on firefly luciferase expression under the control of the respective promoters only. While expression constructs for *Renilla* luciferase were co-transfected to control for transfection efficiency, firefly luciferase values were not normalized to *Renilla* luciferase values. This way of analysis was chosen because RVFV NSs, as a positive control, causes a general transcription block in the host cell (Billecocq *et al.* 2004; Kainulainen *et al.* 2014), which negatively affects *Renilla* luciferase expression values. Absolute *Renilla* luciferase values for the experiments presented in Figure 13 and Figure 15 – Figure 17 are given in Figure 19. Low *Renilla* luciferase values in the presence of RVFV NSs confirmed the general transcription block; however, for other NSs proteins or controls this effect was absent.

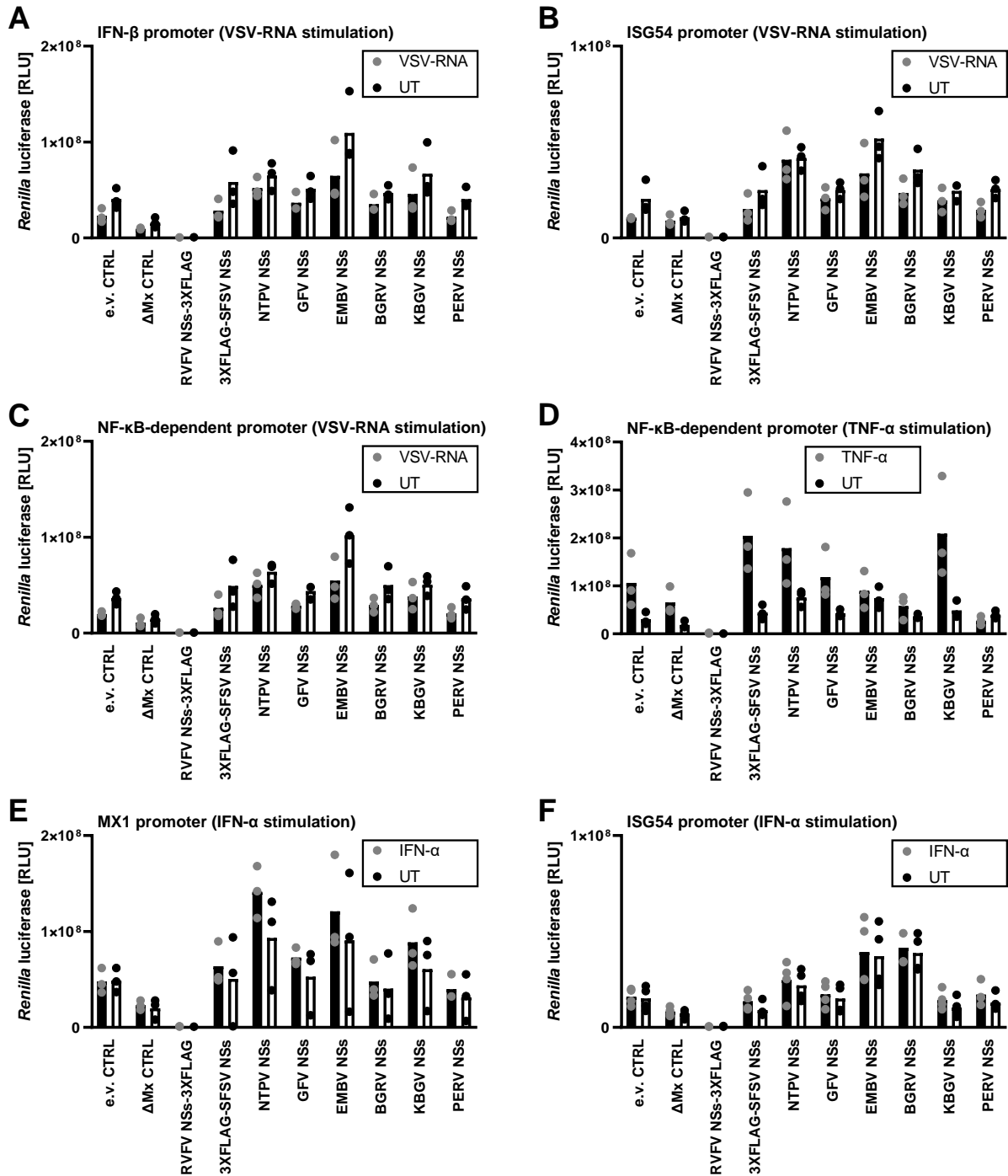


Figure 19: Absolute Renilla luciferase values for reporter assay data of innate immune gene promoter inhibition by phlebovirus NSs proteins. Renilla luciferase values for experiments presented in **Figures 13 and 15–17**. Individual values (dots) and geometric mean values (bars) from three or four biological replicates are shown. RLU, relative luciferase units; UT, untreated.

7.1.5.6 Evaluation of tagged phlebovirus NSs constructs

In the absence of a specific antibody, tagged expression constructs are useful for downstream experiments involving antibody recognition of the NSs proteins. Thereby, tag location is important to consider, as it was observed for SFSV NSs that the presence of a tag at the N-terminus, but not the

C-terminus, abolishes binding to cellular transcription factor eIF2B, while the location of the tag does not affect IFN- β promoter antagonism (Wuerth *et al.* 2020).

To determine for each NSs a tag location that preserves NSs function, the influence of an N- or C-terminal 3 \times FLAG tag on the performance of novel phlebovirus NSs proteins in innate immunity reporter assays was evaluated. To this end, the 3 \times FLAG tag was cloned into expression vectors either up- or downstream of the NSs open reading frame and the resulting constructs were used to repeat luciferase reporter assays, focusing on IFN- β and Mx1 promoter activation as representatives of type I IFN induction and signalling, respectively.

The presence of a 3 \times FLAG tag at either N- or C-terminus did not affect IFN- β promoter inhibition by EMBV, BGRV and PERV NSs (**Figure 20A**). All three constructs counteracted promoter activation in a comparable manner and to the same degree as RVFV NSs. In contrast, NTPV NSs in native as well as C-terminally tagged form efficiently antagonized IFN- β promoter induction; the presence of a tag at the N-terminal end, however, completely negated this function. Untagged as well as N-terminally tagged GFV NSs potently inhibited IFN- β promoter activation, whereas inhibition with C-terminally tagged GFV NSs was slightly less pronounced. Additionally, expression levels of tagged NSs proteins were assessed by immunoblotting. Thereby, expression levels for N- and C-terminally tagged constructs were mostly comparable (**Figure 20B**), except for NTPV and PERV NSs, where C- and N-terminally tagged versions were more strongly expressed, respectively.

KBGV NSs did not show any effect on innate immunity promoter activation in previous experiments. This result could be genuine, in case KBGV does not possess any abilities to interfere with these pathways, or secondary, if the transfected NSs construct is not expressed in the cell. Repeating reporter experiments with tagged KBGV NSs constructs revealed that, in fact, N-terminally tagged KBGV NSs was expressed rather weakly in comparison to other NSs constructs, and C-terminally KBGV NSs was not expressed at all (**Figure 20B**). Weakly expressed N-terminally tagged KBGV NSs was indeed able to slightly reduce IFN- β promoter activation.

A similar overall picture compared to IFN- β promoter activation was observed when evaluating Mx1 promoter activation in the presence of tagged NSs proteins (**Figure 20C, D**). Here, too, a discrepancy in potency depending on tag location was apparent for NTPV, GFV and KBGV NSs. Of note, while the demonstrably expressed N-terminally tagged KBGV NSs caused lower Mx1 promoter induction levels than untagged or C-terminally tagged versions of questionable expression status, promoter induction was still not below control levels. Further, even though neither of the EMBV constructs could counteract Mx1 promoter induction, the C-terminally tagged construct seemed to efficiently boost induction. Lastly, C-terminally tagged BGRV and PERV NSs seemed to be slightly less efficient than their counterparts in Mx1 promoter inhibition.

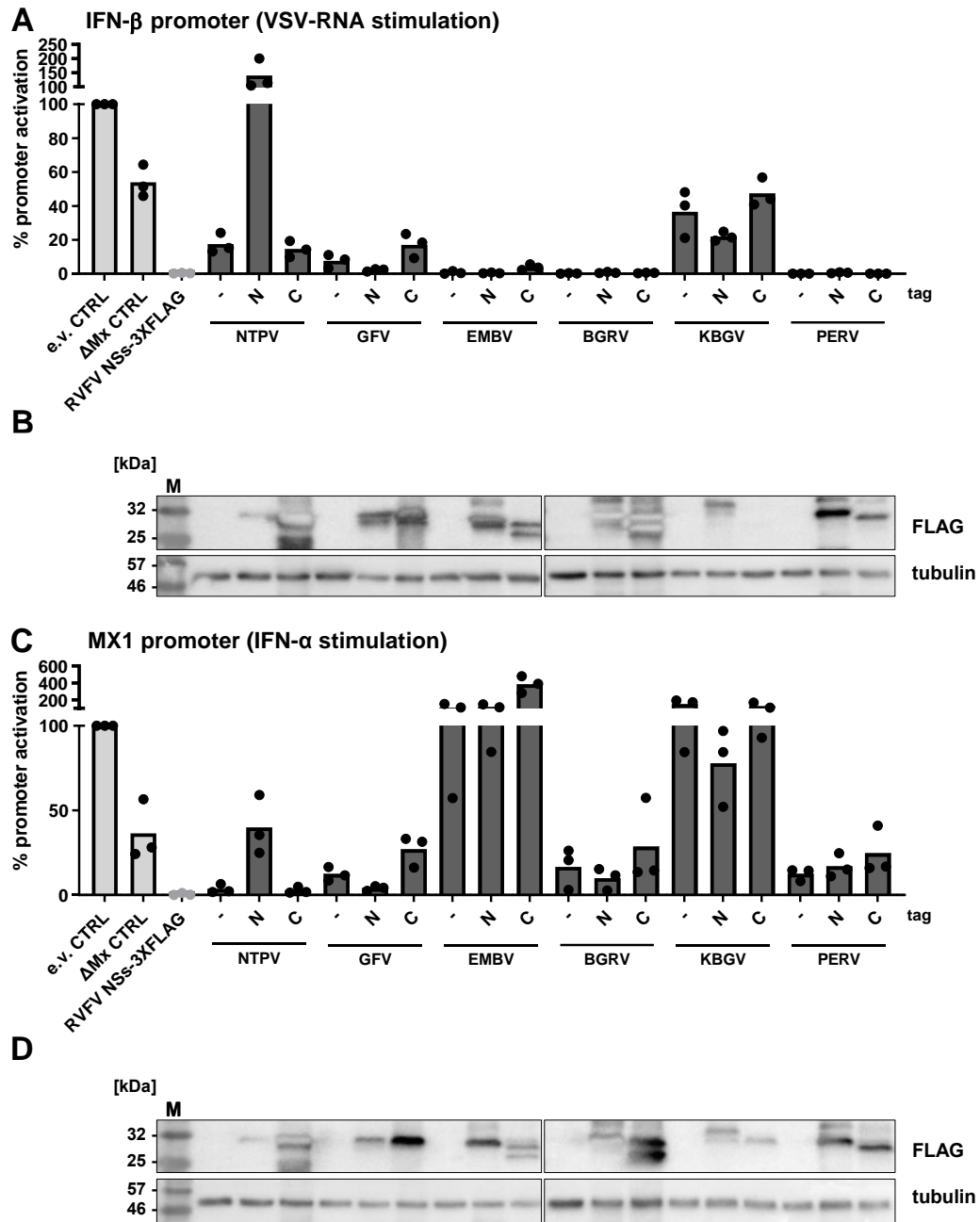


Figure 20: Influence of an N- or C-terminal 3 \times FLAG tag on NSs antagonism of reporter activation. HEK293 cells were transfected with expression plasmids for plebovirus NSs proteins or controls, with reporter constructs coding for firefly luciferase under the control of the respective promoters, as well as with expression plasmids for constitutively expressed *Renilla* luciferase. Reporter luciferase expression was stimulated by transfection of 50 ng/well VSV-RNA (A, B), or by treatment with 50 U/well IFN- α (B/D) (C, D) for 18 h. (A, C) Luciferase activities were measured with a dual-luciferase reporter assay system according to the manufacturer's recommendations. Firefly luciferase values of unstimulated control samples were subtracted from values of stimulated samples, and the resulting values for the empty vector control were set to 100% within each biological replicate. Individual (dots) and geometric mean values (bars) from three biological replicates are shown. (B, D) Cell lysates were analyzed by immunoblotting with antibodies for FLAG tag and tubulin. kDa, kilodalton; M, marker.

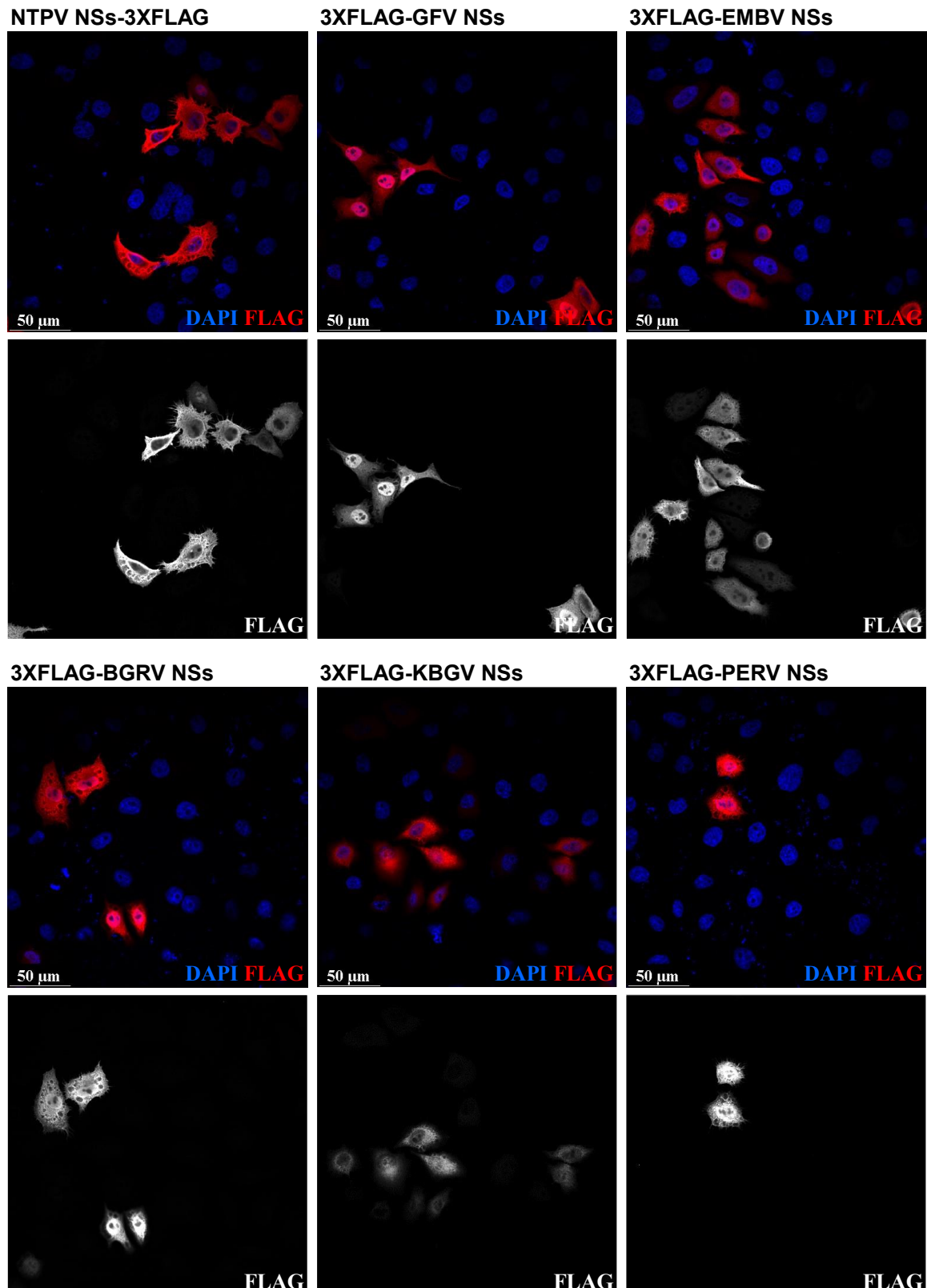


Figure 21: Intracellular location of novel phlebovirus NSs proteins. HeLa cells seeded onto coverslips were reverse transfected with expression constructs for 3×FLAG-tagged NSs of NTPV (C-terminal tag), GFV, EMBV, BGRV, KBGV or PERV (N-terminal tag). 24 h post transfection, cells were fixed with paraformaldehyde, and coverslips were stained using anti-FLAG tag primary and Alexa Fluor 555 donkey anti-mouse secondary antibodies, as well as DAPI. Confocal microscopy was performed using a Leica TCS SP5 confocal microscope and the accompanying software.

In summary, tag location influenced the performance of all tested novel phlebovirus NSs expression constructs in IFN-induction and -signalling reporter assays. In that context, the presence of a tag at either the N- or C-terminus might therefore obscure important NSs domains necessary for possible protein-protein interactions. Thus, for downstream experiments, C-terminally 3×FLAG tagged NTPV NSs as well as N-terminally 3×FLAG tagged GFV, EMBV, BGRV, KBGV and PERV NSs constructs were employed.

7.1.5.7 Subcellular location of phlebovirus NSs

Subcellular location has been found to be distinct for various phenuiviral NSs proteins. For instance, the multi-faceted RVFV NSs acts in the cytoplasm as well as in the nucleus of the infected cell (Ly and Ikegami 2016). It forms characteristic nuclear filament structures which are crucial for its function (Li *et al.* 2019b). Severe fever with thrombocytopenia syndrome virus (SFTSV) NSs has been shown to be distributed in distinct cytoplasmic inclusion bodies, thereby sequestering cellular signalling molecules (Wu *et al.* 2014).

To evaluate the subcellular location of novel phlebovirus NSs, immunofluorescence analyses upon 3×FLAG tagged NSs transfection were performed. As presented in **Figure 21**, NTPV and KBGV NSs mainly showed a diffuse distribution in the cytoplasm, whereas GFV NSs was located predominantly nuclear with low levels still present in the cytoplasm. EMBV, BGRV and PERV NSs seemed evenly distributed throughout cytoplasm and nucleus. Filament or inclusion body structures were not detected.

7.1.5.8 Interactome analysis of novel phlebovirus NSs proteins with host factors

Phenuiviral NSs proteins often exert their immune-modulating functions through direct interaction with host proteins (chapter 4.2.5). The well-characterized RVFV NSs protein, for instance, interacts with histone deacetylase complex subunit SAP30 to inhibit IFN- β promoter induction (Le May *et al.* 2008) and causes a general host transcription shutoff by sequestration of transcription factor TFIID through interaction with subunits p44 and p62 (Billecocq *et al.* 2004; Le May *et al.* 2004; Kalveram *et al.* 2011). In addition, RVFV NSs mediates PKR proteasomal degradation through interaction with the host ubiquitination machinery (Habjan *et al.* 2009b; Ikegami *et al.* 2009; Mudhasani *et al.* 2016).

Thus, the cellular interaction partners of NSs proteins of novel phleboviruses NTPV, EMBV, BGRV, KBGV and PERV as well as poorly characterized phleboviruses GFV, SFSV and two strains of PTV, the virulent Adames strain (PTV-A) and the non-virulent Balliet strain (PTV-B; Palacios *et al.* 2015; see **Figure 12**) were sought to be elucidated. For interactome analysis, 3×FLAG tagged NSs proteins were expressed in HEK293 cells and cellular interacting proteins were isolated by FLAG tag co-immunoprecipitation. As a negative control, again the C-terminally truncated, non-functional Δ Mx was employed. Subsequently, co-immunoprecipitated proteins were analysed by repeated liquid chromatography-tandem mass spectrometry (LC-MS/MS; three technical replicates of three biological replicates: co-immunoprecipitation experiments were repeated three times independently (n=3) and for

each in the mass spectrometry measurement was performed three times, resulting in nine datasets per NSs protein altogether).

Mass spectrometry analyses were performed by Uwe Linne and Tina Krieg (Department of Chemistry, Philipps University Marburg). Evaluation of proteomic data was carried out with the help of Axel Weber (Rudolf Buchheim Institute for Pharmacology, Justus Liebig University Giessen).

Lists of interactors were retrieved by selection for proteins that were (i) identified “by MS/MS” in all nine replicate runs (as opposed to “by similarity”) and (ii) significantly enriched compared to the ΔMx control, as by Student’s t-test ($q < 0.05$). All proteins interacting with the ΔMx control were excluded, as were contaminants detected by the accompanying Maxquant software. Numbers of cellular interactors for each tested NSs identified through these filter criteria are given in **Table 45**.

Table 45: Number of cellular interactors with phlebovirus NSs proteins

<i>Viral NSs</i>	<i># of interactors</i>	<i>Viral NSs</i>	<i># of interactors</i>
NTPV	1548	PERV	1646
GFV	1390	PTV-A	978
EMBV	1422	PTV-B	1625
BGRV	1398	SFSV	642
KBGV	1206		

The Circos plot in **Figure 22** depicts the overlap between the obtained lists of phlebovirus interactors. Most cellular interaction partners were shared between at least two NSs proteins, as shown by the predominantly dark orange colour of inner arcs connected by purple lines. However, NTPV, PERV, and PTV-B NSs also possessed a considerable number of cellular binding partners that were unique among the tested phlebovirus NSs proteins, as shown by the light orange stretches of inner arcs. Numbers of overlapping and unique NSs interactors are further given in **Table 52** (annex).

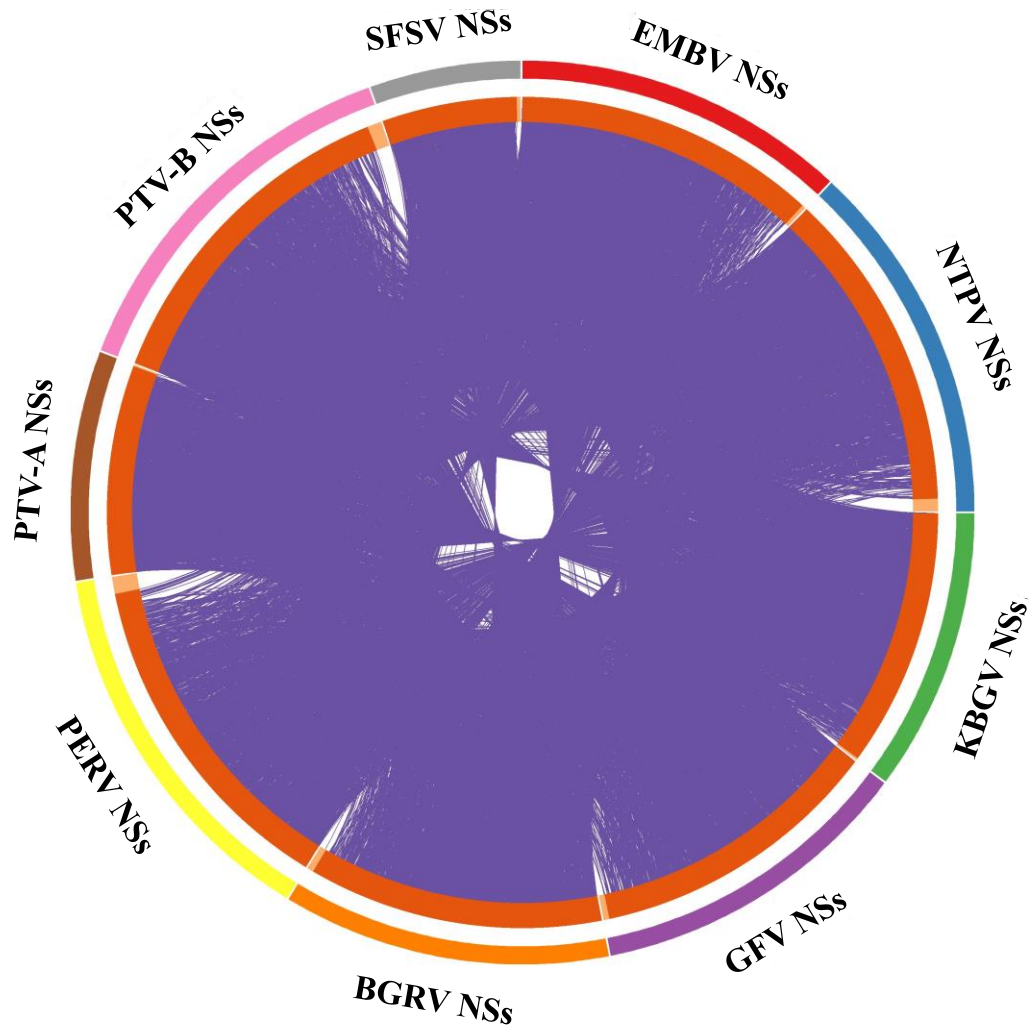


Figure 22: Circos plot depicting overlap between phlebovirus NSs interactor lists. Outer arcs represent the identity of each NSs protein list. Inner arcs represent these protein lists according to absolute number of entries, where each entry has a spot on the arc. Dark orange colour represents proteins that appear in multiple lists and light orange colour represents proteins that are unique across input lists. Purple lines link the same proteins shared by multiple lists. Circos plot was generated using Metascape (Zhou *et al.* 2019).

To identify significantly enriched protein subgroups from the obtained lists of phlebovirus NSs interactors, in a next step, gene ontology (GO) analyses were performed. **Figure 23** shows select statistically enriched GO terms within each phlebovirus NSs interactor list. Novel phlebovirus NSs as well as PTV and SFSV NSs proteins interacted with cellular proteins annotated to a variety of functions, including transcription, mitochondrial functions, apoptosis, transport and cellular localization, or innate immunity.

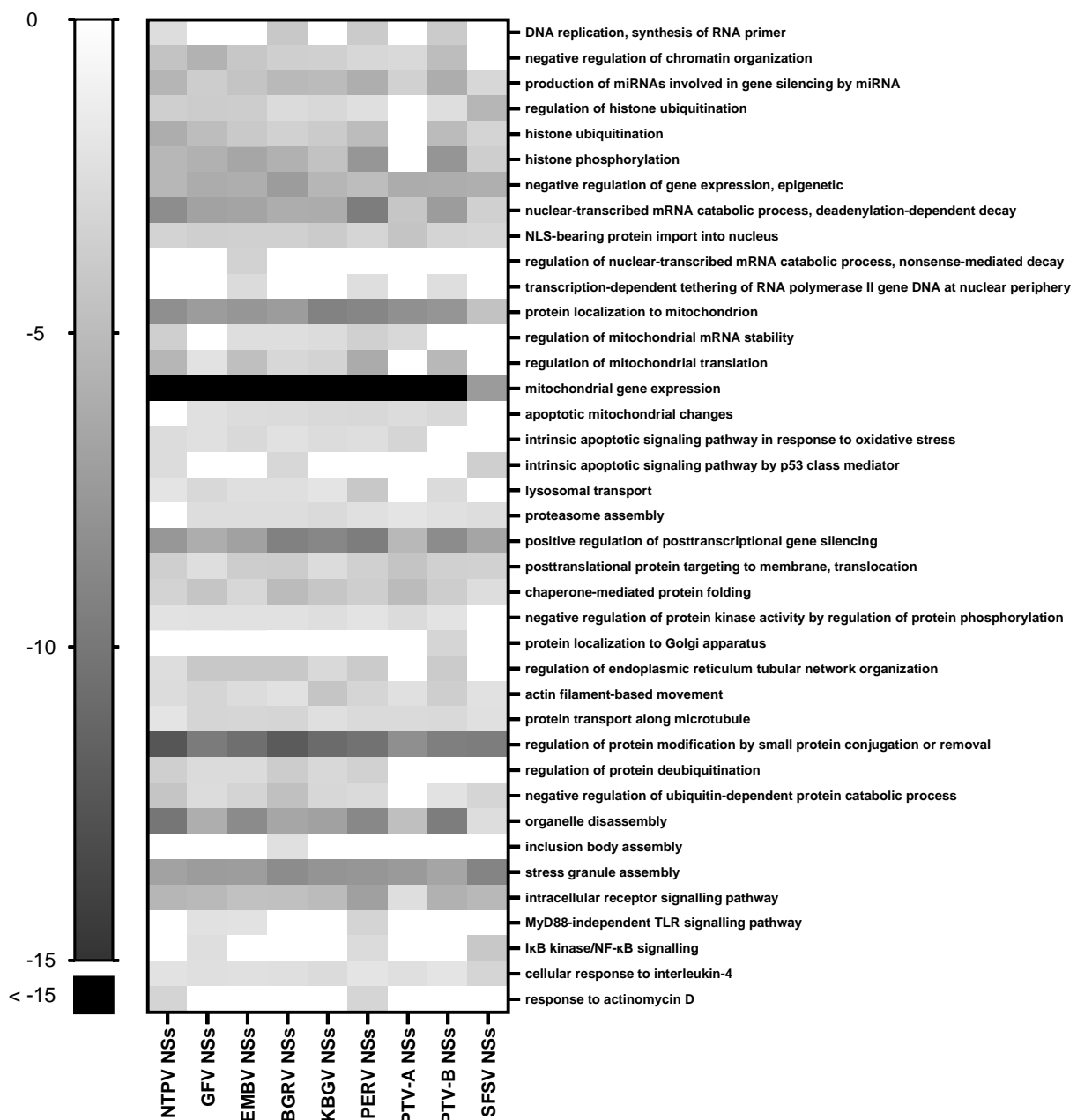


Figure 23: Heatmap depicting select statistically enriched GO terms within phlebovirus NSs host cell interactors. Colour scale depicts p value for each GO term, as analyzed using Metascape (Zhou *et al.* 2019).

With the exception of KBGV and to a lesser extent PTV-B, all tested NSs proteins are either known to have (SFSV, PTV-A; Perrone *et al.* 2007; Nishiyama *et al.* 2016; Wuerth *et al.* 2018) or were shown in this work to have anti-IFN capacities (chapters 7.1.5.1 to 7.1.5.5). Therefore, the next focus lay on NSs-interactors involved in innate immune response functions. To this end, proteins annotated to GO list #0045087 “innate immune response” (obtained from <https://www.ebi.ac.uk/QuickGO/>) were identified within each NSs interactor list. With the generated sub-lists (IIR-lists) gene ontology analysis were performed again to identify subgroup GO terms enriched within each NSs interactor IIR-list. Select statistically enriched GO terms are shown in **Figure 24**.

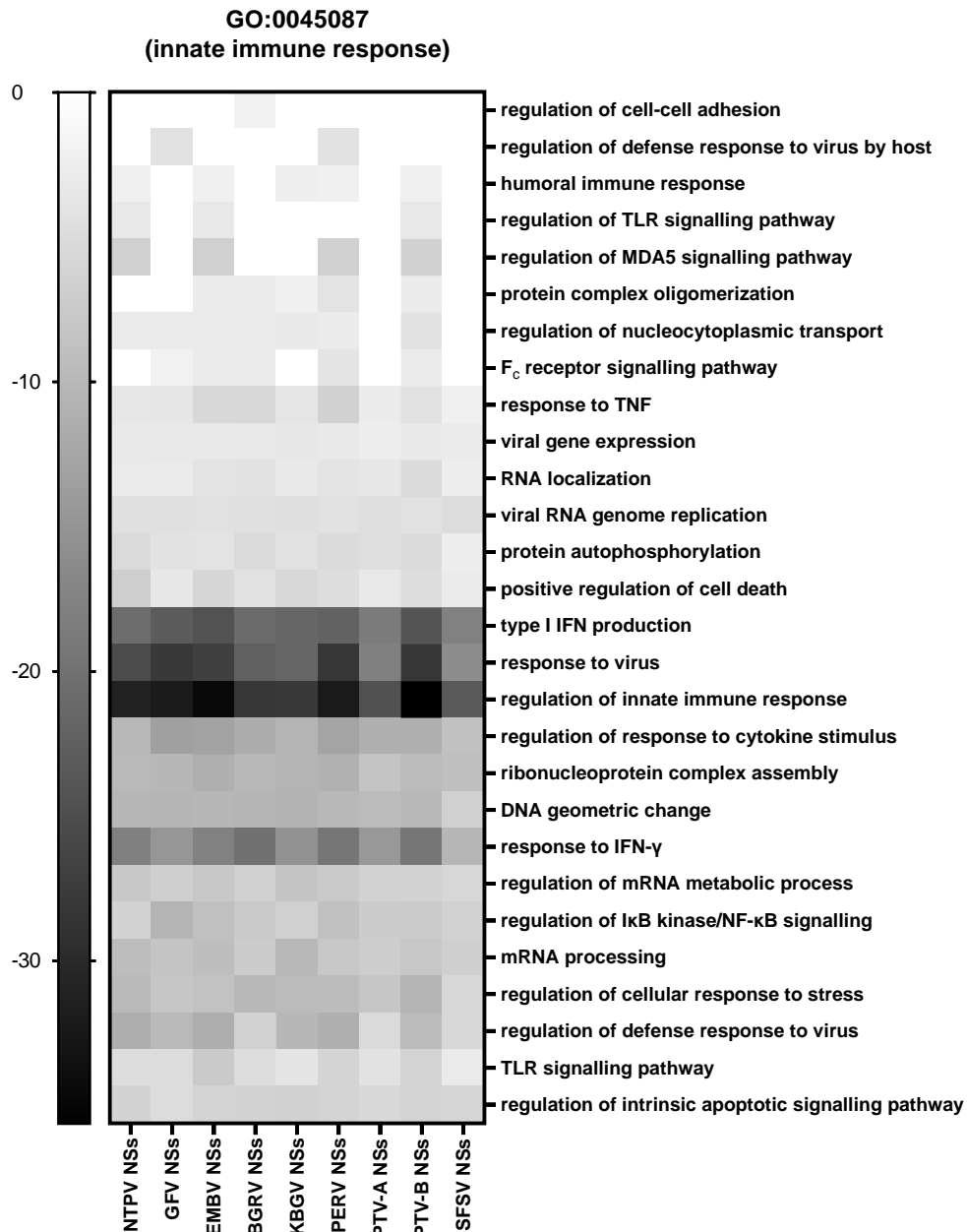


Figure 24: Heatmap depicting select statistically enriched GO terms within phlebovirus NSs host cell interactors annotated to the GO list #0045087, innate immune response. Colour scale depicts p value for each GO term, as analyzed using Metascape (Zhou *et al.* 2019).

Among the NSs interactor IIR-lists, members of general processes like “type I IFN production” and “regulation of innate immune response” were found to be highly enriched across all interactor lists. In addition, more specific pathways including “regulation to cytokine stimulus”, “regulation of NF-κB signalling”, “mRNA processing” or “regulation of intrinsic apoptotic signalling pathways” were also uniformly enriched. Other terms, for instance “regulation of nucleocytoplasmic transport”, “regulation of MDA5 signalling pathway” or “humoral immune response” were only enriched in a subset of interactor lists, indicating distinct mechanisms of NSs action.

Next, single proteins of interest within the innate immune response, which interact with different phlebovirus NSs proteins, were sought to be identified and visualized. To this end, a Venn diagram was created using an online tool (<http://www.interactivenn.net/>, Heberle *et al.* 2015). Because six lists are the maximum amount that can be graphically represented, the focus lay on the five novel phlebovirus NSs proteins together with GFV NSs for this approach. A comprehensive analysis of innate immune response interactors among the nine tested NSs proteins can be found in **Table 53** (annex).

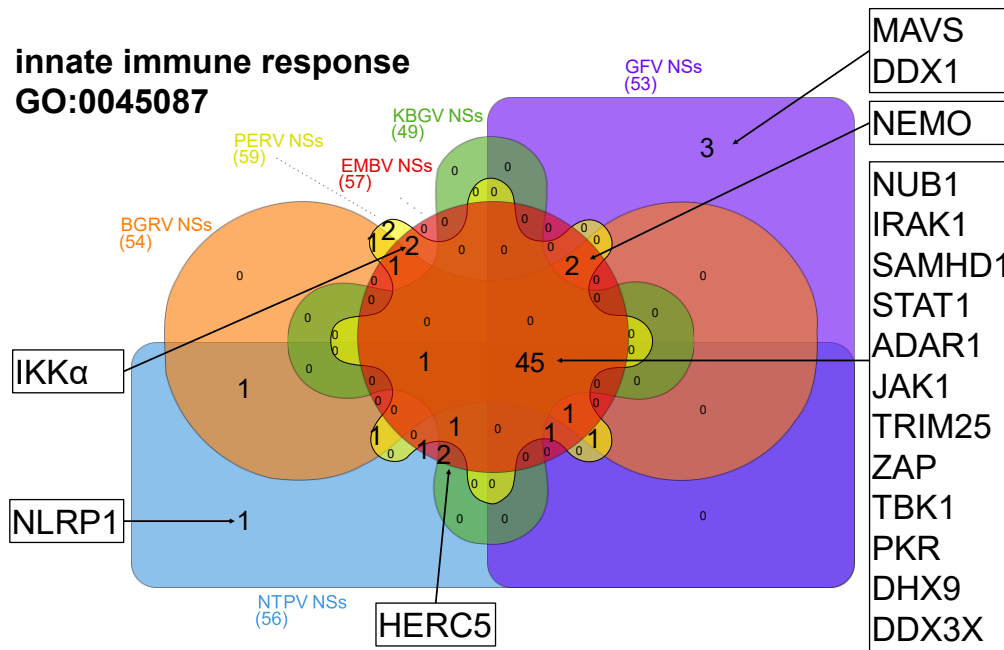


Figure 25: Venn diagram showing shared and unique interactors of phlebovirus NSs, annotated to the GO list #0045087, innate immune response. Venn diagram was created on <http://www.interactivenn.net/> (Heberle *et al.* 2015). Select proteins of interest are highlighted in text boxes.

As shown in **Figure 25**, the majority of interactors (45 out of 67) was shared between the NSs proteins, for example TRIM25 and TBK1, which are involved in IFN induction, or STAT1 (but not STAT2 or STAT3) and JAK1, which are involved in IFN signalling. While these interactions were consistently detected with NSs but not the control proteins, the biological function needs to be investigated further, as not all NSs proteins shared the same capabilities to inhibit IFN induction/signalling. In addition, other players in innate immune signalling pathways not annotated to this GO pathway were identified as shared interactors between multiple NSs proteins, as well as several ISGs (**Table 46**).

Table 48: Host protein interactors with focus on individual phlebovirus NSs proteins (1/3)

Host protein		Interaction with NSs of ...										Host protein cellular function	Remarks
abbr.	UniProt ID	full name	NTPV	GFV	EMBV	BGRV	KBGV	PERV	PTV-A	PTV-B	SFSV		
1. NTPV NSs													
ASH1L	Q9NR48	Histone-lysine N-methyltransferase ASH1L											negative regulation of NF- κ B induction: induces TNFAIP3/A20 transcription, which deubiquitinates NF- κ B signal modulator NEMO (Xia <i>et al.</i> 2013)
ABIN1	Q15025	TNFAIP3-interacting protein 1											related protein ABIN2 was recently identified as a target for SFTSV NSs: SFTSV NSs activated downstream processes which resulted in the upregulation of anti-inflammatory cytokine IL-10 (Choi <i>et al.</i> 2019)
Centrin-2	P41208	Centrin-2											"regulation of nucleocytoplasmic transport" among the enriched GO terms for NTPV NSs interactors
DUSP11	O75319	RNA RNP complex-1-interacting phosphatase											negative regulation of IFN- β induction: reduces RIG-I activation by modifying 5'ppp ends of RNAs (Choi <i>et al.</i> 2020a)
ITPR1	Q14643	Inositol 1,4,5-trisphosphate receptor type 1											NLRP3 inflammasome activation leading to apoptosis (Chen <i>et al.</i> 2017); ITPR3 implicated in antifungal immune responses by activating the TBK1-IRF3 pathway (Yang <i>et al.</i> 2018)
ITPR2	Q14571	Inositol 1,4,5-trisphosphate receptor type 2											
ITPR3	Q14573	Inositol 1,4,5-trisphosphate receptor type 3											
NLRP1	Q9C000	NACHT, LRR and PYD domains-containing protein 1											NLRP1 inflammasome: induces caspase-1 activation, leading to the release of pro-inflammatory cytokines and to cell death
GTF2E2	P29084	Transcription initiation factor IIE subunit beta											RNA polymerase II-mediated transcription: recruits TFIIF to transcription initiation complex
TAF6L	Q9Y6J9	TAF6-like RNA polymerase II p300/CBP-associated factor-associated factor 65 kDa subunit 6L											RNA polymerase II-mediated transcription: component of transcription coactivator PCAF complex
2. GFV NSs													
MAVS	Q7Z434	Mitochondrial antiviral-signalling protein											signalling adapter mediating IFN- β and NF- κ B-dependent gene induction upon PRR signalling
Calnexin	P27824	Calnexin											assembly of newly synthesized proteins at the ER
3. EMBV NSs													
SOGA1	O94964	Protein SOGA1											autophagy regulation
YLPM1	P49750	YLP motif-containing protein 1											transcription regulation
eIF3E	P60228	Eukaryotic translation initiation factor 3 subunit E											translation initiation factor eIF3 subunit
													exceptionally strong intensity in EMBV NSs, considerably weaker for all other NSs proteins

Table 49: Host protein interactors with focus on individual phlebovirus NSs proteins (2/3)

Host protein		Interaction with NSs of ...										Host protein cellular function	Remarks
abbr.	UniProt ID	full name	NTPV	GFV	EMBV	BGRV	KBGV	PERV	PTV-A	PTV-B	SFSV		
4. BGRV NSs													
TRAFD1	O14545	TRAF-type zinc finger domain-containing protein 1										inhibition of IRF3 and NF- κ B activation through interaction with TRIF, MAVS, TRAF3, TRAF6	
mTOR	P42345	Serine/threonine-protein kinase mTOR										mTORC1/2 component; kinase activity	
MLST8	Q9BVC4	Target of rapamycin complex subunit LST8										mTORC1/2 component; positively regulates mTOR kinase activity (Jacinto <i>et al.</i> 2004)	
Raptor	Q8N122	Regulatory-associated protein of mTOR										mTORC1 component; regulation	
MIB2	Q96AX9	E3 ubiquitin-protein ligase MIB2										IFN- β induction: ubiquitinates TBK1 (Ye <i>et al.</i> 2014)	
DNMT3A	Q9Y6K1	DNA (cytosine-5)-methyltransferase 3A										IFN- β induction: maintains high expression of histone deacetylase HDAC9, which enhances TBK1 kinase activity	
SUMO2	P61956	Small ubiquitin-related modifier 2										posttranslational protein modification through covalent attachment: modulates functions including nuclear transport, protein stability, proteasomal degradation	
ZNF169	Q14929	Zinc finger protein 169										poorly characterized	
CHIP	Q9UNE7	E3 ubiquitin-protein ligase CHIP										interaction with p62; mediates ubiquitin-dependent RIPK3 degradation, thereby inhibiting RIPK3-triggered necroptosis upon TNF- α signalling (Seo <i>et al.</i> 2016)	
p62	Q13501	Sequestosome-1										interaction with CHIP; activates the NRF2 pathway through direct interaction with Keap1 to promote the expression of cytoprotective genes; regulation of NF- κ B activation by TNF- α through interaction with RIPK1	
SESN2	P58004	Sestrin-2										interaction with p62; positively regulates p62-Keap2-NRF2 axis; negatively regulates TORC1 signalling	
5. PERV NSs													
TAB1	Q15750	TBK1 and MAP3K7-binding protein 1										as a complex, involved in IKK kinase activation to induce NF- κ B activation (Xu and Lei 2021)	
TAB2	Q9NYJ8	TBK1 and MAP3K7-binding protein 2											
TAB3	Q8N5C8	TBK1 and MAP3K7-binding protein 3											
MAP3K7	O43318	Mitogen-activated protein kinase kinase kinase 7											
STAMBP	O95630	STAM-binding protein										deubiquitinase implicated in PI3K-AKT-mTOR and RAS-MAP signaling pathways as well as inflammasome regulation (Bednash <i>et al.</i> 2017; Bednash <i>et al.</i> 2021)	
RUNX	Q01196	Runt-related transcription factor 1										transcription factor regulating APOBEC3 antiviral immunity (ISG family of enzymes which facilitate viral genome mutations)	
TIMM8B	Q9Y519	Mitochondrial import inner membrane translocase subunit Tim8 B										mitochondrial intermembrane chaperone	

Table 50: Host protein interactors with focus on individual phlebovirus NSs proteins (3/3)

Host protein abbr.	UniProt ID	full name	Interaction with NSs of ...										Host protein cellular function	Remarks	
			NTPV	GFV	EMBV	BGRV	KBGV	PERV	PTV-A	PTV-B	SFSV				
6. KBGV NSs & PTV-B NSs															
DPY19L1	Q2PZ11	Probable C-mannosyltransferase DPY19L1												C-mannosyltransferase	
TET2	Q6N021	Methylcytosine dioxygenase TET2												methylcytosine dioxygenase, active DNA demethylation	
RBM6	P78332	RNA-binding protein 6												RNA-binding protein	
BLM	P54132	Bloom syndrome protein												DNA helicase, DNA replication and repair	
PRMT5	O14744	Protein arginine N-methyltransferase 5												methyltransferase; implicated in Hepatitis B and Bovine Leukemia virus infection (Zhang <i>et al.</i> 2017; Assi <i>et al.</i> 2020); interacts with DNA sensor cGAS to promote type I IFN induction	highest intensity with KBGV and PTV-B NSs
7. PTV-B NSs															
BAP18	Q8IXM2	Chromatin complexes subunit BAP18												chromatin complex subunit	
CSRP2BP	Q9H8E8	Cysteine-rich protein 2-binding protein												histone acetyltransferase	
8. PTV-A NSs															
EloA	Q14241	Elongin-A												elongin proteins; general transcription elongation factors that increase RNA polymerase II transcription elongation	exceptionally high intensity with PTV-A NSs, considerably weaker for all other NSs proteins
EloB	Q15370	Elongin-B													
EloC	Q15369	Elongin-C													
9. SFSV NSs															
TRAF6	Q9Y4K3	TNF receptor-associated factor 6												mediates NF- κ B activation downstream of MAVS signalling	
Rootletin	Q5TZA2	Rootletin												centriole-linker protein; required for influenza A infection (Yamauchi <i>et al.</i> 2011)	
RNF20	Q5VTR2	E3 ubiquitin-protein ligase BRE1A												RNF20/40 E3 ubiquitin-protein ligase complex mediates p53-dependent transcription of apoptotic genes (Wu <i>et al.</i> 2019a)	
RNF40	O75150	E3 ubiquitin-protein ligase BRE1B												E3 ubiquitin-protein ligase	
Calpain-1	P07384	Calpain-1 catalytic subunit												protease implicated in cytoskeletal remodelling; essential for human echovirus replication (Upla <i>et al.</i> 2008)	

Next, common interactors of NSs proteins that are not involved in innate immunity were evaluated (**Table 47**). Thereby, multiple NSs proteins interacted, for example, with cell structure and transport components, or with the cellular proteasomal degradation machinery.

Finally, unique host cellular proteins targeted by respective tested NSs proteins were examined. Interactors of interest are given in **Table 48 – Table 50**. Of note, if a cellular interactor was part of a pathway or cellular function of interest, further proteins involved in those pathways were also included, even if they were common interactors to multiple NSs proteins. In addition, interactors are listed whose enrichment value in one NSs protein exceeded those of others by at least 2-fold.

In summary, functional and interactomic analyses of novel and known phlebovirus NSs proteins uncovered shared as well as distinct characteristics of each tested NSs. All but one novel NSs proteins were able to interfere with the activation of at least one tested innate immunity-related gene in an overexpression context, underscoring their possible pathogenic potential. Moreover, mass spectrometry analyses of host cellular interaction partners of NSs proteins revealed common targeted pathways as well as features that were specific for one phlebovirus NSs.

7.2 Innate immunity characterization of SARS coronavirus 2 (SARS-CoV-2)

Since the start of 2020, the COVID-19 pandemic, with SARS-CoV-2 as causative agent, has had devastating effects on global health. Obviously, it was vital to obtain rapid insights into the interactions of SARS-CoV-2 with the human immune system. To this end, its sensitivity to type I and type III IFN was determined. Additionally, the effect of IFN-signalling inhibitor Ruxolitinib, an FDA-approved drug proposed for COVID-19 treatment, on SARS-CoV-2 replication kinetics was evaluated (Felgenhauer *et al.* 2020). Further, to expand on these findings towards the innate immunity phenotype of SARS-CoV-2, its ability to induce IFN and ISGs was analyzed in depth.

For this, SARS-CoV-2 was compared to its relative SARS-CoV-1, with which it shares approx. 80% genome identity (Zhou *et al.* 2020a). SARS-CoV-1 has been shown to be highly virulent and it efficiently counteracts the induction of IFN, cytokines and ISGs (Spiegel *et al.* 2005; Spiegel and Weber 2006; Thiel and Weber 2008; Lu *et al.* 2011). Reflecting this, the SARS-CoV-1 outbreak in 2002/2003 claimed close to 1,000 deaths among approx. 8,000 cases (WHO 2003). In comparison, at the time of writing, the ongoing SARS-CoV-2 pandemic has caused approx. 4.5 million deaths among more than 222 million confirmed infections (COVID-19 Dashboard, Johns Hopkins University, accessed on 08 September 2021).

7.2.1 Sensitivity of SARS-CoV-2 to type I IFN

First, the effect of type I IFN against a SARS-CoV-2 patient isolate was tested in comparison to a SARS-CoV-1 isolate from 2003. For this, the human bronchial epithelial Calu-3 and the primate kidney epithelial Vero E6 cell line were employed. Both cell lines express the SARS coronavirus receptor ACE2 (Ren *et al.* 2006) and are sensitive to type I IFN. However, Vero E6 cells are unable to produce IFN upon virus infection (Emeny and Morgan 1979) whereas Calu-3 cells produce a functional IFN induction and response (Yoshikawa *et al.* 2010).

Here, cells were pre-treated for 16 h with increasing doses of recombinant human IFN- α (B/D) and SARS coronavirus multistep growth was evaluated after 24 h.

Upon IFN- α pre-treatment of Calu-3 cells (**Figure 26A, B**), a prominent dose-dependent virus titre reduction was observed for both SARS-CoV-2 and SARS-CoV-1. IFN- α pre-treatment of Vero E6 cells (**Figure 26C, D**) resulted in pronounced dose-dependent virus titre reduction for SARS-CoV-2. In contrast, SARS-CoV-1 growth was less efficiently inhibited when using an input MOI of 0.01, and no IFN- α -induced inhibition was observed when using an input MOI of 0.001. Of note, several virus titres were below the plaque assay detection limit and thus set to 1 PFU/ml. Additionally, SARS-CoV-1 growth was impaired in Calu-3 cells, especially when using a low MOI of 0.001 (**Figure 26B**). To account for virus titres below detection limit, a rank correlation test (Spearman's exact rank correlation

test) was applied for statistical dose-response correlation analysis. This approach confirmed that SARS-CoV-2 replication is increasingly inhibited by IFN- α , as shown by statistically significant negative correlation coefficients (CC) for both cell lines. By contrast, even though virus titres were also negatively affected by IFN- α , the effect on SARS-CoV-1 seemed less pronounced.

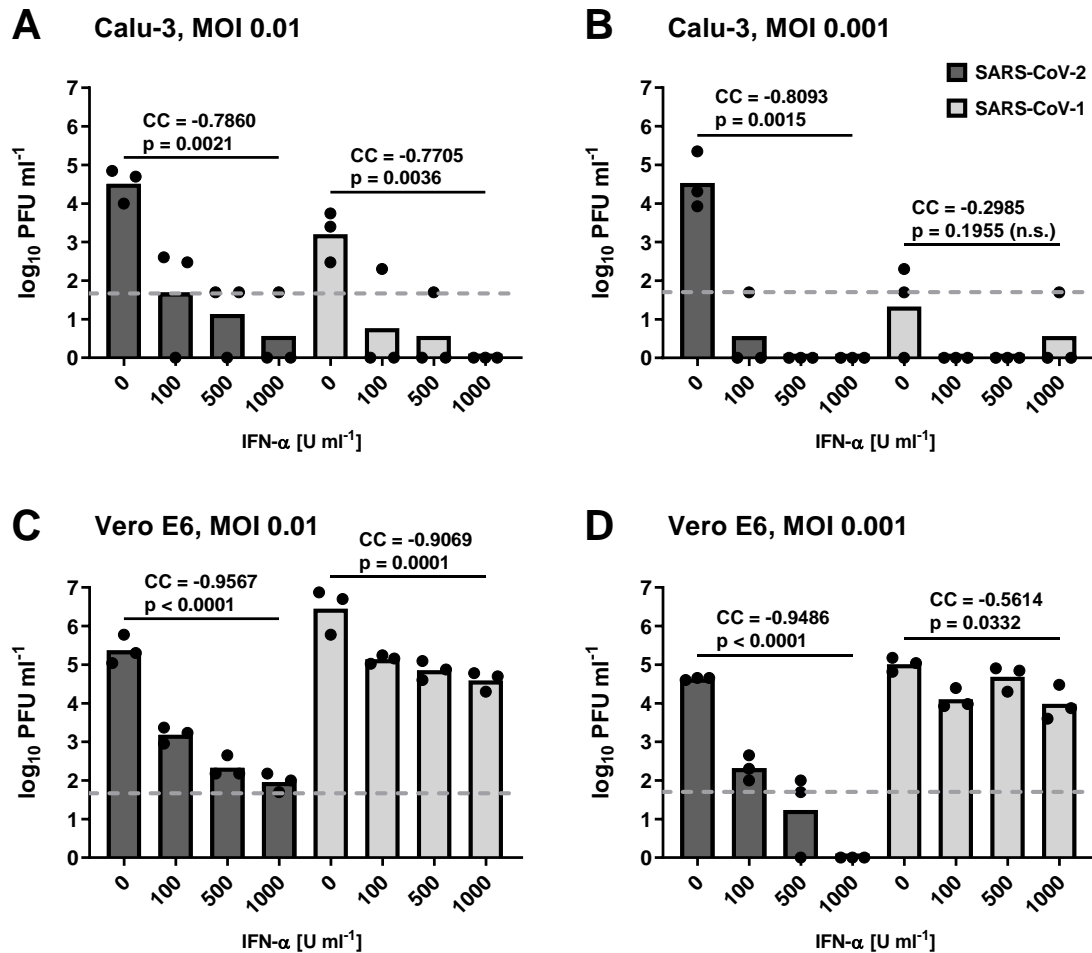


Figure 26: Sensitivity of SARS-CoV-2 and SARS-CoV-1 to increasing doses of type I IFN. Calu-3 (A, B) and Vero E6 (C, D) cells were pre-treated with 0, 100, 500 or 1,000 U/ml IFN- α for 16 h and infected with SARS-CoV-2 or SARS-CoV-1 at an MOI of 0.01 (A, C) or 0.001 (B, D). Virus titres at 24 h post infection were assessed by plaque assay titration of supernatants. Individual titers (dots) and geometric mean values (bars) from three biological replicates are shown. Log-transformed titres were analyzed by Spearman's exact rank correlation test. Correlation coefficients (CC) and exact one-sided p values are provided. Of note, titre values that were below the plaque assay detection limit (50 PFU/ml; indicated by the dashed line) were set to 1 PFU/ml. n.s., not significant.

Thus, the differences between the two viruses were to be more closely investigated. For this, three more replicate experiments were performed with the intermediate dose of 100 U/ml IFN- α and the data were statistically analyzed after pooling with the previous three replicates. Two-way ANOVA was used to simultaneously evaluate the influence of both IFN- α and virus species on virus titres (Figure 27). This analysis confirmed that both viruses are reduced by IFN- α (p(IFN), comparison of 0 versus 100 U/ml IFN- α) and indeed showed differences between the SARS coronavirus species (p(virus), comparison of the virus experiments). Furthermore, the "interaction" p value showed that, at least in Vero E6 cells, the

degree of IFN- α sensitivity depends on the virus species, again indicating that SARS-CoV-2 is more IFN-sensitive than SARS-CoV-1.

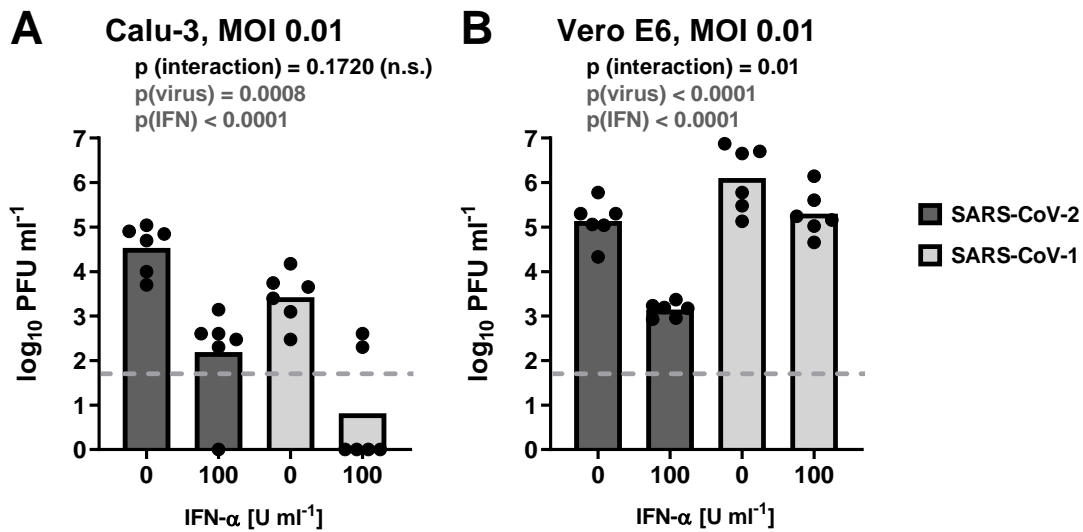


Figure 27: Sensitivity of SARS-CoV-2 and SARS-CoV-1 to intermediate-dose type I IFN. Calu-3 (A) and Vero E6 cells (B) were pre-treated with 100 U/ml IFN- α for 16 h and infected with SARS-CoV-2 or SARS-CoV-1 at an MOI of 0.01. Virus titres at 24 h post infection were assessed by plaque assay titration of supernatants. Individual titers (dots) and geometric mean values (bars) from six biological replicates are shown. Of note, three of the six biological replicates correspond to those of Figure 26. Log-transformed titres were analyzed by two-way ANOVA with factors “IFN” and “virus”, for each of which the specific p values are indicated. $p(\text{interaction})$ designates the probability that IFN sensitivity depends on the virus species. n.s., not significant.

7.2.2 Sensitivity of SARS-CoV-2 to type III IFN

Respiratory viruses, such as coronaviruses, typically invade the host through respiratory or gastrointestinal epithelia (Hulswit *et al.* 2016; Léger *et al.* 2020). On such mucosal barriers, type III IFNs (IFN- λ 1–4) rather than type I IFNs are the predominant antiviral cytokines (Stanifer *et al.* 2019). As mentioned before, type I and type III IFNs induce a similar subset of genes but engage different receptors and therefore differ in their tissue distribution and induction kinetics (chapters 4.1.1 and 4.1.3). IFN- λ has previously been shown to have activity against coronaviruses (Mordstein *et al.* 2010; Kindler *et al.* 2013; Hamming *et al.* 2013) and was proposed as potential COVID-19 treatment (Prokunina-Olsson *et al.* 2020). Therefore, in a next step, the sensitivity of the two SARS coronaviruses to recombinant human IFN- λ was compared.

Upon IFN- λ pre-treatment of Calu-3 and Vero E6 cells (Figure 28A, B), only SARS-CoV-2 titres in Vero E6 cells exhibited a statistically significant dose-dependent reduction. In Calu-3 cells, this reduction was also observed, however was not statistically significant. In contrast, no significant inhibition was observed for SARS-CoV-1 in either cell line. To further investigate the difference between the two viruses, three more replicate experiments were performed with the intermediate dose of 10 ng/ml IFN- λ and the data were statistically analyzed after pooling with the previous three replicates. Because none of the PFU values were below detection limit, conventional statistical analysis

was performed. One-tailed Student's t test confirmed a significant impact of IFN- λ on SARS-CoV-2 and the lack of an effect for SARS-CoV-1. These data thus show that IFN- λ inhibits SARS-CoV-2 but not SARS-CoV-1.

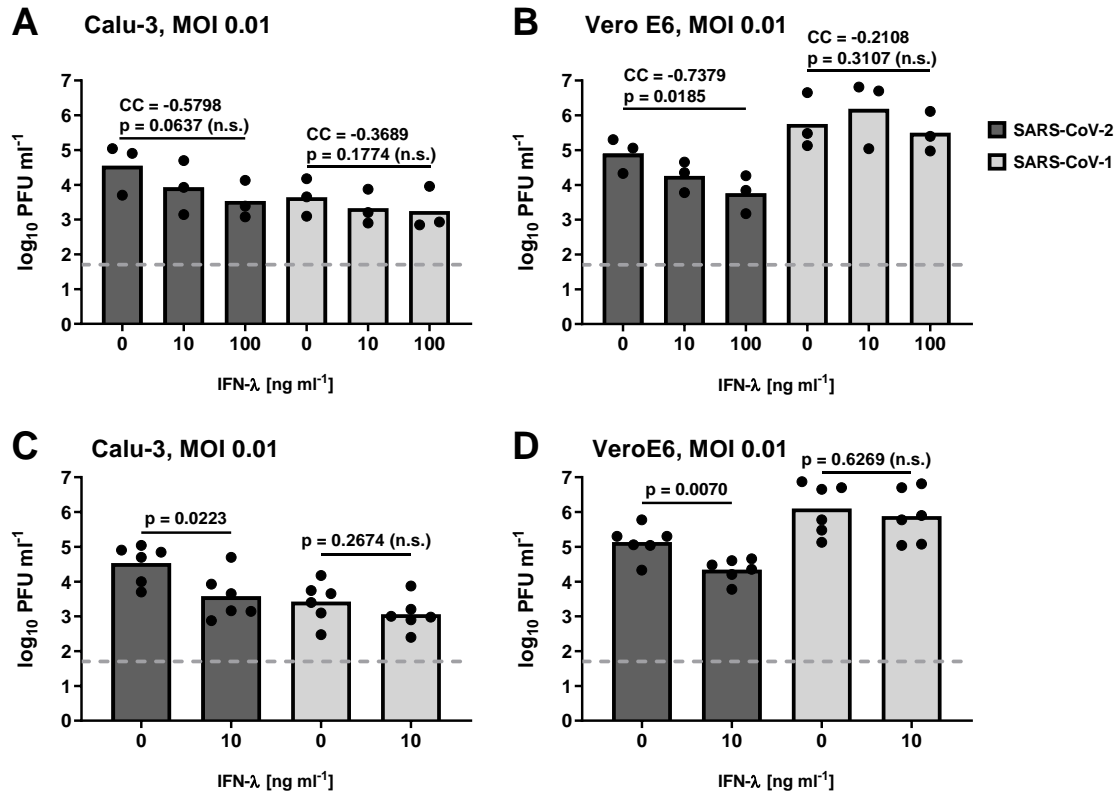


Figure 28: Sensitivity of SARS-CoV-2 and SARS-CoV-1 to type III IFN. Calu-3 (A, C) and Vero E6 (B, D) cells were pre-treated with 0, 10 or 100 ng/ml IFN- λ for 16 h and infected with SARS-CoV-2 or SARS-CoV-1 at an MOI of 0.01. Virus titres at 24 h post infection were assessed by plaque assay titration of supernatants. Individual titers (dots) and geometric mean values (bars) from three (A, B) or six (C, D) biological replicates are shown. Log-transformed titres of virus dose-response experiments (A, B) were analyzed by Spearman's exact rank correlation test. Correlation coefficients (CC) and exact one-sided p values are provided. Log-transformed titres after three additional replicate experiments were analyzed by unpaired one-tailed Student's t test. Of note, three of the six biological replicates in C and D correspond to those of A and B, respectively. n.s., not significant.

7.2.3 Effect of the JAK/STAT inhibitor Ruxolitinib on SARS-CoV-2 replication

Quickly after the emergence of SARS-CoV-2, a virus-host cell interactome study was performed to identify potential target pathways for which FDA-approved drugs are available (Gordon *et al.* 2020). This study proposed the compound Ruxolitinib for COVID-19 treatment. Ruxolitinib interferes with type I and III IFN signalling by targeting kinases JAK1/2 (Davis *et al.* 2011). Having established the sensitivity of SARS-CoV-2 to type I and III IFNs, inhibiting this pathway as a treatment option seems counterintuitive. To clarify the influence of this drug on SARS-CoV-2 replication, cells were pre-treated with 1 μ M Ruxolitinib for 16 h and infected at two different MOIs. Virus titres were determined 24 and 48 h post infection by plaque assay.

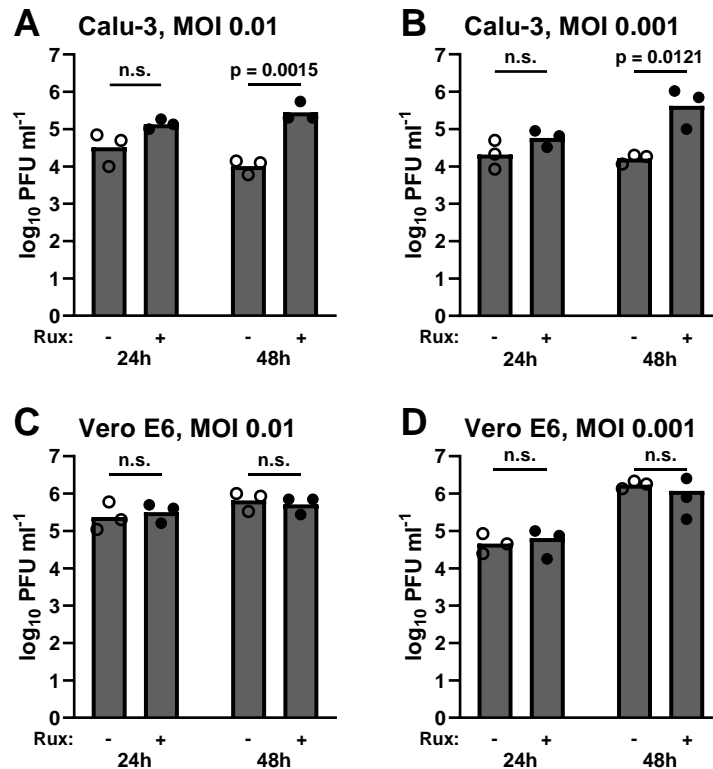


Figure 29: Effect of the JAK/STAT inhibitor Ruxolitinib on SARS-CoV-2 replication. Calu-3 (A, B) and Vero E6 (C, D) cells were pretreated with 1 μ M Ruxolitinib for 16 h and infected with SARS-CoV-2 at an MOI of 0.01 (A, C) or 0.001 (B, D). Virus titres at 24 and 48 h post infection were assessed by plaque assay titration of supernatants. Individual titers (dots) and geometric mean values (bars) from three biological replicates are shown. Log-transformed titres were analyzed by unpaired two-tailed Student's t test. n.s., not significant. Rux, Ruxolitinib.

Upon pre-treatment of Calu-3 cells with Ruxolitinib, SARS-CoV-2 exhibited increased virus growth at 48 h post infection at both input MOIs (Figure 29A, B). Not surprisingly, this clear boosting effect was not observed in Vero E6 cells (Figure 29C, D), which are incapable of IFN induction (Emeny and Morgan 1979). In fact, Ruxolitinib had neither a positive nor a negative effect on SARS-CoV-2 replication in Vero E6 cells. Regardless, the data indicate that (i) if anything, Ruxolitinib is an enhancer rather than an inhibitor of SARS-CoV-2 multiplication, and (ii) the boosting effect is most likely due to inhibition of the antiviral JAK/STAT signalling pathway, because it is not present in the IFN induction-deficient Vero E6 cells.

7.2.4 Comparison of Calu-3 and Vero E6 cell lines

So far, the presented data suggest that (i) SARS-CoV-2 is consistently more sensitive to IFNs than SARS-CoV-1 and that (ii) effects by type I IFN are more pronounced than those of type III IFN. Moreover, a clear difference was observed between Calu-3 and Vero E6 cells. To examine whether basic differences in signalling or subsequent gene expression could account for these phenomena, the ability of the cell lines to respond to the IFNs was tested. For this, cells were treated with type I or III IFN or with Ruxolitinib and protein expression was assessed by immunoblot analysis.

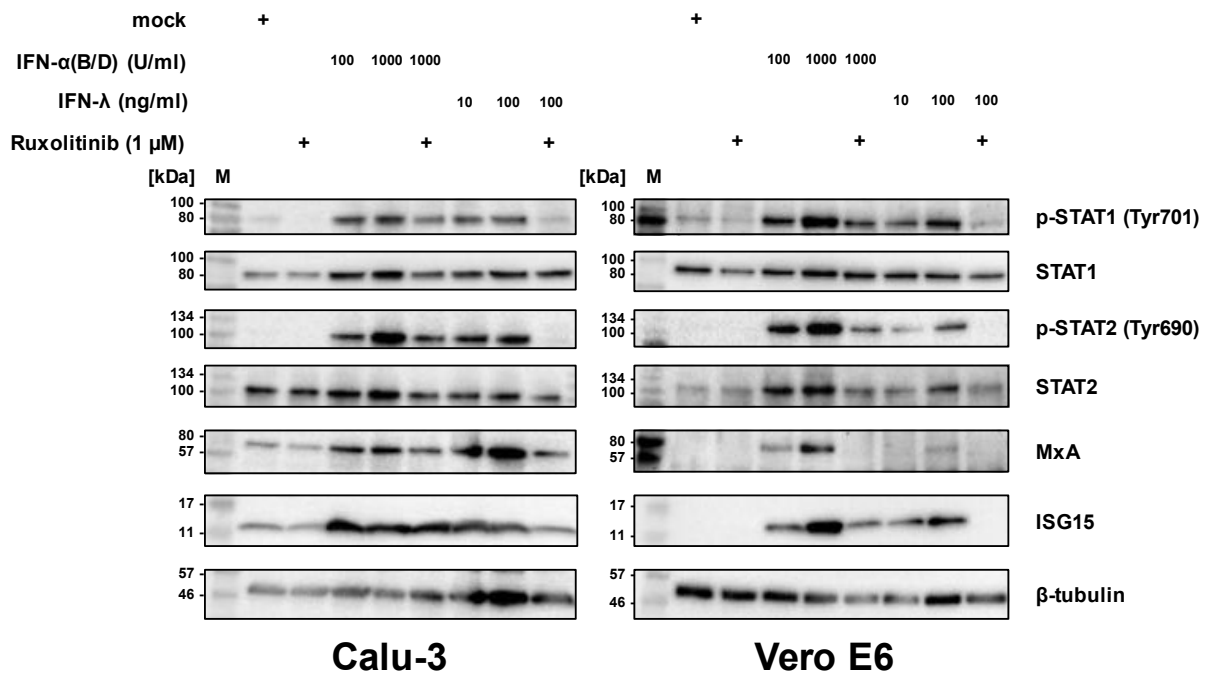


Figure 30: Effect of IFNs and Ruxolitinib on Calu-3 and Vero E6 cells. Calu-3 and Vero E6 cells were treated with the indicated amounts of IFNs and Ruxolitinib (added 1 h before IFN) and 24 h later were analyzed for the indicated antigens using immunoblotting. The data are representative of three independent experiments. Molecular markers are shown on the left sides of the blots. kDa, kilodalton; M, marker; p, phospho.

Calu-3 cells showed a very similar reaction to both types of IFN concerning phosphorylation of STAT1 and STAT2 and expression of the ISGs MxA and ISG15 (**Figure 30**). Vero E6 cells also responded to IFN-λ as expected (Stoltz and Klingström 2010), but the ISG response was lower than to IFN-α. Furthermore, already a background ISG expression could be observed in Calu-3 cells, which was absent in Vero E6 cells. As expected, Ruxolitinib was able to influence these ISG responses but it was more potent against IFN-λ than against IFN-α, and its effects on ISGs were more pronounced in Vero E6 compared to Calu-3 cells. Thus, both cell lines are capable to respond to the different types of IFN, even though IFN-λ showed a reduced potency. This agrees with the above presented observations on SARS coronavirus IFN sensitivity, as well as with previous studies (Pervolaraki *et al.* 2018; Ye *et al.* 2019).

Taken together, this work showed that SARS-CoV-2 was more sensitive to type I IFN than its 2003 counterpart SARS-CoV-1, and that SARS-CoV-2 also exhibited sensitivity to type III IFN, whereas SARS-CoV-1 did not. Consequently, SARS-CoV-2 replication in IFN-competent cells was enhanced upon IFN signalling disruption by the drug Ruxolitinib.

Data presented in **Figure 26** – **Figure 30** have been published (Felgenhauer *et al.* 2020). Statistical analyses for **Figure 26** – **Figure 29** were carried out by Klaus Failing (Unit for Biomathematics and Data Processing, Justus Liebig University Giessen). Experiments that resulted in **Figure 30** were performed by Andreas Schön (Institute for Virology, FB10, Justus Liebig University Giessen).

7.2.5 Differential regulation of innate immune genes upon SARS-CoV-2 infection in human lung cell lines

To expand on the IFN sensitivity data, in a next step, the transcriptional expression of IFN, cytokines and ISGs upon SARS-CoV-2 infection was investigated in one of its primarily targeted tissues, the respiratory tract. For this, three human lung cell lines were compared: (i) H1299, which is a non-small cell lung carcinoma epithelial cell line derived from a lymph node metastasis, and is intermediately susceptible to SARS-CoV-2 infection (Wyler *et al.* 2021); (ii) A549, which is a lung epithelial adenocarcinoma cell line, and is only susceptible to SARS-CoV-2 infection when engineered to express the ACE2 receptor, *e.g.* by stable transduction (Blanco-Melo *et al.* 2020); and (iii) Calu-3, another lung epithelial adenocarcinoma cell line, derived from a pleural effusion metastasis site, which is highly susceptible to SARS-CoV-2 infection (Wyler *et al.* 2021 and **Figure 26** to **Figure 29**).

First, the differential gene expression of a select set of representative innate immune genes upon SARS-CoV-2 infection was assessed in comparison to SARS-CoV-1, which is known to suppress IFN and ISG induction (Spiegel *et al.* 2005; Spiegel and Weber 2006). In addition, RVFV C113 was included as a positive control, because it is an excellent inducer of IFN and ISGs (Billecocq *et al.* 2004 and **Figure 8**).

In H1299 cells, infection with neither SARS coronavirus species led to a notable upregulation of the tested IFN (IFN- β , IFN- λ 1 and IFN- λ 2), cytokine (CCL5, CXCL10) and IFN-stimulated (IFIT1, MX1, RSAD2) genes (**Figure 31A**). Only RVFV C113 as the positive control was able to elicit a strong gene induction. In A549-ACE2 cells, however, infection with both CoVs induced IFN gene expression and expression of the cytokine CXCL10, albeit to a lesser degree than RVFV C113, while the other tested genes were unaffected by CoV infection (**Figure 31D**).

Surprisingly, in Calu-3 cells, SARS-CoV-2 led to a strong upregulation of all tested genes that in magnitude mirrored induction upon RVFV C113 infection (**Figure 31G**). SARS-CoV-1, however, only very weakly induced IFN genes, and had no effect on the expression of other tested genes. Infection of all cell lines was confirmed by qRT-PCR as shown by C_T values of viral E (SARS-CoV) or L (RVFV) gene normalized to 18S RNA control (**Figure 31B, E, H**). The two SARS coronavirus species replicated to similar levels in all cell lines (**Figure 31C, F, I**).

SARS-CoV-2 and SARS-CoV-1 are closely related, thus it is tempting to assume that, like SARS-CoV-1, SARS-CoV-2 would carry means to suppress IFN gene activation. This phenotype was seen in H1299 and A549-ACE2 cells. However, by stark contrast, in Calu-3 cells a distinct upregulation of tested immune genes was observed in this initial experiment after 24 h of infection.

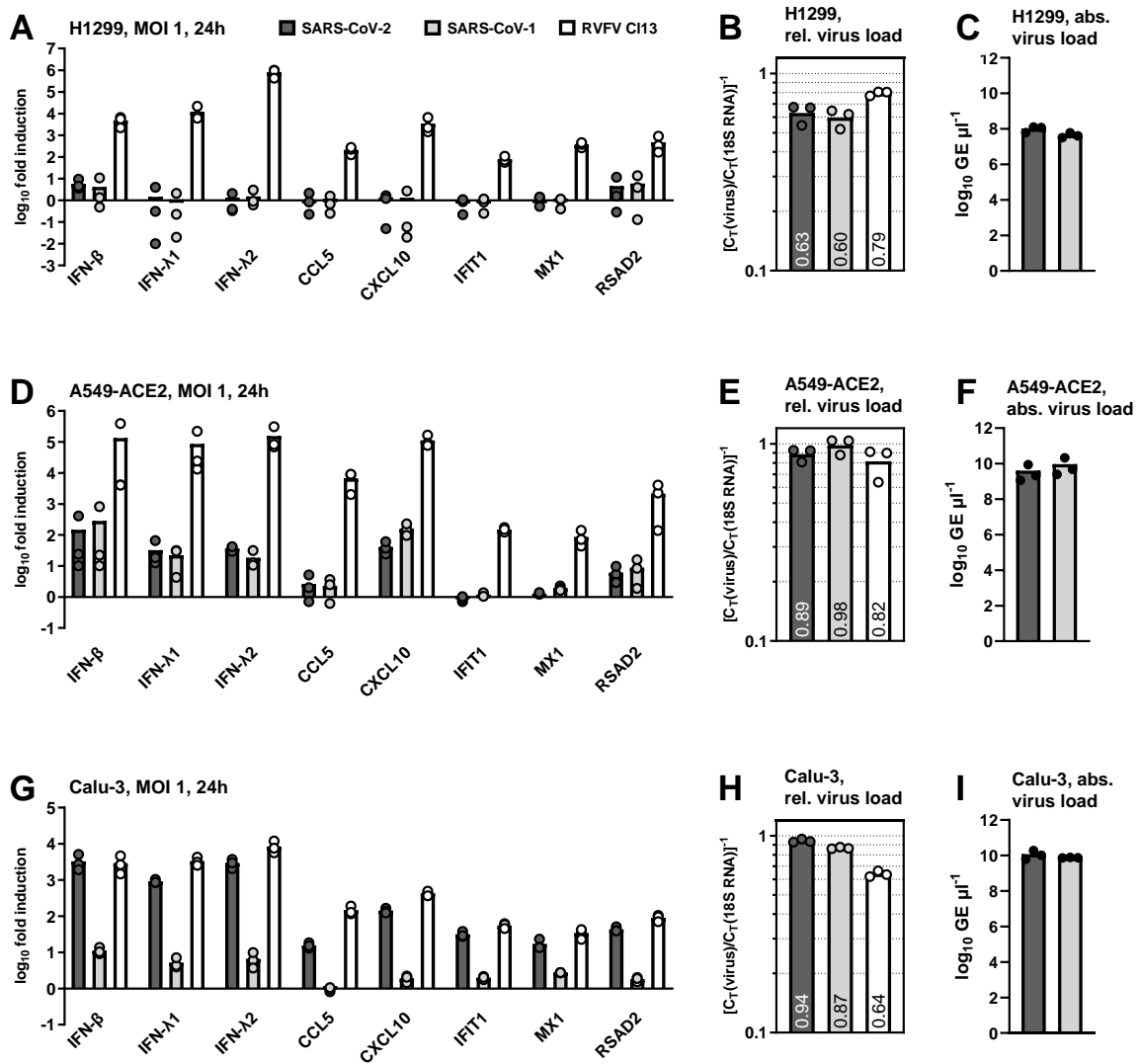


Figure 31: Differential gene expression upon SARS-CoV-2 infection of human lung cell lines. H1299 (A, B, C), A549-ACE2 (D, E, F), and Calu-3 (G, H, I) cells were infected with the indicated virus at an MOI of 1. Cells were lysed at 24 h post infection and subjected to cellular RNA extraction. Gene expression of select IFN genes, ISGs, and cytokines was measured by quantitative real-time PCR. Differential gene expression of innate immune genes (A, D, G) was calculated using the $\Delta\Delta C_T$ method and results are given as fold-induction over the uninfected mock control. 18S rRNA was used as a reference gene. Relative viral gene expression (B, E, H) is pictured as C_T value for viral E (SARS CoVs) or L (RVFV) gene normalized to 18S rRNA control. Absolute viral load of SARS CoVs (C, F, I) is measured in genome equivalent (GE) number, as inferred from a standard curve derived from serial dilutions of a sample with a known genome copy amount.

To exclude the possibility that this result is an artefact of the specific Calu-3 cell clone used, gene induction upon SARS coronavirus infection was assessed in another Calu-3 cell clone. For this, an additional batch of Calu-3 cells was kindly provided by the Institute of Virology at the *Charité Universitätsmedizin*, Berlin. Of note, these “new” cells were approx. of passage 10 and will therefore be deemed “low passage”, while the Calu-3 cells of the initial experiment, kindly provided by the lab of Susanne Herold, Justus Liebig University Giessen, were approx. of passage 60.

To effectively counteract viral infection, cells need to rapidly launch their antiviral response. Therefore, immediate-early innate immune gene activation upon SARS coronavirus infection in Calu-3 cells was

evaluated next. For this, RNA samples were obtained after 8 h of infection in low passage Calu-3 cells and the compilation of marker genes that were shown to react to RNA virus infection was employed (see **Figure 8**).

As shown in **Figure 32**, similar results concerning innate immune gene induction were obtained with the low passage batch of Calu-3 cells. It can therefore be concluded that SARS-CoV-2 infection leads to a genuine upregulation of innate immune genes in Calu-3 cells, and Calu-3 cell batches can be used interchangeably. However, this observed immune gene induction is exclusive to Calu-3 cells.

Moreover, SARS-CoV-2 infection led to a robust upregulation of all tested innate immune genes (**Figure 32A, B**) already at an early time point of 8 h post infection. mRNAs for IFNs (IFN- β , IFN- λ 1 and IFN- λ 2) were upregulated approximately 1,000-fold; for cytokines (CCL4, CCL5, CXCL10, IL-6, TNF- α , TNFSF10) as well as ISGs and other effectors (CH25H, IFIT1, ISG15, OAS1, OAS2, OAS3, PARP14, RSAD2) 10- to 100-fold. IL-8 was thereby the lowest cytokine gene induced by any of the viruses. In stark contrast to SARS-CoV-2, infection with the 2003-emerged SARS-CoV-1 again did not substantially induce the innate immunity markers. Notably, at 8 h post infection, relative and absolute virus loads in Calu-3 cells were higher for SARS-CoV-2- than for SARS-CoV-1-infected cells (**Figure 32C, D**).

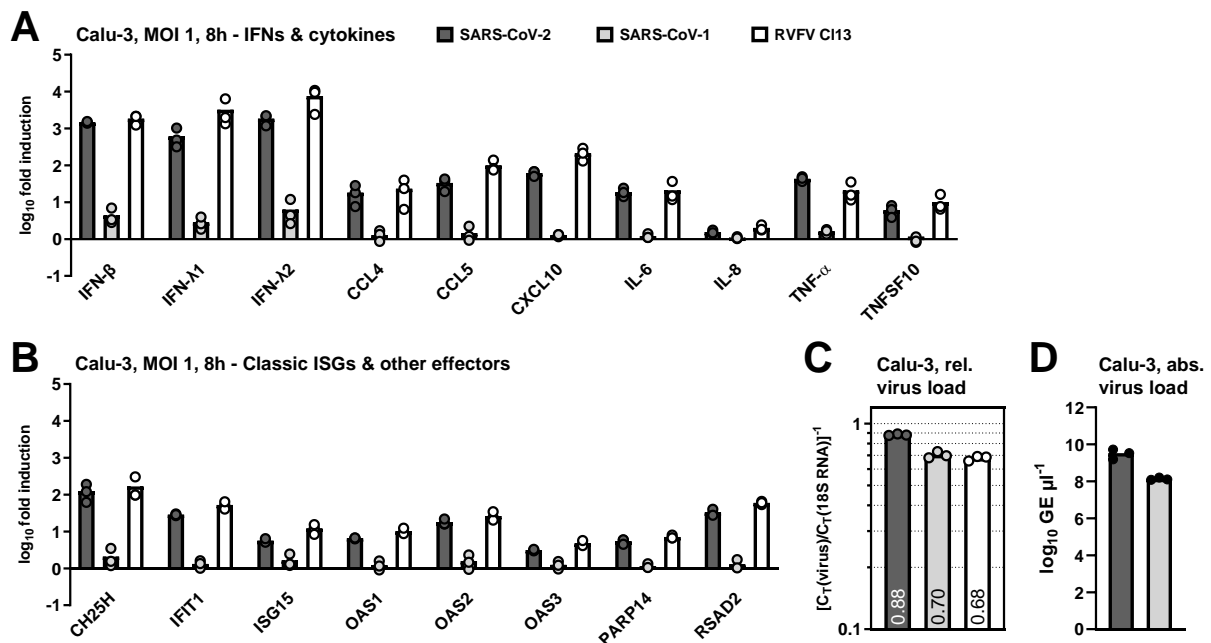


Figure 32: Immediate-early IFN, cytokine and ISG induction profile upon SARS-CoV-2 infection of Calu-3 cells. Calu-3 cells of low passage were infected with the indicated virus at an MOI of 1. Cells were lysed at 8 h post infection and subjected to cellular RNA extraction. Gene expression of IFNs and cytokines (**A**) and classic ISGs and other effectors (**B**) was measured by quantitative real-time PCR. Differential gene expression (**A, B**) was calculated using the $\Delta\Delta C_T$ method and results are given as fold-induction over the uninfected mock control. 18S rRNA was used as a reference gene. Relative viral gene expression (**C**) is pictured as C_T value for viral E (SARS CoVs) or L (RVFV C113) gene normalized to 18S rRNA control. Absolute viral load of SARS CoVs (**D**) is measured in genome equivalent (GE) number.

Previous studies suggest that a certain threshold of SARS-CoV-2 infection is needed for IFN and ISG induction (Blanco-Melo *et al.* 2020). To further investigate this, the experiment was repeated using a 10-fold lower input MOI and samples were analyzed at 8 h and 24 h post infection.

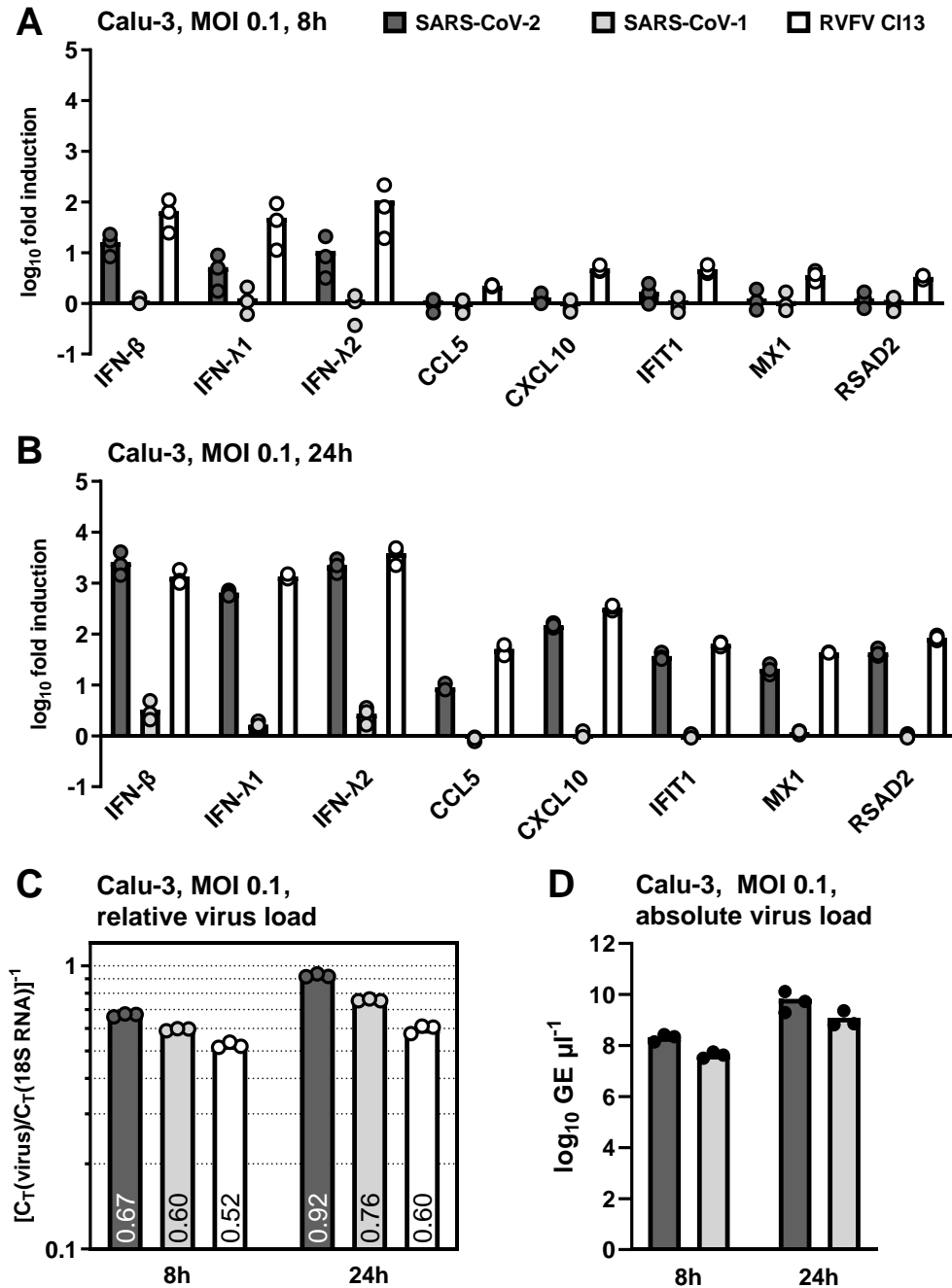


Figure 33: Differential gene expression upon SARS-CoV-2 infection of Calu-3 cells at lower virus loads. Calu-3 cells were infected with the indicated virus at an MOI of 0.1. Cells were lysed at 8 h (A) and 24 h (B) post infection and subjected to cellular RNA extraction. Gene expression was measured by quantitative real-time PCR. Differential gene expression (A, B) was calculated using the $\Delta\Delta C_T$ method and results are given as fold-induction over the uninfected mock control. 18S rRNA was used as a reference gene. Relative viral gene expression (C) is pictured as C_T value for viral E (SARS CoVs) or L (RVFV) gene normalized to 18S rRNA control. Absolute viral load of SARS CoVs (D) is measured in genome equivalent (GE) number.

At 8 h post infection, using an input MOI of 0.1 lowered, but did not abrogate, IFN gene upregulation by SARS-CoV-2; however, upregulation of cytokine genes and ISGs was hardly above mock levels for both SARS coronavirus species (**Figure 33A**). Still, induction of these genes upon RVFV C113 infection was also considerably low under these conditions. At 24 h post infection, both SARS-CoV-2 and RVFV C113 strongly induced expression of all genes tested to a similar degree, even with a lower input MOI (**Figure 33B**). As expected, no immune gene induction was observed upon SARS-CoV-1 infection. These data therefore indeed support the hypothesis that a certain threshold of SARS-CoV-2 virus load in the host cell is needed to induce an antiviral response on transcriptional level. However, this phenomenon was only observed for cytokines and ISGs, as IFN gene induction was independent of virus load and timepoint post infection.

Small differences in viral loads (**Figure 33C, D**) were comparable to the earlier experiments. However, having shown that SARS-CoV-2 infection is able to stimulate IFN gene expression even at a lower virus load in Calu-3 cells at 8 h post infection, compared to no IFN gene induction by SARS-CoV-1 at a higher virus load at 24 h post infection (**Figure 33D**), it can be assumed that the clear differences in gene induction between the two SARS coronavirus species are not due to differences in virus load.

7.2.6 IFN and ISG expression upon SARS-CoV-2 infection in human lung cell lines

Next, it was to be investigated if the transcriptional induction of IFNs and ISGs also translates to an upregulation on a protein level. To evaluate the expression of ISGs upon SARS-CoV-infection, Calu-3, H1299 and A549-ACE2 cells were infected at an MOI of 1, cell lysates were collected 24 h post infection and subjected to immunoblotting (**Figure 34**).

In H1299 and A549-ACE2 cells, ISGs IFIT1 and MxA were expressed only upon infection with the control virus RVFV C113. By contrast, in Calu-3 cells SARS-CoV-2 infection induced expression of MxA to a similar degree as the control virus, while SARS-CoV-1 caused no upregulation. IFIT1 was robustly induced by the control virus and slightly upregulated by infection with either SARS coronavirus species. These observations show that SARS-CoV-2 not only induces expression of IFN and ISGs on mRNA level, but also on protein level, and that this induction again is limited to Calu-3 but not H1299 and A549-ACE2 cells.

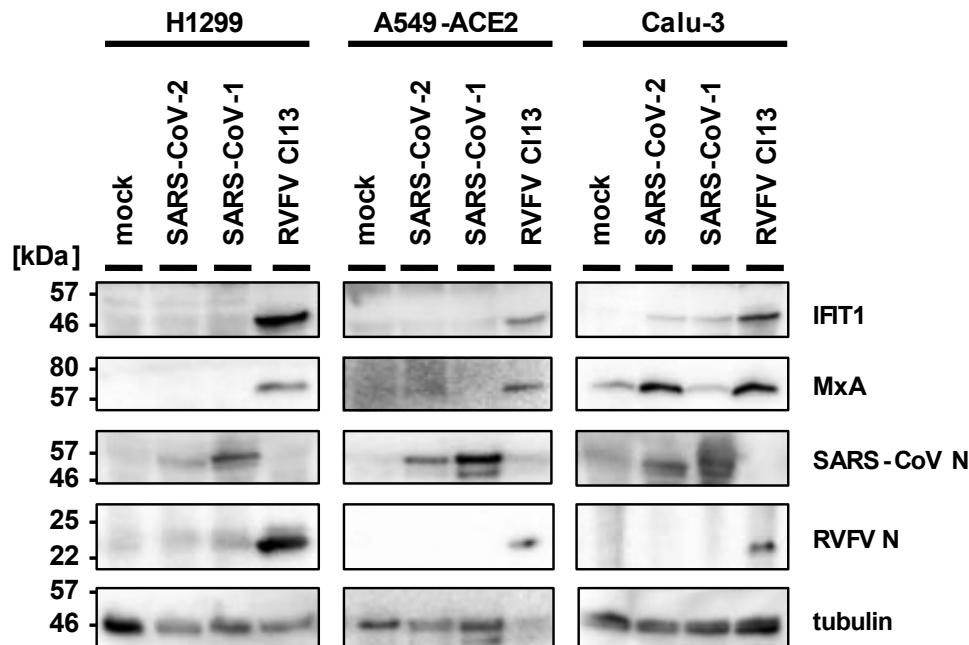


Figure 34: Production of ISGs upon SARS-CoV-2 infection. Cells were infected with the indicated virus at an MOI of 1 for 24 h. Cell lysates were analyzed for the indicated antigens using immunoblotting. The data are representative of three independent experiments. Molecular markers are shown on the left sides of the blots. kDa, kilodalton; N, nucleoprotein.

Further, IFN secretion upon SARS coronavirus infection was assessed. For this, an established IFN bioassay was employed (Kuri *et al.* 2010). To measure the presence and amount of type I IFN, this assay relies on the inhibition of a highly IFN-sensitive reporter virus by type I IFN in a given sample. Here, A549 cells were incubated with supernatants from SARS-CoV-2-, SARS-CoV-1-, and RVFV C113-infected H1299, A549-ACE2, and Calu-3 cells. Supernatants were treated with β -propiolactone thus inactivating infectious virus while preserving IFNs. Pre-incubated A549 cells were subsequently infected with the reporter virus RVFV-delNSs::Renilla. This virus has its gene for the virulence factor NSs replaced by the *Renilla* luciferase gene. Due to the lack of NSs, RVFV-delNSs::Renilla is highly sensitive to IFN. Further, inclusion of the *Renilla* luciferase gene allows for virus quantification via luciferase readout.

Confirming the previous results on gene expression level, the replication of the reporter virus was not affected by treatment with supernatant from SARS-CoV-2- and SARS-CoV-1-infected H1299 and A549-ACE2 cells (**Figure 35**). This indicates that there is no type I IFN released from either of those cell lines upon infection with either coronavirus. As expected, infection of H1299 and A549-ACE2 with control virus RVFV C113 led to a robust type I IFN induction which is mirrored by nearly complete inhibition of reporter virus growth. Supernatant derived from SARS-CoV-2-infected Calu-3 cells, however, was able to inhibit reporter virus growth to a similar degree as RVFV C113. This confirms that biologically active type I IFN is released from SARS-CoV-2-infected Calu-3 cells, while no IFN is detectable upon SARS-CoV-1 infection.

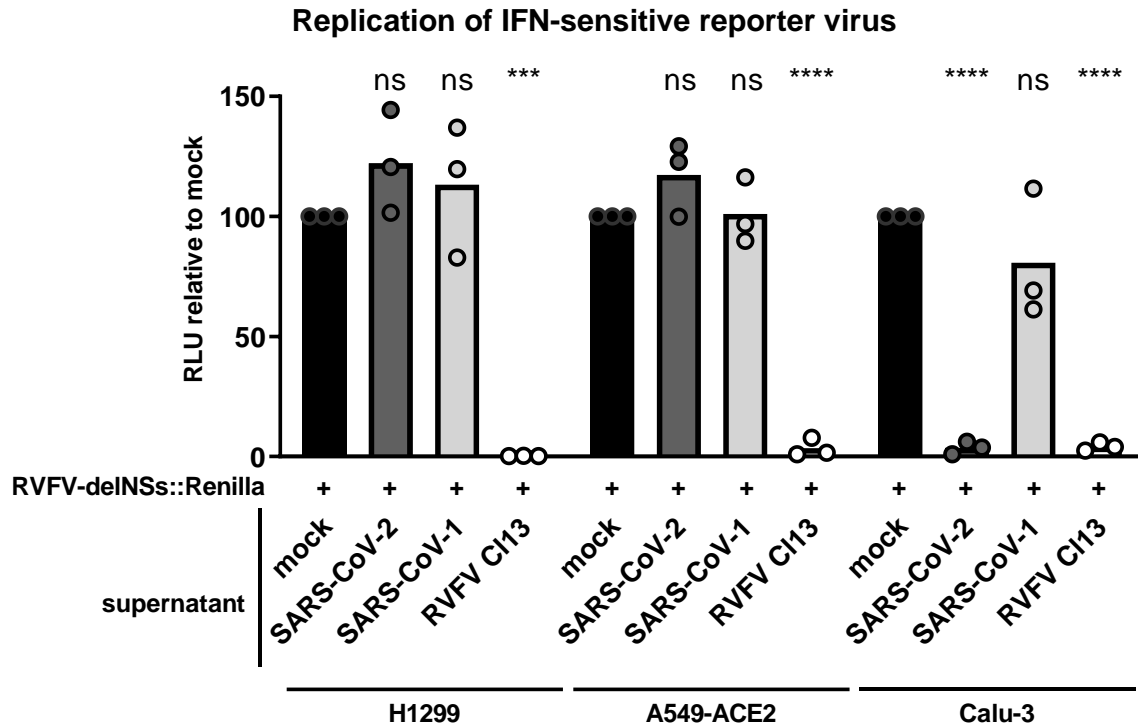


Figure 35: Production of IFN upon SARS-CoV-2 infection. Cells were infected with the indicated virus at an MOI of 1. 24 h post infection, supernatant was collected and inactivated using β -propiolactone. Inactivated supernatant was transferred to A549 cells and incubated for 7 h. A549 cells were then infected with the IFN-sensitive reporter virus RVFV-delINSs::Renilla for 16 h. *Renilla* luciferase was measured as readout for reporter virus growth. Results are given as relative RVFV-delINSs::Renilla growth compared to mock control (100%). Individual values (dots) and geometric mean values (bars) from three biological replicates are shown. Values were analyzed by ordinary one-way ANOVA with Dunnett's post-test compared to mock control. *** $P < 0.0002$; **** $P < 0.0001$; ns, not significant (Graphpad Prism). RLU, relative luciferase units.

7.2.7 Transcriptomic analysis of SARS-CoV-infected human lung cell lines

To investigate the striking differences in innate immune factor induction between the three human lung carcinoma cell lines H1299, A549-ACE2 and Calu-3 following SARS-CoV-2 infection, in a next step, transcriptomic analyses of those cell lines were performed.

On the one hand, transcriptomic signatures upon SARS-CoV-2 and SARS-CoV-1 infection were more closely investigated. On the other hand, the transcriptomic profiles of uninfected cells were compared to identify potential basic differences between the cell lines.

For this, H1299, A549-ACE2 and Calu-3 cells were infected with SARS-CoV-2 or SARS-CoV-1 at an MOI of 1 for 24 h, RNA was obtained from cell lysates and infection was confirmed by qRT-PCR (**Figure 36A–C**). Subsequently, bulk mRNA sequencing was performed on these RNA samples. The percentage of viral reads over total reads is shown in **Figure 36D** and mirrors total genomic RNA assessment in samples.

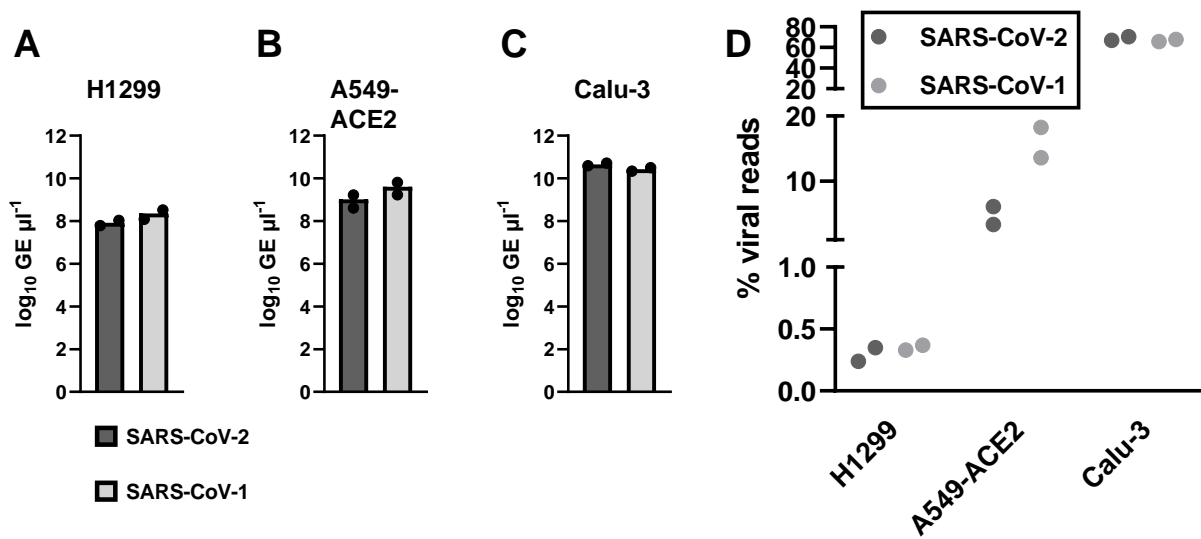


Figure 36: Viral RNA in total cellular RNA for transcriptomic analysis. H1299 (A, D), A549-ACE2 (B, D), and Calu-3 (C, D) cells were infected with the indicated virus at an MOI of 1. Cells were lysed at 24 h post infection and subjected to cellular RNA extraction. (A – C) Total viral RNA per sample was assessed via qRT-PCR. Individual values (dots) and geometric mean values (bars) from two biological replicates are shown. (D) Percentage of virus-aligned reads (over total reads) is indicated for each sample upon RNAseq transcriptomic profiling. Individual values from two biological replicates are shown. GE, genome equivalents.

In line with the previous experiments, viral load was greatest in Calu-3 cells, intermediate in A549-ACE2 cells, and lowest in H1299 cells. Accordingly, differentially expressed gene (DEG) profiles (adjusted p value $P_{\text{adj}} \leq 0.05$; cut off: log₂-fold change < -2 or > 2) compared to uninfected control cells varied between the three cell lines, as expected (Table 51).

Table 51: Number of differentially expressed genes following SARS coronavirus infection

	<i>H1299</i>		<i>A549-ACE2</i>		<i>Calu-3</i>	
	SARS-CoV-2	SARS-CoV-1	SARS-CoV-2	SARS-CoV-1	SARS-CoV-2	SARS-CoV-1
upregulated	0	0	1	3	743	143
downregulated	0	0	0	0	13	1

Top 50 upregulated genes in Calu-3 cells

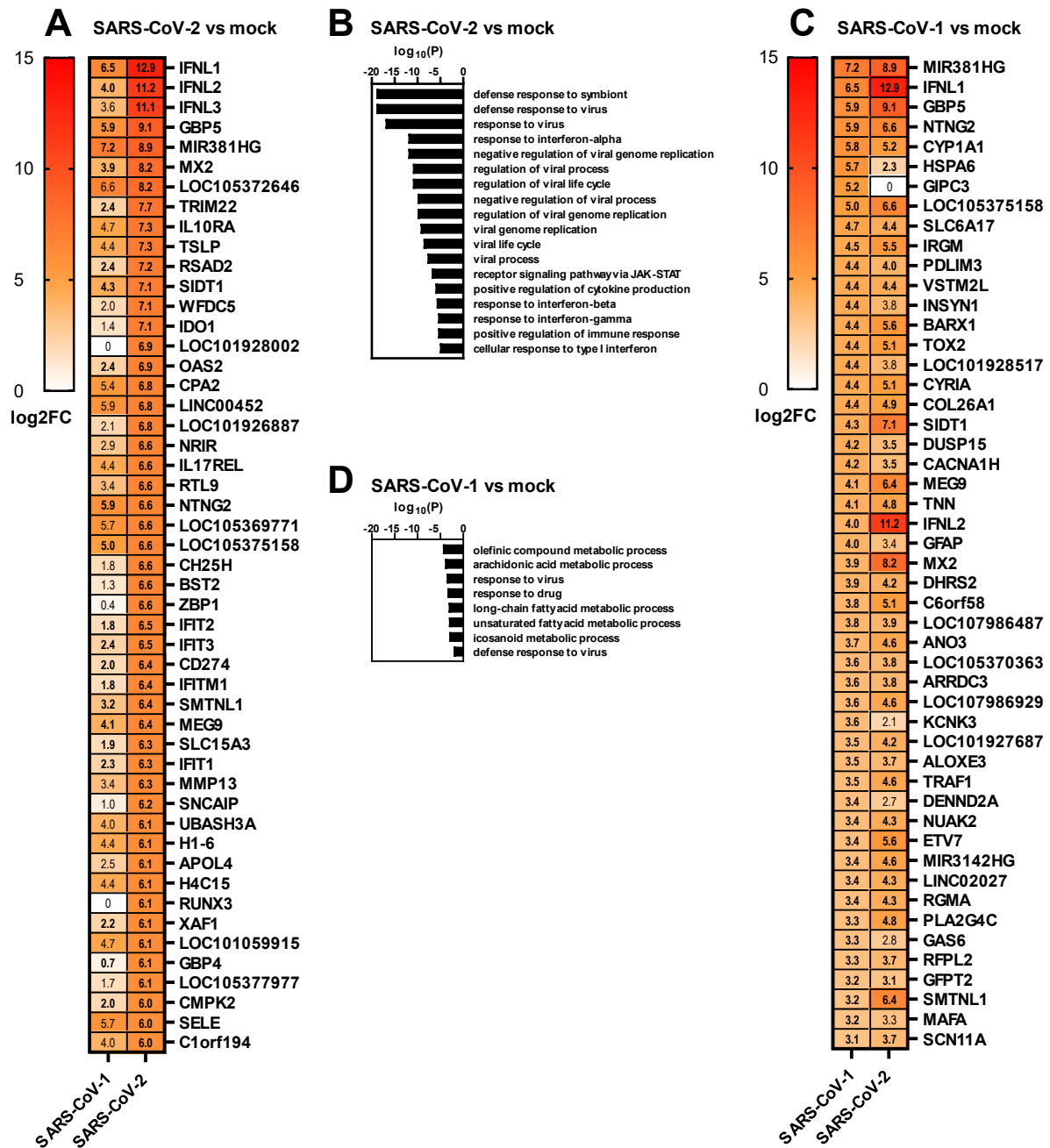


Figure 37: Top 50 upregulated genes upon SARS-CoV-2 (A, B) or SARS-CoV-1 (C, D) infection of Calu-3 cells compared to mock cells. Calu-3 cells were infected with SARS-CoV-2 or SARS-CoV-1 at an MOI of 1 for 24 h, at which point mock and infected samples were harvested for bulk RNAseq analysis. (A, C) Heatmaps displaying the top 50 upregulated genes upon SARS coronavirus infection. The displayed genes were filtered by an adjusted p value ≤ 0.05 , and sorted by absolute log₂-fold change, for which the value is given in each cell. The corresponding log₂-fold change value for the other virus is also shown. Statistical significance (adjusted p value ≤ 0.05) is indicated by bold lettering of the log₂-fold change values. Data are averages from two biological replicates. (B, D) Statistically enriched GO terms within the gene sets displayed in A and C, as analyzed using Metascape (Zhou *et al.* 2019).

Only in Calu-3 cells, SARS coronavirus infection evoked a substantial differential regulation of host cellular genes. Upon SARS-CoV-2 infection, more genes were up- and downregulated than following

SARS-CoV-1 infection. In both cases, more upregulated than downregulated genes were measured (**Table 51**). The top 50 upregulated genes in SARS coronavirus infection of Calu-3 cells are displayed in **Figure 37**. Confirming previous experiments (**Figure 31** and **Figure 32**), the transcriptomic profile of only SARS-CoV-2-infected Calu-3 cells displayed a profound antiviral signature (**Figure 37A, B**). In contrast, Calu-3 infection with SARS-CoV-1 (**Figure 37C, D**) did not elicit this fundamental induction of IFN and IFN-stimulated genes. Moreover, genes were less strongly upregulated in SARS-CoV-1-infected cells, indicated by lower log₂-fold change values.

These differences between the two SARS coronavirus species were further visualized by generating volcano plots of all DEGs upon SARS coronavirus infection and highlighting the genes annotated to the GO list #0009615 “response to virus” (obtained from <https://www.ebi.ac.uk/QuickGO/>). As shown in **Figure 38**, genes belonging to this gene set were profoundly upregulated upon SARS-CoV-2 infection of Calu-3 cells (52 genes upregulated). In contrast, only a modest upregulation of a much smaller number of genes was observed following SARS-CoV-1 infection (9 genes upregulated).

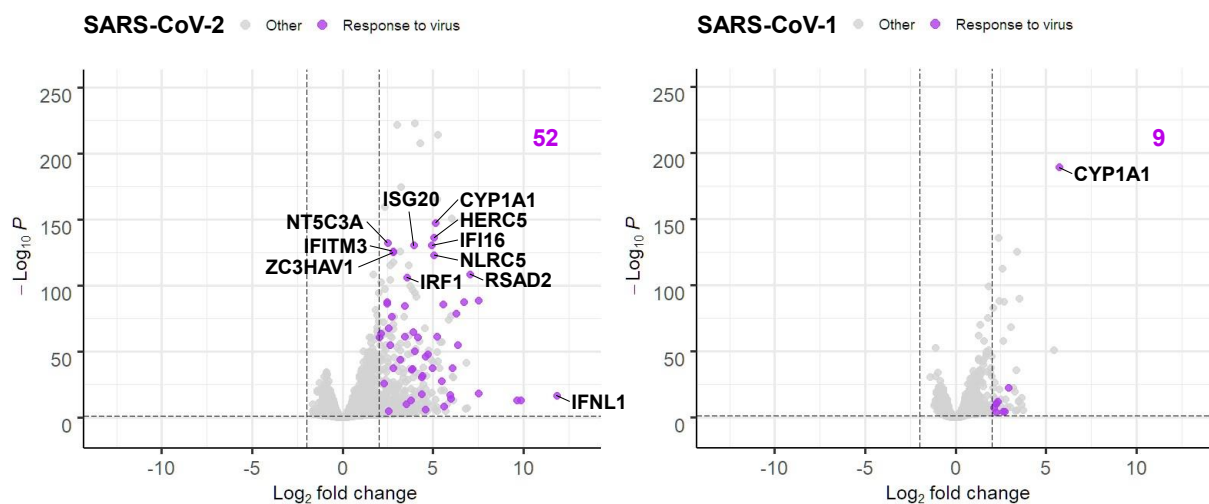


Figure 38: Antiviral signatures of SARS-CoV-infected Calu-3 cells. Calu-3 cells were infected with the indicated virus at an MOI of 1 for 24 h, at which point mock and infected samples were harvested for bulk RNAseq analysis. Volcano plots are shown with all DEGs in gray and the gene set annotated to the GO list #0009615 “response to virus” highlighted in purple. The displayed genes were filtered by an absolute log₂-fold change of 2 and an adjusted p value ≤ 0.05. Data are averages from two biological replicates.

In addition to the upregulated gene signature, downregulated genes in SARS coronavirus-infection were also examined. The top 30 downregulated genes upon infection of Calu-3 cells are displayed in **Figure 39**. Here too, SARS-CoV-2 more strongly downregulated host cell genes than did SARS-CoV-1. Interestingly, among the top downregulated genes upon SARS-CoV-2 infection were *RNR2* and *RNR1*, while these two host genes were slightly upregulated in SARS-CoV-1 infection (**Figure 39A**). *RNR2* and *RNR1* genes code for mitochondrially encoded 16S and 12S RNA, respectively.

Top 30 downregulated genes in Calu-3 cells

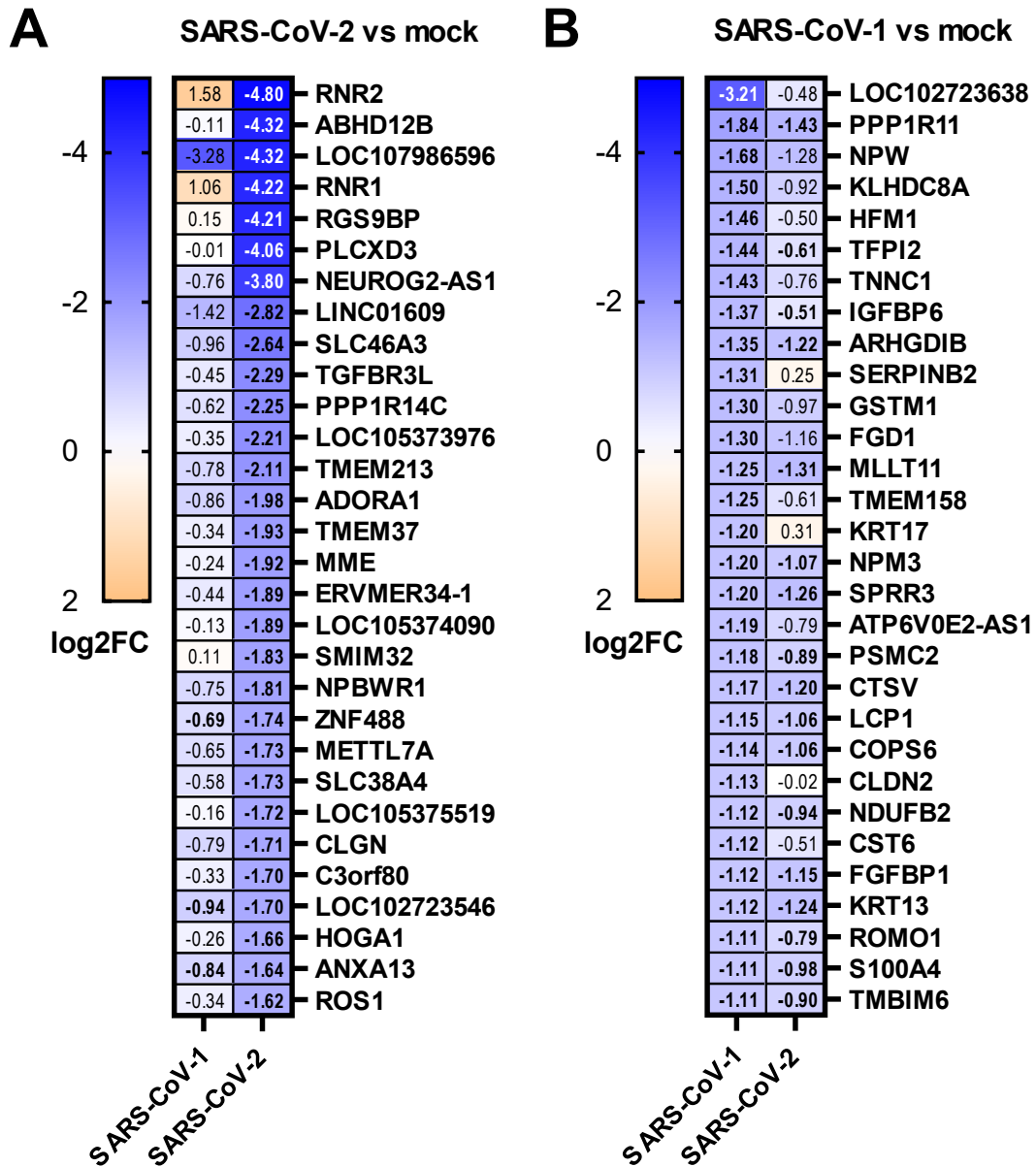


Figure 39: Top 30 downregulated genes upon SARS-CoV-2 (A) or SARS-CoV-1 (B) infection of Calu-3 cells compared to mock cells. Calu-3 cells were infected with SARS-CoV-2 or SARS-CoV-1 at an MOI of 1 for 24 h, at which point mock and infected samples were harvested for bulk RNAseq analysis. The displayed heatmaps show genes filtered by an adjusted p value ≤ 0.05 and sorted by absolute log₂-fold change, for which the value is given in each cell. The corresponding log₂-fold change value for the other virus is also shown. Statistical significance (adjusted p value ≤ 0.05) is indicated by bold lettering of the log₂-fold change values. Data are averages from two biological replicates.

The host cellular transcriptomic response upon SARS coronavirus infection of A549-ACE2 cells was sparse. **Figure 40** shows all significantly differentially regulated genes for these conditions. Notably, the three differentially upregulated genes upon SARS-CoV-2 infection, *EGR1*, *FOSB* and *ATF3*, are upregulated to a comparable degree also in SARS-CoV-1 infection, indicating a similar influence on A549-ACE2 cellular transcription by both viruses.

Differentially regulated genes in A549-ACE2 cells

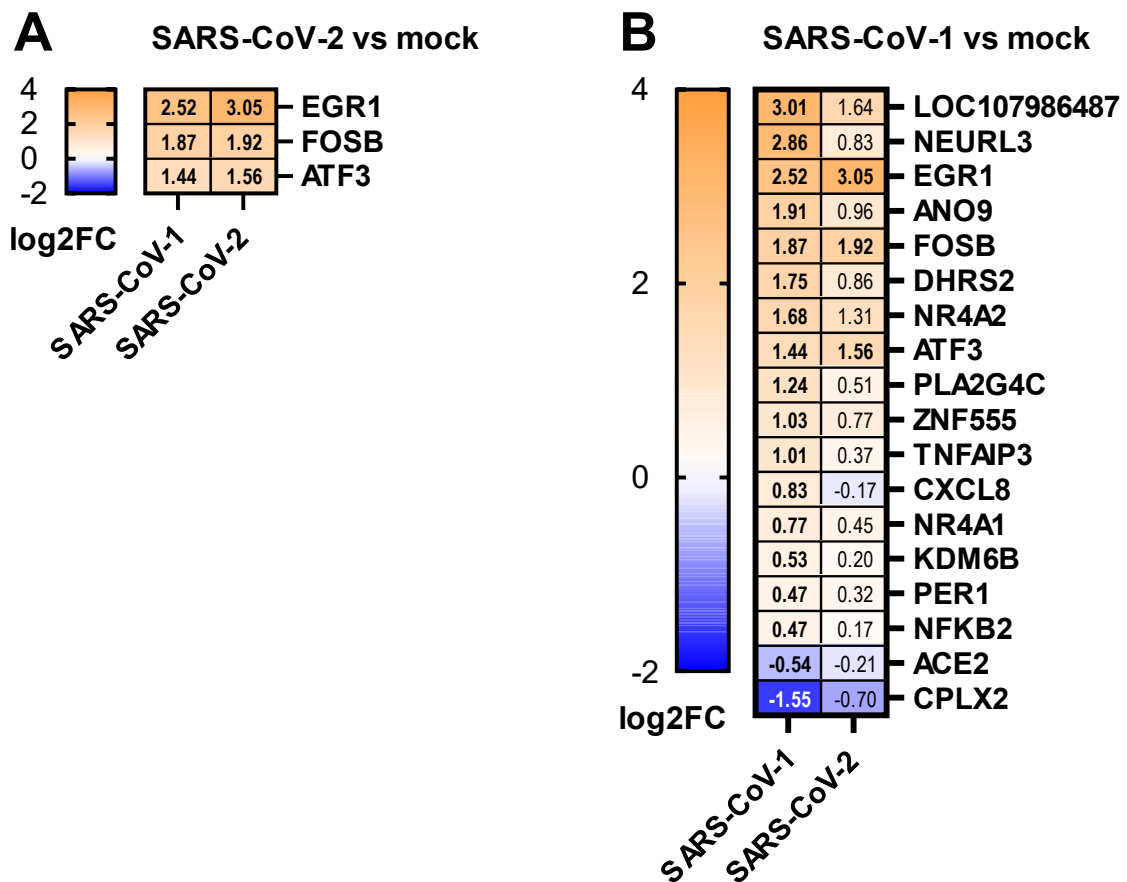


Figure 40: Total differentially regulated genes upon SARS-CoV-2 (A) or SARS-CoV-1 (B) infection of A549-ACE2 cells compared to mock cells. A549-ACE2 cells were infected with SARS-CoV-2 or SARS-CoV-1 at an MOI of 1 for 24 h, at which point mock and infected samples were harvested for bulk RNAseq analysis. The displayed heatmaps show genes filtered by an adjusted p value ≤ 0.05 and sorted by absolute log₂-fold change, for which the value is given in each cell. The corresponding log₂-fold change value for the other virus is also shown. Statistical significance (adjusted p value ≤ 0.05) is indicated by bold lettering of the log₂-fold change values. Data are averages from two biological replicates.

Next, to elucidate potential fundamental differences between the three human lung cell lines, transcriptomic profiles of uninfected H1299, A549-ACE2 and Calu-3 cells were compared. **Figure 41** shows the top 50 upregulated as well as the top 50 downregulated genes in uninfected Calu-3 cells compared to H1299 or A549-ACE2 cells.

Top 50 upregulated genes in Calu-3 mock Top 50 downregulated genes in Calu-3 mock

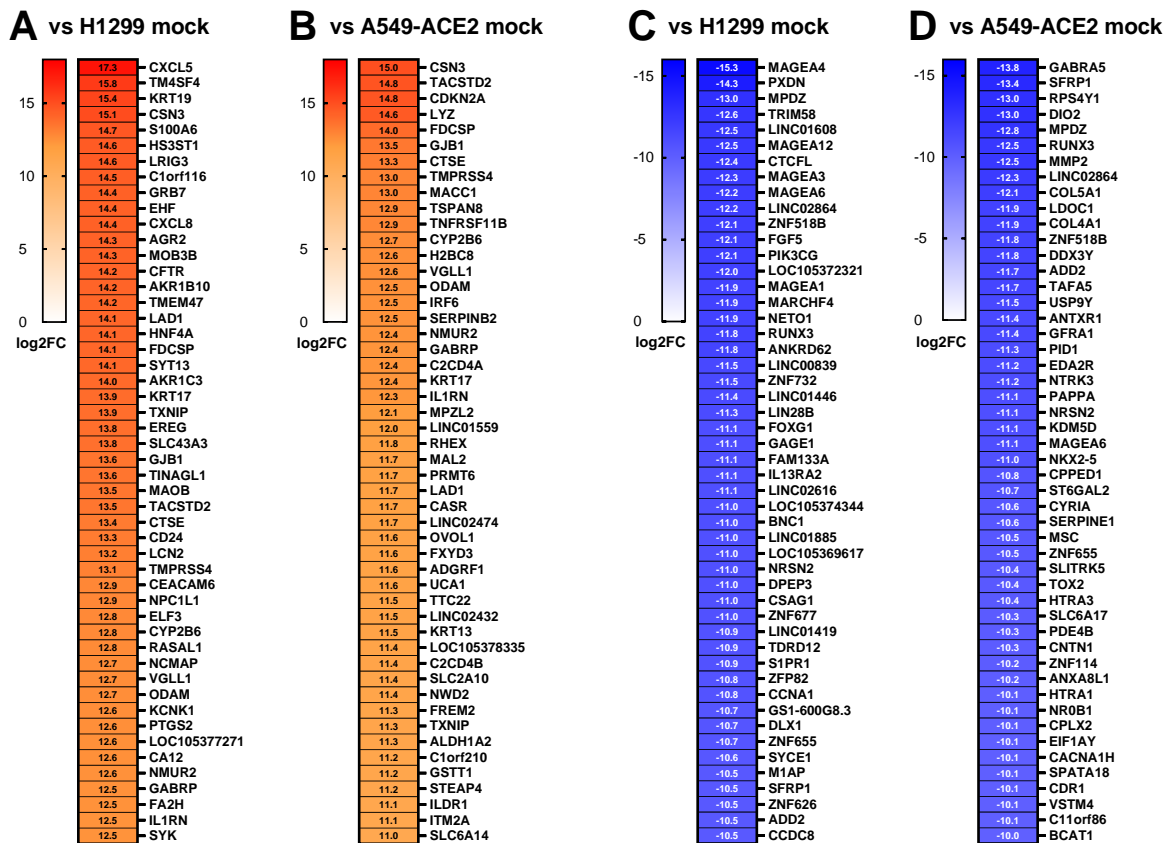


Figure 41: Comparison of transcriptomic profiles of uninfected human lung cell lines. H1299, A549-ACE2 or Calu-3 cells were mock infected for 24 h, at which point samples were harvested for bulk RNAseq analysis. Heatmaps display the top 50 upregulated (A, B) and the top 50 downregulated (C, D) genes in Calu-3 cells versus H1299 (A, C) and A549-ACE2 (B, D) cells. The displayed genes were filtered by an adjusted p value ≤ 0.05 and sorted by absolute log₂-fold change, for which the value is given in each cell. Data are averages from two biological replicates.

In Calu-3 cells, 971 genes were upregulated compared to H1299 cells, and 673 genes compared to A549-ACE2 cells. Thereby, a shared set of 434 genes was upregulated compared to both cell lines (Figure 42A). To further characterize the differences between these cell lines, transcription factor analysis was performed on this overlap of gene lists (upregulated in Calu-3 versus H1299 and A549-ACE2 cells). This revealed that naïve Calu-3 cells displayed a signature characterized by profound enrichment of genes regulated by transcription factors involved in immunity and inflammatory responses, like NF- κ B subunits NFKB1 and RELA or members of the STAT family (Figure 42B).

At the same time, 797 genes were downregulated in Calu-3 cells compared to H1299 cells, and 672 genes compared to A549-ACE2 cells. 250 genes were downregulated in relation to both cell lines (Figure 42C). Transcriptional analysis of this overlap of gene lists rendered less enriched transcription factor targets than analysis of the upregulated overlap (Figure 42D). Of note, target genes of NF- κ B subunit NFKB1 were also enriched in the downregulated overlap, although not as strongly as in the upregulated set. RELA, STAT1 and STAT3 targets were not enriched.

Of note, gene ontology analyses with the sets of overlapping genes were also performed, but were inconclusive and provided no useful information in this case (Figure 49, annex).

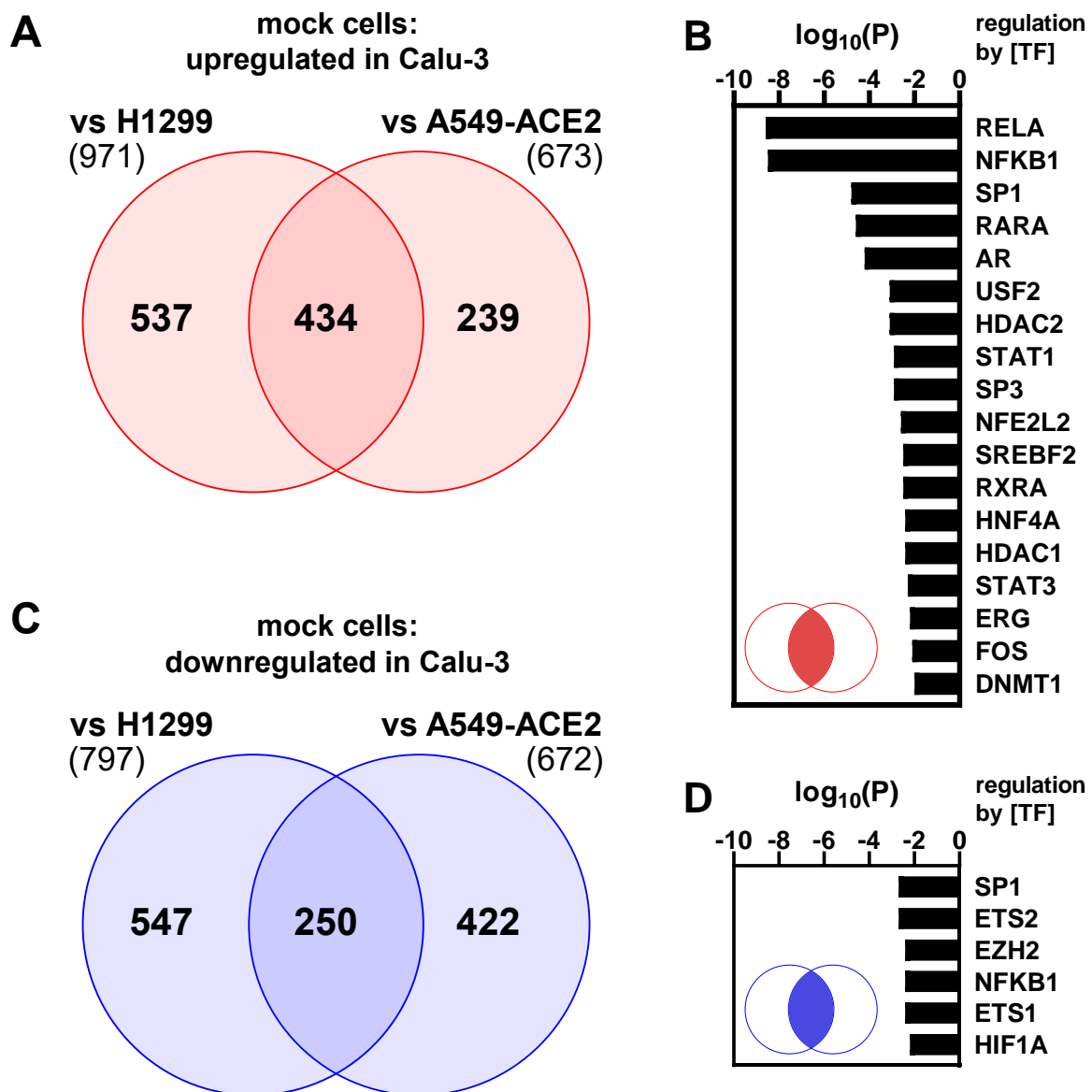


Figure 42: Naïve Calu-3 cells exhibit a “pre-stimulated” state compared to H1299 and A549-ACE2 cells. H1299, A549-ACE2 or Calu-3 cells were mock infected for 24 h, at which point samples were harvested for bulk RNAseq analysis. Genes were filtered by an absolute \log_2 -fold change of 5 and an adjusted p value ≤ 0.05 . Data are averages from two biological replicates. (A, C) Venn diagrams showing the numbers of up- (A) and down- (C) regulated genes in Calu-3 cells versus H1299 and A549-ACE2 cells. (B, D) Statistically enriched transcription factors regulating genes within the overlapping gene set “upregulated in Calu-3 cells compared to H1299 and A549-ACE2 cells” (B) and “downregulated in Calu-3 cells compared to H1299 and A549-ACE2 cells” (D), as analyzed using Metascape (Zhou *et al.* 2019). TF, transcription factor; vs, versus.

Two recent publications corroborate the here presented findings that SARS-CoV-2 induces IFNs and other innate immune genes in Calu-3 cells. Thereby, this phenomenon was attributed on the one hand to lower basal levels of RIG-I (Yamada *et al.* 2021), and on the other hand to higher levels of MDA5 (Li *et al.* 2021) in these cells. Consequently, in a next step of this work, the expression levels of those

PRRs in the three human lung cell lines were assessed. In contrast to Yamada *et al.*, but in agreement with Li *et al.*, Calu-3 cells exhibited higher levels of both RIG-I and MDA5 than did H1299 and A549-ACE2 cells (**Figure 43**).

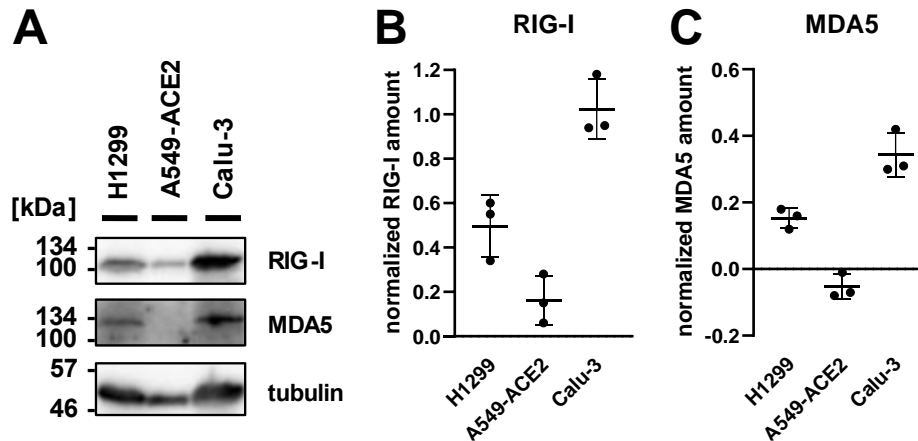


Figure 43: PRR levels in uninfected human lung cell lines. H1299, A549-ACE2 or Calu-3 cells were mock infected for 24 h. (A) Cell lysates were analyzed for the indicated antigens using immunoblotting. The data are representative of three independent experiments. Molecular markers are shown on the left sides of the blots. (B, C) Western Blot bands were quantified using the Image Lab software. Normalized amounts of PRRs are given as intensity of PRR divided by intensity of reference gene tubulin. kDa, kilodalton.

Taken together, this work found that SARS-CoV-2, but not SARS-CoV-1 induces a strong upregulation of IFNs and other innate immune genes, which is limited to Calu-3 cells. Calu-3 cells, in comparison to H1299 and A549-ACE2 cells, were shown to express a transcriptional profile dominated by target genes of innate immunity-associated transcriptions factors. Furthermore, Calu-3 cells expressed higher basal levels of PRRs RIG-I and MDA5. Therefore, it is tempting to hypothesize that Calu-3 cells, as opposed to H1299 and A549-ACE2 cells, exhibit a “pre-stimulated” state which allows for rapid innate immunity activation upon SARS-CoV-2 infection. Still, this innate immune activation is absent in SARS-CoV-1 infection, indicating different properties of the two SARS coronaviruses to suppress Calu-3 antiviral mechanisms.

BSL-3 work involved in data generation for **Figure 31** – **Figure 43** and **Figure 49** was in part performed by Patrick Schmerer and Simone Lau (Institute for Virology, FB10, Justus Liebig University Giessen). RNAseq was performed by Benjamin Ott (Institute of Medical Microbiology, Justus Liebig University Giessen). Transcriptomic and bioinformatic analyses for **Figure 36** – **Figure 42** and **Figure 49** were performed with the great help of Torsten Hain and Benjamin Ott (Institute of Medical Microbiology, Justus Liebig University Giessen).

8 Discussion

Newly emerging viruses pose a great threat to global health and economics. To better understand human infection with novel viruses, it is vital to gain a thorough understanding of these viruses' interactions with the innate immune system, the body's first line of defence against intruding pathogens. This work focused on the characterization of two novel viruses with regard to their innate immunity phenotype. The first analysis concerned the recently described Ntepes virus, a member of the genus *Phlebovirus*, alongside related newly discovered phleboviruses with unknown implications for human disease. The second study focused on SARS coronavirus 2, the causative agent of the ongoing global COVID-19 pandemic, which, at the time of writing, has resulted in more than 222 million infections and claimed approx. 4.5 million deaths worldwide (COVID-19 Dashboard, Johns Hopkins University, accessed on 08 September 2021).

8.1 Newly discovered phleboviruses with potential implications for human health

A sandfly vector surveillance study conducted in 2014 in Kenya identified a previously unknown phlebovirus termed Ntepes virus (NTPV; Tchouassi *et al.* 2019). This work presents the first innate immunity characterization of NTPV. To this end, human cell line susceptibility to NTPV, IFN, cytokine and ISG induction, as well as sensitivity to type I and type III IFN were assessed through infection experiments (chapter 7.1.1 to 7.1.4). Thereby, NTPV was compared to its closest known relative Gabek Forest virus (GFV) and two well-characterized Rift Valley fever virus (RVFV) strains of different pathogenicity. Further, a molecular functional characterization of NTPV virulence factor NSs was conducted (chapter 7.1.5). For these analyses, NSs proteins of four additional newly discovered phleboviruses were included, namely Embossos (EMBV), Bogoria (BGRV), Kiborgoch (KBGV) and Perkerra (PERV) viruses (Marklewitz *et al.* 2020), in comparison to the well-known NSs proteins of Rift Valley fever virus (RVFV), Sandfly fever Sicilian virus (SFSV) and two members of the Punta Toro virus (PTV) species group. NSs proteins were evaluated regarding their ability to counteract the induction of innate immune genes in luciferase-based reporter assays, and host cell binding partners of NSs proteins were identified through mass spectrometry interactome analyses.

8.1.1 Innate immunity characterization of novel phlebovirus Ntepes virus suggests low pathogenicity in humans

The innate immune system, with type I (IFN- α/β) and type III (IFN- λ) IFNs as key players, acts as first-line defence against intruding pathogens. IFNs produced upon virus infection induce the expression of many ISGs of which several have direct antiviral functions (Schoggins *et al.* 2011). Consequently, pathogenic viruses have developed strategies to counteract IFN induction and/or signalling.

This work demonstrated that *in vitro* NTPV infection induces efficient production of IFNs, related cytokines and ISGs on a transcriptional level, thereby mirroring the response to avirulent RVFV C113 infection (**Figure 8**). This suggests that NTPV is unable to inhibit the host innate immune response efficiently and completely. The natural mutant C113 expresses a truncated, non-functional NSs virulence protein (Muller *et al.* 1995) and, as a consequence, is an excellent inducer of innate immune genes (Billecocq *et al.* 2004). In contrast, RVFV vaccine strain MP-12 expresses a functional NSs (Caplen *et al.* 1985) targeting the innate immune system (Eifan *et al.* 2013) and, as expected, led to lower induction levels of IFNs and cytokines. NTPV carries an NSs open reading frame in its S segment, predicted to encode a 30 kDa protein (Tchouassi *et al.* 2019). Possible explanations for this discrepancy are that NTPV NSs is either not as efficient as RVFV NSs in counteracting the innate immune response, or, although less likely, that it is not expressed in the infected cell.

IFN and cytokine induction upon virus infection is critical to combat the infection, but needs to be balanced, as an unchecked pro-inflammatory cytokine expression can lead to pathologic hyperinflammation and increased disease severity. The effects of IFN and cytokine upregulation in phenuivirus infection vary between different virus species. On the one hand, it has been shown for members of the PTV serogroup that the low-pathogenic PTV Balliet strain, but not the more virulent Adames strain, efficiently induces IFNs, cytokines and ISGs in primary mouse macrophages (Mendenhall *et al.* 2009). On the other hand, high levels of pro-inflammatory cytokines such as IL-6, IL-10 or TNF- α , were positively correlated with disease severity in Severe fever with thrombocytopenia syndrome virus (SFTSV), TOSV, and RVFV patients (Jansen van Vuren *et al.* 2015; Liu *et al.* 2017a; Fujikawa *et al.* 2019; Vilibic-Cavlek *et al.* 2020). While *in vitro* NTPV infection leads to a strong upregulation of those pro-inflammatory cytokines, type I and type III IFNs are efficiently induced as well, suggesting a balanced activation of the innate immune system correlated with lower pathogenicity as seen with RVFV C113.

Further, this work shows that NTPV is sensitive to systemically active type I IFN (**Figure 9**), as well as to type III IFN acting on mucosal surfaces (**Figure 10**). Again, IFN sensitivity was comparable to RVFV C113 and increased compared to RVFV MP-12. Inhibitor studies targeting host IFN signalling confirmed that the IFN produced upon NTPV infection can limit NTPV replication *in vitro*, as demonstrated by a titre increase upon IFN signalling disruption by the drug Ruxolitinib (**Figure 11**). This indicates that the host innate immune response is effective against NTPV infection. Of note, there were cell-line dependent differences in IFN and inhibitor assays, with effects being more pronounced in lung A549 cells than in liver Huh7 cells. This hints at the notion that A549 cells respond more efficiently to infection and to paracrine IFN signalling.

Moreover, NTPV behaved differently than its closest relative GFV. GFV consistently exhibited a phenotype similar to RVFV MP-12, except for an increased sensitivity to type III IFN. It may therefore be assumed that GFV has the potential to be more virulent in humans than NTPV. Although known to

infect humans (Tesh *et al.* 1976; Palacios *et al.* 2014), to date, the pathogenicity of GFV in humans is unknown. In hamsters however, GFV infection causes fatal disease resembling RVF (Tesh and Duboise 1987; Fisher *et al.* 2003), which is fitting with the presented *in vitro* data.

NTPV seropositivity has been measured at 13.9% in Kenyan populations (Tchouassi *et al.* 2019). However, to date no acute infection in humans has been documented. The generally short viremic period and a limited availability of molecular diagnostic methods in endemic regions of phleboviruses may result in under-reporting of those infectious diseases. This notion is supported by the universal pathology of phlebovirus infections including common febrile symptoms, complicating differential diagnosis. Recently, the uncharacterized phlebovirus Adria virus, which had been thought to cause solely asymptomatic infections, was found associated with human disease (Anagnostou *et al.* 2011). In other instances, novel phleboviruses were isolated from symptomatic patients (Travassos da Rosa *et al.* 1983; Laubscher *et al.* 2019). Therefore, the possibility that NTPV can cause disease in humans is not to be neglected. However, this work showed that novel phlebovirus NTPV exhibits similar innate immune characteristics to attenuated RVFV strain C113. It is thus tempting to speculate that NTPV is low-pathogenic in humans. Nonetheless, enhanced viral replication upon IFN signalling interruption underscores a potential risk of more severe disease in immunocompromised individuals.

8.1.2 Non-structural proteins NSs of novel phleboviruses exhibit distinct anti-innate immunity characteristics

To counteract innate immunity induction, most members of the *phenuiviridae* family encode a small non-structural protein termed NSs, which for several species has been shown to exhibit anti-IFN characteristics (Eifan *et al.* 2013). The potency of NSs proteins has been observed to dictate phenuivirus pathogenicity. Highly pathogenic RVFV carries a multifunctional NSs targeting several host pathways like IFN induction, host transcription, and protein kinase R (PKR) activation (Le May *et al.* 2008; Billecocq *et al.* 2004; Habjan *et al.* 2009b; Ikegami *et al.* 2009). The natural RVFV variant C113 expresses a truncated, non-functional NSs and is therefore profoundly attenuated (Muller *et al.* 1995; Billecocq *et al.* 2004). By contrast, NSs proteins of non- or intermediately pathogenic phenuiviruses, while exhibiting certain anti-IFN mechanisms, are unable to fully antagonize the host IFN response (Gori Savellini *et al.* 2011; Brisbarre *et al.* 2013; Rezelj *et al.* 2015; Rezelj *et al.* 2017; Wuerth *et al.* 2018). Here, the antagonistic capacities of NSs proteins of novel phleboviruses NTPV, BGRV, EMBV, KBGV, and PERV, as well as GFV were characterized, in comparison to well-known NSs proteins of RVFV, SFSV, and two members of the PTV species group. Luciferase-based reporter assays were used to determine the antagonistic qualities of NSs to counteract the induction of innate immune genes, and mass spectrometry interactome analyses were employed to determine host cell binding partners of NSs proteins.

All NSs proteins of novel phleboviruses, except for KBGV, suppressed IFN- β , ISG54, NF- κ B-dependent and/or Mx1 (IFN-stimulated response element, ISRE) promoter induction through pattern recognition receptor (PRR), TNF and/or type I IFN signalling. Antagonistic profiles were distinct, with only BGRV and PERV NSs exhibiting a similar pattern (**Figure 18**). Therefore, it is tempting to speculate that these novel phlebovirus NSs proteins exhibit unique functions in their ability to counteract different innate immunity pathways.

Interestingly, promoter inhibition was not consistent across promoters nor across stimulation pathways. For instance, IFN- β and ISG54 promoter induction upon VSV-RNA stimulation was not uniformly antagonized. GFV and EMBV NSs inhibited VSV-RNA-stimulated IFN- β , but not ISG54 promoter activation. On the other hand, NTPV NSs counteracted TNF- α -, but not VSV-RNA-induced NF- κ B-dependent promoter induction, and GFV NSs showed the exact opposite picture. Further, IFN- α -stimulated induction of the Mx1 promoter, but not the ISG54 promoter, was suppressed by BGRV and PERV NSs. While both Mx1 and ISG54 promoters contain an ISGF3-responsive ISRE, in contrast to early-induced Mx1 transcription, ISG54 transcription has been shown to be a late event in innate immunity, mediated by distinct phosphorylation of STAT1 as part of the ISGF3 (Perwitasari *et al.* 2011). Thereby, STAT1 Ser708 phosphorylation, mediated by kinase IKK ϵ , increases promoter binding affinity required for ISG54 induction (tenOever *et al.* 2007). One can therefore suggest that BGRV and PERV NSs may interfere with initial STAT1 Tyr701 phosphorylation by JAK/TYK kinases, but not with late Ser708 phosphorylation by IKK ϵ . Indeed, the present interactome analysis identified TYK2 as binding partner of PERV NSs in eight out of nine measurements; JAK1 was found associated with all tested NSs except SFSV. Of note, IKK ϵ in concert with TBK1 also plays a role in IRF3/7 activation downstream of PRR signalling. Both BGRV and PERV NSs were found in this work to inhibit viral RNA-mediated promoter induction downstream of TBK1 but upstream of IRF3. While several binding partners were identified for BGRV NSs that hint at TBK1 inhibition, no such interactors were found for PERV NSs. However, this does not exclude the possibility that PERV NSs acts on TBK1-IRF3 activation through other mechanisms than protein-protein interactions at this level. For instance, PERV NSs could mediate the degradation of host cell proteins. Indeed, interaction of PERV NSs with several Cullin proteins was detected, which are part of the ubiquitination machinery to target proteins for degradation. In any case, absent ISG54 promoter inhibition suggests that IKK ϵ is not inhibited by BGRV and PERV NSs.

Further, focusing on phlebovirus NSs cellular interactors and targeted pathways which were unique among the tested NSs proteins, several proteins of interest were identified that could be involved in innate immune gene repression and further interference with host cellular functions.

NTPV NSs antagonized viral RNA-mediated IFN- β and ISG54 promoter induction upstream of TBK1. Additionally, it strongly inhibited IFN- α -mediated Mx1 and ISG54 induction, and reduced TNF- α -mediated NF- κ B-dependent signalling. Interactome analysis showed NTPV NSs to bind several innate

immunity host factors that could serve to explain this inhibitory phenotype. For instance, NTPV NSs might inhibit IFN- β and ISG54 promoter induction through interaction with DUSP11, which reduces RIG-I activation by modifying 5'ppp ends of RNAs (Choi *et al.* 2020a), and NF- κ B-dependent signalling by association with histone methyltransferase ASH1L, which upregulates factors involved in negative regulation of NF- κ B induction.

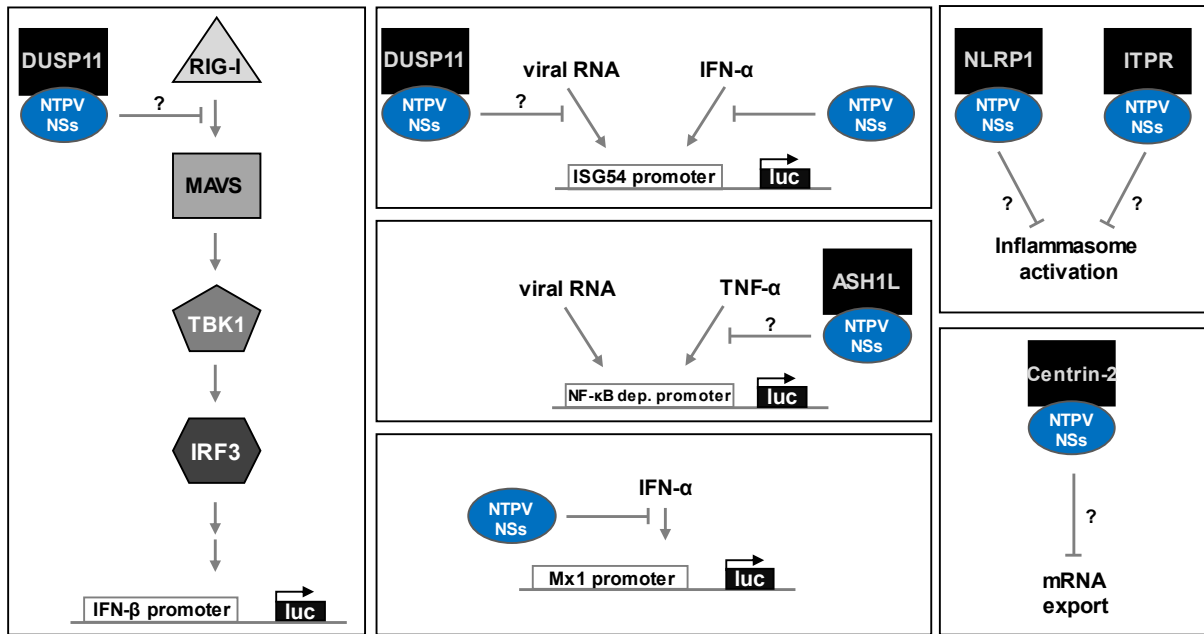


Figure 44: Schematic representation of the antagonistic effect of NTPV NSs protein on innate immune gene induction (see **Figure 18**), together with select interactors of NTPV NSs (as identified by mass spectrometry) and possible biological functions of these interactions. Left panel, NSs influence on the IFN- β promoter activation cascade; middle panels, NSs influence on the activation of ISG54, NF- κ B-dependent and Mx1 promoters; right panel, putative NSs influence on other cellular pathways.

In addition, NTPV NSs might have a negative effect on inflammasome activation. NTPV NSs was found to interact with Inositol 1,4,5-trisphosphate receptors (ITPR), functioning as channels for calcium release from the ER, which induces NLRP3 inflammasome activation leading to apoptosis (Chen *et al.* 2017). The NLRP3 inflammasome has been shown to be activated by infection with a RVFV NSs deletion mutant, but not with MP-12 (Ermler *et al.* 2014), suggesting that RVFV NSs inhibits the NLRP3 inflammasome. Furthermore, NTPV NSs exhibited a strong and unique interaction with inflammasome protein NLRP1. Upon stimulation by pathogens, the NLRP1 inflammasome induces the activation of caspase-1 (CASP1), which leads to the release of pro-inflammatory cytokines like IL-1 β and to cell death. NLRP1 was recently identified to be activated by long dsRNA (Bauernfried *et al.* 2021). Although infection with a negative strand RNA (ss(-)RNA) virus did not lead to NLRP1 infection, presumably because long dsRNA is not produced to detectable levels during ss(-)RNA virus infection (Weber *et al.* 2006), NLRP1 was still responsive to short dsRNA constructs in cell-free systems, suggesting additional mechanisms of activation, which could be fulfilled upon NTPV infection. DNA viruses Vaccinia virus and Kaposi's sarcoma-associated herpes virus have been shown to express proteins that bind to and thereby inhibit NLRP1 (Chavarría-Smith and Vance 2015). A similar mechanism is conceivable for

NTPV NSs, possibly by sequestering NLRP1 from its adapter protein ASC and from CASP1, which were not found in the interactome analysis, indicating a dissociation from NLRP1. Notably, long dsRNA is also recognized by the PRR MDA5, and proteins annotated to the GO term “regulation of MDA5 signalling pathway” were enriched among NTPV interactors. Further experiments are needed to address the question if long dsRNA might be produced during NTPV infection. Lastly, Centrin-2 was also identified as a unique interactor of NTPV NSs. Centrin-2 is involved in microtubule organisation, DNA damage repair and mRNA export. Notably, “regulation of nucleocytoplasmic transport” was among the enriched GO terms for NTPV NSs interactors. RVFV NSs causes an mRNA export block in the host cell (Copeland *et al.* 2015) so it is possible for NTPV NSs to interfere with the nuclear import and export machinery as well, possibly to create a favourable environment for viral transcript translation over host cellular mRNA (see **Figure 44** and **Table 48**).

GFV NSs impeded viral RNA-induced IFN- β and NF- κ B-dependent promoter induction upstream of TBK1, as well as IFN- α -mediated Mx1 and ISG54 promoter induction. Strikingly, GFV NSs strongly interacted with the mitochondrial adapter molecule MAVS, which was unique across all NSs interactor lists. As part of PRR signalling, MAVS governs downstream cascades leading to IRF3/7, NF- κ B and AP-1 induction. Indeed, IFN- β and NF- κ B-dependent promoter expression upon viral RNA stimulation was suppressed in the presence of GFV NSs. However, GFV NSs had no effect on viral RNA-stimulated ISG54 promoter induction. Therefore, either GFV NSs binding to MAVS does not hinder signal transduction, or the promiscuous ISG54 promoter in this case is activated through a different mechanism that is not targeted by GFV NSs (see **Figure 45** and **Table 48**).

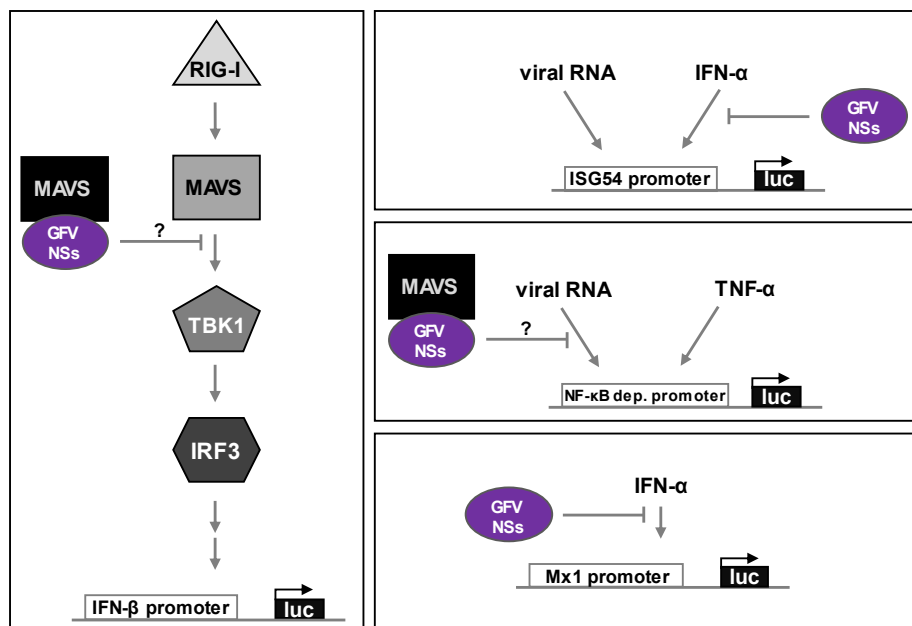


Figure 45: Schematic representation of the antagonistic effect of GFV NSs protein on innate immune gene induction (see **Figure 18**), together with a select interactor of GFV NSs (as identified by mass spectrometry) and possible biological functions of this interaction. Left panel, NSs influence on the IFN- β promoter activation cascade; right panels, NSs influence on the activation of ISG54, NF- κ B-dependent and Mx1 promoters.

EMBV NSs inhibited IFN- β induction downstream of MAVS and upstream of TBK1, and NF- κ B-dependent induction upon stimulation with VSV-RNA as well as with TNF- α . NF- κ B inhibition regardless of stimulus suggests a target after the signalling pathways converge, namely at the IKK α / β /NEMO complex. Indeed, EMBV NSs bound to NEMO, albeit weakly. Furthermore, EMBV NSs interacted with translation initiation factor eIF3 complex subunit eIF3E. This interaction was much more pronounced than with all other NSs proteins, and comparable in magnitude to the interaction of SFSV NSs with eIF2B. SFSV has been shown to exploit this interaction to continue translation in the presence of activated PKR, an ISG which halts viral translation (Wuerth *et al.* 2020). EMBV might pursue a similar strategy to ensure ongoing viral translation (see **Figure 46** and **Table 48**).

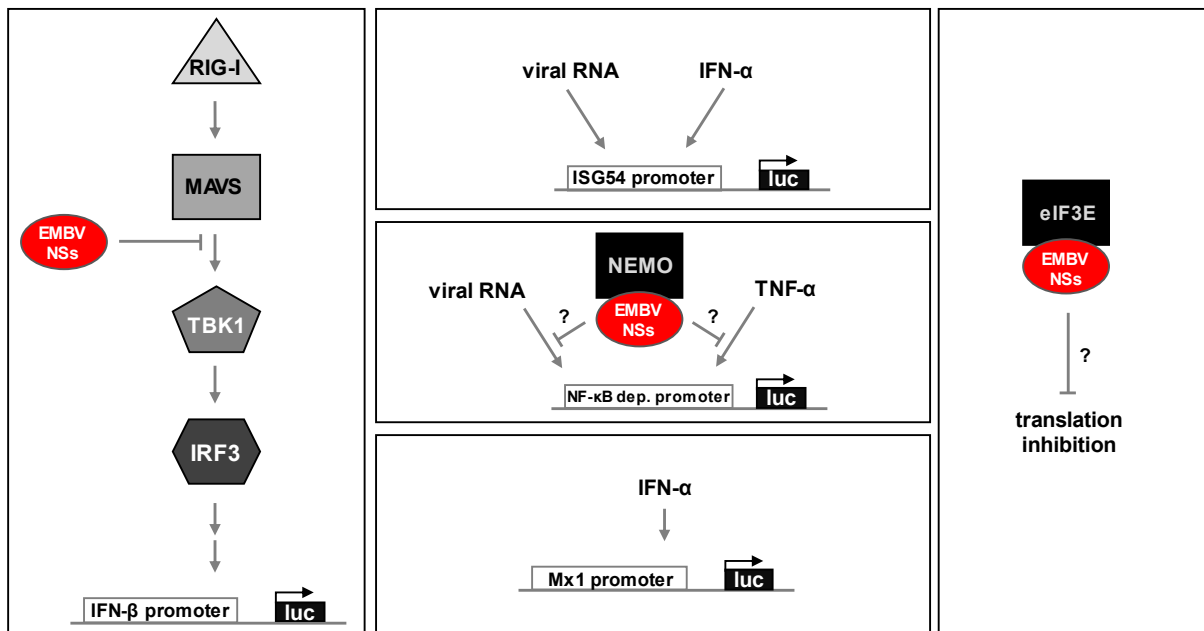


Figure 46: Schematic representation of the antagonistic effect of EMBV NSs protein on innate immune gene induction (see **Figure 18**), together with select interactors of EMBV NSs (as identified by mass spectrometry) and possible biological functions of these interactions. Left panel, NSs influence on the IFN- β promoter activation cascade; middle panels, NSs influence on the activation of ISG54, NF- κ B-dependent and Mx1 promoters; right panel, putative NSs influence on other cellular pathways.

BGRV NSs inhibited viral RNA-induced IFN- β and ISG54 promoter activation downstream of TBK1 but upstream of IRF3, NF- κ B-dependent promoter activation through TNF- α and viral RNA, as well as IFN- α -mediated Mx1, but not ISG54, promoter induction. Interactome analysis revealed BGRV NSs to associate with TRAFD1, which inhibits IRF3 and NF- κ B activation through interaction with TRIF, MAVS, TRAF3 and TRAF6 (Sanada *et al.* 2008). Thus, stabilization of TRAFD1 by BGRV NSs could explain inhibition of IFN- β promoter and NF- κ B-dependent promoter activation. Furthermore, BGRV NSs interacted with several components of the mTORC complex. The mTORC complex is upregulated upon RLR stimulation, and mTOR blockade has been shown to impede antiviral cytokine production by decreasing TBK1 phosphorylation (Fekete *et al.* 2020). By inhibiting mTOR kinase activity through direct interaction with MLST8, which positively regulates mTOR kinase activity within the mTORC1

complex (Jacinto *et al.* 2004), BGRV NSs could inhibit TBK1 phosphorylation and subsequent IRF3-driven innate immune gene induction. Further, BGRV NSs associated with MIB2 and DNMT3A, which are also involved in TBK1 activation (Ye *et al.* 2014). Of note, BGRV NSs was still able to block IFN- β promoter expression upon TBK1 overexpression, indicating that TBK1 inhibition is very strong and likely requires multiple mechanisms, as discussed here. Further, BGRV NSs exhibited a strong unique interaction with E3 ubiquitin ligase CHIP, as well as an interaction with p62 (Sequestosome-1). CHIP and p62 interact with each other, so it is unclear if BGRV interacted directly with both or only one of them. In any case, CHIP inhibits RIPK3-triggered necroptosis upon TNF- α signalling (Seo *et al.* 2016) and p62 promotes the expression of cytoprotective genes by activation of the NRF2-Keap1 pathway. This pathway has been shown to be activated by SFTSV NSs (Choi *et al.* 2020b). Thus, BGRV NSs may, too, be involved in creating a favourable environment for virus replication in the host cell. Alternatively, by inhibiting rather than activating CHIP and p62, BGRV NSs may lead to host cell death. Strong cytopathic effect upon BGRV NSs transfection (data not shown) hints at the latter hypothesis. Additionally, p62 is implicated in regulation of NF- κ B activation by TNF- α through interaction with RIPK1, probably aiding in IKK β recruitment. Inhibition of p62-mediated NF- κ B activation could be another mechanism by which BGRV NSs achieves the observed antagonism of the host innate immune signalling (see **Figure 47** and **Table 49**).

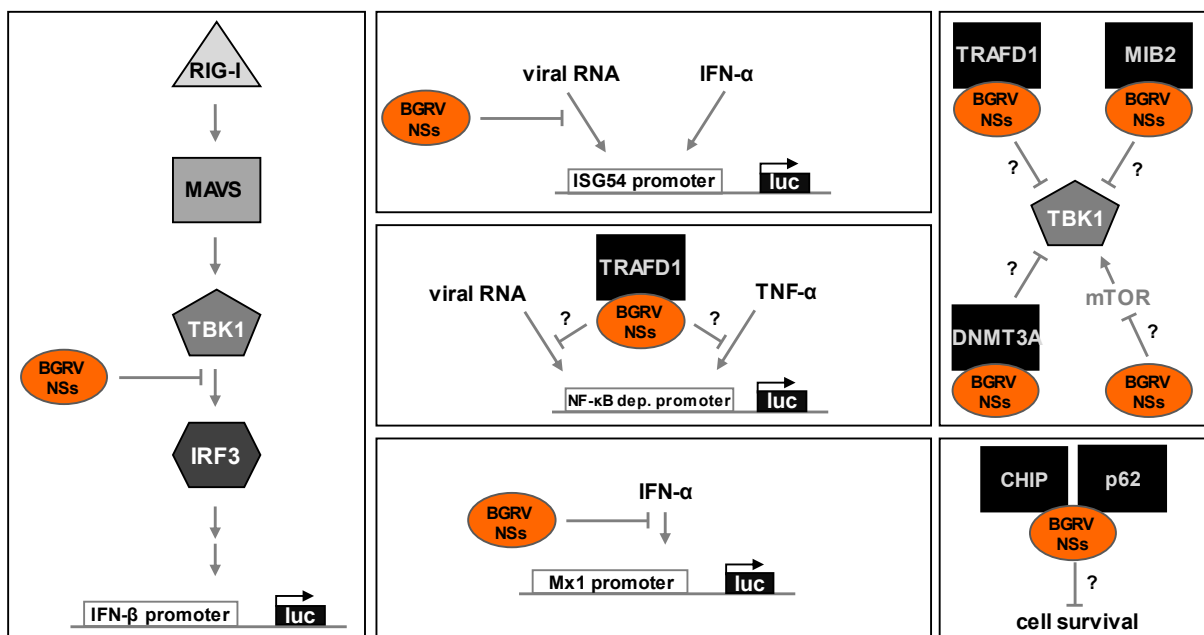


Figure 47: Schematic representation of the antagonistic effect of BGRV NSs protein on innate immune gene induction (see **Figure 18**), together with select interactors of BGRV NSs (as identified by mass spectrometry) and possible biological functions of these interactions. Left panel, NSs influence on the IFN- β promoter activation cascade; middle panels, NSs influence on the activation of ISG54, NF- κ B-dependent and Mx1 promoters; right panel, putative NSs influence on other cellular pathways.

PERV NSs, like **BGRV NSs**, was found to inhibit viral RNA-induced IFN- β and ISG54 promoter activation downstream of TBK1 but upstream of IRF3, NF- κ B-dependent promoter activation through TNF- α and viral RNA, as well as IFN- α -mediated Mx1, but not ISG54, promoter induction. Interactome analysis revealed the complex consisting of TAK1-binding proteins TAB1, 2 and 3, as well as MAP3K7, as unique binding partner of PERV NSs. This complex is involved in the activation of IKK kinases to induce NF- κ B activation (Xu and Lei 2021). A possible disruption of this signalling pathway by PERV NSs could explain its strong effect on NF- κ B-dependent promoter antagonism. Further, PERV NSs also uniquely associated with transcription factor RUNX, which has been shown to regulate APOBEC3 antiviral immunity, an ISG family of enzymes which facilitate viral genome mutations (see **Figure 48** and **Table 49**).

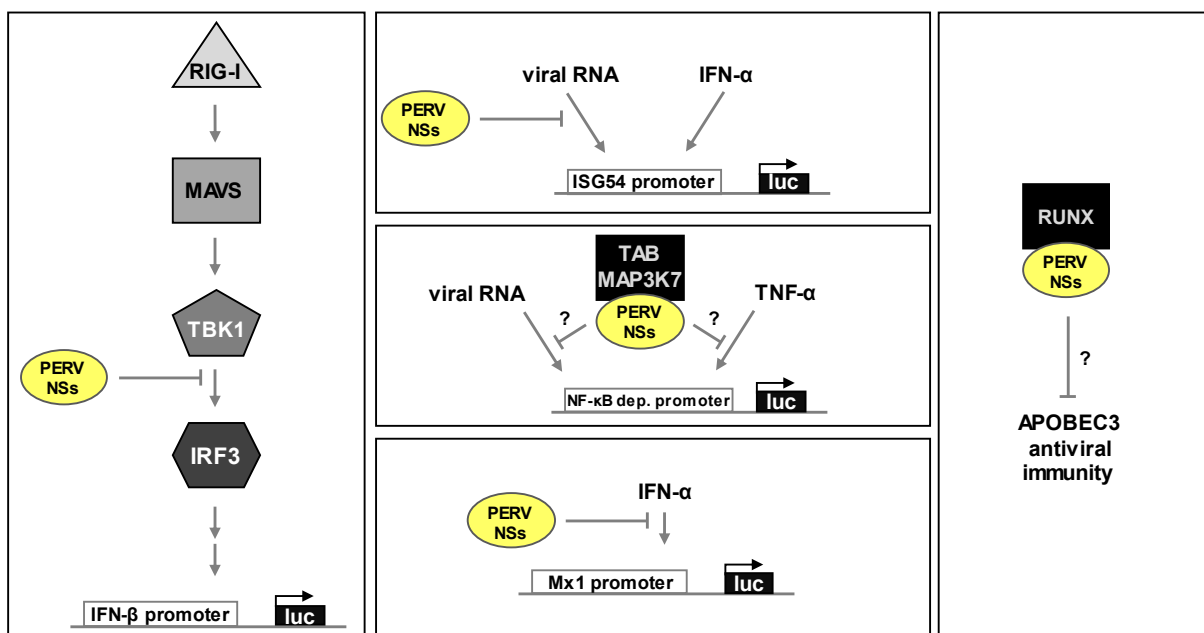


Figure 48: Schematic representation of the antagonistic effect of PERV NSs protein on innate immune gene induction (see **Figure 18**), together with select interactors of PERV NSs (as identified by mass spectrometry) and possible biological functions of these interactions. Left panel, NSs influence on the IFN- β promoter activation cascade; middle panels, NSs influence on the activation of ISG54, NF- κ B-dependent and Mx1 promoters; right panel, putative NSs influence on other cellular pathways.

Only **KBGV NSs** exhibited no antagonistic activity of innate immunity promoters in any tested condition. Similarly, the NSs of avirulent **PTV-B** showed no effect in previous studies (Perrone *et al.* 2007; Wuerth *et al.* 2018). This can either result from an inactive NSs protein or an unstable NSs expression in human cells. Similar observations were made with mosquito-borne phlebovirus Arumowot virus (AMTV), which is non-pathogenic in humans, although serologic evidence confirms human infection (Berthet *et al.* 2016). AMTV NSs has been found to be rapidly degraded in human cell lines; in contrast, AMTV NSs is stable in murine cells, which results in efficient AMTV replication in concert with IFN- β inhibition (Hallam *et al.* 2019). Therefore, it is possible that KBGV and PTV-B NSs exhibit anti-innate immunity characteristics in non-human cells, potentially to ensure efficient viral replication

in amplification hosts. The observed weaker expression levels of KBGV and PTV-B NSs in human cells in comparison with other NSs proteins (**Figure 20** and Wuerth *et al.* 2018 in a similar setting), as well as the association of those NSs proteins with the cellular degradation machinery (*e.g.* members of the Cullin and F-box families, **Table 47**) underscore the hypothesis that those NSs proteins are unstable in human cells. Of note, blood meal analyses showed that sandflies of KBGV-positive pools had fed on cattle instead of humans (Marklewitz *et al.* 2020), further emphasizing the differing phenotype observed here. Importantly, there was a strong overlap between interactors of **KBGV and PTV-B NSs** proteins (see **Table 50**).

The NSs protein of the virulent strain **PTV-A** inhibits IFN- β mRNA synthesis as well as NF- κ B-dependent transcription (Perrone *et al.* 2007; Lihoradova *et al.* 2013; Wuerth *et al.* 2018) and causes a general transcription block in the host cell (Lihoradova *et al.* 2013). The present interactome analysis showed cellular transcription elongation factors Elongin-B and Elongin-C as unique interactors of PTV-A NSs. In addition, Elongin-A also interacted with PTV-A NSs, and with other tested NSs proteins in a weaker manner. Recently, the Weber group identified Elongin-C as a target for orthobunyavirus La Crosse virus (LACV) NSs (Schoen *et al.* 2020). Upon LACV infection, Elongin-C is redistributed from nucleoli and the nucleus, thereby possibly impeding RNA polymerase II transcription and causing the transcriptional shut-off. However, no direct interaction between LACV NSs and Elongin-C has been detected (Schoen *et al.* 2020). An interaction of PTV-A NSs with Elongins A, B and C could explain the observed host transcription block which leads to reduced activation of innate immunity factors. Of note, the interactome signatures of the related PTV-A and PTV-B NSs were markedly different (see **Table 50**).

SFSV NSs strongly impedes IRF3-mediated transcription like IFN- β gene transcription by concealing the IRF3 DNA-binding domain through direct interaction (Wuerth *et al.* 2018). However, this interaction was only sporadically detected in the present interactome analysis, thus the strict application of filter criteria might have caused the omission of biologically relevant interactions. Further, SFSV NSs interacts with the translation initiation factor eIF2B to rescue viral translation in the presence of activated PKR (Wuerth *et al.* 2020). Strong interaction with all five eIF2B subunits was confirmed during the present interactome analysis and, notably, was also observed to similar magnitude in PTV-A NSs. Moreover, SFSV NSs, as the only tested NSs protein, interacted clearly with E3 ubiquitin ligase TRAF6, which mediates NF- κ B activation downstream of MAVS signalling. Curiously, SFSV NSs exhibited no inhibitory effect on NF- κ B-dependent promoter activation (**Figure 16A** and Wuerth *et al.* 2018), so this interaction might serve a different purpose. Further targets of SFSV NSs were both RNF20 and RNF40 of the RNF20/40 E3 ubiquitin-protein ligase complex which mediates p53-dependent transcription of apoptotic genes (Wu *et al.* 2019). Overexpression of SFSV NSs was not associated with cell death (data not shown) and thus the association of SFSV NSs with RNF20/40 could mediate cell survival (see **Table 50**).

In general, mass spectrometry analyses of host cellular binding partners of phlebovirus NSs proteins identified several interactions that could account for the observed antagonism of innate immunity induction. In addition, a broad spectrum of molecular functions and pathways was found to be targeted by the different NSs proteins. For instance, GO terms were enriched that are associated with host transcription and translation, mitochondrial processes, cell death and protein degradation, or, as expected, immunity. Notably, “response to Actinomycin D”, a transcription inhibitor, was found among the enriched pathways for NTPV and PERV NSs interactors, although no general transcription block was observed upon NTPV and PERV NSs overexpression. Interfering with host mRNA and protein synthesis is a common virulence mechanism, employed for example by influenza, Herpes simplex and African Swine Fever viruses, as well as SARS coronavirus 2 (Sánchez *et al.* 2013; Bauer *et al.* 2018; Thoms *et al.* 2020; Wang *et al.* 2020e). Similarly, several viruses target host cell apoptotic pathways to their advantage (Okamoto *et al.* 2017; Ampomah and Lim 2020). It is therefore not surprising that these phleboviruses would interfere with these processes. Phlebovirus NSs proteins examined in this work also interacted with cell structure and transport networks. RVFV NSs was shown to impact cell structure and motility through transcriptional changes, thereby promoting motility to increase the spread of infection (Bamia *et al.* 2020). Other phleboviral NSs proteins might pursue the same effect through protein-protein interaction for virus dissemination and the transport of NSs in the host cell.

The overall great overlap detected between phlebovirus NSs interactors (**Figure 22**) suggests convergent processes to generate advantages for virus replication. Still, many unique interactors were identified for individual NSs proteins, which underscores distinct mechanisms for each different virus. Further studies will be needed to validate these interactions and possibly reveal the mechanisms by which each NSs suppresses innate immunity activation; however, the present data sets a powerful starting point for further investigations, potentially also involving druggable host targets in phlebovirus disease. Nonetheless, it is important to consider that direct protein-protein interactions are not the only way by which cellular processes can be targeted. Other means include the aforementioned transcription/translation interference, protein sequestration, or protein degradation through interaction with intermediary factors.

To summarize, this work characterized NSs proteins of novel phleboviruses identified during vector surveillance studies and showed that all investigated NSs proteins, with the exception of KBGV NSs, potentially suppress the induction of multiple innate immune genes through different pathways. NTPV infection studies, as discussed in chapter 8.1.1, revealed a strong induction of IFNs and other innate immune genes, and showed that NTPV replication is sensitive to exogenously added type I and type III IFN. Taken together with the presented NTPV NSs overexpression studies demonstrating the efficient suppression of innate immune gene promoter induction, this suggests that this antagonism is not as pronounced in an infection context. Similar results have been described for other phenuiviruses, like TOSV (Gori Savellini *et al.* 2011) or SFTSV (Qu *et al.* 2012). One possible explanation for this is that

NSs levels during infection are lower than upon transfection, and thus not able to fully antagonize the potentially large number of PAMPs generated during NTPV infection. Another possibility is that NSs expression is delayed and thus not able to counteract the fast IFN upregulation upon NTPV infection. Potent RVFV NSs is expressed 3 – 4 h into infection, allowing for immediate counteraction of IFN induction (Eifan *et al.* 2013). In contrast, TOSV NSs is weakly expressed at 4 h post infection, reaching peak levels only around 48 – 72 h into infection (Gori Savellini *et al.* 2011). Therefore, during NTPV infection, the IFN response could be initiated before sufficient NSs is produced for innate immune antagonism. Alternatively, if an insufficient number of cells is infected, NTPV NSs could suppress IFN induction in infected cells to minimal levels, however small amounts of IFN might act on neighbouring, uninfected cells to potentiate the immune response.

Although novel phleboviruses are frequently isolated in the course of vector surveillance studies (Charrel *et al.* 2009; Collao *et al.* 2010; Zhioua *et al.* 2010; Remoli *et al.* 2014; Alkan *et al.* 2015; Alkan *et al.* 2016; Bichaud *et al.* 2016; Marklewitz *et al.* 2019), they are rarely characterized. Therefore, gaining important insights into the molecular pathogenesis of novel viruses with zoonotic potential will increase preparedness for future disease in humans.

Serologic studies have confirmed human infection with NTPV, determining 13.9% seropositivity in the Kenyan population (Tchouassi *et al.* 2019). In addition, *in vitro* studies with NTPV isolate have demonstrated the susceptibility of cell lines from a broad range of species (Tchouassi *et al.* 2019). Moreover, blood meal investigations indicated that sandflies of pools positive for BGRV and PERV had fed on humans (Marklewitz *et al.* 2020) suggesting that BGRV and PERV can infect humans. However, EMBV, BGRV, KBGV and PERV remain to be successfully isolated and human serologic data concerning these viruses is lacking. Nonetheless, the present characterization of viral NSs proteins demonstrates that these novel viruses carry powerful virulence factors that target the human innate immune system at various steps. Therefore, zoonotic infections of humans with these newly described viruses and possible subsequent virus adaptations may result in symptomatic, more severe disease, and should be closely monitored.

8.2 Pandemic coronavirus SARS-CoV-2

The recently emerged SARS-CoV-2 as the causative agent for COVID-19 (coronavirus disease 2019) is responsible for major health crises all over the world. The present work used human and animal cell culture systems to compare SARS-CoV-2 with the 2003-emerged SARS-CoV-1. First, SARS-CoV-2 sensitivity to type I and type III IFNs as well as virus replication kinetics in the presence of a proposed COVID-19 drug candidate were assessed (chapter 7.2.1 to 7.2.4). Further, the IFN, cytokine and ISG response upon SARS-CoV-2 infection was characterized in depth in different human lung cell lines (chapter 7.2.5 to 7.2.7).

8.2.1 Inhibition of SARS-CoV-2 by type I and type III interferons

First, this work showed that type I and type III IFNs are able to inhibit SARS-CoV-2 replication, with consistently more profound effects than against SARS-CoV-1 (**Figure 26** to **Figure 28**; Felgenhauer *et al.* 2020). While these differences could be due to the cell types used or due to the observed differences in virus replication, potentially resulting in higher production of viral IFN antagonists, other groups have since corroborated these findings (Mantlo *et al.* 2020; Lokugamage *et al.* 2020; Blanco-Melo *et al.* 2020; Vanderheiden *et al.* 2020; V'kovski *et al.* 2021a; Schroeder *et al.* 2021). Since the start of the pandemic, numerous therapeutic approaches have incorporated the use of well-characterized type I IFNs in COVID-19 treatment, which, although associated with some side effects, are considered safe and have been used to treat millions of patients, and report a favourable outcome from IFN therapy, either alone or in combination with other medications (Hung *et al.* 2020; Zhou *et al.* 2020b; Wang *et al.* 2020c; Zheng *et al.* 2020a; Davoudi-Monfared *et al.* 2020; Rahmani *et al.* 2020; Fu *et al.* 2020; Malhani *et al.* 2021). However, the timing of IFN administration seems to be crucial for a beneficial effect, as late IFN- α treatment has been associated with increased mortality (Wang *et al.* 2020c). Nonetheless, type I IFNs seem promising for COVID-19 treatment.

Initially, scientists argued for the use of type III rather than type I IFN in COVID-19 (Prokunina-Olsson *et al.* 2020; O'Brien *et al.* 2020), as IFN- λ is thought to have fewer side effects because of its restriction to mucosal tissue and the less sudden but more prolonged antiviral response it triggers (Pervolaraki *et al.* 2018; Ye *et al.* 2019). However, large-scale trial data are missing, as phase III clinical trials for hepatitis C virus treatment were abandoned due to the availability of effective direct antivirals, even though phase I and II trials had resulted in excellent tolerance as well as efficacy (Muir *et al.* 2014). To date, little data are available for the therapeutic use of type III in COVID-19 patients. Two phase II clinical trials examined PEGylated IFN- λ for SARS-CoV-2 infection treatment. However, while one study reported on a greater decline in SARS-CoV-2 RNA in patients treated with PEGylated IFN- λ compared to placebo (Feld *et al.* 2021), another report found no difference in duration of viral shedding or symptom improvement between IFN- λ -treated and control groups (Jagannathan *et al.* 2021). Of note, both studies were conducted with outpatients, reflecting mostly mild disease. Thus, it remains to be

determined if IFN- λ holds a beneficial effect for the treatment of severe COVID-19. However, recent reports evoke further concern on the use of IFN- λ as a therapeutic, as it was shown that it can cause damage to the lung epithelium, which increases susceptibility to lethal bacterial superinfections, and impede lung repair (Broggi *et al.* 2020; Major *et al.* 2020), so its use should be with caution.

As the need for COVID-19 therapies is urgent and no direct antivirals are available, in addition to IFN administration several approaches have addressed drug repurposing. IFN signalling inhibitor Ruxolitinib was proposed as a potential treatment against SARS-CoV-2 (Gordon *et al.* 2020; Stebbing *et al.* 2020), reasoning that inhibiting pro-inflammatory responses could alleviate severe COVID-19. However, this work found that Ruxolitinib boosts SARS-CoV-2 replication in IFN-competent Calu-3 cells (**Figure 29**; Felgenhauer *et al.* 2020). This result was confirmed by others and also shown for SARS-CoV-1 infection (Schroeder *et al.* 2021), further indicating that both viruses are affected by IFNs secreted upon infection. Nonetheless, several clinical studies have evaluated the use of Ruxolitinib in COVID-19 treatment. In contrast to the cell culture data, Ruxolitinib treatment in patients resulted in a reduced risk of mortality and a decrease in inflammatory markers in hospitalized patients (Cao *et al.* 2020; D'Alessio *et al.* 2020; Giudice *et al.* 2020). Therefore, the application of *in vitro* data for patient care needs to be cautiously evaluated. Of note, while the three trials involving Ruxolitinib report good tolerance and no severe side effects (Cao *et al.* 2020; D'Alessio *et al.* 2020; Giudice *et al.* 2020), taken together they comprised a total number of only 59 Ruxolitinib-treated patients; and another case report describes two patients who developed purpuric skin lesions and a full-body rash, respectively (Gaspari *et al.* 2020). Thus, large-scale studies are needed to comprehensively analyze the benefit of Ruxolitinib for COVID-19 treatment.

8.2.2 Imperfect inhibition of interferons, cytokines and antiviral gene activation by SARS-CoV-2

Pathogenic viruses have evolved a wide variety of IFN-antagonistic strategies (García-Sastre 2017). A particularly efficient way is to block the induction of IFNs and other cytokines, as this prevents both the establishment of an antiviral state in the surrounding cells and the attraction of immune cells. SARS coronaviruses express a series of factors inhibiting IFN induction and IFN signalling (Kindler *et al.* 2016; Xia *et al.* 2020; chapter 4.3.4.2). The COVID-19 pandemic, with its causative agent SARS-CoV-2, for the last 18 months has run rampant across the globe, causing more than 222 million infections and claiming approx. 4.5 million deaths (COVID-19 Dashboard, Johns Hopkins University, accessed on 08 September 2021). It is therefore crucial to gain a thorough understanding of host cellular molecular responses triggered by SARS-CoV-2 infection.

Herein, the immediate-early innate immune response following SARS-CoV-2 infection was assessed in three human lung cell lines, in comparison with the related SARS-CoV-1, which emerged in 2002/2003. SARS-CoV-2 was able to elicit potent innate immune responses in the Calu-3 cell line, in contrast to

SARS-CoV-1, which efficiently blocks innate immune activation in this cell line. However, innate immune induction was completely absent upon infection with both SARS coronavirus species in the H1299 cell line, and strongly diminished in the A549-ACE2 cell line, but comparable between the two SARS coronaviruses (**Figure 31**).

While much research is being conducted in this field, most studies unfortunately only focus on one cell line, or omit the comparison of SARS-CoV-2 to SARS-CoV-1. The presented data aim to fill this gap and to elucidate the fundamental differences observed between cell lines.

There have been contradicting reports on the expression of innate immune genes upon SARS-CoV-2 infection in cell culture. Nonetheless, in line with this work's results, differential gene expression seems to be highly dependent on the cell line used. In agreement with the findings presented here, it seems that SARS-CoV-2 does not prompt an immune response in lowly permissive cell lines, like H1299 (Wyler *et al.* 2021), Huh7 (Chen *et al.* 2021) or 293FT cells (Saccon *et al.* 2021). One possible explanation for this is that a low level of PAMPs is generated during infection, which causes only a weak activation of innate immune sensors that can efficiently be blocked by viral antagonists. Of note, SARS-CoV-2 may not productively replicate in these cell lines, as an increase in viral genome, but no budding particles were observed in Huh7 and 293FT cells (Saccon *et al.* 2021). Reports on experiments in primary human alveolar epithelial cells are conflicting. While one study presents a pronounced pro-inflammatory response but no IFN induction upon SARS-CoV-2 infection (Vanderheiden *et al.* 2020), another study found SARS-CoV-2, but not SARS-CoV-1, to trigger a profound antiviral as well as pro-inflammatory response in these cells (V'kovski *et al.* 2021a). Notably, different MOIs and sampling time points could account for these differences, as the antiviral response was only reported at 96 h post infection (V'kovski *et al.* 2021a). An infection study of *ex vivo* human lung tissue found an upregulation of some pro-inflammatory cytokines, but no induction of type I, II or III IFNs (Chu *et al.* 2020). In contrast, assessment of SARS-CoV-2 infection in type II pneumocyte-alveolospheres resulted in upregulation of type I and III IFNs, ISGs as well as chemokines (Katsura *et al.* 2020). Notably, the authors report a good agreement of this data with patient bronchioalveolar lavage fluid (BALF) datasets (Katsura *et al.* 2020). Results on immune gene upregulation upon SARS-CoV-2 infection of A549 cells engineered to express ACE2 are also contradicting: a transcriptomic study reports a threshold-dependent upregulation of IFNs and ISGs at a high MOI (Blanco-Melo *et al.* 2020), while a multi-omics study of SARS-CoV-2 and SARS-CoV-1 infection finds IFN and ISGs unaffected with cells exhibiting a pro-inflammatory signature, with no notable differences between the two SARS coronaviruses (Stukalov *et al.* 2021), which is in line with the presented findings. These conflicting outcomes could result from different methods employed to engineer A549 cells to express ACE2. While the present work and Stukalov *et al.* employed a lentiviral vector, Blanco-Melo *et al.* used an adenoviral vector. This might result in different ACE2 expression levels and different permissiveness of the two ACE2-expressing A549 cell lines. In line with this, Blanco-Melo *et al.* report ~54% viral reads in their transcriptomic data, compared to a

much lower 5% in the here presented data (**Figure 36**). Of note, overexpression of the ACE2 receptor does not reflect physiological levels and might further distort the obtained results.

The most consistent reports concern SARS-CoV-2 infection of Calu-3 cells, where, in agreement with the present findings, an induction of IFNs, ISGs and cytokines is observed, that is absent in SARS-CoV-1 infection (Blanco-Melo *et al.* 2020; Wyler *et al.* 2021; Banerjee *et al.* 2021; Grossegeisse *et al.* 2021; Schroeder *et al.* 2021).

From the here presented comparison of transcriptomic profiles of naïve cell lines, it is tempting to hypothesize that Calu-3 cells, compared to H1299 and A549-ACE2 cells, exhibit a “pre-stimulated” condition, reflected in higher basal levels of the PRRs RIG-I and MDA5 (**Figure 43** and Li *et al.* 2021), existing basal levels of ISGs like MxA and ISG15 (**Figure 30**) and an enhanced gene signature regulated by immunity- and inflammation-associated transcription factors in an uninfected state (**Figure 42**). Consequently, SARS-CoV-2 infection might be sensed and combated rapidly and efficiently, to produce IFNs that can further potentiate the immune response. However, not all reports are consistent on observations in Calu-3 cells: One study, contradictory to the results presented in this work, finds lower RIG-I levels in Calu-3 cells, which the authors reason to account for the observed IFN upregulation (Yamada *et al.* 2021).

Further complicating the picture, if IFN and ISG expression is observed, reports are discordant on IFN action: one study employing single-cell analyses of SARS-CoV-2 infection of air liquid interface (ALI) cultures finds ISG expression in infected as well as bystander cells (Ravindra *et al.* 2021) while another study observed ISG expression solely in bystander cells (Lamers *et al.* 2021). Hence, in the latter study viral antagonists counteract IFN signalling while the IFN signature is amplified by uninfected cells that do not harbour viral proteins. It is important to note that the studies used different SARS-CoV-2 isolates, with the latter working with the same isolate as this work (Munich/BavPat1/2020). The here presented data cannot be resolved to the single-cell level, and thus cannot be interpreted accordingly.

Moreover, while most studies focus on transcriptomic changes of IFNs and cytokines in cell culture, this work found that the transcriptional upregulation of innate immune factors in Calu-3 cells translates to the protein level, with ISGs and antivirally active IFNs being produced upon SARS-CoV-2 infection. This is in line with previous inhibitor experiments, showing that blocking IFN signalling with the drug Ruxolitinib enhances SARS-CoV-2 titres in Calu-3 cells (Felgenhauer *et al.* 2020). Thus, at least in some cell types the IFN antagonism of SARS-CoV-2 is non-functional or at least imperfect up to the level of the positive control virus that was employed. Curiously, SARS-CoV-1 did not show this phenomenon, as antiviral immune responses were low or zero in all cell lines and at any time point of infection that was investigated. This could result from one or more IFN antagonists that are more potent or better expressed in SARS-CoV-1 infection. In line with this, one study observed an enhanced expression of the SARS-CoV-1 M protein compared to SARS-CoV-2 in Calu-3 cells (Grossegeisse *et*

al. 2021). Another study reported on reduced potency of SARS-CoV-2 nsp15 compared to its SARS-CoV-1 counterpart, which results in a diminished capacity for IFN induction and signalling counteraction by SARS-CoV-2 nsp15 (Hayn *et al.* 2021).

Basic research relies on the establishment of cellular models that imitate the viral life cycle because the analysis of patient data is often hampered by sample collection being invasive and methods being complex. However, data gained from those *in vitro* experiments do not always adequately translate into intricate *in vivo* patient conditions. Since the COVID-19 pandemic is of exceptional public health concern, a considerable number of studies have therefore also focused on IFN, cytokine and ISG assessment in patients.

SARS-CoV-2 infection can manifest in a broad disease spectrum, ranging from asymptomatic or mild self-limiting infection to life-threatening multi-organ disease (Harrison *et al.* 2020). To successfully combat viral infections while protecting the host by reducing collateral damage, the innate immune system needs to launch IFN-mediated responses preceding pro-inflammatory ones. This order seems to be corrupted in SARS-CoV-2 patients who develop severe COVID-19 (Galani *et al.* 2021). Although reports on the involvement of the innate immune system in COVID-19 patients are often conflicting, owing to study setup, studied materials and a general interpatient variability (genetic predispositions, age-associated factors, co-morbidities etc.), a consensus appears as to a certain temporal innate immunity profile in COVID-19 patients that correlates with disease severity.

Early upregulation of type I IFNs has been shown to be beneficial and crucial in resolving disease, while a delayed induction of type I IFN was associated with a worse disease outcome (Hadjadj *et al.* 2020; Galani *et al.* 2021). This is reflected in trial data using IFN- α as a therapeutic, where late administration of IFN- α was linked to worse clinical outcomes (Wang *et al.* 2020c). Because of the temporal dynamics of IFN induction, the comparison of severe patient profiles with those of mild or moderate cases often shows conflicting results concerning IFN- α/β and also IFN- λ levels, probably owing to sample collection time (Blanco-Melo *et al.* 2020; Cao *et al.* 2021; Scagnolari *et al.* 2021). Nonetheless, patients with severe disease uniformly present with an overshooting pro-inflammatory response, marked by an upregulation of IL-6, IL-8, IL-10, CXCL10, TNFSF10 and TNF- α etc. (Long *et al.* 2020; Bost *et al.* 2020; Banerjee *et al.* 2021). Consequently, late IFN- α expression and a persistent pro-inflammatory signature promote immunopathology and hyperinflammation that can lead to sudden respiratory failure in critical COVID-19 patients (Galani *et al.* 2021; Kim *et al.* 2021). This has also been observed in SARS patients (Cameron *et al.* 2007; Channappanavar *et al.* 2016). Fitting with early IFN induction, ISG expression seems to be elevated in mild over severe cases (Bost *et al.* 2020) but is also robust during moderate and severe disease stages (Cao *et al.* 2021). Notably, the innate immune signature in COVID-19 or SARS differs from other viral pneumonia clinical pictures, like influenza A infection (Galani *et al.* 2021; Olbei *et al.* 2021). Additionally, a recent report suggests that there is also a spatial component to the IFN response in COVID-19 patients: individuals experiencing mild disease presented

with higher IFN- λ 1 and IFN- λ 3 responses in the upper airways, which led to the efficient upregulation of protective ISGs. In contrast, in patients with severe and critical disease, as infection progresses to the lungs, IFN responses were upregulated in the lower airways (Sposito *et al.* 2021).

Since the situation in patients is highly complex, SARS-CoV-2 research would benefit from cell culture systems reflecting severe/critical and mild infections. A meta-analysis of published patient and cell culture RNAseq data (Cao *et al.* 2021) found Calu-3 innate immune profiles upon SARS-CoV-2 infection to cluster with those of BALF samples of severe and moderate COVID-19 cases. Of note, also A549-ACE2 cells infected at a high MOI (MOI 2; Blanco-Melo *et al.* 2020) are part of this cluster. Other cell culture-derived RNAseq profiles form a separate cluster. Unfortunately, RNAseq data for mild or asymptomatic cases were not available.

Therefore, it is possible that Calu-3 cells can reflect conditions of patients with severe COVID-19. The transcriptional landscape observed in naïve Calu-3 cells (**Figure 41**, **Figure 42**) hints at the “pre-stimulated” phenotype proposed here, and leads to robust upregulation of IFN, cytokine and IFN-stimulated genes. However, this model needs to be taken with caution, as one study characterized the pro-inflammatory signature in patients as IRF1-driven (Kim *et al.* 2021), a transcription factor that was absent from the presented list of enriched regulators. Instead, in Calu-3 cells, there is a substantial basal enrichment of NF- κ B subunit p105/p50 (NFKB1) and p65 (RELA) targets. Concerning this, a recent report found a strong NF- κ B activation upon SARS-CoV-2 infection in A549-ACE2 cells, which was crucial for successful SARS-CoV-2 replication, as disruption of NF- κ B signalling impaired virus replication (Nilsson-Payant *et al.* 2021). Thus, SARS-CoV-2 might have a growth advantage in Calu-3 cells, which already provide a suitable transcriptional environment. However, it remains to be determined if there are additional factors distinguishing Calu-3 cells from other cell lines in this regard.

Taken together, this work showed that SARS-CoV-2 elicits a robust but cell type-dependent induction of antiviral IFNs, cytokines and ISGs, with IFN and ISG induction also translating to the protein level. In contrast, SARS-CoV-1 failed to do so in all tested cell lines. The presented work found that the Calu-3 cell line, where SARS-CoV-2 causes innate immunity activation, exhibits a “pre-stimulated” state which could account for insufficient viral anti-IFN mechanisms. Comparisons with patient data suggest that Calu-3 cells might be a model for severe COVID-19. However, ultimately, data generated from cell culture need to be adequately and cautiously interpreted for the translation to *in vivo* conditions.

9 List of abbreviations

µl	microlitre
5'PPP	5' triphosphate
aa	amino acid
abbr.	abbreviation
AmpR	ampicillin resistance
approx.	approximately
APS	ammonium persulfate
ATP	adenosine triphosphate
BGRV	Bogoria virus
bp	basepair
BSA	bovine serum albumin
C-	carboxy-
CARD	caspase activation and recruitment domain
cDNA	copy DNA
CoV	coronavirus
CTRL	control
d	day(s)
DAPI	4',6-diamidino-2-phenylindole
DMEM	Dulbecco's modified Eagle's medium
DNA	deoxyribonucleic acid
dNTP	deoxyribonucleotide triphosphate
dsRNA	double-stranded RNA
e.g.	for example, <i>exempli gratia</i>
EDTA	ethylenediaminetetraacetic acid
EMBV	Embossos virus
FBS	fetal bovine serum
FDA	United States Food and Drug Administration
fwd	forward
g	g-force
GFV	Gabek Forest virus
GO	gene ontology
GOI	gene of interest
h	hour(s)
HCl	hydrochloric acid
HCoV	human coronavirus
HF	high fidelity
HRP	horseradish peroxidase
i.e.	that is, <i>id est</i>
IF	immunofluorescence
IFN	interferon
IKK	IκB kinase
IRF	interferon regulatory transcription factor
ISG	interferon-stimulated gene
ISRE	interferon-stimulated response element
kb	kilobase
KBGV	Kiborgoch virus
kDa	kilodalton
LB	lysogeny broth
LGP2	laboratory of genetics and physiology 2
Luc	luciferase

MAVS	mitochondrial antiviral signalling protein
MDA5	melanoma differentiation-associated gene 5
MEM	minimum essential medium
MERS-CoV	Middle East respiratory syndrome coronavirus
min	minute(s)
ml	millilitre
MOI	multiplicity of infection
Mx	Myxovirus resistance protein
N-	amino-
n.a.	not applicable
NaCl	sodium chloride
NF-κB	nuclear factor kappa B
NSs	small nonstructural protein
nt	nucleotide
NTPV	Ntepes virus
ORF	open reading frame
P/S/Q	penicillin-streptomycin-glutamine
PAGE	polyacrylamide gel electrophoresis
PAMP	pathogen-associated molecular pattern
PBS_{def}	phosphate buffered saline deficient
PCR	polymerase chain reaction
PERV	Perkerra virus
PFA	paraformaldehyde
PRR	pattern recognition receptor
PTV-A	Punta Toro virus Adames strain
PTV-B	Punta Toro virus Balliet strain
PVDF	polyvinylidene fluoride
rev	reverse
RIG-I	retinoic acid-inducible gene I
RLR	RIG-I-like receptor
RLU	relative luciferase unit(s)
RNA	ribonucleic acid
RNAseq	RNA sequencing
RNP	ribonucleoprotein
rpm	revolutions per minute
RT	room temperature (22°C)
Rux	Ruxolitinib
RVFV	Rift Valley fever virus
sec	second(s)
SARS-CoV	Severe acute respiratory syndrome coronavirus
SDS	sodium dodecyl sulfate
SFSV	Sandfly fever Sicilian virus
TAE buffer	tris-acetate-EDTA buffer
TANK	TRAF family member-associated NF- κ B activator
TBK1	TANK-binding kinase 1
TBS	tris buffered saline
TE buffer	tris-EDTA buffer
TEMED	tetramethylethylenediamine
TRIM25	tripartite motif-containing 25
U	unit(s)
UTR	untranslated region
VSV	Vesicular stomatitis virus

10 List of figures

Figure 1: Interferon (IFN) induction through Toll-like receptor (TLR) and RIG-I-like receptor (RLR) signalling	12
Figure 2: Type I and type III interferon signalling.....	15
Figure 3: Phlebovirus taxonomy, genome organization, and virion	21
Figure 4: Phlebovirus replication cycle.....	24
Figure 5: Coronavirus taxonomy, genome organization, and virion.....	27
Figure 6: Coronavirus replication cycle	29
Figure 7: Human cell line susceptibility to NTPV and related phleboviruses	66
Figure 8: Differential regulation of innate immune genes upon phlebovirus infection	67
Figure 9: Sensitivity of phleboviruses to type I interferon.....	69
Figure 10: Sensitivity of phleboviruses to type III interferon	70
Figure 11: Effect of the JAK/STAT inhibitor Ruxolitinib on phlebovirus replication	71
Figure 12: Phylogenetic relationship and amino acid sequence identity of phlebovirus NSs proteins.....	72
Figure 13: Antagonistic effect on IFN- β promoter induction of virulence factor NSs of novel phleboviruses.....	73
Figure 14: Antagonistic effect on pattern recognition receptor signalling cascade of virulence factor NSs of novel phleboviruses.....	75
Figure 15: Antagonistic effect on ISG54 promoter induction of virulence factor NSs of novel phleboviruses.....	76
Figure 16: Antagonistic effect on NF- κ B-dependent promoter induction of virulence factor NSs of novel phleboviruses.....	77
Figure 17: Antagonistic effect on type I IFN signalling of virulence factor NSs of novel phleboviruses.....	78
Figure 18: Heatmap summarizing the antagonistic effect of novel phlebovirus NSs proteins on innate immune gene induction	79
Figure 19: Absolute Renilla luciferase values for reporter assay data of innate immune gene promoter inhibition by phlebovirus NSs proteins	80
Figure 20: Influence of an N- or C-terminal 3 \times FLAG tag on NSs antagonism of reporter activation.....	82
Figure 21: Intracellular location of novel phlebovirus NSs proteins	83
Figure 22: Circos plot depicting overlap between phlebovirus NSs interactor lists	86
Figure 23: Heatmap depicting select statistically enriched GO terms within phlebovirus NSs host cell interactors	87
Figure 24: Heatmap depicting select statistically enriched GO terms within phlebovirus NSs host cell interactors annotated to the GO list #0045087, innate immune response	88
Figure 25: Venn diagram showing shared and unique interactors of phlebovirus NSs, annotated to the GO list #0045087, innate immune response.....	89
Figure 26: Sensitivity of SARS-CoV-2 and SARS-CoV-1 to increasing doses of type I IFN.....	97
Figure 27: Sensitivity of SARS-CoV-2 and SARS-CoV-1 to intermediate-dose type I IFN.....	98
Figure 28: Sensitivity of SARS-CoV-2 and SARS-CoV-1 to type III IFN.....	99
Figure 29: Effect of the JAK/STAT inhibitor Ruxolitinib on SARS-CoV-2 replication.....	100
Figure 30: Effect of IFNs and Ruxolitinib on Calu-3 and Vero E6 cells	101
Figure 31: Differential gene expression upon SARS-CoV-2 infection of human lung cell lines	103
Figure 32: Immediate-early IFN, cytokine and ISG induction profile upon SARS-CoV-2 infection of Calu-3 cells.....	104
Figure 33: Differential gene expression upon SARS-CoV-2 infection of Calu-3 cells at lower virus loads	105
Figure 34: Production of ISGs upon SARS-CoV-2 infection	107
Figure 35: Production of IFN upon SARS-CoV-2 infection.....	108
Figure 36: Viral RNA in total cellular RNA for transcriptomic analysis.....	109

Figure 37: Top 50 upregulated genes upon SARS-CoV-2 or SARS-CoV-1 infection of Calu-3 cells compared to mock cells.....	110
Figure 38: Antiviral signatures of SARS-CoV-infected Calu-3 cells	111
Figure 39: Top 30 downregulated genes upon SARS-CoV-2 or SARS-CoV-1 infection of Calu-3 cells compared to mock cells.....	112
Figure 40: Total differentially regulated genes upon SARS-CoV-2 or SARS-CoV-1 infection of A549-ACE2 cells compared to mock cells	113
Figure 41: Comparison of transcriptomic profiles of uninfected human lung cell lines.....	114
Figure 42: Naïve Calu-3 cells exhibit a “pre-stimulated” state compared to H1299 and A549-ACE2 cells.....	115
Figure 43: PRR levels in uninfected human lung cell lines	116
Figure 44: Schematic representation of the antagonistic effect of NTPV NSs protein on innate immune gene induction, together with select interactors of NTPV NSs (as identified by mass spectrometry) and possible biological functions of these interactions	121
Figure 45: Schematic representation of the antagonistic effect of GFV NSs protein on innate immune gene induction, together with a select interactor of GFV NSs (as identified by mass spectrometry) and possible biological functions of this interactions	122
Figure 46: Schematic representation of the antagonistic effect of EMBV NSs protein on innate immune gene induction, together with select interactors of EMBV NSs (as identified by mass spectrometry) and possible biological functions of these interactions	123
Figure 47: Schematic representation of the antagonistic effect of BGRV NSs protein on innate immune gene induction, together with select interactors of BGRV NSs (as identified by mass spectrometry) and possible biological functions of these interactions	124
Figure 48: Schematic representation of the antagonistic effect of PERV NSs protein on innate immune gene induction, together with select interactors of PERV NSs (as identified by mass spectrometry) and possible biological functions of these interactions	125
Figure 49: Statistically enriched GO terms within the overlapping gene sets “upregulated in Calu-3 cells compared to H1299 and A549-ACE2 cells” and “downregulated in Calu-3 cells compared to H1299 and A549-ACE2 cells”	177

11 List of tables

Table 1: Viruses used in this work	35
Table 2: Eukaryotic cell lines used in this work.....	35
Table 3: Prokaryotic cells used in this work.....	36
Table 4: Cell culture reagents for eukaryotic cells	36
Table 5: Transfection reagents for eukaryotic cells.....	36
Table 6: Cytokines and inhibitors.....	37
Table 7: Media and solutions for prokaryotic cells	37
Table 8: Buffers and reagents for SDS PAGE	37
Table 9: Buffers for Western blot.....	37
Table 10: Lysis buffers.....	38
Table 11: Buffers and solutions for immunofluorescence (IF)	38
Table 12: Buffers and reagents for agarose gel electrophoresis	38
Table 13: Additional buffers and solutions	38
Table 14: Polymerases.....	39
Table 15: Restriction Enzymes.....	39

Table 16: Other PCR reagents.....	39
Table 17: Primary antibodies for Western blotting	39
Table 18: Secondary antibodies for Western blotting	39
Table 19: Antibodies for immunofluorescence microscopy.....	40
Table 20: Expression plasmids for viral NSs proteins.....	40
Table 21: Expression plasmids for luciferase reporter assays	41
Table 22: Primers for cloning NSs expression plasmids	42
Table 23: Sequencing primers	44
Table 24: Miscellaneous primers.....	44
Table 25: qRT-PCR primers and probes for viral gene targets	44
Table 26: qRT-PCR primers for human gene targets	45
Table 27: Commercial reagents.....	45
Table 28: Commercial kits for co-immunoprecipitation, DNA- and RNA-isolation	46
Table 29: Commercial kits for cloning.....	46
Table 30: Commercial kits for (q)RT-PCR.....	46
Table 31: Commercial kits for luciferase assays	46
Table 32: Consumables and other materials.....	47
Table 33: Instruments	47
Table 34: Software	48
Table 35: PCR settings for mycoplasma PCR test	50
Table 36: Phusion® polymerase protocol	56
Table 37: KOD polymerase protocol.....	56
Table 38: Restriction endonuclease digest reaction	57
Table 39: Ligation reaction	57
Table 40: Colony PCR reaction.....	58
Table 41: Two-step SYBR green qRT-PCR protocol	60
Table 42: Two-step probe qRT-PCR protocol	60
Table 43: One-step probe qRT-PCR protocol	61
Table 44: SDS gel composition	61
Table 45: Number of cellular interactors with phlebovirus NSs proteins	85
Table 46: Host protein interactors involved in innate immunity shared between multiple phlebovirus NSs proteins	90
Table 47: Host protein interactors NOT involved in innate immunity shared between multiple phlebovirus NSs proteins.....	91
Table 48: Host protein interactors with focus on individual phlebovirus NSs proteins (1/3)	92
Table 49: Host protein interactors with focus on individual phlebovirus NSs proteins (2/3)	93
Table 50: Host protein interactors with focus on individual phlebovirus NSs proteins (3/3)	94
Table 51: Number of differentially expressed genes following SARS coronavirus infection	109
Table 52: Total numbers of cellular interactors of indicated phlebovirus NSs proteins	175
Table 53: Phlebovirus NSs interactors annotated to GO list #0045087 “innate immune response” ..	176

12 References

- Alkan, C., Alwassouf, S., Piorkowski, G., Bichaud, L., Tezcan, S., Dincer, E., Ergunay, K., Ozbel, Y., Alten, B., Lamballerie, X. de, Charrel, R.N., 2015. Isolation, genetic characterization, and seroprevalence of Adana virus, a novel phlebovirus belonging to the Salehabad virus complex, in Turkey. *Journal of virology* 89, 4080–4091. doi:10.1128/JVI.03027-14.
- Alkan, C., Erisoz Kasap, O., Alten, B., Lamballerie, X. de, Charrel, R.N., 2016. Sandfly-Borne Phlebovirus Isolations from Turkey: New Insight into the Sandfly fever Sicilian and Sandfly fever Naples Species. *PLoS neglected tropical diseases* 10, e0004519. doi:10.1371/journal.pntd.0004519.
- Alkan, C., Moin Vaziri, V., Ayhan, N., Badakhshan, M., Bichaud, L., Rahbarian, N., Javadian, E.-A., Alten, B., Lamballerie, X. de, Charrel, R.N., 2017. Isolation and sequencing of Dashli virus, a novel Sicilian-like virus in sandflies from Iran; genetic and phylogenetic evidence for the creation of one novel species within the Phlebovirus genus in the Phenuiviridae family. *PLoS neglected tropical diseases* 11, e0005978. doi:10.1371/journal.pntd.0005978.
- Amaro, F., Hanke, D., Zé-Zé, L., Alves, M.J., Becker, S.C., Höper, D., 2016. Genetic characterization of Arrabida virus, a novel phlebovirus isolated in South Portugal. *Virus research* 214, 19–25. doi:10.1016/j.virusres.2016.01.004.
- Amaro, F., Zé-Zé, L., Alves, M.J., Börstler, J., Clos, J., Lorenzen, S., Becker, S.C., Schmidt-Chanasit, J., Cadar, D., 2015. Co-circulation of a novel phlebovirus and Massilia virus in sandflies, Portugal. *Virology journal* 12, 174. doi:10.1186/s12985-015-0407-0.
- Ampomah, P.B., Lim, L.H.K., 2020. Influenza A virus-induced apoptosis and virus propagation. *Apoptosis : an international journal on programmed cell death* 25, 1–11. doi:10.1007/s10495-019-01575-3.
- Amroun, A., Priet, S., Lamballerie, X. de, Quérat, G., 2017. Bunyaviridae RdRps: structure, motifs, and RNA synthesis machinery. *Critical reviews in microbiology* 43, 753–778. doi:10.1080/1040841X.2017.1307805.
- Anagnostou, V., Pardalos, G., Athanasiou-Metaxa, M., Papa, A., 2011. Novel phlebovirus in febrile child, Greece. *Emerging infectious diseases* 17, 940–941. doi:10.3201/eid1705.101958.
- Aso, H., Ito, J., Koyanagi, Y., Sato, K., 2019. Comparative Description of the Expression Profile of Interferon-Stimulated Genes in Multiple Cell Lineages Targeted by HIV-1 Infection. *Frontiers in microbiology* 10, 429. doi:10.3389/fmicb.2019.00429.
- Atkins, C., Evans, C.W., Nordin, B., Patricelli, M.P., Reynolds, R., Wennerberg, K., Noah, J.W., 2014. Global Human-Kinase Screening Identifies Therapeutic Host Targets against Influenza. *Journal of biomolecular screening* 19, 936–946. doi:10.1177/1087057113518068.
- Atrekhany, K.-S.N., Gogoleva, V.S., Drutskaya, M.S., Nedospasov, S.A., 2020. Distinct modes of TNF signaling through its two receptors in health and disease. *Journal of leukocyte biology* 107, 893–905. doi:10.1002/JLB.2MR0120-510R.
- Bamia, A., Marcato, V., Boissière, M., Mansuroglu, Z., Tamiatti, C., Romani, M., Simon, D., Tian, G., Niedergang, F., Panthier, J.-J., Flamand, M., Souès, S., Bonnefoy, E., 2020. The NSs Protein Encoded by the Virulent Strain of Rift Valley Fever Virus Targets the Expression of Abl2 and the Actin Cytoskeleton of the Host, Affecting Cell Mobility, Cell Shape, and Cell-Cell Adhesion. *Journal of virology* 95. doi:10.1128/JVI.01768-20.

- Banerjee, A., El-Sayes, N., Budyłowski, P., Jacob, R.A., Richard, D., Maan, H., Aguiar, J.A., Demian, W.L., Baid, K., D'Agostino, M.R., Ang, J.C., Murdza, T., Tremblay, B.J.-M., Afkhami, S., Karimzadeh, M., Irving, A.T., Yip, L., Ostrowski, M., Hirota, J.A., Kozak, R., Capellini, T.D., Miller, M.S., Wang, B., Mubareka, S., McGeer, A.J., McArthur, A.G., Doxey, A.C., Mossman, K., 2021. Experimental and natural evidence of SARS-CoV-2-infection-induced activation of type I interferon responses. *iScience* 24, 102477. doi:10.1016/j.isci.2021.102477.
- Barr, J.N., 2007. Bunyavirus mRNA synthesis is coupled to translation to prevent premature transcription termination. *RNA (New York, N.Y.)* 13, 731–736. doi:10.1261/rna.436607.
- Bauer, D.L.V., Tellier, M., Martínez-Alonso, M., Nojima, T., Proudfoot, N.J., Murphy, S., Fodor, E., 2018. Influenza Virus Mounts a Two-Pronged Attack on Host RNA Polymerase II Transcription. *Cell reports* 23, 2119–2129.e3. doi:10.1016/j.celrep.2018.04.047.
- Bauernfried, S., Scherr, M.J., Pichlmair, A., Duderstadt, K.E., Hornung, V., 2021. Human NLRP1 is a sensor for double-stranded RNA. *Science (New York, N.Y.)* 371. doi:10.1126/science.abd0811.
- Berke, I.C., Modis, Y., 2012. MDA5 cooperatively forms dimers and ATP-sensitive filaments upon binding double-stranded RNA. *The EMBO journal* 31, 1714–1726. doi:10.1038/emboj.2012.19.
- Berthet, N., Nakouné, E., Gessain, A., Manuguerra, J.-C., Kazanji, M., 2016. Complete Genome Characterization of the Arumowot Virus (Unclassified Phlebovirus) Isolated from *Turdus libonyanus* Birds in the Central African Republic. *Vector borne and zoonotic diseases (Larchmont, N.Y.)* 16, 139–143. doi:10.1089/vbz.2015.1830.
- Betakova, T., Kostrabova, A., Lachova, V., Turianova, L., 2017. Cytokines Induced During Influenza Virus Infection. *Current pharmaceutical design* 23, 2616–2622. doi:10.2174/1381612823666170316123736.
- Bichaud, L., Dachraoui, K., Alwassouf, S., Alkan, C., Mensi, M., Piorkowski, G., Sakhria, S., Seston, M., Fares, W., Lamballerie, X. de, Zhioua, E., Charrel, R.N., 2016. Isolation, full genomic characterization and neutralization-based human seroprevalence of Medjerda Valley virus, a novel sandfly-borne phlebovirus belonging to the Salehabad virus complex in northern Tunisia. *The Journal of general virology* 97, 602–610. doi:10.1099/jgv.0.000389.
- Billecocq, A., Spiegel, M., Vialat, P., Kohl, A., Weber, F., Bouloy, M., Haller, O., 2004. NSs protein of Rift Valley fever virus blocks interferon production by inhibiting host gene transcription. *Journal of virology* 78, 9798–9806. doi:10.1128/JVI.78.18.9798-9806.2004.
- Bino, S., Velo, E., Kadriaj, P., Kota, M., Moureau, G., Lamballerie, X. de, Bagramian, A., Charrel, R.N., Ayhan, N., 2019. Detection of a Novel Phlebovirus (Drin Virus) from Sand Flies in Albania. *Viruses* 11. doi:10.3390/v11050469.
- Bird, B.H., Bawiec, D.A., Ksiazek, T.G., Shoemaker, T.R., Nichol, S.T., 2007. Highly sensitive and broadly reactive quantitative reverse transcription-PCR assay for high-throughput detection of Rift Valley fever virus. *Journal of clinical microbiology* 45, 3506–3513. doi:10.1128/JCM.00936-07.
- Bird, B.H., Ksiazek, T.G., Nichol, S.T., Maclachlan, N.J., 2009. Rift Valley fever virus. *Journal of the American Veterinary Medical Association* 234, 883–893. doi:10.2460/javma.234.7.883.
- Birra, D., Benucci, M., Landolfi, L., Merchionda, A., Loi, G., Amato, P., Licata, G., Quartuccio, L., Triggiani, M., Moscato, P., 2020. COVID 19: a clue from innate immunity. *Immunologic Research*, 1–8. doi:10.1007/s12026-020-09137-5.
- Bixler, S.L., Goff, A.J., 2015. The Role of Cytokines and Chemokines in Filovirus Infection. *Viruses* 7, 5489–5507. doi:10.3390/v7102892.

- Blanco-Melo, D., Nilsson-Payant, B.E., Liu, W.-C., Uhl, S., Hoagland, D., Møller, R., Jordan, T.X., Oishi, K., Panis, M., Sachs, D., Wang, T.T., Schwartz, R.E., Lim, J.K., Albrecht, R.A., tenOever, B.R., 2020. Imbalanced Host Response to SARS-CoV-2 Drives Development of COVID-19. *Cell* 181, 1036-1045.e9. doi:10.1016/j.cell.2020.04.026.
- Blighe, K., Rana, S., Lewis, M., 2019. EnhancedVolcano: Publication-ready volcano plots with enhanced colouring and labeling. R package version, 1(0).
- Blumer, T., Coto-Llerena, M., Duong, F.H.T., Heim, M.H., 2017. SOCS1 is an inducible negative regulator of interferon λ (IFN- λ)-induced gene expression in vivo. *The Journal of biological chemistry* 292, 17928–17938. doi:10.1074/jbc.M117.788877.
- Bolen, C.R., Ding, S., Robek, M.D., Kleinstein, S.H., 2014. Dynamic expression profiling of type I and type III interferon-stimulated hepatocytes reveals a stable hierarchy of gene expression. *Hepatology (Baltimore, Md.)* 59, 1262–1272. doi:10.1002/hep.26657.
- Bost, P., Giladi, A., Liu, Y., Bendjelal, Y., Xu, G., David, E., Blecher-Gonen, R., Cohen, M., Medaglia, C., Li, H., Deczkowska, A., Zhang, S., Schwikowski, B., Zhang, Z., Amit, I., 2020. Host-Viral Infection Maps Reveal Signatures of Severe COVID-19 Patients. *Cell* 181, 1475-1488.e12. doi:10.1016/j.cell.2020.05.006.
- Bouloy, M., Janzen, C., Vialat, P., Khun, H., Pavlovic, J., Huerre, M., Haller, O., 2001. Genetic Evidence for an Interferon-Antagonistic Function of Rift Valley Fever Virus Nonstructural Protein NSs. *Journal of virology* 75, 1371–1377. doi:10.1128/JVI.75.3.1371-1377.2001.
- Brisbarre, N.M., Plumet, S., Micco, P. de, Leparac-Goffart, I., Emonet, S.F., 2013. Toscana virus inhibits the interferon beta response in cell cultures. *Virology* 442, 189–194. doi:10.1016/j.virol.2013.04.016.
- Brisse, M., Ly, H., 2019. Comparative Structure and Function Analysis of the RIG-I-Like Receptors: RIG-I and MDA5. *Frontiers in Immunology* 10, 1586.
- Broggi, A., Ghosh, S., Sposito, B., Spreafico, R., Balzarini, F., Lo Cascio, A., Clementi, N., Santis, M. de, Mancini, N., Granucci, F., Zanoni, I., 2020. Type III interferons disrupt the lung epithelial barrier upon viral recognition. *Science (New York, N.Y.)* 369, 706–712. doi:10.1126/science.abc3545.
- Bruns, A.M., Leser, G.P., Lamb, R.A., Horvath, C.M., 2014. The innate immune sensor LGP2 activates antiviral signaling by regulating MDA5-RNA interaction and filament assembly. *Molecular cell* 55, 771–781. doi:10.1016/j.molcel.2014.07.003.
- Calisher, C.H., Calzolari, M., 2021. Taxonomy of Phleboviruses, Emphasizing Those That Are Sandfly-Borne. *Viruses* 13. doi:10.3390/v13050918.
- Cameron, M.J., Ran, L., Xu, L., Danesh, A., Bermejo-Martin, J.F., Cameron, C.M., Muller, M.P., Gold, W.L., Richardson, S.E., Poutanen, S.M., Willey, B.M., DeVries, M.E., Fang, Y., Seneviratne, C., Bosinger, S.E., Persad, D., Wilkinson, P., Greller, L.D., Somogyi, R., Humar, A., Keshavjee, S., Louie, M., Loeb, M.B., Brunton, J., McGeer, A.J., Kelvin, D.J., 2007. Interferon-mediated immunopathological events are associated with atypical innate and adaptive immune responses in patients with severe acute respiratory syndrome. *Journal of virology* 81, 8692–8706. doi:10.1128/JVI.00527-07.
- Cao, Y., Wei, J., Zou, L., Jiang, T., Wang, G., Chen, L., Huang, L., Meng, F., Huang, L., Wang, N., Zhou, X., Luo, H., Mao, Z., Chen, X., Xie, J., Liu, J., Cheng, H., Zhao, J., Huang, G., Wang, W., Zhou, J., 2020. Ruxolitinib in treatment of severe coronavirus disease 2019 (COVID-19): A

- multicenter, single-blind, randomized controlled trial. *The Journal of allergy and clinical immunology* 146, 137-146.e3. doi:10.1016/j.jaci.2020.05.019.
- Cao, Y., Xu, X., Kitanovski, S., Song, L., Wang, J., Hao, P., Hoffmann, D., 2021. Comprehensive Comparison of RNA-Seq Data of SARS-CoV-2, SARS-CoV and MERS-CoV Infections: Alternative Entry Routes and Innate Immune Responses. *Frontiers in Immunology* 12, 656433. doi:10.3389/fimmu.2021.656433.
- Caplen, H., Peters, C.J., Bishop, D.H., 1985. Mutagen-directed attenuation of Rift Valley fever virus as a method for vaccine development. *The Journal of general virology* 66 (Pt 10), 2271–2277. doi:10.1099/0022-1317-66-10-2271.
- Carty, M., Goodbody, R., Schröder, M., Stack, J., Moynagh, P.N., Bowie, A.G., 2006. The human adaptor SARM negatively regulates adaptor protein TRIF-dependent Toll-like receptor signaling. *Nature immunology* 7, 1074–1081. doi:10.1038/ni1382.
- Carty, M., Guy, C., Bowie, A.G., 2021. Detection of Viral Infections by Innate Immunity. *Biochemical pharmacology* 183, 114316. doi:10.1016/j.bcp.2020.114316.
- Carvalho, M.S. de, Lara Pinto, A.Z. de, Pinheiro, A., Rodrigues, J.S.V., Melo, F.L., da Silva, L.A., Ribeiro, B.M., Dezengrini-Slhessarenko, R., 2018. Viola phlebovirus is a novel Phlebotomus fever serogroup member identified in *Lutzomyia (Lutzomyia) longipalpis* from Brazilian Pantanal. *Parasites & vectors* 11, 405. doi:10.1186/s13071-018-2985-3.
- Channappanavar, R., Fehr, A.R., Vijay, R., Mack, M., Zhao, J., Meyerholz, D.K., Perlman, S., 2016. Dysregulated Type I Interferon and Inflammatory Monocyte-Macrophage Responses Cause Lethal Pneumonia in SARS-CoV-Infected Mice. *Cell Host & Microbe* 19, 181–193. doi:10.1016/j.chom.2016.01.007.
- Charrel, R.N., Moureau, G., Temmam, S., Izri, A., Marty, P., Parola, P., da Rosa, A.T., Tesh, R.B., Lamballerie, X. de, 2009. Massilia virus, a novel Phlebovirus (Bunyaviridae) isolated from sandflies in the Mediterranean. *Vector borne and zoonotic diseases (Larchmont, N.Y.)* 9, 519–530. doi:10.1089/vbz.2008.0131.
- Chavarría-Smith, J., Vance, R.E., 2015. The NLRP1 inflammasomes. *Immunological reviews* 265, 22–34. doi:10.1111/imr.12283.
- Chen, C.-Y., Yang, C.-H., Tsai, Y.-F., Liaw, C.-C., Chang, W.-Y., Hwang, T.-L., 2017. Ugonin U stimulates NLRP3 inflammasome activation and enhances inflammasome-mediated pathogen clearance. *Redox biology* 11, 263–274. doi:10.1016/j.redox.2016.12.018.
- Chen, H., Li, Y., Zhang, J., Ran, Y., Wei, J., Yang, Y., Shu, H.-B., 2013. RAVER1 is a coactivator of MDA5-mediated cellular antiviral response. *Journal of molecular cell biology* 5, 111–119. doi:10.1093/jmcb/mjt006.
- Chen, X., Saccon, E., Appelberg, K.S., Mikaeloff, F., Rodriguez, J.E., Vinhas, B.S., Frisan, T., Végvári, Á., Mirazimi, A., Neogi, U., Gupta, S., 2021. Type-I interferon signatures in SARS-CoV-2 infected Huh7 cells. *Cell Death Discovery* 7. doi:10.1038/s41420-021-00487-z.
- Chen, Y., Cai, H., Pan, J., Xiang, N., Tien, P., Ahola, T., Guo, D., 2009. Functional screen reveals SARS coronavirus nonstructural protein nsp14 as a novel cap N7 methyltransferase. *Proceedings of the National Academy of Sciences* 106, 3484–3489. doi:10.1073/pnas.0808790106.
- Chen, Y., Su, C., Ke, M., Jin, X., Xu, L., Zhang, Z., Wu, A., Sun, Y., Yang, Z., Tien, P., Ahola, T., Liang, Y., Liu, X., Guo, D., 2011. Biochemical and Structural Insights into the Mechanisms of SARS Coronavirus RNA Ribose 2'-O-Methylation by nsp16/nsp10 Protein Complex. *PLoS pathogens* 7, e1002294. doi:10.1371/journal.ppat.1002294.

- Ching, J.C.-Y., Chan, K.Y.K., Lee, E.H.L., Xu, M.-S., Ting, C.K.P., So, T.M.K., Sham, P.C., Leung, G.M., Peiris, J.S.M., Khoo, U.-S., 2010. Significance of the myxovirus resistance A (MxA) gene - 123Ca single-nucleotide polymorphism in suppressed interferon beta induction of severe acute respiratory syndrome coronavirus infection. *The Journal of infectious diseases* 201, 1899–1908. doi:10.1086/652799.
- Choi, J.H., Burke, J.M., Szymanik, K.H., Nepal, U., Battenhouse, A., Lau, J.T., Stark, A., Lam, V., Sullivan, C.S., 2020a. DUSP11-mediated control of 5'-triphosphate RNA regulates RIG-I sensitivity. *Genes & development* 34, 1697–1712. doi:10.1101/gad.340604.120.
- Choi, Y., Jiang, Z., Shin, W.-J., Jung, J.U., 2020b. Severe Fever with Thrombocytopenia Syndrome Virus NSs Interacts with TRIM21 To Activate the p62-Keap1-Nrf2 Pathway. *Journal of virology* 94. doi:10.1128/JVI.01684-19.
- Christova, I., Panayotova, E., Trifonova, I., Taseva, E., Gladnishka, T., Ivanova, V., 2020. Serologic evidence of widespread Toscana virus infection in Bulgaria. *Journal of infection and public health* 13, 164–166. doi:10.1016/j.jiph.2019.07.008.
- Chu, H., Chan, J.F.-W., Wang, Y., Yuen, T.T.-T., Chai, Y., Hou, Y., Shuai, H., Yang, D., Hu, B., Huang, X., Zhang, X., Cai, J.-P., Zhou, J., Yuan, S., Kok, K.-H., To, K.K.-W., Chan, I.H.-Y., Zhang, A.J., Sit, K.-Y., Au, W.-K., Yuen, K.-Y., 2020. Comparative replication and immune activation profiles of SARS-CoV-2 and SARS-CoV in human lungs: an ex vivo study with implications for the pathogenesis of COVID-19. *Clinical Infectious Diseases: An Official Publication of the Infectious Diseases Society of America*. doi:10.1093/cid/ciaa410.
- Ciota, A.T., Keyel, A.C., 2019. The Role of Temperature in Transmission of Zoonotic Arboviruses. *Viruses* 11. doi:10.3390/v11111013.
- Collao, X., Palacios, G., Ory, F. de, Sanbonmatsu, S., Pérez-Ruiz, M., Navarro, J.M., Molina, R., Hutchison, S.K., Lipkin, W.I., Tenorio, A., Sánchez-Seco, M.P., 2010. Granada virus: a natural phlebovirus reassortant of the sandfly fever Naples serocomplex with low seroprevalence in humans. *The American journal of tropical medicine and hygiene* 83, 760–765. doi:10.4269/ajtmh.2010.09-0697.
- Copeland, A.M., van Deusen, N.M., Schmaljohn, C.S., 2015. Rift Valley fever virus NSS gene expression correlates with a defect in nuclear mRNA export. *Virology* 486, 88–93. doi:10.1016/j.virol.2015.09.003.
- Corman, V.M., Landt, O., Kaiser, M., Molenkamp, R., Meijer, A., Chu, D.K., Bleicker, T., Brünink, S., Schneider, J., Schmidt, M.L., Mulders, D.G., Haagmans, B.L., van der Veer, B., van den Brink, S., Wijsman, L., Goderski, G., Romette, J.-L., Ellis, J., Zambon, M., Peiris, M., Goossens, H., Reusken, C., Koopmans, M.P., Drosten, C., 2020. Detection of 2019 novel coronavirus (2019-nCoV) by real-time RT-PCR. *Euro surveillance : bulletin Europeen sur les maladies transmissibles = European communicable disease bulletin* 25. doi:10.2807/1560-7917.ES.2020.25.3.2000045.
- Corman, V.M., Muth, D., Niemeyer, D., Drosten, C., 2018. Hosts and Sources of Endemic Human Coronaviruses. *Advances in Virus Research* 100, 163–188. doi:10.1016/bs.aivir.2018.01.001.
- COVID-19 Dashboard, Johns Hopkins University, accessed on 08 September 2021, 2021. <https://gisanddata.maps.arcgis.com/apps/dashboards/bda7594740fd40299423467b48e9ecf6>.
- Daamen, A.R., Bachali, P., Owen, K.A., Kingsmore, K.M., Hubbard, E.L., Labonte, A.C., Robl, R., Shrotri, S., Grammer, A.C., Lipsky, P.E., 2021. Comprehensive transcriptomic analysis of COVID-19 blood, lung, and airway. *Scientific reports* 11, 7052. doi:10.1038/s41598-021-86002-x.

- Daffis, S., Samuel, M.A., Keller, B.C., Gale, M., Diamond, M.S., 2007. Cell-specific IRF-3 responses protect against West Nile virus infection by interferon-dependent and -independent mechanisms. *PLoS pathogens* 3, e106. doi:10.1371/journal.ppat.0030106.
- D'Alessio, A., Del Poggio, P., Bracchi, F., Cesana, G., Sertori, N., Di Mauro, D., Fagnoli, A., Motta, M., Giussani, C., Moro, P., Vitale, G., Giacomini, M., Borra, G., 2020. Low-dose ruxolitinib plus steroid in severe SARS-CoV-2 pneumonia. *Leukemia* 35, 635–638. doi:10.1038/s41375-020-01087-z.
- Davis, M.I., Hunt, J.P., Herrgard, S., Ciceri, P., Wodicka, L.M., Pallares, G., Hocker, M., Treiber, D.K., Zarrinkar, P.P., 2011. Comprehensive analysis of kinase inhibitor selectivity. *Nature biotechnology* 29, 1046–1051. doi:10.1038/nbt.1990.
- Davoudi-Monfared, E., Rahmani, H., Khalili, H., Hajiabdolbaghi, M., Salehi, M., Abbasian, L., Kazemzadeh, H., Yekaninejad, M.S., 2020. A Randomized Clinical Trial of the Efficacy and Safety of Interferon β -1a in Treatment of Severe COVID-19. *Antimicrobial agents and chemotherapy* 64. doi:10.1128/AAC.01061-20.
- de Weerd, N.A., Samarajiwa, S.A., Hertzog, P.J., 2007. Type I interferon receptors: biochemistry and biological functions. *The Journal of biological chemistry* 282, 20053–20057. doi:10.1074/jbc.R700006200.
- Dellgren, C., Gad, H.H., Hamming, O.J., Melchjorsen, J., Hartmann, R., 2009. Human interferon-lambda3 is a potent member of the type III interferon family. *Genes and immunity* 10, 125–131. doi:10.1038/gene.2008.87.
- Devaraj, S.G., Wang, N., Chen, Z., Chen, Z., Tseng, M., Barretto, N., Lin, R., Peters, C.J., Tseng, C.-T.K., Baker, S.C., Li, K., 2007. Regulation of IRF-3-dependent Innate Immunity by the Papain-like Protease Domain of the Severe Acute Respiratory Syndrome Coronavirus. *Journal of Biological Chemistry* 282, 32208–32221. doi:10.1074/jbc.m704870200.
- Drappier, M., Michiels, T., 2015. Inhibition of the OAS/RNase L pathway by viruses. *Current opinion in virology* 15, 19–26. doi:10.1016/j.coviro.2015.07.002.
- Dzimianski, J.V., Scholte, F.E.M., Bergeron, É., Pegan, S.D., 2019. ISG15: It's Complicated. *Journal of molecular biology* 431, 4203–4216. doi:10.1016/j.jmb.2019.03.013.
- Eifan, S., Schnettler, E., Dietrich, I., Kohl, A., Blomström, A.-L., 2013. Non-structural proteins of arthropod-borne bunyaviruses: roles and functions. *Viruses* 5, 2447–2468. doi:10.3390/v5102447.
- Elliott, R.M., Brennan, B., 2014. Emerging phleboviruses. *Current opinion in virology* 5, 50–57. doi:10.1016/j.coviro.2014.01.011.
- Emeny, J.M., Morgan, M.J., 1979. Regulation of the interferon system: evidence that Vero cells have a genetic defect in interferon production. *The Journal of general virology* 43, 247–252. doi:10.1099/0022-1317-43-1-247.
- Ermler, M.E., Traylor, Z., Patel, K., Schattgen, S.A., Vanaja, S.K., Fitzgerald, K.A., Hise, A.G., 2014. Rift Valley fever virus infection induces activation of the NLRP3 inflammasome. *Virology* 449, 174–180. doi:10.1016/j.virol.2013.11.015.
- Esser, H.J., Mögling, R., Cleton, N.B., van der Jeugd, H., Sprong, H., Stroo, A., Koopmans, M.P.G., Boer, W.F. de, Reusken, C.B.E.M., 2019. Risk factors associated with sustained circulation of six zoonotic arboviruses: a systematic review for selection of surveillance sites in non-endemic areas. *Parasites & vectors* 12, 265. doi:10.1186/s13071-019-3515-7.

- Fajgenbaum, D.C., June, C.H., 2020. Cytokine Storm. *New England Journal of Medicine* 383, 2255–2273. doi:10.1056/nejmra2026131.
- Fan, X., Jin, T., 2019. Structures of RIG-I-Like Receptors and Insights into Viral RNA Sensing. *Advances in experimental medicine and biology* 1172, 157–188. doi:10.1007/978-981-13-9367-9_8.
- Fehr, A.R., Perlman, S., 2015. Coronaviruses: an overview of their replication and pathogenesis. *Methods in molecular biology (Clifton, N.J.)* 1282, 1–23. doi:10.1007/978-1-4939-2438-7_1.
- Fekete, T., Ágics, B., Bencze, D., Bene, K., Szántó, A., Tarr, T., Veréb, Z., Bácsi, A., Pázmándi, K., 2020. Regulation of RLR-Mediated Antiviral Responses of Human Dendritic Cells by mTOR. *Frontiers in Immunology* 11, 572960. doi:10.3389/fimmu.2020.572960.
- Feld, J.J., Kandel, C., Biondi, M.J., Kozak, R.A., Zahoor, M.A., Lemieux, C., Borgia, S.M., Boggild, A.K., Powis, J., McCready, J., Tan, D.H.S., Chan, T., Coburn, B., Kumar, D., Humar, A., Chan, A., O'Neil, B., Noureldin, S., Booth, J., Hong, R., Smookler, D., Aleyadeh, W., Patel, A., Barber, B., Casey, J., Hiebert, R., Mistry, H., Choong, I., Hislop, C., Santer, D.M., Lorne Tyrrell, D., Glenn, J.S., Gehring, A.J., Janssen, H.L.A., Hansen, B.E., 2021. Peginterferon lambda for the treatment of outpatients with COVID-19: a phase 2, placebo-controlled randomised trial. *The Lancet. Respiratory Medicine* 9, 498–510. doi:10.1016/S2213-2600(20)30566-X.
- Felgenhauer, U., Schoen, A., Gad, H.H., Hartmann, R., Schaubmar, A.R., Failing, K., Drosten, C., Weber, F., 2020. Inhibition of SARS-CoV-2 by type I and type III interferons. *The Journal of biological chemistry* 295, 13958–13964. doi:10.1074/jbc.AC120.013788.
- Fensterl, V., Sen, G.C., 2011. The ISG56/IFIT1 gene family. *Journal of interferon & cytokine research : the official journal of the International Society for Interferon and Cytokine Research* 31, 71–78. doi:10.1089/jir.2010.0101.
- Ferron, F., Weber, F., La Torre, J.C. de, Reguera, J., 2017. Transcription and replication mechanisms of Bunyaviridae and Arenaviridae L proteins. *Virus research* 234, 118–134. doi:10.1016/j.virusres.2017.01.018.
- Finkel, Y., Mizrahi, O., Nachshon, A., Weingarten-Gabbay, S., Morgenstern, D., Yahalom-Ronen, Y., Tamir, H., Achdout, H., Stein, D., Israeli, O., Beth-Din, A., Melamed, S., Weiss, S., Israely, T., Paran, N., Schwartz, M., Stern-Ginossar, N., 2021. The coding capacity of SARS-CoV-2. *Nature* 589, 125–130. doi:10.1038/s41586-020-2739-1.
- Fisher, A.F., Tesh, R.B., Tonry, J., Guzman, H., Liu, D., Xiao, S.-Y., 2003. Induction of severe disease in hamsters by two sandfly fever group viruses, Punta toro and Gabek Forest (Phlebovirus, Bunyaviridae), similar to that caused by Rift Valley fever virus. *The American journal of tropical medicine and hygiene* 69, 269–276.
- Fitzgerald, K.A., Kagan, J.C., 2020. Toll-like Receptors and the Control of Immunity. *Cell* 180, 1044–1066. doi:10.1016/j.cell.2020.02.041.
- Forero, A., Ozarkar, S., Li, H., Lee, C.H., Hemann, E.A., Nadsjombati, M.S., Hendricks, M.R., So, L., Green, R., Roy, C.N., Sarkar, S.N., Moltke, J. von, Anderson, S.K., Gale, M., Savan, R., 2019. Differential activation of the transcription factor IRF1 underlies the distinct immune responses elicited by type I and type III interferons. *Immunity* 51, 451–464.e6. doi:10.1016/j.immuni.2019.07.007.
- Forni, D., Cagliani, R., Clerici, M., Sironi, M., 2017. Molecular Evolution of Human Coronavirus Genomes. *Trends in microbiology* 25, 35–48. doi:10.1016/j.tim.2016.09.001.

- Fraser, D.D., Cepinskas, G., Slessarev, M., Martin, C., Daley, M., Miller, M.R., O’Gorman, D.B., Gill, S.E., Patterson, E.K., Dos Santos, C.C., 2020. Inflammation Profiling of Critically Ill Coronavirus Disease 2019 Patients. *Critical care explorations* 2, e0144. doi:10.1097/CCE.000000000000144.
- Frese, M., Kochs, G., Feldmann, H., Hertkorn, C., Haller, O., 1996. Inhibition of bunyaviruses, phleboviruses, and hantaviruses by human MxA protein. *Journal of virology* 70, 915–923. doi:10.1128/JVI.70.2.915-923.1996.
- Freundt, E.C., Yu, L., Park, E., Lenardo, M.J., Xu, X.-N., 2009. Molecular Determinants for Subcellular Localization of the Severe Acute Respiratory Syndrome Coronavirus Open Reading Frame 3b Protein. *Journal of virology* 83, 6631–6640. doi:10.1128/jvi.00367-09.
- Frieman, M., Heise, M., Baric, R., 2007a. SARS coronavirus and innate immunity. *Virus research* 133, 101–112. doi:10.1016/j.virusres.2007.03.015.
- Frieman, M., Yount, B., Heise, M., Kopecky-Bromberg, S.A., Palese, P., Baric, R.S., 2007b. Severe Acute Respiratory Syndrome Coronavirus ORF6 Antagonizes STAT1 Function by Sequestering Nuclear Import Factors on the Rough Endoplasmic Reticulum/Golgi Membrane. *Journal of virology* 81, 9812–9824. doi:10.1128/jvi.01012-07.
- Fu, W., Liu, Y., Liu, L., Hu, H., Cheng, X., Liu, P., Song, Z., Zha, L., Bai, S., Xu, T., Yuan, S., Lu, F., Shang, Z., Zhao, Y., Wang, J., Zhao, J., Ding, L., Chen, J., Zhang, L., Zhu, T., Zhang, X., Lu, H., Xu, J., 2020. An open-label, randomized trial of the combination of IFN- κ plus TFF2 with standard care in the treatment of patients with moderate COVID-19. *EClinicalMedicine* 27. doi:10.1016/j.eclinm.2020.100547.
- Fuchs, S., Kaiser-Labusch, P., Bank, J., Ammann, S., Kolb-Kokocinski, A., Edelbusch, C., Omran, H., Ehl, S., 2016. Tyrosine kinase 2 is not limiting human antiviral type III interferon responses. *European journal of immunology* 46, 2639–2649. doi:10.1002/eji.201646519.
- Fujikawa, K., Koga, T., Honda, T., Uchida, T., Okamoto, M., Endo, Y., Mihara, T., Kondo, A., Shimada, S., Hayasaka, D., Morita, K., Mizokami, A., Kawakami, A., 2019. Serial analysis of cytokine and chemokine profiles and viral load in severe fever with thrombocytopenia syndrome: Case report and review of literature. *Medicine* 98, e17571. doi:10.1097/MD.00000000000017571.
- Fung, K.Y., Mangan, N.E., Cumming, H., Horvat, J.C., Mayall, J.R., Stifter, S.A., Weerd, N. de, Roisman, L.C., Rossjohn, J., Robertson, S.A., Schjenken, J.E., Parker, B., Gargett, C.E., Nguyen, H.P.T., Carr, D.J., Hansbro, P.M., Hertzog, P.J., 2013. Interferon- ϵ protects the female reproductive tract from viral and bacterial infection. *Science (New York, N.Y.)* 339, 1088–1092. doi:10.1126/science.1233321.
- Fung, T.S., Liu, D.X., 2019. Human Coronavirus: Host-Pathogen Interaction. *Annual review of microbiology* 73, 529–557. doi:10.1146/annurev-micro-020518-115759.
- Gack, M.U., Shin, Y.C., Joo, C.-H., Urano, T., Liang, C., Sun, L., Takeuchi, O., Akira, S., Chen, Z., Inoue, S., Jung, J.U., 2007. TRIM25 RING-finger E3 ubiquitin ligase is essential for RIG-I-mediated antiviral activity. *Nature* 446, 916–920. doi:10.1038/nature05732.
- Galani, I.-E., Rovina, N., Lampropoulou, V., Triantafyllia, V., Manioudaki, M., Pavlos, E., Koukaki, E., Fragkou, P.C., Panou, V., Rapti, V., Koltsida, O., Mentis, A., Koulouris, N., Tsiodras, S., Koutsoukou, A., Andreacos, E., 2021. Untuned antiviral immunity in COVID-19 revealed by temporal type I/III interferon patterns and flu comparison. *Nature immunology* 22, 32–40. doi:10.1038/s41590-020-00840-x.
- García-Sastre, A., 2017. Ten Strategies of Interferon Evasion by Viruses. *Cell Host & Microbe* 22, 176–184. doi:10.1016/j.chom.2017.07.012.

- Gaspari, V., Zengarini, C., Greco, S., Vangeli, V., Mastroianni, A., 2020. Side effects of ruxolitinib in patients with SARS-CoV-2 infection: Two case reports. *International journal of antimicrobial agents* 56, 106023. doi:10.1016/j.ijantimicag.2020.106023.
- Gerdts, J., Brace, E.J., Sasaki, Y., DiAntonio, A., Milbrandt, J., 2015. SARM1 activation triggers axon degeneration locally via NAD⁺ destruction. *Science (New York, N.Y.)* 348, 453–457. doi:10.1126/science.1258366.
- Gerlach, T., Hensen, L., Matrosovich, T., Bergmann, J., Winkler, M., Peteranderl, C., Klenk, H.-D., Weber, F., Herold, S., Pöhlmann, S., Matrosovich, M., 2017. pH Optimum of Hemagglutinin-Mediated Membrane Fusion Determines Sensitivity of Influenza A Viruses to the Interferon-Induced Antiviral State and IFITMs. *Journal of virology* 91. doi:10.1128/JVI.00246-17.
- Ghosh, S., Dellibovi-Ragheb, T.A., Kerviel, A., Pak, E., Qiu, Q., Fisher, M., Takvorian, P.M., Bleck, C., Hsu, V.W., Fehr, A.R., Perlman, S., Achar, S.R., Straus, M.R., Whittaker, G.R., Haan, C.A.M. de, Kehrl, J., Altan-Bonnet, G., Altan-Bonnet, N., 2020. β -Coronaviruses Use Lysosomes for Egress Instead of the Biosynthetic Secretory Pathway. *Cell* 183, 1520-1535.e14. doi:10.1016/j.cell.2020.10.039.
- Giudice, V., Pagliano, P., Vatrella, A., Masullo, A., Poto, S., Polverino, B.M., Gammaldi, R., Maglio, A., Sellitto, C., Vitale, C., Serio, B., Cuffa, B., Borrelli, A., Vecchione, C., Filippelli, A., Selleri, C., 2020. Combination of Ruxolitinib and Eculizumab for Treatment of Severe SARS-CoV-2-Related Acute Respiratory Distress Syndrome: A Controlled Study. *Frontiers in pharmacology* 11, 857. doi:10.3389/fphar.2020.00857.
- Goodbourn, S., 1990. The regulation of beta-interferon gene expression. *Seminars in cancer biology* 1, 89–95.
- Gordon, D.E., Jang, G.M., Bouhaddou, M., Xu, J., Obernier, K., White, K.M., O'Meara, M.J., Rezelj, V.V., Guo, J.Z., Swaney, D.L., Tummino, T.A., Hüttenhain, R., Kaake, R.M., Richards, A.L., Tutuncuoglu, B., Foussard, H., Batra, J., Haas, K., Modak, M., Kim, M., Haas, P., Polacco, B.J., Braberg, H., Fabius, J.M., Eckhardt, M., Soucheray, M., Bennett, M.J., Cakir, M., McGregor, M.J., Li, Q., Meyer, B., Roesch, F., Vallet, T., Mac Kain, A., Miorin, L., Moreno, E., Naing, Z.Z.C., Zhou, Y., Peng, S., Shi, Y., Zhang, Z., Shen, W., Kirby, I.T., Melnyk, J.E., Chorba, J.S., Lou, K., Dai, S.A., Barrio-Hernandez, I., Memon, D., Hernandez-Armenta, C., Lyu, J., Mathy, C.J.P., Perica, T., Pilla, K.B., Ganesan, S.J., Saltzberg, D.J., Rakesh, R., Liu, X., Rosenthal, S.B., Calviello, L., Venkataramanan, S., Liboy-Lugo, J., Lin, Y., Huang, X.-P., Liu, Y., Wankowicz, S.A., Bohn, M., Safari, M., Ugur, F.S., Koh, C., Savar, N.S., Tran, Q.D., Shengjuler, D., Fletcher, S.J., O'Neal, M.C., Cai, Y., Chang, J.C.J., Broadhurst, D.J., Klippsten, S., Sharp, P.P., Wenzell, N.A., Kuzuoglu-Ozturk, D., Wang, H.-Y., Trenker, R., Young, J.M., Cavero, D.A., Hiatt, J., Roth, T.L., Rathore, U., Subramanian, A., Noack, J., Hubert, M., Stroud, R.M., Frankel, A.D., Rosenberg, O.S., Verba, K.A., Agard, D.A., Ott, M., Emerman, M., Jura, N., Zastrow, M. von, Verdin, E., Ashworth, A., Schwartz, O., d'Enfert, C., Mukherjee, S., Jacobson, M., Malik, H.S., Fujimori, D.G., Ideker, T., Craik, C.S., Floor, S.N., Fraser, J.S., Gross, J.D., Sali, A., Roth, B.L., Ruggero, D., Taunton, J., Kortemme, T., Beltrao, P., Vignuzzi, M., García-Sastre, A., Shokat, K.M., Shoichet, B.K., Krogan, N.J., 2020. A SARS-CoV-2 protein interaction map reveals targets for drug repurposing. *Nature* 583, 459–468. doi:10.1038/s41586-020-2286-9.
- Gori Savellini, G., Anichini, G., Gandolfo, C., Prathyumnan, S., Cusi, M.G., 2019. Toscana virus non-structural protein NSs acts as E3 ubiquitin ligase promoting RIG-I degradation. *PLoS pathogens* 15, e1008186. doi:10.1371/journal.ppat.1008186.

- Gori Savellini, G., Weber, F., Terrosi, C., Habjan, M., Martorelli, B., Cusi, M.G., 2011. Toscana virus induces interferon although its NSs protein reveals antagonistic activity. *The Journal of general virology* 92, 71–79. doi:10.1099/vir.0.025999-0.
- Goubau, D., Deddouche, S., Reis e Sousa, C., 2013. Cytosolic Sensing of Viruses. *Immunity* 38, 855–869. doi:10.1016/j.immuni.2013.05.007.
- Goubau, D., van der Veen, A.G., Chakravarty, P., Lin, R., Rogers, N., Rehwinkel, J., Deddouche, S., Rosewell, I., Hiscott, J., Reis e Sousa, C., 2015. Mouse superkiller-2-like helicase DDX60 is dispensable for type I IFN induction and immunity to multiple viruses. *European journal of immunology* 45, 3386–3403. doi:10.1002/eji.201545794.
- Grossegeisse, M., Bourquain, D., Neumann, M., Schaade, L., Nitsche, A., Doellinger, J., 2021. Deep time course proteomics of SARS-CoV- and SARS-CoV-2-infected human lung epithelial cells (Calu-3) reveals strong induction of interferon-stimulated gene (ISG) expression by SARS-CoV-2 in contrast to SARS-CoV.
- Guu, T.S.Y., Zheng, W., Tao, Y.J., 2012. Bunyavirus: structure and replication. *Advances in experimental medicine and biology* 726, 245–266. doi:10.1007/978-1-4614-0980-9_11.
- Habjan, M., Andersson, I., Klingström, J., Schumann, M., Martin, A., Zimmermann, P., Wagner, V., Pichlmair, A., Schneider, U., Mühlberger, E., Mirazimi, A., Weber, F., 2008a. Processing of Genome 5' Termini as a Strategy of Negative-Strand RNA Viruses to Avoid RIG-I-Dependent Interferon Induction. *PLoS ONE* 3. doi:10.1371/journal.pone.0002032.
- Habjan, M., Penski, N., Spiegel, M., Weber, F., 2008b. T7 RNA polymerase-dependent and -independent systems for cDNA-based rescue of Rift Valley fever virus. *Journal of General Virology* 89, 2157–2166. doi:10.1099/vir.0.2008/002097-0.
- Habjan, M., Penski, N., Wagner, V., Spiegel, M., Overby, A.K., Kochs, G., Huiskonen, J.T., Weber, F., 2009a. Efficient production of Rift Valley fever virus-like particles: The antiviral protein MxA can inhibit primary transcription of bunyaviruses. *Virology* 385, 400–408. doi:10.1016/j.virol.2008.12.011.
- Habjan, M., Pichlmair, A., Elliott, R.M., Overby, A.K., Glatter, T., Gstaiger, M., Superti-Furga, G., Unger, H., Weber, F., 2009b. NSs protein of rift valley fever virus induces the specific degradation of the double-stranded RNA-dependent protein kinase. *Journal of virology* 83, 4365–4375. doi:10.1128/JVI.02148-08.
- Hackbart, M., Deng, X., Baker, S.C., 2020. Coronavirus endoribonuclease targets viral polyuridine sequences to evade activating host sensors. *Proceedings of the National Academy of Sciences* 117, 8094–8103. doi:10.1073/pnas.1921485117.
- Hadjadj, J., Yatim, N., Barnabei, L., Corneau, A., Boussier, J., Smith, N., Péré, H., Charbit, B., Bondet, V., Chenevier-Gobeaux, C., Breillat, P., Carlier, N., Gauzit, R., Morbieu, C., Pène, F., Marin, N., Roche, N., Szwebel, T.-A., Merklung, S.H., Treluyer, J.-M., Veyer, D., Mouthon, L., Blanc, C., Tharaux, P.-L., Rozenberg, F., Fischer, A., Duffy, D., Rieux-Laucat, F., Kernéis, S., Terrier, B., 2020. Impaired type I interferon activity and inflammatory responses in severe COVID-19 patients. *Science (New York, N.Y.)* 369, 718–724. doi:10.1126/science.abc6027.
- Hall, T.A., 1999. BioEdit : a user-friendly biological sequence alignment editor and analysis program for Windows 95/98/NT. *Nucleic Acids Symp. Ser.* 41, 95–98.
- Hallam, H.J., Lokugamage, N., Ikegami, T., 2019. Rescue of infectious Arumowot virus from cloned cDNA: Posttranslational degradation of Arumowot virus NSs protein in human cells. *PLoS neglected tropical diseases* 13, e0007904. doi:10.1371/journal.pntd.0007904.

- Haller, O., Kochs, G., 2011. Human MxA protein: an interferon-induced dynamin-like GTPase with broad antiviral activity. *Journal of interferon & cytokine research : the official journal of the International Society for Interferon and Cytokine Research* 31, 79–87. doi:10.1089/jir.2010.0076.
- Hamming, O.J., Terczyńska-Dyla, E., Vieyres, G., Dijkman, R., Jørgensen, S.E., Akhtar, H., Siupka, P., Pietschmann, T., Thiel, V., Hartmann, R., 2013. Interferon lambda 4 signals via the IFN λ receptor to regulate antiviral activity against HCV and coronaviruses. *The EMBO journal* 32, 3055–3065. doi:10.1038/emboj.2013.232.
- Han, H., Ma, Q., Li, C., Liu, R., Zhao, L., Wang, W., Zhang, P., Liu, X., Gao, G., Liu, F., Jiang, Y., Cheng, X., Zhu, C., Xia, Y., 2020. Profiling serum cytokines in COVID-19 patients reveals IL-6 and IL-10 are disease severity predictors. *Emerging microbes & infections* 9, 1123–1130. doi:10.1080/22221751.2020.1770129.
- Harcourt, J., Tamin, A., Lu, X., Kamili, S., Sakthivel, S.K., Murray, J., Queen, K., Tao, Y., Paden, C.R., Zhang, J., Li, Y., Uehara, A., Wang, H., Goldsmith, C., Bullock, H.A., Wang, L., Whitaker, B., Lynch, B., Gautam, R., Schindewolf, C., Lokugamage, K.G., Scharton, D., Plante, J.A., Mirchandani, D., Widen, S.G., Narayanan, K., Makino, S., Ksiazek, T.G., Plante, K.S., Weaver, S.C., Lindstrom, S., Tong, S., Menachery, V.D., Thornburg, N.J., 2020. Isolation and characterization of SARS-CoV-2 from the first US COVID-19 patient. *bioRxiv : the preprint server for biology*. doi:10.1101/2020.03.02.972935.
- Harrison, A.G., Lin, T., Wang, P., 2020. Mechanisms of SARS-CoV-2 Transmission and Pathogenesis. *Trends in Immunology* 41, 1100–1115. doi:10.1016/j.it.2020.10.004.
- Hartmann, G., 2017. Nucleic Acid Immunity. *Advances in immunology* 133, 121–169. doi:10.1016/bs.ai.2016.11.001.
- Hayakawa, S., Shiratori, S., Yamato, H., Kameyama, T., Kitatsuji, C., Kashigi, F., Goto, S., Kameoka, S., Fujikura, D., Yamada, T., Mizutani, T., Kazumata, M., Sato, M., Tanaka, J., Asaka, M., Ohba, Y., Miyazaki, T., Imamura, M., Takaoka, A., 2011. ZAPS is a potent stimulator of signaling mediated by the RNA helicase RIG-I during antiviral responses. *Nature immunology* 12, 37–44. doi:10.1038/ni.1963.
- Hayn, M., Hirschenberger, M., Koepke, L., Nchioua, R., Straub, J.H., Klute, S., Hunszinger, V., Zech, F., Prelli Bozzo, C., Aftab, W., Christensen, M.H., Conzelmann, C., Müller, J.A., Srinivasachar Badarinarayan, S., Stürzel, C.M., Forne, I., Stenger, S., Conzelmann, K.-K., Münch, J., Schmidt, F.I., Sauter, D., Imhof, A., Kirchhoff, F., Sparrer, K.M.J., 2021. Systematic functional analysis of SARS-CoV-2 proteins uncovers viral innate immune antagonists and remaining vulnerabilities. *Cell reports* 35, 109126. doi:10.1016/j.celrep.2021.109126.
- He, J., Feng, D., Vlas, S.J. de, Wang, H., Fontanet, A., Zhang, P., Plancoulaine, S., Tang, F., Zhan, L., Yang, H., Wang, T., Richardus, J.H., Habbema, J.D.F., Cao, W., 2006. Association of SARS susceptibility with single nucleic acid polymorphisms of OAS1 and MxA genes: a case-control study. *BMC infectious diseases* 6, 106. doi:10.1186/1471-2334-6-106.
- Heberle, H., Meirelles, G.V., da Silva, F.R., Telles, G.P., Minghim, R., 2015. InteractiVenn: a web-based tool for the analysis of sets through Venn diagrams. *BMC bioinformatics* 16, 169. doi:10.1186/s12859-015-0611-3.
- Hoffmann, M., Kleine-Weber, H., Schroeder, S., Krüger, N., Herrler, T., Erichsen, S., Schiergens, T.S., Herrler, G., Wu, N.-H., Nitsche, A., Müller, M.A., Drosten, C., Pöhlmann, S., 2020. SARS-CoV-2 Cell Entry Depends on ACE2 and TMPRSS2 and Is Blocked by a Clinically Proven Protease Inhibitor. *Cell* 181, 271-280.e8. doi:10.1016/j.cell.2020.02.052.

- Holbrook, J., Lara-Reyna, S., Jarosz-Griffiths, H., McDermott, M., 2019. Tumour necrosis factor signalling in health and disease. *F1000Research* 8. doi:10.12688/f1000research.17023.1.
- Hölzer, M., Schoen, A., Wulle, J., Müller, M.A., Drost, C., Marz, M., Weber, F., 2019. Virus- and Interferon Alpha-Induced Transcriptomes of Cells from the Microbat *Myotis daubentonii*. *iScience* 19, 647–661. doi:10.1016/j.isci.2019.08.016.
- Hong, Y., Bai, M., Qi, X., Li, C., Liang, M., Li, D., Cardona, C.J., Xing, Z., 2019. Suppression of the IFN- α and - β Induction through Sequestering IRF7 into Viral Inclusion Bodies by Nonstructural Protein NSs in Severe Fever with Thrombocytopenia Syndrome Bunyavirus Infection. *Journal of immunology (Baltimore, Md. : 1950)* 202, 841–856. doi:10.4049/jimmunol.1800576.
- Horisberger, M.A., Staritzky, K. de, 1987. A recombinant human interferon-alpha B/D hybrid with a broad host-range. *The Journal of general virology* 68 (Pt 3), 945–948. doi:10.1099/0022-1317-68-3-945.
- Hornung, V., Ellegast, J., Kim, S., Brzózka, K., Jung, A., Kato, H., Poeck, H., Akira, S., Conzelmann, K.-K., Schlee, M., Endres, S., Hartmann, G., 2006. 5'-Triphosphate RNA is the ligand for RIG-I. *Science (New York, N.Y.)* 314, 994–997. doi:10.1126/science.1132505.
- Hou, F., Sun, L., Zheng, H., Skaug, B., Jiang, Q.-X., Chen, Z.J., 2011. MAVS Forms Functional Prion-Like Aggregates To Activate and Propagate Antiviral Innate Immune Response. *Cell* 146, 448–461. doi:10.1016/j.cell.2011.06.041.
- Hu, Y., Li, W., Gao, T., Cui, Y., Jin, Y., Li, P., Ma, Q., Liu, X., Cao, C., 2017. The Severe Acute Respiratory Syndrome Coronavirus Nucleocapsid Inhibits Type I Interferon Production by Interfering with TRIM25-Mediated RIG-I Ubiquitination. *Journal of virology* 91. doi:10.1128/jvi.02143-16.
- Huang, C., Lokugamage, K.G., Rozovics, J.M., Narayanan, K., Semler, B.L., Makino, S., 2011. SARS Coronavirus nsp1 Protein Induces Template-Dependent Endonucleolytic Cleavage of mRNAs: Viral mRNAs Are Resistant to nsp1-Induced RNA Cleavage. *PLoS pathogens* 7, e1002433. doi:10.1371/journal.ppat.1002433.
- Huang, C., Wang, Y., Li, X., Ren, L., Zhao, J., Hu, Y., Zhang, L., Fan, G., Xu, J., Gu, X., Cheng, Z., Yu, T., Xia, J., Wei, Y., Wu, W., Xie, X., Yin, W., Li, H., Liu, M., Xiao, Y., Gao, H., Guo, L., Xie, J., Wang, G., Jiang, R., Gao, Z., Jin, Q., Wang, J., Cao, B., 2020. Clinical features of patients infected with 2019 novel coronavirus in Wuhan, China. *The Lancet* 395, 497–506. doi:10.1016/S0140-6736(20)30183-5.
- Hug, H., Costas, M., Staeheli, P., Aebi, M., Weissmann, C., 1988. Organization of the murine Mx gene and characterization of its interferon- and virus-inducible promoter. *Molecular and cellular biology* 8, 3065–3079. doi:10.1128/mcb.8.8.3065.
- Hulswit, R.J.G., Haan, C.A.M. de, Bosch, B.-J., 2016. Coronavirus Spike Protein and Tropism Changes. *Advances in Virus Research* 96, 29–57. doi:10.1016/bs.aivir.2016.08.004.
- Hung, I.F.-N., Lung, K.-C., Tso, E.Y.-K., Liu, R., Chung, T.W.-H., Chu, M.-Y., Ng, Y.-Y., Lo, J., Chan, J., Tam, A.R., Shum, H.-P., Chan, V., Wu, A.K.-L., Sin, K.-M., Leung, W.-S., Law, W.-L., Lung, D.C., Sin, S., Yeung, P., Yip, C.C.-Y., Zhang, R.R., Fung, A.Y.-F., Yan, E.Y.-W., Leung, K.-H., Ip, J.D., Chu, A.W.-H., Chan, W.-M., Ng, A.C.-K., Lee, R., Fung, K., Yeung, A., Wu, T.-C., Chan, J.W.-M., Yan, W.-W., Chan, W.-M., Chan, J.F.-W., Lie, A.K.-W., Tsang, O.T.-Y., Cheng, V.C.-C., Que, T.-L., Lau, C.-S., Chan, K.-h., To, K.K.-W., Yuen, K.-Y., 2020. Triple combination of interferon beta-1b, lopinavir-ritonavir, and ribavirin in the treatment of patients admitted to hospital with COVID-19: an open-label, randomised, phase 2 trial. *Lancet (London, England)* 395, 1695–1704. doi:10.1016/S0140-6736(20)31042-4.

- Ibsen, M.S., Gad, H.H., Andersen, L.L., Hornung, V., Julkunen, I., Sarkar, S.N., Hartmann, R., 2015. Structural and functional analysis reveals that human OASL binds dsRNA to enhance RIG-I signaling. *Nucleic acids research* 43, 5236–5248. doi:10.1093/nar/gkv389.
- ICTV, 2020. <https://talk.ictvonline.org/taxonomy/>: accessed on 17 February 2021.
- Ikegami, T., Narayanan, K., Won, S., Kamitani, W., Peters, C.J., Makino, S., 2009. Rift Valley fever virus NSs protein promotes post-transcriptional downregulation of protein kinase PKR and inhibits eIF2alpha phosphorylation. *PLoS pathogens* 5, e1000287. doi:10.1371/journal.ppat.1000287.
- Ivanov, K.A., Thiel, V., Dobbe, J.C., van der Meer, Y., Snijder, E.J., Ziebuhr, J., 2004. Multiple Enzymatic Activities Associated with Severe Acute Respiratory Syndrome Coronavirus Helicase. *Journal of virology* 78, 5619–5632. doi:10.1128/jvi.78.11.5619-5632.2004.
- Ivashkiv, L.B., Donlin, L.T., 2014. Regulation of type I interferon responses. *Nature reviews. Immunology* 14, 36–49. doi:10.1038/nri3581.
- Iversen, M.B., Paludan, S.R., 2010. Mechanisms of type III interferon expression. *Journal of interferon & cytokine research : the official journal of the International Society for Interferon and Cytokine Research* 30, 573–578. doi:10.1089/jir.2010.0063.
- Iwata, H., Goettsch, C., Sharma, A., Ricchiuto, P., Goh, W.W.B., Halu, A., Yamada, I., Yoshida, H., Hara, T., Wei, M., Inoue, N., Fukuda, D., Mojcher, A., Mattson, P.C., Barabási, A.-L., Boothby, M., Aikawa, E., Singh, S.A., Aikawa, M., 2016. PARP9 and PARP14 cross-regulate macrophage activation via STAT1 ADP-ribosylation. *Nature communications* 7, 12849. doi:10.1038/ncomms12849.
- Jacinto, E., Loewith, R., Schmidt, A., Lin, S., Rüegg, M.A., Hall, A., Hall, M.N., 2004. Mammalian TOR complex 2 controls the actin cytoskeleton and is rapamycin insensitive. *Nature cell biology* 6, 1122–1128. doi:10.1038/ncb1183.
- Jagannathan, P., Andrews, J.R., Bonilla, H., Hedlin, H., Jacobson, K.B., Balasubramanian, V., Purington, N., Kamble, S., Vries, C.R. de, Quintero, O., Feng, K., Ley, C., Winslow, D., Newberry, J., Edwards, K., Hislop, C., Choong, I., Maldonado, Y., Glenn, J., Bhatt, A., Blish, C., Wang, T., Khosla, C., Pinsky, B.A., Desai, M., Parsonnet, J., Singh, U., 2021. Peginterferon Lambda-1a for treatment of outpatients with uncomplicated COVID-19: a randomized placebo-controlled trial. *Nature communications* 12. doi:10.1038/s41467-021-22177-1.
- Jaks, E., Gavutis, M., Uzé, G., Martal, J., Piehler, J., 2007. Differential receptor subunit affinities of type I interferons govern differential signal activation. *Journal of molecular biology* 366, 525–539. doi:10.1016/j.jmb.2006.11.053.
- Jansen van Vuren, P., Shalekoff, S., Grobbelaar, A.A., Archer, B.N., Thomas, J., Tiemessen, C.T., Paweska, J.T., 2015. Serum levels of inflammatory cytokines in Rift Valley fever patients are indicative of severe disease. *Virology journal* 12, 159. doi:10.1186/s12985-015-0392-3.
- Jennings, S., Martínez-Sobrido, L., García-Sastre, A., Weber, F., Kochs, G., 2005. Thogoto virus ML protein suppresses IRF3 function. *Virology* 331, 63–72. doi:10.1016/j.virol.2004.10.015.
- Jiang, H.-w., Zhang, H.-n., Meng, Q.-f., Xie, J., Li, Y., Chen, H., Zheng, Y.-x., Wang, X.-n., Qi, H., Zhang, J., Wang, P.-H., Han, Z.-G., Tao, S.-c., 2020. SARS-CoV-2 Orf9b suppresses type I interferon responses by targeting TOM70. *Cellular & Molecular Immunology* 17, 998–1000. doi:10.1038/s41423-020-0514-8.
- Jiang, X., Kinch, L.N., Brautigam, C.A., Chen, X., Du, F., Grishin, N.V., Chen, Z.J., 2012. Ubiquitin-Induced Oligomerization of the RNA Sensors RIG-I and MDA5 Activates Antiviral Innate Immune Response. *Immunity* 36, 959–973. doi:10.1016/j.immuni.2012.03.022.

- Jorns, C., Holzinger, D., Thimme, R., Spangenberg, H.C., Weidmann, M., Rasenack, J., Blum, H.E., Haller, O., Kochs, G., 2006. Rapid and simple detection of IFN-neutralizing antibodies in chronic hepatitis C non-responsive to IFN-alpha. *Journal of medical virology* 78, 74–82. doi:10.1002/jmv.20506.
- Jungreis, I., Nelson, C.W., Ardern, Z., Finkel, Y., Krogan, N.J., Sato, K., Ziebuhr, J., Stern-Ginossar, N., Pavese, A., Firth, A.E., Gorbalenya, A.E., Kellis, M., 2021. Conflicting and ambiguous names of overlapping ORFs in the SARS-CoV-2 genome: A homology-based resolution. *Virology* 558, 145–151. doi:10.1016/j.virol.2021.02.013.
- Kainulainen, M., Habjan, M., Hubel, P., Busch, L., Lau, S., Colinge, J., Superti-Furga, G., Pichlmair, A., Weber, F., 2014. Virulence factor NSs of rift valley fever virus recruits the F-box protein FBXO3 to degrade subunit p62 of general transcription factor TFIID. *Journal of virology* 88, 3464–3473. doi:10.1128/JVI.02914-13.
- Kainulainen, M., Lau, S., Samuel, C.E., Hornung, V., Weber, F., 2016. NSs Virulence Factor of Rift Valley Fever Virus Engages the F-Box Proteins FBXW11 and β -TRCP1 To Degrade the Antiviral Protein Kinase PKR. *Journal of virology* 90, 6140–6147. doi:10.1128/JVI.00016-16.
- Kalveram, B., Lihoradova, O., Ikegami, T., 2011. NSs protein of rift valley fever virus promotes posttranslational downregulation of the TFIID subunit p62. *Journal of virology* 85, 6234–6243. doi:10.1128/JVI.02255-10.
- Kasuga, Y., Zhu, B., Jang, K.-J., Yoo, J.-S., 2021. Innate immune sensing of coronavirus and viral evasion strategies. *Experimental & molecular medicine* 53, 723–736. doi:10.1038/s12276-021-00602-1.
- Kato, H., Takeuchi, O., Mikamo-Satoh, E., Hirai, R., Kawai, T., Matsushita, K., Hiiragi, A., Dermody, T.S., Fujita, T., Akira, S., 2008. Length-dependent recognition of double-stranded ribonucleic acids by retinoic acid-inducible gene-I and melanoma differentiation-associated gene 5. *Journal of Experimental Medicine* 205, 1601–1610. doi:10.1084/jem.20080091.
- Katsura, H., Sontake, V., Tata, A., Kobayashi, Y., Edwards, C.E., Heaton, B.E., Konkimalla, A., Asakura, T., Mikami, Y., Fritch, E.J., Lee, P.J., Heaton, N.S., Boucher, R.C., Randell, S.H., Baric, R.S., Tata, P.R., 2020. Human Lung Stem Cell-Based Alveolospheres Provide Insights into SARS-CoV-2-Mediated Interferon Responses and Pneumocyte Dysfunction. *Cell Stem Cell* 27, 890–904.e8. doi:10.1016/j.stem.2020.10.005.
- Kawai, T., Takahashi, K., Sato, S., Coban, C., Kumar, H., Kato, H., Ishii, K.J., Takeuchi, O., Akira, S., 2005. IPS-1, an adaptor triggering RIG-I- and Mda5-mediated type I interferon induction. *Nature immunology* 6, 981–988. doi:10.1038/ni1243.
- Kemp, G.E., Causey, O.R., Setzer, H.W., Moore, D.L., 1974. Isolation of viruses from wild mammals in West Africa, 1966–1970. *Journal of wildlife diseases* 10, 279–293. doi:10.7589/0090-3558-10.3.279.
- Kibbe, W.A., 2007. OligoCalc: an online oligonucleotide properties calculator. *Nucleic acids research* 35, W43–6. doi:10.1093/nar/gkm234.
- Kim, M.-H., Salloum, S., Wang, J.Y., Lai Ping, W., Regan, J., Lefteri, K., Manickas-Hill, Z., Gao, C., Li, J.Z., Sadreyev, R.I., Yu, X.G., Chung, R.T., 2021. Type I, II, and III interferon signatures correspond to COVID-19 disease severity. *The Journal of infectious diseases*. doi:10.1093/infdis/jiab288.
- Kindler, E., Gil-Cruz, C., Spanier, J., Li, Y., Wilhelm, J., Rabouw, H.H., Züst, R., Hwang, M., V'kovski, P., Stalder, H., Marti, S., Habjan, M., Cervantes-Barragan, L., Elliot, R., Karl, N.,

- Gaughan, C., van Kuppeveld, F.J.M., Silverman, R.H., Keller, M., Ludewig, B., Bergmann, C.C., Ziebuhr, J., Weiss, S.R., Kalinke, U., Thiel, V., 2017. Early endonuclease-mediated evasion of RNA sensing ensures efficient coronavirus replication. *PLoS pathogens* 13, e1006195. doi:10.1371/journal.ppat.1006195.
- Kindler, E., Jónsdóttir, H.R., Muth, D., Hamming, O.J., Hartmann, R., Rodriguez, R., Geffers, R., Fouchier, R.A.M., Drosten, C., Müller, M.A., Dijkman, R., Thiel, V., 2013. Efficient replication of the novel human betacoronavirus EMC on primary human epithelium highlights its zoonotic potential. *mBio* 4, e00611-12. doi:10.1128/mBio.00611-12.
- Kindler, E., Thiel, V., Weber, F., 2016. Interaction of SARS and MERS Coronaviruses with the Antiviral Interferon Response. *Advances in Virus Research* 96, 219–243. doi:10.1016/bs.aivir.2016.08.006.
- Klemm, T., Ebert, G., Calleja, D.J., Allison, C.C., Richardson, L.W., Bernardini, J.P., Lu, B.G.C., Kuchel, N.W., Grohmann, C., Shibata, Y., Gan, Z.Y., Cooney, J.P., Doerflinger, M., Au, A.E., Blackmore, T.R., Heden van Noort, Gerbrand J, Geurink, P.P., Ovaa, H., Newman, J., Riboldi-Tunncliffe, A., Czabotar, P.E., Mitchell, J.P., Feltham, R., Lechtenberg, B.C., Lowes, K.N., Dewson, G., Pellegrini, M., Lessene, G., Komander, D., 2020. Mechanism and inhibition of the papain-like protease, PLpro, of SARS-CoV-2. *The EMBO journal* 39. doi:10.15252/embj.2020106275.
- Knoblach, B., Ishida, R., Hobman, T.C., Rachubinski, R.A., 2021. Peroxisomes exhibit compromised structure and matrix protein content in SARS-CoV-2-infected cells. *Molecular biology of the cell*, mbcE21020074. doi:10.1091/mbc.E21-02-0074.
- Konno, Y., Kimura, I., Uriu, K., Fukushi, M., Irie, T., Koyanagi, Y., Sauter, D., Gifford, R.J., Nakagawa, S., Sato, K., 2020. SARS-CoV-2 ORF3b Is a Potent Interferon Antagonist Whose Activity Is Increased by a Naturally Occurring Elongation Variant. *Cell reports* 32, 108185. doi:10.1016/j.celrep.2020.108185.
- Konstantoulas, C.J., Indik, S., 2014. Mouse mammary tumor virus-based vector transduces non-dividing cells, enters the nucleus via a TNPO3-independent pathway and integrates in a less biased fashion than other retroviruses. *Retrovirology* 11, 34. doi:10.1186/1742-4690-11-34.
- Kopecky-Bromberg, S.A., Martínez-Sobrido, L., Frieman, M., Baric, R.A., Palese, P., 2007. Severe acute respiratory syndrome coronavirus open reading frame (ORF) 3b, ORF 6, and nucleocapsid proteins function as interferon antagonists. *Journal of virology* 81, 548–557. doi:10.1128/JVI.01782-06.
- Kotenko, S.V., Gallagher, G., Baurin, V.V., Lewis-Antes, A., Shen, M., Shah, N.K., Langer, J.A., Sheikh, F., Dickensheets, H., Donnelly, R.P., 2003. IFN-lambdas mediate antiviral protection through a distinct class II cytokine receptor complex. *Nature immunology* 4, 69–77. doi:10.1038/ni875.
- Kowalinski, E., Lunardi, T., McCarthy, A.A., Loubser, J., Brunel, J., Grigorov, B., Gerlier, D., Cusack, S., 2011. Structural basis for the activation of innate immune pattern-recognition receptor RIG-I by viral RNA. *Cell* 147, 423–435. doi:10.1016/j.cell.2011.09.039.
- Krafcikova, P., Silhan, J., Nencka, R., Boura, E., 2020. Structural analysis of the SARS-CoV-2 methyltransferase complex involved in RNA cap creation bound to sinefungin. *Nature communications* 11. doi:10.1038/s41467-020-17495-9.
- Krähling, V., Stein, D.A., Spiegel, M., Weber, F., Mühlberger, E., 2009. Severe acute respiratory syndrome coronavirus triggers apoptosis via protein kinase R but is resistant to its antiviral activity. *Journal of virology* 83, 2298–2309. doi:10.1128/JVI.01245-08.

- Ksiazek, T.G., Erdman, D., Goldsmith, C.S., Zaki, S.R., Peret, T., Emery, S., Tong, S., Urbani, C., Comer, J.A., Lim, W., Rollin, P.E., Dowell, S.F., Ling, A.E., Humphrey, C.D., Shieh, W.J., Guarner, J., Paddock, C.D., Rota, P., Fields, B., DeRisi, J., Yang, J.Y., Cox, N., Hughes, J.M., LeDuc, J.W., Bellini, W.J., Anderson, L.J., 2003. A novel coronavirus associated with severe acute respiratory syndrome. *The New England journal of medicine* 348. doi:10.1056/NEJMoa030781.
- Kumar, S., Stecher, G., Li, M., Knyaz, C., Tamura, K., 2018. MEGA X: Molecular Evolutionary Genetics Analysis across Computing Platforms. *Molecular biology and evolution* 35, 1547–1549. doi:10.1093/molbev/msy096.
- Kuri, T., Habjan, M., Penski, N., Weber, F., 2010. Species-independent bioassay for sensitive quantification of antiviral type I interferons. *Virology journal* 7, 50. doi:10.1186/1743-422X-7-50.
- LaFleur, D.W., Nardelli, B., Tsareva, T., Mather, D., Feng, P., Semenuk, M., Taylor, K., Buerger, M., Chinchilla, D., Roshke, V., Chen, G., Ruben, S.M., Pitha, P.M., Coleman, T.A., Moore, P.A., 2001. Interferon-kappa, a novel type I interferon expressed in human keratinocytes. *The Journal of biological chemistry* 276, 39765–39771. doi:10.1074/jbc.M102502200.
- Lagunas-Rangel, F.A., Chávez-Valencia, V., 2020. High IL-6/IFN- γ ratio could be associated with severe disease in COVID-19 patients. *Journal of medical virology* 92, 1789–1790. doi:10.1002/jmv.25900.
- Lamers, M.M., van der Vaart, J., Knoops, K., Riesebosch, S., Breugem, T.I., Mykytyn, A.Z., Beumer, J., Schipper, D., Bezstarosti, K., Koopman, C.D., Groen, N., Ravelli, R.B.G., Duimel, H.Q., Demmers, J.A.A., Verjans, G.M.G.M., Koopmans, M.P.G., Muraro, M.J., Peters, P.J., Clevers, H., Haagmans, B.L., 2021. An organoid-derived bronchioalveolar model for SARS-CoV-2 infection of human alveolar type II-like cells. *The EMBO journal* 40. doi:10.15252/embj.2020105912.
- Lang, X., Tang, T., Jin, T., Ding, C., Zhou, R., Jiang, W., 2017. TRIM65-catalyzed ubiquitination is essential for MDA5-mediated antiviral innate immunity. *The Journal of Experimental Medicine* 214, 459–473. doi:10.1084/jem.20160592.
- Larkin, M.A., Blackshields, G., Brown, N.P., Chenna, R., McGettigan, P.A., McWilliam, H., Valentin, F., Wallace, I.M., Wilm, A., Lopez, R., Thompson, J.D., Gibson, T.J., Higgins, D.G., 2007. Clustal W and Clustal X version 2.0. *Bioinformatics (Oxford, England)* 23, 2947–2948. doi:10.1093/bioinformatics/btm404.
- Lau, S., Weber, F., 2020. Nuclear pore protein Nup98 is involved in replication of Rift Valley fever virus and nuclear import of virulence factor NSs. *The Journal of general virology* 101, 712–716. doi:10.1099/jgv.0.001347.
- Laubscher, F., Cordey, S., Hartley, M.-A., Vieille, G., Boillat-Blanco, N., Samaka, J., Mlaganile, T., d'Acremont, V., Kaiser, L., 2019. Nearly Complete Genome Sequence of a Novel Phlebovirus-Like Virus Detected in a Human Plasma Sample by High-Throughput Sequencing. *Microbiology Resource Announcements* 8. doi:10.1128/MRA.00764-19.
- Le May, N., Dubaele, S., Santis, L.P. de, Billecocq, A., Bouloy, M., Egly, J.-M., 2004. TFIIF Transcription Factor, a Target for the Rift Valley Hemorrhagic Fever Virus. *Cell* 116, 541–550. doi:10.1016/s0092-8674(04)00132-1.
- Le May, N., Mansuroglu, Z., Léger, P., Josse, T., Blot, G., Billecocq, A., Flick, R., Jacob, Y., Bonnefoy, E., Bouloy, M., 2008. A SAP30 complex inhibits IFN-beta expression in Rift Valley fever virus infected cells. *PLoS pathogens* 4, e13. doi:10.1371/journal.ppat.0040013.
- Léger, P., Lozach, P.-Y., 2015. Bunyaviruses: from transmission by arthropods to virus entry into the mammalian host first-target cells. *Future Virology* 10, 859–881. doi:10.2217/fvl.15.52.

- Léger, P., Nachman, E., Richter, K., Tamiatti, C., Koch, J., Burk, R., Kummer, S., Xin, Q., Stanifer, M., Bouloy, M., Boulant, S., Kräusslich, H.-G., Montagutelli, X., Flamand, M., Nussbaum-Krammer, C., Lozach, P.-Y., 2020. NSs amyloid formation is associated with the virulence of Rift Valley fever virus in mice. *Nature communications* 11, 3281. doi:10.1038/s41467-020-17101-y.
- Lei, C.-Q., Zhong, B., Zhang, Y., Zhang, J., Wang, S., Shu, H.-B., 2010. Glycogen synthase kinase 3 β regulates IRF3 transcription factor-mediated antiviral response via activation of the kinase TBK1. *Immunity* 33, 878–889. doi:10.1016/j.immuni.2010.11.021.
- Letko, M., Marzi, A., Munster, V., 2020. Functional assessment of cell entry and receptor usage for SARS-CoV-2 and other lineage B betacoronaviruses. *Nature microbiology* 5, 562–569. doi:10.1038/s41564-020-0688-y.
- Levitz, R., Gao, Y., Dozmorov, I., Song, R., Wakeland, E.K., Kahn, J.S., 2017. Distinct patterns of innate immune activation by clinical isolates of respiratory syncytial virus. *PLoS ONE* 12, e0184318. doi:10.1371/journal.pone.0184318.
- Levy, D.E., Darnell, J.E., 2002. Stats: transcriptional control and biological impact. *Nature reviews. Molecular cell biology* 3, 651–662.
- Levy, D.E., Marié, I.J., Durbin, J.E., 2011. Induction and function of type I and III interferon in response to viral infection. *Current opinion in virology* 1, 476–486. doi:10.1016/j.coviro.2011.11.001.
- Li, H., Handsaker, B., Wysoker, A., Fennell, T., Ruan, J., Homer, N., Marth, G., Abecasis, G., Durbin, R., 2009. The Sequence Alignment/Map format and SAMtools. *Bioinformatics* 25, 2078–2079. doi:10.1093/bioinformatics/btp352.
- Li, L., Zhao, H., Liu, P., Li, C., Quanquin, N., Ji, X., Sun, N., Du, P., Qin, C.-F., Lu, N., Cheng, G., 2018. PARP12 suppresses Zika virus infection through PARP-dependent degradation of NS1 and NS3 viral proteins. *Science signaling* 11. doi:10.1126/scisignal.aas9332.
- Li, M.M.H., Aguilar, E.G., Michailidis, E., Pabon, J., Park, P., Wu, X., Jong, Y.P. de, Schneider, W.M., Molina, H., Rice, C.M., MacDonald, M.R., 2019a. Characterization of Novel Splice Variants of Zinc Finger Antiviral Protein (ZAP). *Journal of virology* 93. doi:10.1128/JVI.00715-19.
- Li, S., Zhu, X., Guan, Z., Huang, W., Zhang, Y., Kortekaas, J., Lozach, P.-Y., Peng, K., 2019b. NSs Filament Formation Is Important but Not Sufficient for RVFV Virulence In Vivo. *Viruses* 11. doi:10.3390/v11090834.
- Li, Y., Renner, D.M., Comar, C.E., Whelan, J.N., Reyes, H.M., Cardenas-Diaz, F.L., Truitt, R., Tan, L.H., Dong, B., Alysandratos, K.D., Huang, J., Palmer, J.N., Adappa, N.D., Kohanski, M.A., Kotton, D.N., Silverman, R.H., Yang, W., Morrissey, E.E., Cohen, N.A., Weiss, S.R., 2021. SARS-CoV-2 induces double-stranded RNA-mediated innate immune responses in respiratory epithelial-derived cells and cardiomyocytes. *Proceedings of the National Academy of Sciences of the United States of America* 118. doi:10.1073/pnas.2022643118.
- Liao, Y., Smyth, G.K., Shi, W., 2013. The Subread aligner: fast, accurate and scalable read mapping by seed-and-vote. *Nucleic acids research* 41, e108-e108. doi:10.1093/nar/gkt214.
- Lihoradova, O.A., Indran, S.V., Kalveram, B., Lokugamage, N., Head, J.A., Gong, B., Tigabu, B., Juelich, T.L., Freiberg, A.N., Ikegami, T., 2013. Characterization of Rift Valley fever virus MP-12 strain encoding NSs of Punta Toro virus or sandfly fever Sicilian virus. *PLoS neglected tropical diseases* 7, e2181. doi:10.1371/journal.pntd.0002181.

- Lin, R., Heylbroeck, C., Pitha, P.M., Hiscott, J., 1998. Virus-dependent phosphorylation of the IRF-3 transcription factor regulates nuclear translocation, transactivation potential, and proteasome-mediated degradation. *Molecular and cellular biology* 18, 2986–2996. doi:10.1128/mcb.18.5.2986.
- Linthicum, K.J., Britch, S.C., Anyamba, A., 2016. Rift Valley Fever: An Emerging Mosquito-Borne Disease. *Annual review of entomology* 61, 395–415. doi:10.1146/annurev-ento-010715-023819.
- Liu, M.-M., Lei, X.-Y., Yu, H., Zhang, J.-z., Yu, X.-J., 2017a. Correlation of cytokine level with the severity of severe fever with thrombocytopenia syndrome. *Virology journal* 14. doi:10.1186/s12985-016-0677-1.
- Liu, S.-Y., Aliyari, R., Chikere, K., Li, G., Marsden, M.D., Smith, J.K., Pernet, O., Guo, H., Nusbaum, R., Zack, J.A., Freiberg, A.N., Su, L., Lee, B., Cheng, G., 2013. Interferon-inducible cholesterol-25-hydroxylase broadly inhibits viral entry by production of 25-hydroxycholesterol. *Immunity* 38, 92–105. doi:10.1016/j.immuni.2012.11.005.
- Liu, T., Zhang, L., Joo, D., Sun, S.-C., 2017b. NF- κ B signaling in inflammation. *Signal transduction and targeted therapy* 2. doi:10.1038/sigtrans.2017.23.
- Livak, K.J., Schmittgen, T.D., 2001. Analysis of relative gene expression data using real-time quantitative PCR and the 2(-Delta Delta C(T)) Method. *Methods (San Diego, Calif.)* 25, 402–408. doi:10.1006/meth.2001.1262.
- Lokugamage, K.G., Hage, A., Vries, M. de, Valero-Jimenez, A.M., Schindewolf, C., Dittmann, M., Rajsbaum, R., Menachery, V.D., 2020. Type I Interferon Susceptibility Distinguishes SARS-CoV-2 from SARS-CoV. *Journal of virology* 94. doi:10.1128/JVI.01410-20.
- Long, Q.-X., Tang, X.-J., Shi, Q.-L., Li, Q., Deng, H.-J., Yuan, J., Hu, J.-L., Xu, W., Zhang, Y., Lv, F.-J., Su, K., Zhang, F., Gong, J., Wu, B., Liu, X.-M., Li, J.-J., Qiu, J.-F., Chen, J., Huang, A.-L., 2020. Clinical and immunological assessment of asymptomatic SARS-CoV-2 infections. *Nature medicine* 26, 1200–1204. doi:10.1038/s41591-020-0965-6.
- Love, M.I., Huber, W., Anders, S., 2014. Moderated estimation of fold change and dispersion for RNA-seq data with DESeq2. *Genome Biology* 15. doi:10.1186/s13059-014-0550-8.
- Lowery, S.A., Sariol, A., Perlman, S., 2021. Innate immune and inflammatory responses to SARS-CoV-2: Implications for COVID-19. *Cell Host & Microbe*. doi:10.1016/j.chom.2021.05.004.
- Lu, X., Pan, J.'a., Tao, J., Guo, D., 2011. SARS-CoV nucleocapsid protein antagonizes IFN- β response by targeting initial step of IFN- β induction pathway, and its C-terminal region is critical for the antagonism. *Virus genes* 42, 37–45. doi:10.1007/s11262-010-0544-x.
- Ly, H.J., Ikegami, T., 2016. Rift Valley fever virus NSs protein functions and the similarity to other bunyavirus NSs proteins. *Virology journal* 13, 118. doi:10.1186/s12985-016-0573-8.
- Major, J., Crotta, S., Llorian, M., McCabe, T.M., Gad, H.H., Priestnall, S.L., Hartmann, R., Wack, A., 2020. Type I and III interferons disrupt lung epithelial repair during recovery from viral infection. *Science (New York, N.Y.)* 369, 712–717. doi:10.1126/science.abc2061.
- Malhani, A.A., Enani, M.A., Sharif-Askari, F.S., Alghareeb, M.R., Bin-Brikan, R.T., AlShahrani, S.A., Halwani, R., Tleyjeh, I.M., 2021. Combination of (interferon beta-1b, lopinavir/ritonavir and ribavirin) versus favipiravir in hospitalized patients with non-critical COVID-19: A cohort study. *PLoS ONE* 16. doi:10.1371/journal.pone.0252984.
- Mantlo, E., Bukreyeva, N., Maruyama, J., Paessler, S., Huang, C., 2020. Antiviral activities of type I interferons to SARS-CoV-2 infection. *Antiviral research* 179, 104811. doi:10.1016/j.antiviral.2020.104811.

- Mariani, M.K., Dasmeh, P., Fortin, A., Caron, E., Kalamujic, M., Harrison, A.N., Hotea, D.I., Kasumba, D.M., Cervantes-Ortiz, S.L., Mukawera, E., Serohijos, A.W.R., Grandvaux, N., 2019. The Combination of IFN β and TNF Induces an Antiviral and Immunoregulatory Program via Non-Canonical Pathways Involving STAT2 and IRF9. *Cells* 8. doi:10.3390/cells8080919.
- Marklewitz, M., Dutari, L.C., Paraskevopoulou, S., Page, R.A., Loaiza, J.R., Junglen, S., 2019. Diverse novel phleboviruses in sandflies from the Panama Canal area, Central Panama. *The Journal of general virology* 100, 938–949. doi:10.1099/jgv.0.001260.
- Marklewitz, M., Tchouassi, D.P., Hieke, C., Heyde, V., Torto, B., Sang, R., Junglen, S., 2020. Insights into the Evolutionary Origin of Mediterranean Sandfly Fever Viruses. *mSphere* 5. doi:10.1128/mSphere.00598-20.
- Martin, A.P.J., Jacquemyn, M., Lipecka, J., Chhuon, C., Aushev, V.N., Meunier, B., Singh, M.K., Carpi, N., Piel, M., Codogno, P., Hergovich, A., Parrini, M.C., Zalcman, G., Guerrera, I.C., Daelemans, D., Camonis, J.H., 2019. STK38 kinase acts as XPO1 gatekeeper regulating the nuclear export of autophagy proteins and other cargoes. *EMBO Reports* 20. doi:10.15252/embr.201948150.
- Matzinger, S.R., Carroll, T.D., Dutra, J.C., Ma, Z.-M., Miller, C.J., 2013. Myxovirus resistance gene A (MxA) expression suppresses influenza A virus replication in alpha interferon-treated primate cells. *Journal of virology* 87, 1150–1158. doi:10.1128/JVI.02271-12.
- Menachery, V.D., Yount, B.L., Josset, L., Gralinski, L.E., Scobey, T., Agnihothram, S., Katze, M.G., Baric, R.S., 2014. Attenuation and Restoration of Severe Acute Respiratory Syndrome Coronavirus Mutant Lacking 2'-O-Methyltransferase Activity. *Journal of virology* 88, 4251–4264. doi:10.1128/jvi.03571-13.
- Mendenhall, M., Wong, M.-H., Skirpstunas, R., Morrey, J.D., Gowen, B.B., 2009. Punta Toro virus (Bunyaviridae, Phlebovirus) infection in mice: strain differences in pathogenesis and host interferon response. *Virology* 395, 143–151. doi:10.1016/j.virol.2009.09.003.
- Mesev, E.V., LeDesma, R.A., Ploss, A., 2019. Decoding type I and III interferon signalling during viral infection. *Nature microbiology* 4, 914–924. doi:10.1038/s41564-019-0421-x.
- Min, Y.-Q., Ning, Y.-J., Wang, H., Deng, F., 2020. A RIG-I-like receptor directs antiviral responses to a bunyavirus and is antagonized by virus-induced blockade of TRIM25-mediated ubiquitination. *The Journal of biological chemistry* 295, 9691–9711. doi:10.1074/jbc.RA120.013973.
- Minakshi, R., Padhan, K., Rani, M., Khan, N., Ahmad, F., Jameel, S., 2009. The SARS Coronavirus 3a Protein Causes Endoplasmic Reticulum Stress and Induces Ligand-Independent Downregulation of the Type 1 Interferon Receptor. *PLoS ONE* 4, e8342. doi:10.1371/journal.pone.0008342.
- Miorin, L., Kehrer, T., Sanchez-Aparicio, M.T., Zhang, K., Cohen, P., Patel, R.S., Cupic, A., Makio, T., Mei, M., Moreno, E., Danziger, O., White, K.M., Rathnasinghe, R., Uccellini, M., Gao, S., Aydililo, T., Mena, I., Yin, X., Martin-Sancho, L., Krogan, N.J., Chanda, S.K., Schotsaert, M., Wozniak, R.W., Ren, Y., Rosenberg, B.R., Fontoura, B.M.A., García-Sastre, A., 2020. SARS-CoV-2 Orf6 hijacks Nup98 to block STAT nuclear import and antagonize interferon signaling. *Proceedings of the National Academy of Sciences of the United States of America* 117, 28344–28354. doi:10.1073/pnas.2016650117.
- Miyashita, M., Oshiumi, H., Matsumoto, M., Seya, T., 2011. DDX60, a DEXD/H box helicase, is a novel antiviral factor promoting RIG-I-like receptor-mediated signaling. *Molecular and cellular biology* 31, 3802–3819. doi:10.1128/MCB.01368-10.

- Mordstein, M., Neugebauer, E., Ditt, V., Jessen, B., Rieger, T., Falcone, V., Sorgeloos, F., Ehl, S., Mayer, D., Kochs, G., Schwemmle, M., Günther, S., Drosten, C., Michiels, T., Staeheli, P., 2010. Lambda interferon renders epithelial cells of the respiratory and gastrointestinal tracts resistant to viral infections. *Journal of virology* 84, 5670–5677. doi:10.1128/JVI.00272-10.
- Mu, J., Fang, Y., Yang, Q., Shu, T., Wang, A., Huang, M., Jin, L., Deng, F., Qiu, Y., Zhou, X., 2020. SARS-CoV-2 N protein antagonizes type I interferon signaling by suppressing phosphorylation and nuclear translocation of STAT1 and STAT2. *Cell Discovery* 6. doi:10.1038/s41421-020-00208-3.
- Mudhasani, R., Tran, J.P., Retterer, C., Kota, K.P., Whitehouse, C.A., Bavari, S., 2016. Protein Kinase R Degradation Is Essential for Rift Valley Fever Virus Infection and Is Regulated by SKP1-CUL1-F-box (SCF)FBXW11-NSs E3 Ligase. *PLoS pathogens* 12, e1005437. doi:10.1371/journal.ppat.1005437.
- Muir, A.J., Arora, S., Everson, G., Flisiak, R., George, J., Ghalib, R., Gordon, S.C., Gray, T., Greenbloom, S., Hassanein, T., Hillson, J., Horga, M.A., Jacobson, I.M., Jeffers, L., Kowdley, K.V., Lawitz, E., Lueth, S., Rodriguez-Torres, M., Rustgi, V., Shemanski, L., Shiffman, M.L., Srinivasan, S., Vargas, H.E., Vierling, J.M., Xu, D., Lopez-Talavera, J.C., Zeuzem, S., 2014. A randomized phase 2b study of peginterferon lambda-1a for the treatment of chronic HCV infection. *Journal of hepatology* 61, 1238–1246. doi:10.1016/j.jhep.2014.07.022.
- Mukherjee, P., Woods, T.A., Moore, R.A., Peterson, K.E., 2013. Activation of the Innate Signaling Molecule MAVS by Bunyavirus Infection Upregulates the Adaptor Protein SARM1, Leading to Neuronal Death. *Immunity* 38, 705–716. doi:10.1016/j.immuni.2013.02.013.
- Muller, R., Saluzzo, J.F., Lopez, N., Dreier, T., Turell, M., Smith, J., Bouloy, M., 1995. Characterization of clone 13, a naturally attenuated avirulent isolate of Rift Valley fever virus, which is altered in the small segment. *The American journal of tropical medicine and hygiene* 53, 405–411. doi:10.4269/ajtmh.1995.53.405.
- Nchioua, R., Kmiec, D., Müller, J.A., Conzelmann, C., Groß, R., Swanson, C.M., Neil, S.J.D., Stenger, S., Sauter, D., Münch, J., Sparrer, K.M.J., Kirchhoff, F., 2020. SARS-CoV-2 Is Restricted by Zinc Finger Antiviral Protein despite Preadaptation to the Low-CpG Environment in Humans. *mBio* 11. doi:10.1128/mBio.01930-20.
- Negishi, H., Taniguchi, T., Yanai, H., 2018. The Interferon (IFN) Class of Cytokines and the IFN Regulatory Factor (IRF) Transcription Factor Family. *Cold Spring Harbor perspectives in biology* 10. doi:10.1101/cshperspect.a028423.
- Nelson, C.W., Ardern, Z., Goldberg, T.L., Meng, C., Kuo, C.-H., Ludwig, C., Kolokotronis, S.-O., Wei, X., 2020. Dynamically evolving novel overlapping gene as a factor in the SARS-CoV-2 pandemic. *eLife* 9. doi:10.7554/eLife.59633.
- Neuwirth, E., 2011. Package ‘RColorBrewer’. CRAN 2011-06-17 08: 34: 00. Apache License 2.0.
- Nilsson-Payant, B.E., Uhl, S., Grimont, A., Doane, A.S., Cohen, P., Patel, R.S., Higgins, C.A., Acklin, J.A., Bram, Y., Chandar, V., Blanco-Melo, D., Panis, M., Lim, J.K., Elemento, O., Schwartz, R.E., Rosenberg, B.R., Chandwani, R., tenOever, B.R., 2021. The NF- κ B transcriptional footprint is essential for SARS-CoV-2 replication. *Journal of virology*, JVI0125721. doi:10.1128/JVI.01257-21.
- Ning, Y.-J., Feng, K., Min, Y.-Q., Cao, W.-C., Wang, M., Deng, F., Hu, Z., Wang, H., 2015. Disruption of type I interferon signaling by the nonstructural protein of severe fever with thrombocytopenia syndrome virus via the hijacking of STAT2 and STAT1 into inclusion bodies. *Journal of virology* 89, 4227–4236. doi:10.1128/JVI.00154-15.

- Ning, Y.-J., Feng, K., Min, Y.-Q., Deng, F., Hu, Z., Wang, H., 2017. Heartland virus NSs protein disrupts host defenses by blocking the TBK1 kinase-IRF3 transcription factor interaction and signaling required for interferon induction. *The Journal of biological chemistry* 292, 16722–16733. doi:10.1074/jbc.M117.805127.
- Nishiyama, S., Slack, O.A.L., Lokugamage, N., Hill, T.E., Juelich, T.L., Zhang, L., Smith, J.K., Perez, D., Gong, B., Freiberg, A.N., Ikegami, T., 2016. Attenuation of pathogenic Rift Valley fever virus strain through the chimeric S-segment encoding sandfly fever phlebovirus NSs or a dominant-negative PKR. *Virulence* 7, 871–881. doi:10.1080/21505594.2016.1195528.
- O'Brien, T.R., Thomas, D.L., Jackson, S.S., Prokunina-Olsson, L., Donnelly, R.P., Hartmann, R., 2020. Weak Induction of Interferon Expression by Severe Acute Respiratory Syndrome Coronavirus 2 Supports Clinical Trials of Interferon- λ to Treat Early Coronavirus Disease 2019. *Clinical infectious diseases : an official publication of the Infectious Diseases Society of America* 71, 1410–1412. doi:10.1093/cid/ciaa453.
- Odendall, C., Kagan, J.C., 2015. The unique regulation and functions of type III interferons in antiviral immunity. *Current opinion in virology* 12, 47–52. doi:10.1016/j.coviro.2015.02.003.
- Okamoto, T., Suzuki, T., Kusakabe, S., Tokunaga, M., Hirano, J., Miyata, Y., Matsuura, Y., 2017. Regulation of Apoptosis during Flavivirus Infection. *Viruses* 9. doi:10.3390/v9090243.
- Olbei, M., Hautefort, I., Modos, D., Treveil, A., Poletti, M., Gul, L., Shannon-Lowe, C.D., Korcsmaros, T., 2021. SARS-CoV-2 Causes a Different Cytokine Response Compared to Other Cytokine Storm-Causing Respiratory Viruses in Severely Ill Patients. *Frontiers in Immunology* 12. doi:10.3389/fimmu.2021.629193.
- Oshiumi, H., Miyashita, M., Okamoto, M., Morioka, Y., Okabe, M., Matsumoto, M., Seya, T., 2015. DDX60 Is Involved in RIG-I-Dependent and Independent Antiviral Responses, and Its Function Is Attenuated by Virus-Induced EGFR Activation. *Cell reports* 11, 1193–1207. doi:10.1016/j.celrep.2015.04.047.
- Palacios, G., Tesh, R.B., Savji, N., Travassos da Rosa, A.P.A., Guzman, H., Bussetti, A.V., Desai, A., Ladner, J., Sanchez-Seco, M., Lipkin, W.I., 2014. Characterization of the Sandfly fever Naples species complex and description of a new Karimabad species complex (genus Phlebovirus, family Bunyaviridae). *The Journal of general virology* 95, 292–300. doi:10.1099/vir.0.056614-0.
- Palacios, G., Wiley, M.R., Travassos da Rosa, A.P.A., Guzman, H., Quiroz, E., Savji, N., Carrera, J.-P., Bussetti, A.V., Ladner, J.T., Ian Lipkin, W., Tesh, R.B., 2015. Characterization of the Punta Toro species complex (genus Phlebovirus, family Bunyaviridae). *The Journal of general virology* 96, 2079–2085. doi:10.1099/vir.0.000170.
- Papa, A., Velo, E., Bino, S., 2011. A novel phlebovirus in Albanian sandflies. *Clinical microbiology and infection : the official publication of the European Society of Clinical Microbiology and Infectious Diseases* 17, 585–587. doi:10.1111/j.1469-0691.2010.03371.x.
- Parker, M.D., Lindsey, B.B., Leary, S., Gaudieri, S., Chopra, A., Wyles, M., Angyal, A., Green, L.R., Parsons, P., Tucker, R.M., Brown, R., Groves, D., Johnson, K., Carrilero, L., Heffer, J., Partridge, D.G., Evans, C., Raza, M., Keeley, A.J., Smith, N., Filipe, A.D.S., Shepherd, J.G., Davis, C., Bennett, S., Sreenu, V.B., Kohl, A., Aranday-Cortes, E., Tong, L., Nichols, J., Thomson, E.C., Wang, D., Mallal, S., Silva, T.I. de, 2021. Subgenomic RNA identification in SARS-CoV-2 genomic sequencing data. *Genome Research* 31, 645–658. doi:10.1101/gr.268110.120.
- Paulson, M., Press, C., Smith, E., Tanese, N., Levy, D.E., 2002. IFN-Stimulated transcription through a TBP-free acetyltransferase complex escapes viral shutoff. *Nature cell biology* 4, 140–147. doi:10.1038/ncb747.

- Peng, J., Yuan, Q., Lin, B., Panneerselvam, P., Wang, X., Luan, X.L., Lim, S.K., Leung, B.P., Ho, B., Ding, J.L., 2010. SARM inhibits both TRIF- and MyD88-mediated AP-1 activation. *European journal of immunology* 40, 1738–1747. doi:10.1002/eji.200940034.
- Perlman, S., Netland, J., 2009. Coronaviruses post-SARS: update on replication and pathogenesis. *Nature reviews. Microbiology* 7, 439–450. doi:10.1038/nrmicro2147.
- Perreira, J.M., Chin, C.R., Feeley, E.M., Brass, A.L., 2013. IFITMs Restrict the Replication of Multiple Pathogenic Viruses. *Journal of molecular biology* 425, 4937–4955. doi:10.1016/j.jmb.2013.09.024.
- Perrone, L.A., Narayanan, K., Worthy, M., Peters, C.J., 2007. The S segment of Punta Toro virus (Bunyaviridae, Phlebovirus) is a major determinant of lethality in the Syrian hamster and codes for a type I interferon antagonist. *Journal of virology* 81, 884–892. doi:10.1128/JVI.01074-06.
- Pervolaraki, K., Rastgou Talemi, S., Albrecht, D., Bormann, F., Bamford, C., Mendoza, J.L., Garcia, K.C., McLauchlan, J., Höfer, T., Stanifer, M.L., Boulant, S., 2018. Differential induction of interferon stimulated genes between type I and type III interferons is independent of interferon receptor abundance. *PLoS pathogens* 14, e1007420. doi:10.1371/journal.ppat.1007420.
- Perwitasari, O., Cho, H., Diamond, M.S., Gale, M., 2011. Inhibitor of κ B kinase epsilon (IKK(epsilon)), STAT1, and IFIT2 proteins define novel innate immune effector pathway against West Nile virus infection. *The Journal of biological chemistry* 286, 44412–44423. doi:10.1074/jbc.M111.285205.
- Pestka, S., Krause, C.D., Sarkar, D., Walter, M.R., Shi, Y., Fisher, P.B., 2004a. Interleukin-10 and related cytokines and receptors. *Annual review of immunology* 22, 929–979. doi:10.1146/annurev.immunol.22.012703.104622.
- Pestka, S., Krause, C.D., Walter, M.R., 2004b. Interferons, interferon-like cytokines, and their receptors. *Immunological reviews* 202, 8–32. doi:10.1111/j.0105-2896.2004.00204.x.
- Pichlmair, A., Lassnig, C., Eberle, C.A., Góna, M.W., Baumann, C.L., Burkard, T.R., Bürckstümmer, T., Stefanovic, A., Krieger, S., Bennett, K.L., Rüllicke, T., Weber, F., Colinge, J., Müller, M., Superti-Furga, G., 2011. IFIT1 is an antiviral protein that recognizes 5'-triphosphate RNA. *Nature immunology* 12. doi:10.1038/ni.2048.
- Pichlmair, A., Schulz, O., Tan, C.P., Näslund, T.I., Liljeström, P., Weber, F., Reis e Sousa, C., 2006. RIG-I-mediated antiviral responses to single-stranded RNA bearing 5'-phosphates. *Science (New York, N.Y.)* 314, 997–1001. doi:10.1126/science.1132998.
- Pichlmair, A., Schulz, O., Tan, C.-P., Rehwinkel, J., Kato, H., Takeuchi, O., Akira, S., Way, M., Schiavo, G., Reis e Sousa, C., 2009. Activation of MDA5 requires higher-order RNA structures generated during virus infection. *Journal of virology* 83, 10761–10769. doi:10.1128/JVI.00770-09.
- Pindel, A., Sadler, A., 2011. The role of protein kinase R in the interferon response. *Journal of interferon & cytokine research : the official journal of the International Society for Interferon and Cytokine Research* 31, 59–70. doi:10.1089/jir.2010.0099.
- Prokunina-Olsson, L., Alphonse, N., Dickenson, R.E., Durbin, J.E., Glenn, J.S., Hartmann, R., Kotenko, S.V., Lazear, H.M., O'Brien, T.R., Odendall, C., Onabajo, O.O., Piontkivska, H., Santer, D.M., Reich, N.C., Wack, A., Zanoni, I., 2020. COVID-19 and emerging viral infections: The case for interferon lambda. *The Journal of Experimental Medicine* 217. doi:10.1084/jem.20200653.
- Prokunina-Olsson, L., Muchmore, B., Tang, W., Pfeiffer, R.M., Park, H., Dickensheets, H., Hergott, D., Porter-Gill, P., Mumy, A., Kohaar, I., Chen, S., Brand, N., Tarway, M., Liu, L., Sheikh, F., Astemborski, J., Bonkovsky, H.L., Edlin, B.R., Howell, C.D., Morgan, T.R., Thomas, D.L.,

- Rehermann, B., Donnelly, R.P., O'Brien, T.R., 2013. A variant upstream of IFNL3 (IL28B) creating a novel interferon gene IFNL4 is associated with impaired clearance of hepatitis C virus. *Nature genetics* 45, 164–171. doi:10.1038/ng.2521.
- Qu, B., Qi, X., Wu, X., Liang, M., Li, C., Cardona, C.J., Xu, W., Tang, F., Li, Z., Wu, B., Powell, K., Wegner, M., Li, D., Xing, Z., 2012. Suppression of the interferon and NF- κ B responses by severe fever with thrombocytopenia syndrome virus. *Journal of virology* 86, 8388–8401. doi:10.1128/JVI.00612-12.
- Quicke, K.M., Kim, K.Y., Horvath, C.M., Suthar, M.S., 2019. RNA Helicase LGP2 Negatively Regulates RIG-I Signaling by Preventing TRIM25-Mediated Caspase Activation and Recruitment Domain Ubiquitination. *Journal of interferon & cytokine research : the official journal of the International Society for Interferon and Cytokine Research* 39, 669–683. doi:10.1089/jir.2019.0059.
- Rabouw, H.H., Langereis, M.A., Knaap, R.C.M., Dalebout, T.J., Canton, J., Sola, I., Enjuanes, L., Bredenbeek, P.J., Kikkert, M., Groot, R.J. de, van Kuppeveld, F.J.M., 2016. Middle East Respiratory Coronavirus Accessory Protein 4a Inhibits PKR-Mediated Antiviral Stress Responses. *PLoS pathogens* 12, e1005982. doi:10.1371/journal.ppat.1005982.
- Rahmani, H., Davoudi-Monfared, E., Nourian, A., Khalili, H., Hajizadeh, N., Jalalabadi, N.Z., Fazeli, M.R., Ghazaeian, M., Yekaninejad, M.S., 2020. Interferon β -1b in treatment of severe COVID-19: A randomized clinical trial. *International immunopharmacology* 88, 106903. doi:10.1016/j.intimp.2020.106903.
- Ravindra, N.G., Alfajaro, M.M., Gasque, V., Huston, N.C., Wan, H., Szigeti-Buck, K., Yasumoto, Y., Greaney, A.M., Habet, V., Chow, R.D., Chen, J.S., Wei, J., Filler, R.B., Wang, B., Wang, G., Niklason, L.E., Montgomery, R.R., Eisenbarth, S.C., Chen, S., Williams, A., Iwasaki, A., Horvath, T.L., Foxman, E.F., Pierce, R.W., Pyle, A.M., van Dijk, D., Wilen, C.B., 2021. Single-cell longitudinal analysis of SARS-CoV-2 infection in human airway epithelium identifies target cells, alterations in gene expression, and cell state changes. *PLoS Biology* 19, e3001143. doi:10.1371/journal.pbio.3001143.
- Rehwinkel, J., Gack, M.U., 2020. RIG-I-like receptors: their regulation and roles in RNA sensing. *Nature reviews. Immunology* 20, 537–551. doi:10.1038/s41577-020-0288-3.
- Remoli, M.E., Fortuna, C., Marchi, A., Bucci, P., Argentini, C., Bongiorno, G., Maroli, M., Gradoni, L., Gramiccia, M., Ciufolini, M.G., 2014. Viral isolates of a novel putative phlebovirus in the Marche Region of Italy. *The American journal of tropical medicine and hygiene* 90, 760–763. doi:10.4269/ajtmh.13-0457.
- Ren, X., Glende, J., Al-Falah, M., Vries, V. de, Schwegmann-Wessels, C., Qu, X., Tan, L., Tschernig, T., Deng, H., Naim, H.Y., Herrler, G., 2006. Analysis of ACE2 in polarized epithelial cells: surface expression and function as receptor for severe acute respiratory syndrome-associated coronavirus. *The Journal of general virology* 87, 1691–1695. doi:10.1099/vir.0.81749-0.
- Rezelj, V.V., Li, P., Chaudhary, V., Elliott, R.M., Jin, D.-Y., Brennan, B., 2017. Differential Antagonism of Human Innate Immune Responses by Tick-Borne Phlebovirus Nonstructural Proteins. *mSphere* 2. doi:10.1128/mSphere.00234-17.
- Rezelj, V.V., Överby, A.K., Elliott, R.M., 2015. Generation of mutant Uukuniemi viruses lacking the nonstructural protein NSs by reverse genetics indicates that NSs is a weak interferon antagonist. *Journal of virology* 89, 4849–4856. doi:10.1128/JVI.03511-14.

- Riedel, C., Lamp, B., Hagen, B., Indik, S., Rümenapf, T., 2017. The core protein of a pestivirus protects the incoming virus against IFN-induced effectors. *Scientific reports* 7, 44459. doi:10.1038/srep44459.
- Rodrigo, W.W.S.I., Ortiz-Riaño, E., Pythoud, C., Kunz, S., La Torre, J.C. de, Martínez-Sobrido, L., 2012. Arenavirus nucleoproteins prevent activation of nuclear factor kappa B. *Journal of virology* 86, 8185–8197. doi:10.1128/JVI.07240-11.
- Saccon, E., Chen, X., Mikaeloff, F., Rodriguez, J.E., Szekely, L., Vinhas, B.S., Krishnan, S., Byrreddy, S.N., Frisan, T., Végvári, Á., Mirazimi, A., Neogi, U., Gupta, S., 2021. Cell-type-resolved quantitative proteomics map of interferon response against SARS-CoV-2. *iScience* 24, 102420. doi:10.1016/j.isci.2021.102420.
- Sadler, A.J., Williams, B.R., 2008. Interferon-inducible antiviral effectors. *Nature reviews. Immunology* 8. doi:10.1038/nri2314.
- Sanada, T., Takaesu, G., Mashima, R., Yoshida, R., Kobayashi, T., Yoshimura, A., 2008. FLN29 Deficiency Reveals Its Negative Regulatory Role in the Toll-like Receptor (TLR) and Retinoic Acid-inducible Gene I (RIG-I)-like Helicase Signaling Pathway*. *The Journal of biological chemistry* 283, 33858–33864. doi:10.1074/jbc.M806923200.
- Sánchez, E.G., Quintas, A., Nogal, M., Castelló, A., Revilla, Y., 2013. African swine fever virus controls the host transcription and cellular machinery of protein synthesis. *Virus research* 173, 58–75. doi:10.1016/j.virusres.2012.10.025.
- Scagnolari, C., Pierangeli, A., Frasca, F., Bitossi, C., Viscido, A., Oliveto, G., Scordio, M., Mazzuti, L., Di Carlo, D., Gentile, M., Solimini, A., Ceccarelli, G., Pugliese, F., Mastroianni, C.M., d'Etto, G., Turriziani, O., Antonelli, G., 2021. Differential induction of type I and III interferon genes in the upper respiratory tract of patients with coronavirus disease 2019 (COVID-19). *Virus research* 295, 198283. doi:10.1016/j.virusres.2020.198283.
- Schlee, M., Roth, A., Hornung, V., Hagmann, C.A., Wimmenauer, V., Barchet, W., Coch, C., Janke, M., Mihailovic, A., Wardle, G., Juraneck, S., Kato, H., Kawai, T., Poeck, H., Fitzgerald, K.A., Takeuchi, O., Akira, S., Tuschl, T., Latz, E., Ludwig, J., Hartmann, G., 2009. Recognition of 5'-triphosphate by RIG-I helicase requires short blunt double-stranded RNA as contained in panhandle of negative strand virus. *Immunity* 31, 25–34. doi:10.1016/j.immuni.2009.05.008.
- Schmidt, A., Schwerd, T., Hamm, W., Hellmuth, J.C., Cui, S., Wenzel, M., Hoffmann, F.S., Michallet, M.-C., Besch, R., Hopfner, K.-P., Endres, S., Rothenfusser, S., 2009. 5'-triphosphate RNA requires base-paired structures to activate antiviral signaling via RIG-I. *Proceedings of the National Academy of Sciences of the United States of America* 106, 12067–12072. doi:10.1073/pnas.0900971106.
- Schneider, W.M., Chevillotte, M.D., Rice, C.M., 2014. Interferon-stimulated genes: a complex web of host defenses. *Annual review of immunology* 32, 513–545. doi:10.1146/annurev-immunol-032713-120231.
- Schoen, A., Lau, S., Verbruggen, P., Weber, F., 2020. Elongin C Contributes to RNA Polymerase II Degradation by the Interferon Antagonist NSs of La Crosse Orthobunyavirus. *Journal of virology* 94. doi:10.1128/JVI.02134-19.
- Schoggins, J.W., Wilson, S.J., Panis, M., Murphy, M.Y., Jones, C.T., Bieniasz, P., Rice, C.M., 2011. A diverse array of gene products are effectors of the type I interferon antiviral response. *Nature* 472, 481–485. doi:10.1038/nature09907.

- Schroeder, S., Pott, F., Niemeyer, D., Veith, T., Richter, A., Muth, D., Goffinet, C., Müller, M.A., Drosten, C., 2021. Interferon antagonism by SARS-CoV-2: a functional study using reverse genetics. *The Lancet. Microbe* 2, e210-8. doi:10.1016/S2666-5247(21)00027-6.
- Schwerk, J., Soveg, F.W., Ryan, A.P., Thomas, K.R., Hatfield, L.D., Ozarkar, S., Forero, A., Kell, A.M., Roby, J.A., So, L., Hyde, J.L., Gale, M., Daugherty, M.D., Savan, R., 2019. RNA-binding protein isoforms ZAP-S and ZAP-L have distinct antiviral and immune resolution functions. *Nature immunology* 20, 1610–1620. doi:10.1038/s41590-019-0527-6.
- Seo, J., Lee, E.-W., Sung, H., Seong, D., Dondelinger, Y., Shin, J., Jeong, M., Lee, H.-K., Kim, J.-H., Han, S.Y., Lee, C., Seong, J.K., Vandenabeele, P., Song, J., 2016. CHIP controls necroptosis through ubiquitylation- and lysosome-dependent degradation of RIPK3. *Nature cell biology* 18, 291–302. doi:10.1038/ncb3314.
- Sharma, S., tenOever, B.R., Grandvaux, N., Zhou, G.P., Lin, R., Hiscott, J., 2003. Triggering the interferon antiviral response through an IKK-related pathway. *Science (New York, N.Y.)* 300. doi:10.1126/science.1081315.
- Shaw, A.E., Hughes, J., Gu, Q., Behdenna, A., Singer, J.B., Dennis, T., Orton, R.J., Varela, M., Gifford, R.J., Wilson, S.J., Palmarini, M., 2017. Fundamental properties of the mammalian innate immune system revealed by multispecies comparison of type I interferon responses. *PLoS Biology* 15. doi:10.1371/journal.pbio.2004086.
- Sheppard, P., Kindsvogel, W., Xu, W., Henderson, K., Schlutsmeyer, S., Whitmore, T.E., Kuestner, R., Garrigues, U., Birks, C., Roraback, J., Ostrander, C., Dong, D., Shin, J., Presnell, S., Fox, B., Haldeman, B., Cooper, E., Taft, D., Gilbert, T., Grant, F.J., Tackett, M., Krivan, W., McKnight, G., Clegg, C., Foster, D., Klucher, K.M., 2003. IL-28, IL-29 and their class II cytokine receptor IL-28R. *Nature immunology* 4, 63–68. doi:10.1038/ni873.
- Shi, C.-S., Qi, H.-Y., Boularan, C., Huang, N.-N., Abu-Asab, M., Shelhamer, J.H., Kehrl, J.H., 2014. SARS-Coronavirus Open Reading Frame-9b Suppresses Innate Immunity by Targeting Mitochondria and the MAVS/TRAF3/TRAF6 Signalosome. *The Journal of Immunology* 193, 3080–3089. doi:10.4049/jimmunol.1303196.
- Shi, H.-X., Yang, K., Liu, X., Liu, X.-Y., Wei, B., Shan, Y.-F., Zhu, L.-H., Wang, C., 2010. Positive regulation of interferon regulatory factor 3 activation by Herc5 via ISG15 modification. *Molecular and cellular biology* 30, 2424–2436. doi:10.1128/MCB.01466-09.
- Shin, D., Mukherjee, R., Grewe, D., Bojkova, D., Baek, K., Bhattacharya, A., Schulz, L., Widera, M., Mehdipour, A.R., Tascher, G., Geurink, P.P., Wilhelm, A., van Heden Noort, G.J., Ovaa, H., Müller, S., Knobloch, K.-P., Rajalingam, K., Schulman, B.A., Cinatl, J., Hummer, G., Ciesek, S., Dikic, I., 2020. Papain-like protease regulates SARS-CoV-2 viral spread and innate immunity. *Nature* 587, 657–662. doi:10.1038/s41586-020-2601-5.
- Shu, T., Huang, M., Di Wu, Ren, Y., Zhang, X., Han, Y., Mu, J., Wang, R., Qiu, Y., Zhang, D.-Y., Zhou, X., 2020. SARS-Coronavirus-2 Nsp13 Possesses NTPase and RNA Helicase Activities That Can Be Inhibited by Bismuth Salts. *Virologica Sinica* 35, 321–329. doi:10.1007/s12250-020-00242-1.
- Siu, K.-L., Chan, C.-P., Kok, K.-H., Chiu-Yat Woo, P., Jin, D.-Y., 2014. Suppression of innate antiviral response by severe acute respiratory syndrome coronavirus M protein is mediated through the first transmembrane domain. *Cellular & Molecular Immunology* 11, 141–149. doi:10.1038/cmi.2013.61.
- Sjaastad, L.E., Fay, E.J., Fiege, J.K., Macchietto, M.G., Stone, I.A., Markman, M.W., Shen, S., Langlois, R.A., 2018. Distinct antiviral signatures revealed by the magnitude and round of

- influenza virus replication in vivo. *Proceedings of the National Academy of Sciences of the United States of America* 115, 9610–9615. doi:10.1073/pnas.1807516115.
- Slowikowski, K., Schep, A., Hughes, S., Dang, T.K., Lukauskas, S., Irisson, J.-O., Kamvar, Z.N., Ryan, T., Christophe, D., Hiroaki, Y., Gramme, P., Abdol, A.M., Barrett, M., Cannoodt, R., Krassowski, M., Chirico, M., Aphalo, P., 2021. ggrepel: Automatically Position Non-Overlapping Text Labels with „ggplot2“ (0.9.1).
- Sola, I., Almazán, F., Zúñiga, S., Enjuanes, L., 2015. Continuous and Discontinuous RNA Synthesis in Coronaviruses. *Annual review of virology* 2, 265–288. doi:10.1146/annurev-virology-100114-055218.
- Sommereyans, C., Paul, S., Staeheli, P., Michiels, T., 2008. IFN-lambda (IFN-lambda) is expressed in a tissue-dependent fashion and primarily acts on epithelial cells in vivo. *PLoS pathogens* 4, e1000017. doi:10.1371/journal.ppat.1000017.
- Spiegel, M., Pichlmair, A., Martínez-Sobrido, L., Cros, J., García-Sastre, A., Haller, O., Weber, F., 2005. Inhibition of Beta Interferon Induction by Severe Acute Respiratory Syndrome Coronavirus Suggests a Two-Step Model for Activation of Interferon Regulatory Factor 3. *Journal of virology* 79, 2079–2086. doi:10.1128/JVI.79.4.2079-2086.2005.
- Spiegel, M., Pichlmair, A., Mühlberger, E., Haller, O., Weber, F., 2004. The antiviral effect of interferon-beta against SARS-coronavirus is not mediated by MxA protein. *Journal of clinical virology : the official publication of the Pan American Society for Clinical Virology* 30, 211–213. doi:10.1016/j.jcv.2003.11.013.
- Spiegel, M., Plegge, T., Pöhlmann, S., 2016. The Role of Phlebovirus Glycoproteins in Viral Entry, Assembly and Release. *Viruses* 8. doi:10.3390/v8070202.
- Spiegel, M., Weber, F., 2006. Inhibition of cytokine gene expression and induction of chemokine genes in non-lymphatic cells infected with SARS coronavirus. *Virology journal* 3, 17. doi:10.1186/1743-422X-3-17.
- Sposito, B., Broggi, A., Pandolfi, L., Crotta, S., Clementi, N., Ferrarese, R., Sisti, S., Criscuolo, E., Spreafico, R., Long, J.M., Ambrosi, A., Liu, E., Frangipane, V., Saracino, L., Bozzini, S., Marongiu, L., Facchini, F.A., Bottazzi, A., Fossali, T., Colombo, R., Clementi, M., Tagliabue, E., Chou, J., Pontiroli, A.E., Meloni, F., Wack, A., Mancini, N., Zanoni, I., 2021. The interferon landscape along the respiratory tract impacts the severity of COVID-19. *Cell* 184, 4953-4968.e16. doi:10.1016/j.cell.2021.08.016.
- Stanifer, M.L., Pervolaraki, K., Boulant, S., 2019. Differential Regulation of Type I and Type III Interferon Signaling. *International journal of molecular sciences* 20. doi:10.3390/ijms20061445.
- Stebbing, J., Phelan, A., Griffin, I., Tucker, C., Oechsle, O., Smith, D., Richardson, P., 2020. COVID-19: combining antiviral and anti-inflammatory treatments. *The Lancet Infectious Diseases* 20, 400–402. doi:10.1016/S1473-3099(20)30132-8.
- Stephens, M., 2016. False discovery rates: a new deal. *Biostatistics*, kxw041. doi:10.1093/biostatistics/kxw041.
- Stoltz, M., Klingström, J., 2010. Alpha/beta interferon (IFN-alpha/beta)-independent induction of IFN-lambda1 (interleukin-29) in response to Hantaan virus infection. *Journal of virology* 84, 9140–9148. doi:10.1128/JVI.00717-10.
- Stukalov, A., Girault, V., Grass, V., Karayel, O., Bergant, V., Urban, C., Haas, D.A., Huang, Y., Oubraham, L., Wang, A., Hamad, M.S., Piras, A., Hansen, F.M., Tanzer, M.C., Paron, I., Zinzula, L., Engleitner, T., Reinecke, M., Lavacca, T.M., Ehmann, R., Wölfel, R., Jores, J., Kuster, B.,

- Protzer, U., Rad, R., Ziebuhr, J., Thiel, V., Scaturro, P., Mann, M., Pichlmair, A., 2021. Multilevel proteomics reveals host perturbations by SARS-CoV-2 and SARS-CoV. *Nature* 594, 246–252. doi:10.1038/s41586-021-03493-4.
- Stutz, A., Kolbe, C.-C., Stahl, R., Horvath, G.L., Franklin, B.S., van Ray, O., Brinkschulte, R., Geyer, M., Meissner, F., Latz, E., 2017. NLRP3 inflammasome assembly is regulated by phosphorylation of the pyrin domain. *The Journal of Experimental Medicine* 214, 1725–1736. doi:10.1084/jem.20160933.
- Sutejo, R., Yeo, D.S., Myaing, M. zu, Hui, C., Xia, J., Ko, D., Cheung, P.C.F., Tan, B.-H., Sugrue, R.J., 2012. Activation of type I and III interferon signalling pathways occurs in lung epithelial cells infected with low pathogenic avian influenza viruses. *PLoS ONE* 7, e33732. doi:10.1371/journal.pone.0033732.
- Szretter, K.J., Samuel, M.A., Gilfillan, S., Fuchs, A., Colonna, M., Diamond, M.S., 2009. The Immune Adaptor Molecule SARM Modulates Tumor Necrosis Factor Alpha Production and Microglia Activation in the Brainstem and Restricts West Nile Virus Pathogenesis. *Journal of virology* 83, 9329–9338. doi:10.1128/JVI.00836-09.
- Takeuchi, O., Akira, S., 2010. Pattern Recognition Receptors and Inflammation. *Cell* 140, 805–820. doi:10.1016/j.cell.2010.01.022.
- Tamura, K., Nei, M., 1993. Estimation of the number of nucleotide substitutions in the control region of mitochondrial DNA in humans and chimpanzees. *Molecular biology and evolution* 10, 512–526. doi:10.1093/oxfordjournals.molbev.a040023.
- Taylor, J.K., Coleman, C.M., Postel, S., Sisk, J.M., Bernbaum, J.G., Venkataraman, T., Sundberg, E.J., Frieman, M.B., 2015. Severe Acute Respiratory Syndrome Coronavirus ORF7a Inhibits Bone Marrow Stromal Antigen 2 Virion Tethering through a Novel Mechanism of Glycosylation Interference. *Journal of virology* 89, 11820–11833. doi:10.1128/JVI.02274-15.
- Tchouassi, D.P., Marklewitz, M., Chepkorir, E., Zirkel, F., Agha, S.B., Tigoi, C.C., Koskei, E., Drosten, C., Borgemeister, C., Torto, B., Junglen, S., Sang, R., 2019. Sand Fly-Associated Phlebovirus with Evidence of Neutralizing Antibodies in Humans, Kenya. *Emerging infectious diseases* 25, 681–690. doi:10.3201/eid2504.180750.
- tenOever, B.R., Ng, S.L., Chua, M.A., McWhirter, S.M., García-Sastre, A., Maniatis, T., 2007. Multiple functions of the IKK-related kinase IKKepsilon in interferon-mediated antiviral immunity. *Science (New York, N.Y.)* 315. doi:10.1126/science.1136567.
- Tesh, R.B., Duboise, S.M., 1987. Viremia and immune response with sequential phlebovirus infections. *The American journal of tropical medicine and hygiene* 36, 662–668. doi:10.4269/ajtmh.1987.36.662.
- Tesh, R.B., Saidi, S., Gajdamovic, S.J., Rodhain, F., Vesenjask-Hirjan, J., 1976. Serological studies on the epidemiology of sandfly fever in the Old World. *Bulletin of the World Health Organization* 54, 663–674.
- Thiel, V., Weber, F., 2008. Interferon and cytokine responses to SARS-coronavirus infection. *Cytokine & Growth Factor Reviews* 19, 121–132. doi:10.1016/j.cytogfr.2008.01.001.
- Thoms, M., Buschauer, R., Ameisemeier, M., Koepke, L., Denk, T., Hirschenberger, M., Kratzat, H., Hayn, M., Mackens-Kiani, T., Cheng, J., Straub, J.H., Stürzel, C.M., Fröhlich, T., Berninghausen, O., Becker, T., Kirchhoff, F., Sparrer, K.M.J., Beckmann, R., 2020. Structural basis for translational shutdown and immune evasion by the Nsp1 protein of SARS-CoV-2. *Science (New York, N.Y.)* 369, 1249–1255. doi:10.1126/science.abc8665.

- Tiwari, R., La Torre, J.C. de, McGavern, D.B., Nayak, D., 2019. Beyond Tethering the Viral Particles: Immunomodulatory Functions of Tetherin (BST-2). *DNA and cell biology* 38, 1170–1177. doi:10.1089/dna.2019.4777.
- Traoré-Lamizana, M., Fontenille, D., Diallo, M., Bâ, Y., Zeller, H.G., Mondo, M., Adam, F., Thonon, J., Maïga, A., 2001. Arbovirus surveillance from 1990 to 1995 in the Barkedji area (Ferlo) of Senegal, a possible natural focus of Rift Valley fever virus. *Journal of medical entomology* 38, 480–492. doi:10.1603/0022-2585-38.4.480.
- Travassos da Rosa, A.P., Tesh, R.B., Pinheiro, F.P., Travassos da Rosa, J.F., Peterson, N.E., 1983. Characterization of eight new phlebotomus fever serogroup arboviruses (Bunyaviridae: Phlebovirus) from the Amazon region of Brazil. *The American journal of tropical medicine and hygiene* 32, 1164–1171. doi:10.4269/ajtmh.1983.32.1164.
- Tyanova, S., Temu, T., Cox, J., 2016a. The MaxQuant computational platform for mass spectrometry-based shotgun proteomics. *Nature protocols* 11, 2301–2319. doi:10.1038/nprot.2016.136.
- Tyanova, S., Temu, T., Sinitcyn, P., Carlson, A., Hein, M.Y., Geiger, T., Mann, M., Cox, J., 2016b. The Perseus computational platform for comprehensive analysis of (prote)omics data. *Nature methods* 13, 731–740. doi:10.1038/nmeth.3901.
- Upadhyay, A.S., Vonderstein, K., Pichlmair, A., Stehling, O., Bennett, K.L., Dobler, G., Guo, J.-T., Superti-Furga, G., Lill, R., Överby, A.K., Weber, F., 2014. Viperin is an iron-sulfur protein that inhibits genome synthesis of tick-borne encephalitis virus via radical SAM domain activity. *Cellular microbiology* 16, 834–848. doi:10.1111/cmi.12241.
- van Kuppeveld, F.J., van der Logt, J.T., Angulo, A.F., van Zoest, M.J., Quint, W.G., Niesters, H.G., Galama, J.M., Melchers, W.J., 1992. Genus- and species-specific identification of mycoplasmas by 16S rRNA amplification. *Applied and Environmental Microbiology* 58, 2606–2615. doi:10.1128/AEM.58.8.2606-2615.1992.
- van Kuppeveld, F.J., van der Logt, J.T., Angulo, A.F., van Zoest, M.J., Quint, W.G., Niesters, H.G., Galama, J.M., Melchers, W.J., 1993. Genus- and species-specific identification of mycoplasmas by 16S rRNA amplification. *Applied and Environmental Microbiology* 59, 655.
- Vanderheiden, A., Ralfs, P., Chirkova, T., Upadhyay, A.A., Zimmerman, M.G., Bedoya, S., Aoued, H., Tharp, G.M., Pellegrini, K.L., Manfredi, C., Sorscher, E., Mainou, B., Lobby, J.L., Kohlmeier, J.E., Lowen, A.C., Shi, P.-Y., Menachery, V.D., Anderson, L.J., Grakoui, A., Bosinger, S.E., Suthar, M.S., 2020. Type I and Type III Interferons Restrict SARS-CoV-2 Infection of Human Airway Epithelial Cultures. *Journal of virology* 94. doi:10.1128/JVI.00985-20.
- Vazquez, C., Swanson, S.E., Negatu, S.G., Dittmar, M., Miller, J., Ramage, H.R., Cherry, S., Jurado, K.A., 2021. SARS-CoV-2 viral proteins NSP1 and NSP13 inhibit interferon activation through distinct mechanisms. *PLoS ONE* 16, e0253089. doi:10.1371/journal.pone.0253089.
- Verbruggen, P., Ruf, M., Blakqori, G., Överby, A.K., Heidemann, M., Eick, D., Weber, F., 2011. Interferon antagonist NSs of La Crosse virus triggers a DNA damage response-like degradation of transcribing RNA polymerase II. *The Journal of biological chemistry* 286, 3681–3692. doi:10.1074/jbc.M110.154799.
- Vilibic-Cavlek, T., Zidovec-Lepej, S., Ledina, D., Knezevic, S., Savic, V., Tabain, I., Ivic, I., Slavuljica, I., Bogdanic, M., Grgic, I., Gorenc, L., Stevanovic, V., Barbic, L., 2020. Clinical, Virological, and Immunological Findings in Patients with Toscana Neuroinvasive Disease in Croatia: Report of Three Cases. *Tropical medicine and infectious disease* 5. doi:10.3390/tropicalmed5030144.

- V'kovski, P., Gultom, M., Kelly, J.N., Steiner, S., Russeil, J., Mangeat, B., Cora, E., Pezoldt, J., Holwerda, M., Kratzel, A., Laloli, L., Wider, M., Portmann, J., Tran, T., Ebert, N., Stalder, H., Hartmann, R., Gardeux, V., Alpern, D., Deplancke, B., Thiel, V., Dijkman, R., 2021a. Disparate temperature-dependent virus–host dynamics for SARS-CoV-2 and SARS-CoV in the human respiratory epithelium. *PLoS Biology* 19. doi:10.1371/journal.pbio.3001158.
- V'kovski, P., Kratzel, A., Steiner, S., Stalder, H., Thiel, V., 2021b. Coronavirus biology and replication: implications for SARS-CoV-2. *Nature reviews. Microbiology* 19, 155–170. doi:10.1038/s41579-020-00468-6.
- Wack, A., Openshaw, P., O'Garra, A., 2011. Contribution of cytokines to pathology and protection in virus infection. *Current opinion in virology* 1, 184–195. doi:10.1016/j.coviro.2011.05.015.
- Wack, A., Terczyńska-Dyla, E., Hartmann, R., 2015. Guarding the frontiers: the biology of type III interferons. *Nature immunology* 16, 802–809. doi:10.1038/ni.3212.
- Walter, C.T., Barr, J.N., 2011. Recent advances in the molecular and cellular biology of bunyaviruses. *The Journal of general virology* 92, 2467–2484. doi:10.1099/vir.0.035105-0.
- Wang, J., Fu, S., Xu, Z., Cheng, J., Shi, M., Fan, N., Song, J., Tian, X., Cheng, J., Ni, S., He, Y., Lei, W., Li, F., Peng, H., Wang, B., Wang, H., Lu, X., Ma, Y., Liang, G., 2020a. Emerging Sand Fly-Borne Phlebovirus in China. *Emerging infectious diseases* 26, 2435–2438. doi:10.3201/eid2610.191374.
- Wang, J., Li, H., Xue, B., Deng, R., Huang, X., Xu, Y., Chen, S., Tian, R., Wang, X., Xun, Z., Sang, M., Zhu, H., 2020b. IRF1 Promotes the Innate Immune Response to Viral Infection by Enhancing the Activation of IRF3. *Journal of virology* 94. doi:10.1128/JVI.01231-20.
- Wang, N., Zhan, Y., Zhu, L., Hou, Z., Liu, F., Song, P., Qiu, F., Wang, X., Zou, X., Wan, D., Qian, X., Wang, S., Guo, Y., Yu, H., Cui, M., Tong, G., Xu, Y., Zheng, Z., Lu, Y., Hong, P., 2020c. Retrospective Multicenter Cohort Study Shows Early Interferon Therapy Is Associated with Favorable Clinical Responses in COVID-19 Patients. *Cell Host & Microbe* 28, 455-464.e2. doi:10.1016/j.chom.2020.07.005.
- Wang, S., Li, W., Hui, H., Tiwari, S.K., Zhang, Q., Croker, B.A., Rawlings, S., Smith, D., Carlin, A.F., Rana, T.M., 2020d. Cholesterol 25-Hydroxylase inhibits SARS-CoV-2 and other coronaviruses by depleting membrane cholesterol. *The EMBO journal* 39, e106057. doi:10.15252/embj.2020106057.
- Wang, X., Hennig, T., Whisnant, A.W., Erhard, F., Prusty, B.K., Friedel, C.C., Forouzmand, E., Hu, W., Erber, L., Chen, Y., Sandri-Goldin, R.M., Dölken, L., Shi, Y., 2020e. Herpes simplex virus blocks host transcription termination via the bimodal activities of ICP27. *Nature communications* 11, 293. doi:10.1038/s41467-019-14109-x.
- Wang, X., Hinson, E.R., Cresswell, P., 2007. The interferon-inducible protein viperin inhibits influenza virus release by perturbing lipid rafts. *Cell Host & Microbe* 2, 96–105. doi:10.1016/j.chom.2007.06.009.
- Wathelet, M.G., Orr, M., Frieman, M.B., Baric, R.S., 2007. Severe Acute Respiratory Syndrome Coronavirus Evades Antiviral Signaling: Role of nsp1 and Rational Design of an Attenuated Strain. *Journal of virology* 81, 11620–11633. doi:10.1128/jvi.00702-07.
- Weber, F., Wagner, V., Rasmussen, S.B., Hartmann, R., Paludan, S.R., 2006. Double-Stranded RNA Is Produced by Positive-Strand RNA Viruses and DNA Viruses but Not in Detectable Amounts by Negative-Strand RNA Viruses. *Journal of virology* 80, 5059–5064. doi:10.1128/JVI.80.10.5059-5064.2006.

- WHO, 2003. Consensus document on the epidemiology of severe acute respiratory syndrome, <https://www.who.int/csr/sars/en/WHOconsensus.pdf>.
- Wickham, H., 2016. *ggplot2: Elegant Graphics for Data Analysis*, Springer International Publishing, ISBN 978-3-319-24275-0.
- Woelfl, F., Léger, P., Oreshkova, N., Pahmeier, F., Windhaber, S., Koch, J., Stanifer, M., Roman Sosa, G., Uckeley, Z.M., Rey, F.A., Boulant, S., Kortekaas, J., Wichgers Schreur, P.J., Lozach, P.-Y., 2020. Novel Toscana Virus Reverse Genetics System Establishes NSs as an Antagonist of Type I Interferon Responses. *Viruses* 12. doi:10.3390/v12040400.
- Wright, D., Kortekaas, J., Bowden, T.A., Warimwe, G.M., 2019. Rift Valley fever: biology and epidemiology. *The Journal of general virology* 100, 1187–1199. doi:10.1099/jgv.0.001296.
- Wu, C., Cui, Y., Liu, X., Zhang, F., Lu, L.-Y., Yu, X., 2019. The RNF20/40 complex regulates p53-dependent gene transcription and mRNA splicing. *Journal of molecular cell biology* 12, 113–124. doi:10.1093/jmcb/mjz045.
- Wu, X., Qi, X., Qu, B., Zhang, Z., Liang, M., Li, C., Cardona, C.J., Li, D., Xing, Z., 2014. Evasion of antiviral immunity through sequestering of TBK1/IKK ϵ /IRF3 into viral inclusion bodies. *Journal of virology* 88, 3067–3076. doi:10.1128/JVI.03510-13.
- Wuerth, J.D., Habjan, M., Kainulainen, M., Berisha, B., Bertheloot, D., Superti-Furga, G., Pichlmair, A., Weber, F., 2020. eIF2B as a Target for Viral Evasion of PKR-Mediated Translation Inhibition. *mBio* 11. doi:10.1128/mBio.00976-20.
- Wuerth, J.D., Habjan, M., Wulle, J., Superti-Furga, G., Pichlmair, A., Weber, F., 2018. NSs Protein of Sandfly Fever Sicilian Phlebovirus Counteracts Interferon (IFN) Induction by Masking the DNA-Binding Domain of IFN Regulatory Factor 3. *Journal of virology* 92. doi:10.1128/JVI.01202-18.
- Wuerth, J.D., Weber, F., 2016. Phleboviruses and the Type I Interferon Response. *Viruses* 8. doi:10.3390/v8060174.
- Wyler, E., Mösbauer, K., Franke, V., Diag, A., Gottula, L.T., Arsiè, R., Klironomos, F., Koppstein, D., Hönzke, K., Ayoub, S., Buccitelli, C., Hoffmann, K., Richter, A., Legnini, I., Ivanov, A., Mari, T., Del Giudice, S., Papiès, J., Praktiknjo, S., Meyer, T.F., Müller, M.A., Niemeyer, D., Hocke, A., Selbach, M., Akalin, A., Rajewsky, N., Drosten, C., Landthaler, M., 2021. Transcriptomic profiling of SARS-CoV-2 infected human cell lines identifies HSP90 as target for COVID-19 therapy. *iScience* 24, 102151. doi:10.1016/j.isci.2021.102151.
- Xia, H., Cao, Z., Xie, X., Zhang, X., Chen, J.Y.-C., Wang, H., Menachery, V.D., Rajsbaum, R., Shi, P.-Y., 2020. Evasion of Type I Interferon by SARS-CoV-2. *Cell reports* 33, 108234. doi:10.1016/j.celrep.2020.108234.
- Xu, J., Zhang, L., Xu, Y., Zhang, H., Gao, J., Wang, Q., Tian, Z., Xuan, L., Chen, H., Wang, Y., 2019. PP2A Facilitates Porcine Reproductive and Respiratory Syndrome Virus Replication by Deactivating irf3 and Limiting Type I Interferon Production. *Viruses* 11. doi:10.3390/v11100948.
- Xu, Y.-R., Lei, C.-Q., 2021. TAK1-TABs Complex: A Central Signalosome in Inflammatory Responses. *Frontiers in Immunology* 11. doi:10.3389/fimmu.2020.608976.
- Yamada, T., Sato, S., Sotoyama, Y., Orba, Y., Sawa, H., Yamauchi, H., Sasaki, M., Takaoka, A., 2021. RIG-I triggers a signaling-abortive anti-SARS-CoV-2 defense in human lung cells. *Nature immunology* 22, 820–828. doi:10.1038/s41590-021-00942-0.
- Yang, Y., Shen, C., Li, J., Yuan, J., Wei, J., Huang, F., Wang, F., Li, G., Li, Y., Xing, L., Peng, L., Yang, M., Cao, M., Zheng, H., Wu, W., Zou, R., Li, D., Xu, Z., Wang, H., Zhang, M., Zhang, Z.,

- Gao, G.F., Jiang, C., Liu, L., Liu, Y., 2020a. Plasma IP-10 and MCP-3 levels are highly associated with disease severity and predict the progression of COVID-19. *The Journal of allergy and clinical immunology* 146, 119-127.e4. doi:10.1016/j.jaci.2020.04.027.
- Yang, Z., Zhang, X., Wang, F., Wang, P., Kuang, E., Li, X., 2020b. Suppression of MDA5-mediated antiviral immune responses by NSP8 of SARS-CoV-2, <http://dx.doi.org/10.1101/2020.08.12.247767>.
- Yarilina, A., Park-Min, K.-H., Antoniv, T., Hu, X., Ivashkiv, L.B., 2008. TNF activates an IRF1-dependent autocrine loop leading to sustained expression of chemokines and STAT1-dependent type I interferon-response genes. *Nature immunology* 9, 378–387. doi:10.1038/ni1576.
- Ye, J.S., Kim, N., Lee, K.J., Nam, Y.R., Lee, U., Joo, C.H., 2014. Lysine 63-linked TANK-binding kinase 1 ubiquitination by mindbomb E3 ubiquitin protein ligase 2 is mediated by the mitochondrial antiviral signaling protein. *Journal of virology* 88, 12765–12776. doi:10.1128/JVI.02037-14.
- Ye, L., Schnepf, D., Staeheli, P., 2019. Interferon- λ orchestrates innate and adaptive mucosal immune responses. *Nature reviews. Immunology* 19, 614–625. doi:10.1038/s41577-019-0182-z.
- Yin, X., Riva, L., Pu, Y., Martin-Sancho, L., Kanamune, J., Yamamoto, Y., Sakai, K., Gotoh, S., Miorin, L., Jesus, P.D. de, Yang, C.-C., Herbert, K.M., Yoh, S., Hultquist, J.F., García-Sastre, A., Chanda, S.K., 2021. MDA5 Governs the Innate Immune Response to SARS-CoV-2 in Lung Epithelial Cells. *Cell reports* 34, 108628. doi:10.1016/j.celrep.2020.108628.
- Yoneyama, M., Suhara, W., Fukuhara, Y., Fukuda, M., Nishida, E., Fujita, T., 1998. Direct triggering of the type I interferon system by virus infection: activation of a transcription factor complex containing IRF-3 and CBP/p300. *The EMBO journal* 17, 1087–1095. doi:10.1093/emboj/17.4.1087.
- Yoshikawa, T., Hill, T.E., Yoshikawa, N., Popov, V.L., Galindo, C.L., Garner, H.R., Peters, C.J., Tseng, C.-T.K., 2010. Dynamic innate immune responses of human bronchial epithelial cells to severe acute respiratory syndrome-associated coronavirus infection. *PLoS ONE* 5, e8729. doi:10.1371/journal.pone.0008729.
- Yoshinaka, T., Kosako, H., Yoshizumi, T., Furukawa, R., Hirano, Y., Kuge, O., Tamada, T., Koshiba, T., 2019. Structural Basis of Mitochondrial Scaffolds by Prohibitin Complexes: Insight into a Role of the Coiled-Coil Region. *iScience* 19, 1065–1078. doi:10.1016/j.isci.2019.08.056.
- Zaki, A.M., van Boheemen, S., Bestebroer, T.M., Osterhaus, A.D.M.E., Fouchier, R.A.M., 2012. Isolation of a novel coronavirus from a man with pneumonia in Saudi Arabia. *The New England journal of medicine* 367, 1814–1820. doi:10.1056/NEJMoa1211721.
- Zang, R., Case, J.B., Yutuc, E., Ma, X., Shen, S., Gomez Castro, M.F., Liu, Z., Zeng, Q., Zhao, H., Son, J., Rothlauf, P.W., Kreutzberger, A.J.B., Hou, G., Zhang, H., Bose, S., Wang, X., Vahey, M.D., Mani, K., Griffiths, W.J., Kirchhausen, T., Fremont, D.H., Guo, H., Diwan, A., Wang, Y., Diamond, M.S., Whelan, S.P.J., Ding, S., 2020. Cholesterol 25-hydroxylase suppresses SARS-CoV-2 replication by blocking membrane fusion. *Proceedings of the National Academy of Sciences of the United States of America* 117, 32105–32113. doi:10.1073/pnas.2012197117.
- Zhao, X., Li, J., Winkler, C.A., An, P., Guo, J.-T., 2018. IFITM Genes, Variants, and Their Roles in the Control and Pathogenesis of Viral Infections. *Frontiers in microbiology* 9, 3228. doi:10.3389/fmicb.2018.03228.
- Zheng, F., Zhou, Y., Zhou, Z., Ye, F., Huang, B., Huang, Y., Ma, J., Zuo, Q., Tan, X., Xie, J., Niu, P., Wang, W., Xu, Y., Peng, F., Zhou, N., Cai, C., Tang, W., Xiao, X., Li, Y., Zhou, Z., Jiang, Y., Xie,

- Y., Tan, W., Gong, G., 2020a. SARS-CoV-2 clearance in COVID-19 patients with Novaferon treatment: A randomized, open-label, parallel-group trial. *International journal of infectious diseases : IJID : official publication of the International Society for Infectious Diseases* 99, 84–91. doi:10.1016/j.ijid.2020.07.053.
- Zheng, Y., Zhuang, M.-W., Han, L., Zhang, J., Nan, M.-L., Zhan, P., Kang, D., Liu, X., Gao, C., Wang, P.-H., 2020b. Severe acute respiratory syndrome coronavirus 2 (SARS-CoV-2) membrane (M) protein inhibits type I and III interferon production by targeting RIG-I/MDA-5 signaling. *Signal transduction and targeted therapy* 5. doi:10.1038/s41392-020-00438-7.
- Zhioua, E., Moureau, G., Chelbi, I., Ninove, L., Bichaud, L., Derbali, M., Champs, M., Cherni, S., Salez, N., Cook, S., Lamballerie, X. de, Charrel, R.N., 2010. Punique virus, a novel phlebovirus, related to sandfly fever Naples virus, isolated from sandflies collected in Tunisia. *The Journal of general virology* 91, 1275–1283. doi:10.1099/vir.0.019240-0.
- Zhong, N.S., Zheng, B.J., Li, Y.M., Poon, Xie, Z.H., Chan, K.H., Li, P.H., Tan, S.Y., Chang, Q., Xie, J.P., Liu, X.Q., Xu, J., Li, D.X., Yuen, K.Y., Peiris, Guan, Y., 2003. Epidemiology and cause of severe acute respiratory syndrome (SARS) in Guangdong, People's Republic of China, in February, 2003. *Lancet (London, England)* 362, 1353–1358. doi:10.1016/s0140-6736(03)14630-2.
- Zhou, B., Li, J., Liang, X., Yang, Z., Jiang, Z., 2017. Transcriptome profiling of influenza A virus-infected lung epithelial (A549) cells with laticiresinol-4- β -D-glucopyranoside treatment. *PLoS ONE* 12, e0173058. doi:10.1371/journal.pone.0173058.
- Zhou, P., Yang, X.-L., Wang, X.-G., Hu, B., Zhang, L., Zhang, W., Si, H.-R., Zhu, Y., Li, B., Huang, C.-L., Chen, H.-D., Chen, J., Luo, Y., Guo, H., Jiang, R.-D., Liu, M.-Q., Chen, Y., Shen, X.-R., Wang, X., Zheng, X.-S., Zhao, K., Chen, Q.-J., Deng, F., Liu, L.-L., Yan, B., Zhan, F.-X., Wang, Y.-Y., Xiao, G.-F., Shi, Z.-L., 2020a. A pneumonia outbreak associated with a new coronavirus of probable bat origin. *Nature* 579, 270–273. doi:10.1038/s41586-020-2012-7.
- Zhou, Q., Chen, V., Shannon, C.P., Wei, X.-S., Xiang, X., Wang, X., Wang, Z.-H., Tebbutt, S.J., Kollmann, T.R., Fish, E.N., 2020b. Interferon- α 2b Treatment for COVID-19. *Frontiers in Immunology* 11, 1061. doi:10.3389/fimmu.2020.01061.
- Zhou, Y., Zhou, B., Pache, L., Chang, M., Khodabakhshi, A.H., Tanaseichuk, O., Benner, C., Chanda, S.K., 2019. Metascape provides a biologist-oriented resource for the analysis of systems-level datasets. *Nature communications* 10, 1523. doi:10.1038/s41467-019-09234-6.
- Zhu, N., Zhang, D., Wang, W., Li, X., Yang, B., Song, J., Zhao, X., Huang, B., Shi, W., Lu, R., Niu, P., Zhan, F., Ma, X., Wang, D., Xu, W., Wu, G., Gao, G.F., Tan, W., 2020. A Novel Coronavirus from Patients with Pneumonia in China, 2019. *The New England journal of medicine* 382, 727–733. doi:10.1056/NEJMoa2001017.
- Zielecki, F., Weber, M., Eickmann, M., Spiegelberg, L., Zaki, A.M., Matrosovich, M., Becker, S., Weber, F., 2013. Human cell tropism and innate immune system interactions of human respiratory coronavirus EMC compared to those of severe acute respiratory syndrome coronavirus. *Journal of virology* 87, 5300–5304. doi:10.1128/JVI.03496-12.

13 Addendum

13.1 Peer-reviewed publications

Han, N., Hwang, W., Tzelepis, K., Schmerer, P., Yankova, E., MacMahon, M., Lei, W., M. Katritsis, N., Liu, A., **Felgenhauer, U.**, Schuldt, A., Harris, R., Chapman, K., McCaughan, F., Weber, F., Kouzarides, T., 2021. **Identification of SARS-CoV-2-induced pathways reveals drug repurposing strategies.** *Science Advances* 7, eabh3032. doi:10.1126/sciadv.abh3032

Felgenhauer, U., Schoen, A., Gad, H.H., Hartmann, R., Schaubmar, A.R., Failing, K., Drosten, C., Weber, F., 2020. **Inhibition of SARS-CoV-2 by type I and type III interferons.** *The Journal of biological chemistry* 295, 13958–13964. doi:10.1074/jbc.AC120.013788.

Weber, M., Sediri, H., **Felgenhauer, U.**, Binzen, I., Bänfer, S., Jacob, R., Brunotte, L., García-Sastre, A., Schmid-Burgk, J.L., Schmidt, T., Hornung, V., Kochs, G., Schwemmler, M., Klenk, H.-D., Weber, F., 2015. **Influenza virus adaptation PB2-627K modulates nucleocapsid inhibition by the pathogen sensor RIG-I.** *Cell Host & Microbe* 17, 309–319. doi:10.1016/j.chom.2015.01.005

13.2 Conference presentations

Felgenhauer, U., Marklewitz, M., Tchouassi, D.P., Torto, B., Sang, R., Junglen, S., Weber, F. **Towards the innate immunity phenotype of newly emerging viruses.** Zoonoses 2021 – International Symposium on Zoonoses Research, 13 – 15 October 2021, digital. Oral presentation.

Felgenhauer, U., Marklewitz, M., Tchouassi, D.P., Torto, B., Sang, R., Junglen, S., Weber, F. **Towards the innate immunity phenotype of newly emerging viruses.** 30th Annual Meeting of the Society for Virology, 24 – 26 March 2021, digital. Poster presentation.

Felgenhauer, U., Karl, N., Ziebuhr, J., Weber, F. **Innate immunity phenotype of viruses.** Zoonoses 2019 – International Symposium on Zoonoses Research, 16 – 18 October 2019, Berlin, Germany. Poster presentation.

Felgenhauer, U., Karl, N., Ziebuhr, J., Weber, F. **Innate immunity phenotype of viruses.** 3rd Novel Concepts in Innate Immunity Conference, 12 – 14 June 2019, Tübingen, Germany. Poster presentation.

Felgenhauer, U., Karl, N., Ziebuhr, J., Weber, F. **Innate immunity phenotype of viruses.** 7th European Congress of Virology, 28 April – 1 May 2019, Rotterdam, the Netherlands. Poster presentation.

Weber-Gerlach M., Fehling, S.K., Wolff, S., **Felgenhauer, U.**, Bank-Wolf, B., Kainulainen, M.H., Jacob, R., Wulle, J., Becker, S., Strecker, T., Weber, F. **Activation and inhibition of PKR by ambisense RNA viruses.** 28th Annual Meeting of the Society for Virology, 14 – 17 March 2018, Würzburg, Germany. Poster presentation.

14 Danksagung

Zuallererst möchte ich Friedemann Weber für die Ausbildung in den letzten acht Jahren danken (mit Unterbrechung). Für die Unterstützung, die Leitung, die offene Tür und das Vertrauen, mich wieder aufzunehmen.

Ein besonderer Dank geht auch an Sandra Hake in der Rolle meiner Erstgutachterin. Dafür, dass sie mich während meiner Doktorarbeitszeit in Gießen betreut und unterstützt hat, für die netten Gespräche und ihre Zeit.

Ganz herzlich danke ich auch Stefan Bauer und John Ziebuhr, für ihre Bereitschaft, meine Disputation mit zu prüfen.

Weiterhin danke ich allen Mitgliedern von AG Weber und AG Lamp und dem gesamten Institut für Virologie des FB10 für die schöne und lehrreiche Zeit hier in Gießen. Simone, Akis, Babsi und Tim für ein großartiges Büroklima und immer die Zeit für einen kleinen Spaß; Patrick, meinem „Leidensgenossen“, dafür, dass er sich immer meine Geschichten angehört hat und dafür, dass er ein guter Freund ist; Carina dafür, dass sie da ist und wir irgendwie sofort Freunde geworden sind, und auch für die ganze Hilfe bei dem organisatorischen Kram; sowie Stéph, Andreas, Lyudmila, Besim, Kelly, Gleyder, Lisa, Kai, Kathi und auch Jen und Michi – und Benjamin, den man immer alles fragen kann. Ganz herzlichen Dank auch an Frau Zitzlaff und Frau Biedenkopf für die exzellente administrative Unterstützung, und an alle Mitglieder der Diagnostik, ganz besonders Sibylle. Und danke an alle, die jemals Kuchen mitgebracht haben!

Ein riesiges Dankeschön geht an das ganze Institut für Virologie der Charité Berlin: Marcel Müller, Daniela Niemeyer, Sandra Junglen und Christian Drosten, Kirstin, Lina, Verena, Anja, Fabian, Julia, Jan, Rieke, Simon, Julian, Andrea, Jackson, Bengisu, Selina, Tobi, Anne und an alle anderen, sowie Anja Köstler, Ilia Semmler und Naemi Smolka. Ihr habt mich ohne zu zögern aufgenommen und ich hatte eine wundervolle Zeit bei euch.

Danke an alle, die mir während meiner Doktorarbeitszeit geholfen haben und mit denen ich zusammenarbeiten durfte: Nadja Karl, John Ziebuhr, Sandra Junglen, Marco Marklewitz, Uwe Linne, Axel Weber, Torsten Hain, Ben Ott, Rune Hartmann und allen weiteren, die bei der Datenanalyse und Vorbereitung von Manuskripten geholfen haben, sowie Patrick, Andreas und Simone, die meine S3-Versuche in Gießen gemacht haben.

Ein besonderes Dankeschön an meine alte Arbeitsgruppe in Vancouver und das gesamte *Centre for Blood Research*: Ed, Scott, Michael, Bryan, Frank, Rolinda, Tseday, Kim und auch Chanel, Fred, Elena, Brana, Katherine und alle. Ich werde es nie bereuen, dass ich diesen „Umweg“ gegangen bin. Ihr seid super. An dieser Stelle auch noch ein Riesendank an Dirk Lange – ohne dich wäre vieles gar nicht möglich gewesen.

Ein immens großes Ultradankeschön geht an alle, die meine Doktorarbeit Korrektur gelesen haben: Carina und Jan, und auch Johanna, Helle, Anika, Lisa, Laura, Simone und Patrick. Ihr seid spitze!

Danke Mama und Papa für alles. Ihr habt mich immer unterstützt, egal was war, und ich kann euch dafür gar nicht genug danken. Danke auch an meine ganze Familie.

Jan. Danke, dass du mein Leben so viel schöner machst. Und für alles, was ich von dir gelernt hab und noch lernen werde. Ente!

Johanna, danke, dass du so ein guter Mensch bist. Ich bin so froh, dass wir zusammen vergessen wurden und dass du Flummis Freundin geworden und geblieben bist.

Martin, danke, dass du mich immer auf den Boden der Tatsachen zurückgeholt und dabei nie allein gelassen hast. Für alle Gespräche und Abenteuer, und für alles was noch kommt.

Ich danke Frauke, Thomas, den J's, Helle, Connie, Anne, Miri, Gwen und dem Rest des grandiosesten Hubi-Jahrgangs der Welt, sowie Marcel und Christian, Maria, Anika, Janina aka Renaade, dem ehemaligen OE-Team, Conny und Julia aka der besten WG der Welt, Helmut, Dede, Julia, Laura und Shawn aka den besten Nachbarn, die man sich wünschen kann, und ganz besonders Ina (besser spät als nie).

Allen wundervollen Menschen in Kanada danke für alles: Myles, Zoë, Evan, Zeus, Zach, Wesley, Jessyca, Fabian, Katie, Jewlee, Bryan, Jorie, Tomas, Bashar, Alex, Tina, Cam, Kasey, Karina, Steve und ganz besonders Ellen und Jim.

Ich danke Henni (siehst du, muss ich doch nicht putzen! – oder zumindest kann ich jetzt gut ausgebildet putzen... Danke für knapp 30 Jahre einer wundervollen Freundschaft), Vanessa aka meinem größten Fan (danke für deine Unterstützung und dein Vertrauen) und Stefan Mützel (das ist hier zwar keine Dankesrede für den Nobelpreis, aber wer weiß, wie lange du dich bis dahin noch gedulden musst).

Vielen Dank auch an alle meine Lehrer an der Schule, an der Uni und im Leben und danke an alle, deren Bekanntschaften und Freundschaften mich zu dem Menschen gemacht haben, der ich jetzt bin.

Zu guter Letzt danke an alle, deren Musik mich durch mein Leben begleitet und getragen hat: Depeche Mode, David Bowie, Queen, Placebo, Ultravox – und besonders Midge Ure für die erfrischende Ablenkung während des letzten Jahres.

15 Annex

Table 52: Total numbers of cellular interactors of indicated phlebovirus NSs proteins

NTPV	GFV	EMBV	BGRV	KBGV	PERV	PTV-A	PTV-B	SFSV	Number of NSs interactors	NTPV	GFV	EMBV	BGRV	KBGV	PERV	PTV-A	PTV-B	SFSV	Number of NSs interactors	NTPV	GFV	EMBV	BGRV	KBGV	PERV	PTV-A	PTV-B	SFSV	Number of NSs interactors
									554										26									8	
									278										1									1	
									2										1									2	
									21										3									1	
									1										1									7	
									5										2									7	
									3										2									4	
									3										1									3	
									2										1									4	
									5										1									27	
									3										1									1	
									125										6									1	
									1										1									3	
									1										1									3	
									1										4									1	
									1										4									1	
									22										1									5	
									1										1									1	
									3										1									8	
									8										1									1	
									11										2									1	
									4										5									1	
									5										1									5	
									1										3									5	
									1										1									9	
									2										2									3	
									2										12									5	
									3										1									7	
									71										2									4	
									1										2									2	
									19										1									11	
									3										1									2	
									6										1									24	
									4										16									3	
									1										1									1	
									1										1									2	
									27										1									6	
									1										1									3	
									1										1									6	
									2										6									6	
									1										4									5	
									1										1									7	
									9										4									1	
									1										2									7	
									2										1									2	
									4										3									5	
									4										6									8	
									9										1									1	
									1										1									1	
									1										4									46	
									1										1									2	
									18										3									58	
									1										1									25	
									1										6									16	
									1										2									28	
									14										1									8	
									1										2									78	
									2										1									4	
									1										2									64	
									1										3									15	
									1										1									1	
									1										8									2037	

Table 53: Phlebovirus NSs interactors annotated to GO list #0045087 “innate immune response”

Host protein		Interaction with NSs of...								
UniProt entry ID	UniProt entry name	NTPV	GFV	EMBV	BGRV	KBGV	PERV	PTV-A	PTV-B	SFSV
Q9NVI7	ATD3A_HUMAN									
P08670	VIME_HUMAN									
P61160	ARP2_HUMAN									
Q9Y5A9	YTHD2_HUMAN									
P23246	SFPQ_HUMAN									
Q13283	G3BP1_HUMAN									
P35232	PHB_HUMAN									
Q13263	TIF1B_HUMAN									
P51617	IRAK1_HUMAN									
P14174	MIF_HUMAN									
Q96SB4	SRPK1_HUMAN									
Q9Y3Z3	SAMH1_HUMAN									
P12956	XRCC6_HUMAN									
P78527	PRKDC_HUMAN									
O00571	DDX3X_HUMAN									
Q9NR30	DDX21_HUMAN									
O00159	MYO1C_HUMAN									
Q96PK6	RBM14_HUMAN									
O60506	HNRPQ_HUMAN									
P42224	STAT1_HUMAN									
Q9NX58	LYAR_HUMAN									
Q15233	NONO_HUMAN									
P40429	RL13A_HUMAN									
P55265	DSRAD_HUMAN									
Q14258	TRI25_HUMAN									
Q7Z2W4	ZCCHV_HUMAN									
O75179	ANR17_HUMAN									
Q9UHD2	TBK1_HUMAN									
Q15366	PCBP2_HUMAN									
P62861	RS30_HUMAN									
Q08211	DHX9_HUMAN									
P07814	SYEP_HUMAN									
Q92974	ARHG2_HUMAN									
P13010	XRCC5_HUMAN									
Host protein	Interaction with NSs of...									
UniProt entry ID	UniProt entry name	NTPV	GFV	EMBV	BGRV	KBGV	PERV	PTV-A	PTV-B	SFSV
Q01804	OTUD4_HUMAN									
Q9Y5A7	NUB1_HUMAN									
Q96S55	WRIP1_HUMAN									
O95373	IPO7_HUMAN									
Q9H2U1	DHX36_HUMAN									
P23458	JAK1_HUMAN									
Q13557	KCC2D_HUMAN									
P19525	E2AK2_HUMAN									
P62891	RL39_HUMAN									
Q96J02	ITCH_HUMAN									
P78362	SRPK2_HUMAN									
O00186	STXB3_HUMAN									
P04637	P53_HUMAN									
Q3LXA3	TKFC_HUMAN									
Q9H078	CLPB_HUMAN									
Q07021	C1QBP_HUMAN									
Q9Y6K9	NEMO_HUMAN									
P05423	RPC4_HUMAN									
Q8WXF1	PSPC1_HUMAN									
Q05397	FAK1_HUMAN									
Q9UN86	G3BP2_HUMAN									
Q9UII4	HERC5_HUMAN									
Q6SZW1	SARM1_HUMAN									
Q13555	KCC2G_HUMAN									
Q9BXS9	S26A6_HUMAN									
O15111	IKKA_HUMAN									
P23443	KS6B1_HUMAN									
Q9C000	NLRP1_HUMAN									
Q7Z434	MAVS_HUMAN									
P19367	HXK1_HUMAN									
Q92499	DDX1_HUMAN									
P34897	GLYM_HUMAN									
Q8TDB6	DTX3L_HUMAN									
Q9NW08	RPC2_HUMAN									
Q9BYW2	SETD2_HUMAN									

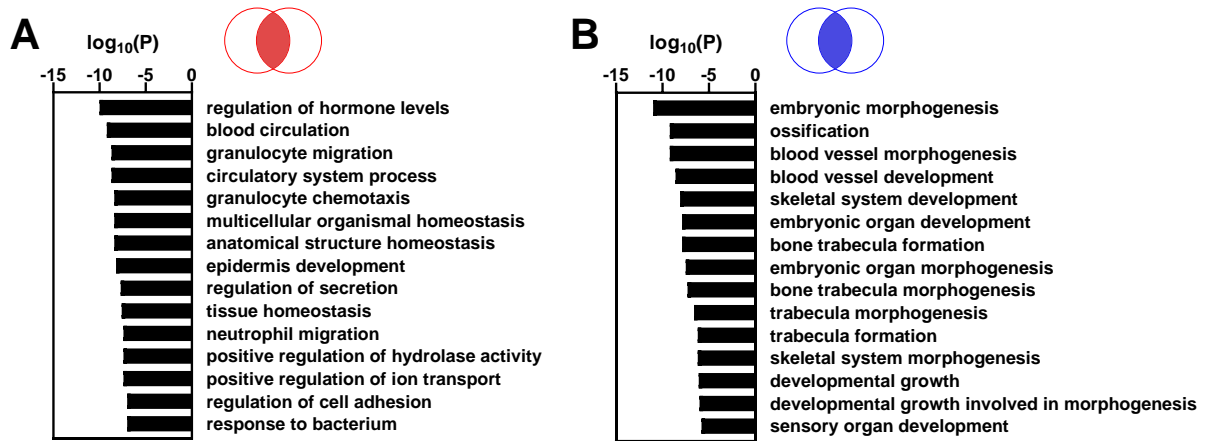


Figure 49: Statistically enriched GO terms within the overlapping gene sets “upregulated in Calu-3 cells compared to H1299 and A549-ACE2 cells” (A) and “downregulated in Calu-3 cells compared to H1299 and A549-ACE2 cells” (B). H1299, A549-ACE2 or Calu-3 cells were mock infected for 24 h, at which point samples were harvested for bulk RNAseq analysis. Genes were filtered by an absolute log₂-fold change of 5 and an adjusted p value ≤ 0.05 . Statistically enriched GO terms within the indicated gene sets are displayed as analyzed using Metascape (Zhou *et al.* 2019). Data are averages from two biological replicates.